RESIDUAL STRESS EVALUATION OF ALUMINIUM DRILL RODS

by

Andrew Michael Segal

A Dissertation Submitted in Partial Fulfilment of the Requirements for the Degree M.Sc. (Engineering)

Department of Mechanical Engineering
University of Cape Town
Pretoria, February 1995

SYNOPSIS

This thesis describes the design, construction and calibration of an air abrasive centre hole (AACH) residual stress measuring facility as well as its use in an experimental study of residual stresses developed in extruded high strength aluminium drill rods. These drill rods were manufactured by Hulett Aluminium for the mining industry for surface drilling exploration work.

Initially a review of available residual stress measurement techniques was undertaken to establish which technique was the most suitable, particularly for residual stress measurement in aluminium rods as a function of processing route, and preferably with the advantages of being reliable, easy to perform, and nominally portable. Furthermore, it was required to establish a residual stress measurement technique which would be well suited for incorporation into the production line of the extruded aluminium drill rods.

The AACH drilling unit, based on Beaney and Procter's design[1-3], appeared to facilitate reliable and accurate residual stress measurement. The facility incorporated a drilling unit and a compatible optical unit, both of which were inserted into a common guide bush which was accurately positioned and aligned above a targeted strain gauge rosette on a test specimen containing residual stress. The required hole in the specimen was then abraded away or "drilled" through the centre of the strain gauge rosette, which in turn monitored any strain relaxation. Subsequently the drilled hole diameter, side wall normality and relative position were checked and measured using the optical facility.

The ring splitting technique was chosen as the technique suited to a production line, since it was a quick and easy method of determining the average hoop residual stresses in the aluminium drill rods. The technique involved between 10 and 30 diameter measurements (both external and internal) depending on the specimen length, and one longitudinal cutting operation to "split" the rod specimens. Various specimen lengths were used to

check whether this factor had any influence on the results. Net average hoop stresses in the rods led to small but consistent changes in diameter which were interpreted in residual stress terms.

Prior to the determination of the residual stresses present in the rods, a geometric evaluation of the rods was conducted. The curvature of the rods was determined in order to establish whether it had any influence on the residual stress distribution in the rods.

Residual stresses were analysed in aluminium drill rods from three different processing routes to establish how induced residual stresses varied between them. The first rod (rod A) was manufactured by a so called "old route" method which entailed extruding a bloom, annealing, tagging, drawing, solution heat treatment, straightening through a series of reels, cutting and ageing. The second rod (rod E) was manufactured according to a so called "stretch route" method which differed from the "old route" method in that the straightening operation was performed by means of stretching the rods axially instead of passing them through reels. The third rod (rod F) was manufactured by a so called "new route" method which differed from the "old route" method in that the sequence of operations was changed. Rod F was also passed through the straightening reels on two different occasions.

Results from the AACH drilling measurements showed that residual tensile stresses were as high as 136.9 MPa at 78.7° to the longitudinal direction of rod A, and 215.2 MPa at 88.6° to the longitudinal direction of rod F, on their outer surfaces. The residual stresses on the outer surface of rod E were compressive, with the lowest measured value being -39.6 MPa at 19.9° to the longitudinal direction. Residual stress measurements performed on the inside surface of the rods showed that stress reversal occurred through the thickness of the rods, and that the magnitude of these residual stresses were substantially lower than those measured on the outside surface.

Interesting trends occurred in the results for rods A and F (which had been passed through series of reels as opposed to having a simple stretch to straighten them as in the case of rod E). These were that the maximum principal stresses were generally in the circumferential direction of the rods; the maximum longitudinal stresses around the circumference of the rods tended to be on the bottom of the curve of the rods and the minimum longitudinal stresses on the top side of the curve (note that the rods were slightly bent in the shape of an arc - the bottom and top sides of the curve of the rods refer to the concave and convex sides respectively); the stress flow direction (calculated from the vector addition of σ_1 and σ_2) tended to act in the direction in which the reels spiralled along the rods, and there appeared to be evidence of periodicity in the distribution of the residual stresses along the length of the rods caused by the spiralling effect of the reels.

It was found in rod E, which had undergone a simple stretch, that the residual stresses had been reoriented, since the stresses that were applied to perform the stretch were slightly in excess of the 0.2% proof stress of the aluminium alloy. Presumably for this reason, it was found that rod E had the smallest amount of curvature of the three rods.

The ring splitting results exhibited similar trends to the AACH drilling results. They were however lower than those for the AACH drilling technique, as expected, due to the averaging nature of the ring splitting technique.

An evaluation of the error associated with the AACH drilling results was undertaken. Various factors such as hole geometry, hole eccentricity and hole measurement were taken into account. It was found that the errors associated with the technique were typically within 6.2%.

From the experimental study of the residual stresses induced in the aluminium drill rods during manufacture, it was found that by incorporating a controlled stretch operation into the processing route, the residual stresses could be significantly

reduced. It was also established that the ring splitting technique could be used as a quick and easy method of residual stress measurement, provided its limitations were taken into account.

DEDICATION

I dedicate this thesis to my wife, Celeste, who has given me constant understanding, love, support and encouragement, as well as sacrificed much valuable time during my studies.

DECLARATION

I declare that this dissertation contains only my own original work, except where reference is made with acknowledgement to contributions from others. I also declare that this material has not been submitted for any purpose or examination to any other Department or University.

Signed this.....day of.....

.....
Andrew Michael Segal

ACKNOWLEDGEMENTS

I would like to thank the following people for their contributions in helping me complete this thesis:

- Prof. R.B. Tait for his supervision and guidance.
- Hulett Aluminium for sponsoring the project, and particularly Dr T. Hurd and Dr B. Harty for their helpfulness.
- Mr C. Clarke for his input during the design stage.
- Mr G. da Silva Pauleta for his input during the experimentation stage.
- Mr M. Batho and his team in the workshop for their help in manufacturing the components for the design work, as well as specimen machining.
- Mr J. Meyer who helped me with strain gauging and the associated electronic equipment.
- Mr M. du Toit for allowing me to use the Mitotoyo Profile Projector at the Cape Town Technikon.
- Mrs C.M. Segal for helping me type this document.
- My colleagues in the Department of Mechanical Engineering for their support and advice.
- My boss, Mr B. Ballantyne, for his consideration during the final stages of this thesis.
- Some of my colleagues at Transwerk, especially Mr C. Jones, for their assistance in preparing certain figures in this document.

TABLE OF CONTENTS

LIST OF ILLUSTRATIONS

Tables

LIST OF SYMBOLS AND ABBREVIATIONS/NOMENCLATURE

Abbreviations

AACH - Air abrasive centre hole.

eqn - Equation.

Symbols

$1/K_1$ - Equation constant used to calculate residual stresses using the air abrasive centre hole drilling technique.

A, A_i - Equation constant used to calculate residual stresses using the air abrasive centre hole drilling technique.

B, B_i - Equation constant used to calculate residual stresses using the air abrasive centre hole drilling technique.

d - Hole diameter.

d_L - Lattice spacing.

d_t - Deflection of cut out tongue.

d_o - Unstressed lattice spacing.

$d_{\phi\psi}$ - Lattice spacing when x-rays are directed with a tilt of ψ.

D - Determinant used to calculate residual stresses when using the air abrasive centre hole drilling technique, defined in eqn A.14.

D_o - Initial diameter of tube or rod.

D_1 - Diameter of tube or rod after ring splitting.

D_X - Determinant used to calculate residual stresses when using the air abrasive centre hole drilling technique, defined in eqn A.15.

D_{YC} - Determinant used to calculate residual stresses when using the air abrasive centre hole drilling technique, defined in eqn A.16.

D_{YS} - Determinant used to calculate residual stresses when using the air abrasive centre hole drilling technique, defined in eqn A.17.

e - Eccentricity of drilled hole with respect to a strain gauge rosette.

E - Young's modulus.

E' - Young's modulus for plane strain.

G_1 - First strain gauge of a strain gauge rosette.

G_2 - Second strain gauge of a strain gauge rosette.

G_3 - Third strain gauge of a strain gauge rosette.

I - Second moment of area.

ID - Inner diameter.

ID_o - Initial inner diameter.

K_1 - Proportionality constant.

K_2 - Proportionality constant.

K_{IC} - Linear elastic fracture toughness.

L - Length of cut.

M - Bending moment.

OD - Outer diameter.

OD_o - Initial outer diameter.

OD_1 - Outer diameter after ring split.

r - Ratio of r_h/R.

r_h - Radius of drilled hole using the AACH drilling technique.

r_i - Ratio of r_h/R_i.

R - Distance from hole centre to centre of strain gauge.

R_o - Initial radius before ring splitting.

R_1 - Radius after ring splitting.

R_i - Distance from hole centre to centre strain gauge i.

S_i - X-ray elastic constants.

t - Thickness.

W - Specimen coordinate system

X - Maximum principal stress plus minimum principal stress.

y - Distance from neutral axis.

Y - Maximum principal stress minus minimum principal stress.

α - Angle measured form the first strain gauge of a strain gauge rosette to the direction of maximum principal stress.

β - Angle between x-axis and direction of eccentricity of an off-centred hole.

γ_i - Angle between direction of maximum principal stress and strain gauge i.

δ_x - Change in length of cored out hole.

ε - Strain.

ε_1 - Strain measured by the first strain gauge of a strain gauge rosette.

ε_2 - Strain measured by the second strain gauge of a strain gauge rosette.

ε_3 - Strain measured by the third strain gauge of a strain gauge rosette.

ε_i - Strain measured by strain gauge i.

ε_{max} - Maximum principal strain.

ε_{min} - Minimum principal strain.

ε_A - Applied axial strain.

ε'_A - Relaxed axial strain.

ε'_T - Relaxed transverse strain.

θ - Angle between maximum principal stress and the circumferential direction of the rods.

θ_i - Angle between the x'-axis and the direction of strain gauge i as measured from the centre of the off-centred hole.

θ_x - Angle of x-ray diffraction.

K - Curvature.

λ - Wave length.

ν - Poisson's ratio.

$\nu K_2/K_1$ - Equation constant used to calculate residual stresses using the air abrasive centre hole drilling technique.

ξ_i - Angle between x-axis and direction of strain gauge i.

σ - Stress.

σ_1 - Maximum principal stress.

σ_{11} - Stress in the W_1 direction.

σ_2 - Minimum principal stress.

σ_{22} - Stress in the W_2 direction.

σ_h or σ_{hoop} - Circumferential or hoop stress.

σ_l or σ_{long} - Longitudinal stress.

σ_{max} - Maximum principal stress.

σ_r - Radial stress.

σ_{shear} - Shear stress.

σ_u - Stress in the direction of the u-axis.

σ'_u - Stress in the direction of the u'-axis.

σ_{uv} - Shear stress in the uv plane.

σ_v - Stress in the direction of the v-axis.

σ'_v - Stress in the direction of the v'-axis.

σ_X - Stress in the direction of the x-axis.

σ_y - Yield stress.

σ_Y - Stress in the direction of the y-axis.

σ_ϕ - Stress in the ϕ direction.

τ - Shear stress.

ϕ_i - Angle between u and u' axes.

ψ - Angle of tilt.

1. INTRODUCTION AND BACKGROUND

1.1 Background

Residual stress is the term applied to a stress or stress system which is induced in an article during its manufacture, and which does not disappear during the natural relaxation of the article when all external constraints are removed[4]. Although such residual stresses tend to exist unnoticed, they are as real as any stress arising from applied loads or service conditions. Residual stresses are thus very common and can arise from various sources, such as transient temperature gradients, non uniform plastic deformation, or property changes arising from fabrication or heat treatment operations. They can arise from virtually every fabrication process[5,6], for example: casting[7], rolling[7,8], forming[7], stamping[7], drawing[4,9,10], extrusion[7], machining[6,7,11], or welding[7,12,13]. These locked-in stresses consist of a configuration of tensile and compressive stresses which are necessarily in equilibrium, and are independent of any applied loads or stresses. Although their presence in components and structures has long been recognised[7,10,14-17], it is only in the past few decades that emphasis been placed on their significance which has consequently led to the need for accurate quantification[2-6,11-13,18-69].

Residual stresses can have a marked influence on the behaviour of components in service. For example the stress-corrosion sensitivity[5,6,56], fatigue[5,6,62,63], and fracture toughness[70] properties can all be influenced by the magnitude and direction of residual stresses and hence they can have a significant impact on safety and reliability. Once present in a product, or component, residual stress can only be removed, and then usually only partially, by special forms of post-processing, such as stretching[8,71], vibration[71,72], annealing[7,8,71] or other forms of heat treatment[64,71] - eg. post weld heat treatment (PWHT). When the presence of residual stress is ignored, or when stress-relief is not feasible, the residual stress ordinarily remains in the product or component,

except for some possible shakedown in service, and may subsequently interact with the applied stresses. Therefore the risk of failure arising from the presence of residual stresses is a major source of concern in design.

Residual stresses do not necessarily have an adverse affect on a component. They may either have a favourable or unfavourable effect as seen from the engineering point of view. They are generally harmful if they act in the same direction as the critical applied stress, as in the case of the American "Liberty Bell"[7], which will be discussed shortly. On the other hand, they can be beneficial if acting in the opposite direction to the local applied stress, as in the case of carburised gear teeth. This superposition of local residual stress in both an adverse and beneficial situation is illustrated in Fig 1.1[8].

Adverse effects of residual stress may include increased susceptibility to fast fracture, particularly due to stress corrosion cracking and fatigue, resulting in premature failure. It has been noted that fatigue frequently begins on the surface of structural parts due to the presence of high residual stresses. In such cases the subtle role played by residual stress often goes completely unnoticed.

An example of the destructive power of residual stresses is evident in the American "Liberty Bell"[7]. When cast, the inner surface cooled first, and as the outer surface tried to shrink, the contraction was prevented by the already rigid inner portion. Therefore the outer surface was left in a state of residual tensile stress. After many years of service, including cyclic loading due to the clapper, a crack appeared in the lip of the bell. The crack continued to grow, despite some attempts at repair, and continued even after the bell was retired from service due to a loss in acoustic properties. This example is one of the earliest documented cases of the deleterious effects of residual stresses.

Since the most common mode of failure arises as a result of tensile stress application, the usual practice is to induce

residual compressive stresses particularly in the surface areas of components which are normally subjected to high tensile service stresses or wear rates. Examples of such practice are not hard to find: carburised gear teeth[7,8], shot-peened machine parts[58,59], prestressed concrete[7] and autofrettaged gun barrels[7], are examples of this beneficial use of residual stress.

Another example is that of so called toughened "safety glass". The glass is heated until it is soft, it is then cooled rapidly by blowing cold air on its surfaces (accounting for the periodic spotted appearance of car windows when seen through polarised dark glasses). The outside cools and hardens first but as the inside attempts to cool and contract, it is restrained by the rigid outer surface. The resulting residual stress distribution is that of an inner tensile stress, and an outer compressive stress, as illustrated in Fig 1.2. The toughened glass can withstand greater impact and tolerates minor surface cracks, but if the inner core is cracked the glass shatters into small numerous nominally "harmless" pieces.

1.2 Formation of Residual Stresses

As mentioned previously, residual stresses may arise from a variety of processes such as the following[8,12], which are discussed below:

i. Transient temperature gradients

ii. Non-uniform plastic deformation

iii. Property changes arising from heat treatment operations, and indeed almost all other manufacturing processes.

1.2.1 Transient Temperature Gradients

An example of this case of residual stress formation arises from the welding process[12,13]. Residual stresses are induced in the local welding area, since in this area the metal is momentarily molten. Upon cooling it is restrained by the surrounding cooler metal while contracting. As a result the hotter material goes

into a state of localised tension and the cooler metal into a state of local compression. The resulting stress distribution of a typical weld run is shown in Fig 1.3[12].

A further example is that of the non-uniform cooling of an ingot, as shown in Fig 1.4[8]. The ingot is initially at a high temperature and stress free (a). As the outside of the ingot cools, it contracts (b). The centre of the ingot is still hot and thus opposes the contraction of the outer material. This results in a compressive stress in the centre and a tensile stress in the outer material. The yield strength of the centre is low since it is hot, and therefore readily contracts plastically, following the colder outer material. As cooling continues (c), the centre contracts thermally and no longer plastically. Eventually the entire body reaches a uniform temperature. Since the centre had previously shrunk plastically, its total thermal plus plastic contraction exceeds that of the outer material. The differential contraction is opposed by the outer material so that, finally, a tensile stress develops in the centre and a compressive stress in the outer material (d).

1.2.2 Non-uniform Plastic Deformation

Essentially all cold working operations on metals (except perhaps simple stretching) may cause non-uniform plastic deformation. Therefore almost all worked members have in them residual stresses unless they have been subsequently removed by special processes such as heat treatments[8]. An elastic-plastic stress distribution is caused by yielding due to applied manufacturing loads. After processing the component will partially return to its original state, except for the permanent state of strain induced during the plastic deformation.

An interesting example is the rolling of a metal strip[8]. If small rolls are used and small reductions per pass are made, then surface working is favoured. Here the surface stresses are compressive and the inner tensile, since the surface metal wants to elongate more than the relatively rigid inner core will allow. This can be seen in Fig 1.5(a). If large rolls are used,

however, and large reductions are made, then the centre is worked more and results in the opposite stress distribution, to that previously described. This is because a lagging zone borders the rolls causing the centre to deform more than the surface. This is illustrated in Fig 1.5(b).

1.2.3 Property Changes Arising from Heat Treatment Operations

One of the most common commercial thermal operations is the rapid cooling (quenching) of steel. Normally materials contract on cooling and the residual stress pattern that develops is similar to that described for the cooling ingot case discussed previously. Steel, in addition, undergoes a phase change from face-centred cubic austenite to body-centred cubic ferrite while cooling. Because ferrite is less dense than austenite, the metal expands rather than contracts in the temperature range of the phase change during cooling[8]. If the steel has a low concentration of alloying elements, the phase change occurs at such a high temperature that it does not influence the residual stress pattern. Certain alloying elements such as nickel cause the phase change to occur at lower temperatures. As a result the residual stress pattern in a nickel-free steel and one containing 16.9% nickel are essentially opposite each other, as can be seen in Fig 1.6[8].

A similar process is that of the rapid quenching of steel to form martensite[73]. If a 0.8% Carbon steel (which is a eutectoid steel) is allowed to cool slowly from a temperature of 723°C or higher, then pearlite is formed, which consists of a stable body centred cubic ferrite and cementite. On the other hand, if the steel is rapidly quenched, the iron atoms transform to body centred cubic martensite so rapidly that the carbon atoms are "frozen" in place and remain in their original positions. Under normal conditions body centred cubic iron can only dissolve 0.035% carbon, therefore the martensite is heavily oversaturated with carbon and something must give. The carbon atoms make room for themselves by stretching the lattice along one of the cube directions to form a body centered tetragonal unit cell, causing the structure to be highly strained.

Martensite grains can therefore be seen to be larger than pearlite grains and resultantly would induce residual stresses when formed.

1.3 Project Motivation

It is thus clearly evident that residual stresses are important in engineering applications and there is a need to quantify them accurately and with confidence. Engineers need to be able to determine the magnitudes, directions and effects of these stresses so that failures can be avoided.

1.3.1 The Residual Stress Problem Experienced by Hulett Aluminium

A situation where residual stress was believed to play a role was in the apparent premature failure of high strength extruded aluminium tubes. These tubes were manufactured by Hulett Aluminium for use as drill rods in the mining industry for surface drilling exploration work[74]. The basic drill rod was extruded from a billet into a seamless tubular section, typically 2.5 m long, and subsequently straightened and heat treated (see Section 5.4.2 to follow). For service these drill rods were made up by manufacturing standard taper pipe threads on the inner diameter at both ends of the drill rods. Steel fittings were coupled to the ends of the drill rods, as shown in Fig 1.7, and tightened to a specified torque[74].

Alleged premature failures of some drill rods led to concern about their quality - but it was uncertain whether the failure arose from poor handling and usage by the drill team or whether there were more insiduous material manufacturing problems with the drill rods themselves. In an attempt to resolve this question, Hulett Aluminium wanted to ascertain whether the drill rods were indeed within specification and that the problems experienced by the customers were rather due to the latters' poor handling methods, rather than intrinsic manufacturing problems. They therefore conducted an investigation which consisted initially of conducting tests on the failed aluminium

drill rods[74,75]. The aim of the investigation was to show that the drill rods were within specification and that they compared to nominally identical Canadian drill rods.

Initially mechanical tests were conducted on the drill rods, namely: evaluation of the 0.2% proof stress, tensile strength and percentage elongation[74]. Chemical tests were then carried out so as to ascertain the chemical composition of the aluminium alloy, followed by a visual inspection. Next the microstructure was examined and finally linear elastic fracture toughness tests were carried out.

The results of the mechanical, chemical and fracture toughness tests showed that the rods were indeed within specification[74]. Microstructural tests indicated that there were no unusual inclusions or phases in the material that may have been detrimental to the rods' properties[74] or performance. However examination under a scanning electron microscope revealed some limited evidence of environmentally assisted fatigue cracking[74]. The visual inspection indicated that fracture had generally occurred transversely through the rod wall at the "first engaged" thread of the steel coupling and that the machined threads did not correspond to those of the Canadian rods[74]. Indeed the machined threads gave rise to a higher stress concentration factor than those in the Canadian rods[74]. The last of the tests, linear elastic fracture toughness tests[75], showed that the linear elastic fracture toughness (K_{IC}) of the rods produced by Hulett Aluminium was approximately the same as that of the Canadian rods, within the limits of scatter.

It was thus concluded that the rods could possibly have failed due to the high stress concentration factor of the sharply machined threads and that crack growth was caused by environmentally assisted fatigue cracking. The question that needed to be answered was... what had initiated crack growth? There were two possible suggestions: (i) the over-torque of the steel fittings, which was a problem that had been known to occur in the field, and (ii) the presence of residual

stress[76]. It was decided by Hulett Aluminium to have tests conducted by the Department of Mechanical Engineering at the University of Cape Town in order to measure any residual stress in the rods so that it could be determined whether this was indeed a contributory cause of failure. It was agreed that this work would form part of the author's masters programme.

1.3.2 Residual Stress Measurement Techniques

As can be reasoned thus far, there is a need to determine residual stress in components and structures. Since it is extremely difficult to calculate residual stress by analytical methods[52], an effective residual stress measurement technique was sought. There are many available[1-3,8,12,14,15,20,29,65], however, each with their own characteristic advantages and disadvantages. Since Hulett Aluminium had requested that work be carried out in this field, the author conducted research in order to determine which residual stress technique would best suit the problem at hand as well as any future related problems.

The air abrasive centre hole drilling technique was chosen as the main method of residual stress measurement. For convenience, in the rest of this thesis, air abrasive centre hole will be abbreviated to AACH. A ring splitting technique was also chosen so that a quick and easy shop floor technique could be compared to the more reliable AACH drilling approach. The principle of the AACH drilling device design given in this thesis is similar to that created by Beaney and Procter[1-3], which although commercially available is expensive. The design attempts to create a less expensive model where most of the components are manufactured locally with the exception of a few key components obtained from Procter in the United Kingdom.

1.4 Thesis Content and Structure

This thesis involves the design, construction and development of an AACH drilling device for use in residual stress measurement. It also involves the calibration and utilisation of the device as well as the ring splitting technique in order to determine

the residual stress distribution in high strength extruded aluminium rods manufactured by Hulett Aluminium.

The thesis begins by giving information and background on residual stress. Various residual stress measurement techniques are then outlined, followed by the theory of the chosen residual stress measurement techniques. Next the design of the AACH drilling device is presented. Experimental details - which included calibration, specimen identification and the test programme follow; after which the results, discussion, conclusions and recommendations conclude the main text of the document.

1.5 Thesis Objectives

The objectives of the thesis are the following:

i. To review the residual stress measurement techniques available.

ii. To design and construct a working prototype of an AACH drilling device for residual stress measurement.

iii. To calibrate the AACH drilling device.

iv. To use the AACH drilling device in the measurement of the residual stresses, both in magnitude and distribution, in high strength aluminium tubes.

v. To use the ring splitting technique as an approximate but easy comparative measurement of the hoop residual stresses.

vi. To attempt to draw interpretations from the results and thus make recommendations where necessary.

1.6 Summary

In this introductory chapter the following information has been given: background to residual stresses, formation of residual stresses and motivation for the thesis. In the next chapter various residual stress measuring techniques are examined so that a reliable technique can be chosen in order to perform

accurate residual stress measurements in extruded aluminium tubes.

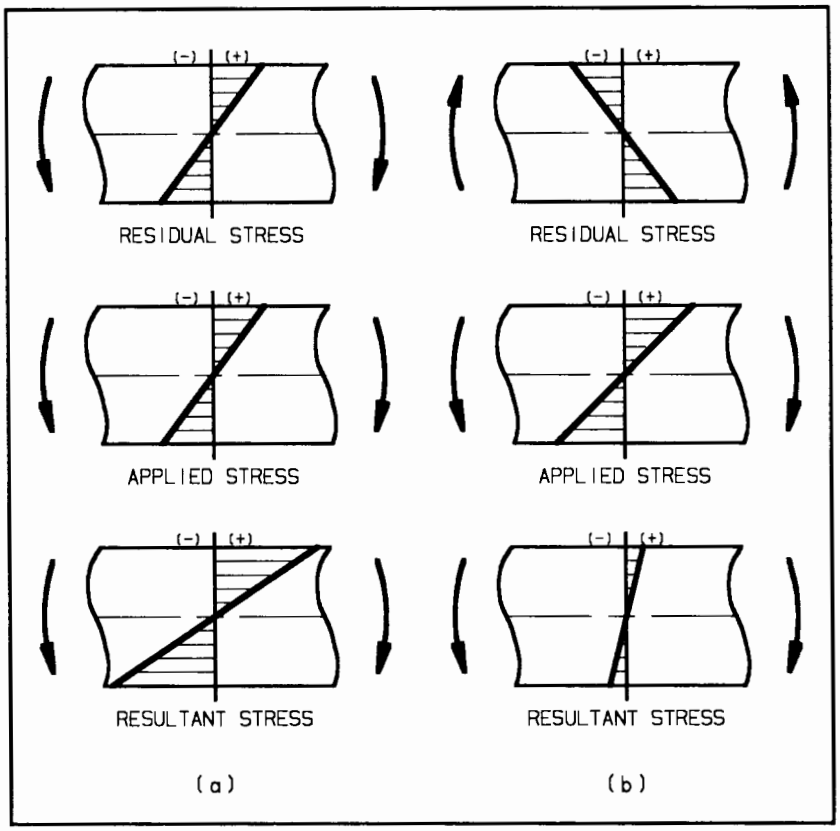

Fig 1.1 - Adverse (a) and beneficial (b) effects of residual stress. The applied stress field is superimposed on the residual stress field to create a resultant stress as illustrated.

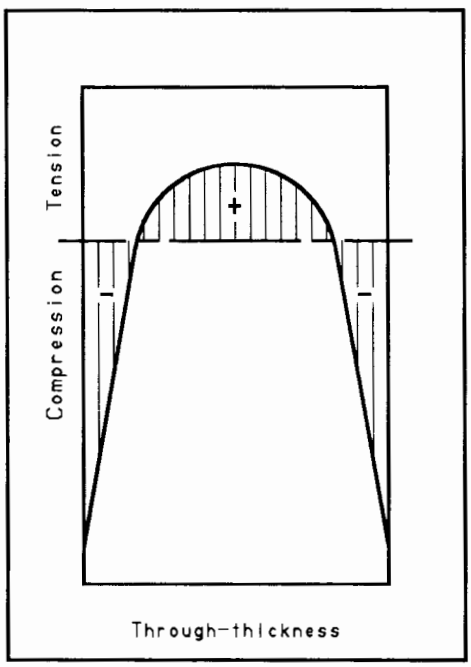

Fig 1.2 - Thermal toughening of glass, where the outer skin is put into a state of compression, thus resisting crack initiation.

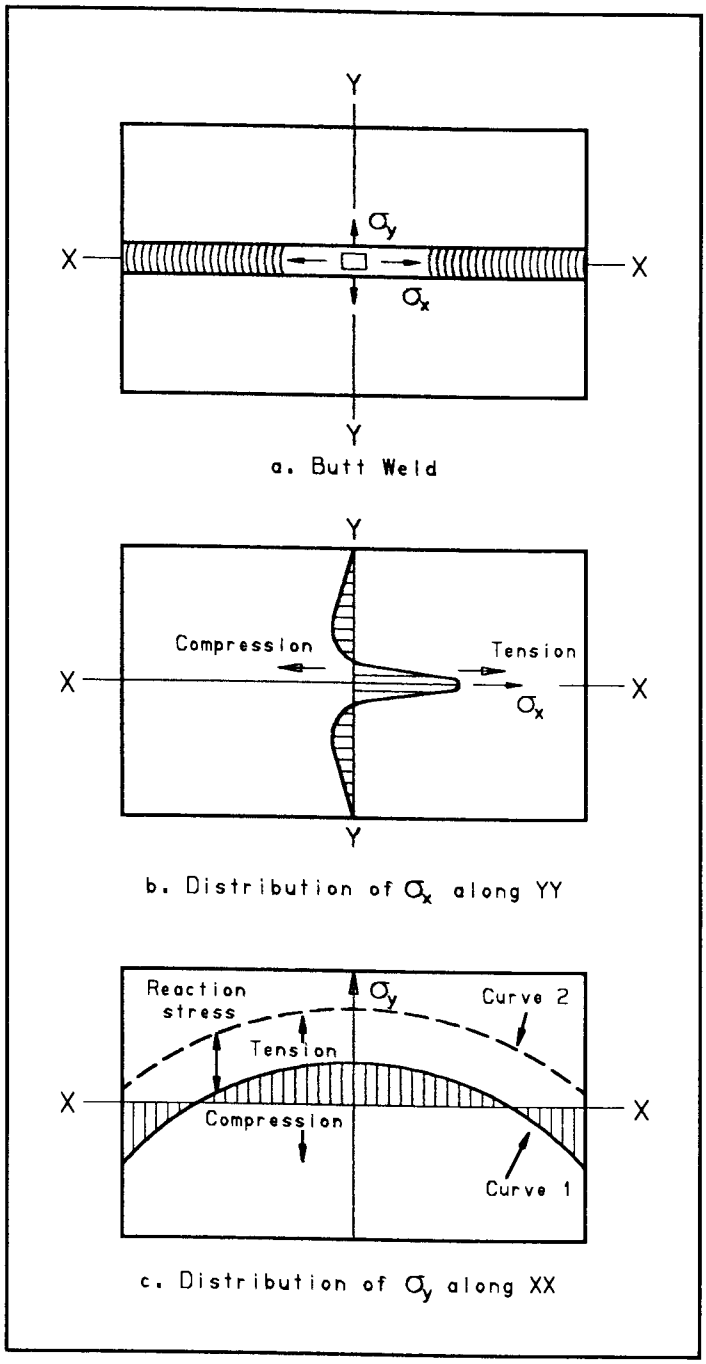

Fig 1.3 - Typical distribution of residual stress in a butt weld. The material furthest from the weld cools first and as a result prevents the inner material from contracting upon cooling. This gives rise to the stress pattern shown.

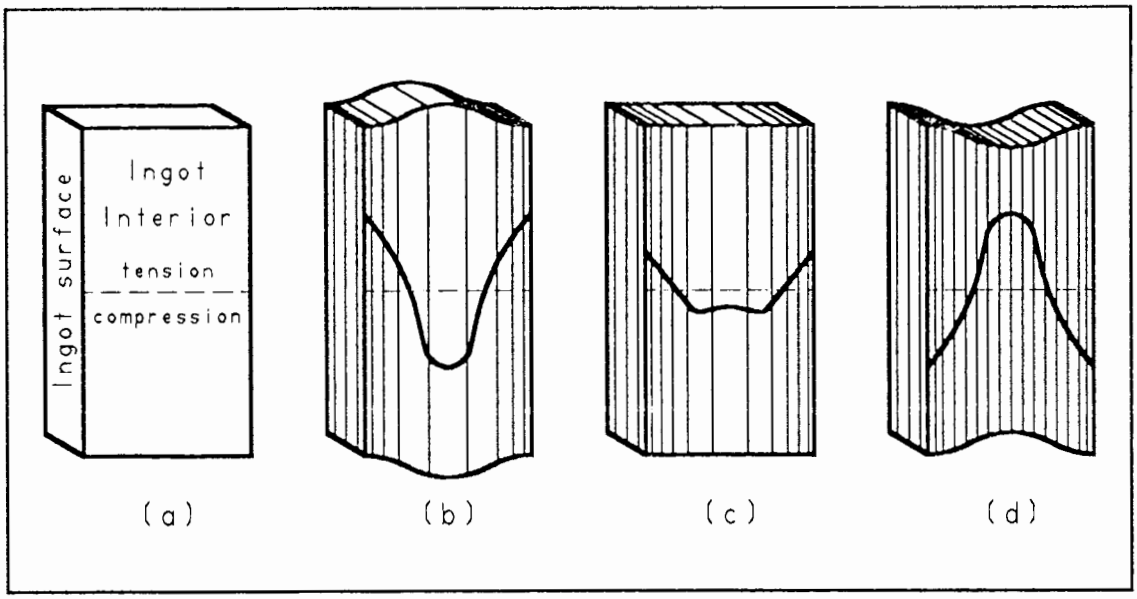

Fig 1.4 - Stresses resulting from differential expansion and contraction in non-uniform cooling. The ingot is initially at an elevated temperature (a) and stress free. As the outside cools, it contracts (b). The centre is however still hot and opposes contraction. Its yield strength is low (since it is hot) and therefore contracts plastically, following the colder and therefore harder outer material. As cooling continues (c), the centre which had flowed plastically continues to contract thermally. Eventually the entire ingot reaches a uniform temperature (d). Since the centre had prevously shrunk plastically, its total thermal plus plastic contraction exceeds that of the outer material. The differential contraction is opposed by the outer material, resulting in the stress pattern shown.

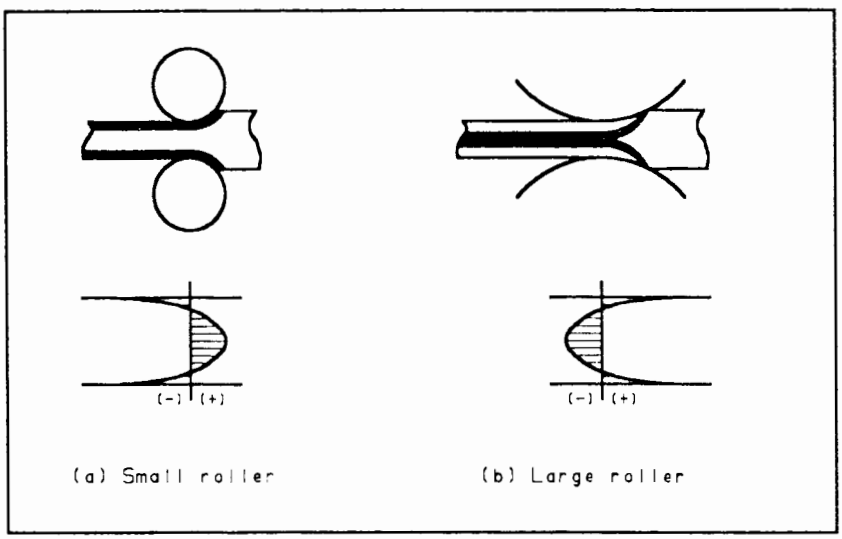

Fig 1.5 - Residual stresses in rolling. When using small rolls (a), surface working is favoured. As a result the surface metal wants to elongate more than the relatively rigid core which creates the stress pattern shown. When using larger rolls (b), the centre is worked more and an opposite stress distribution results.

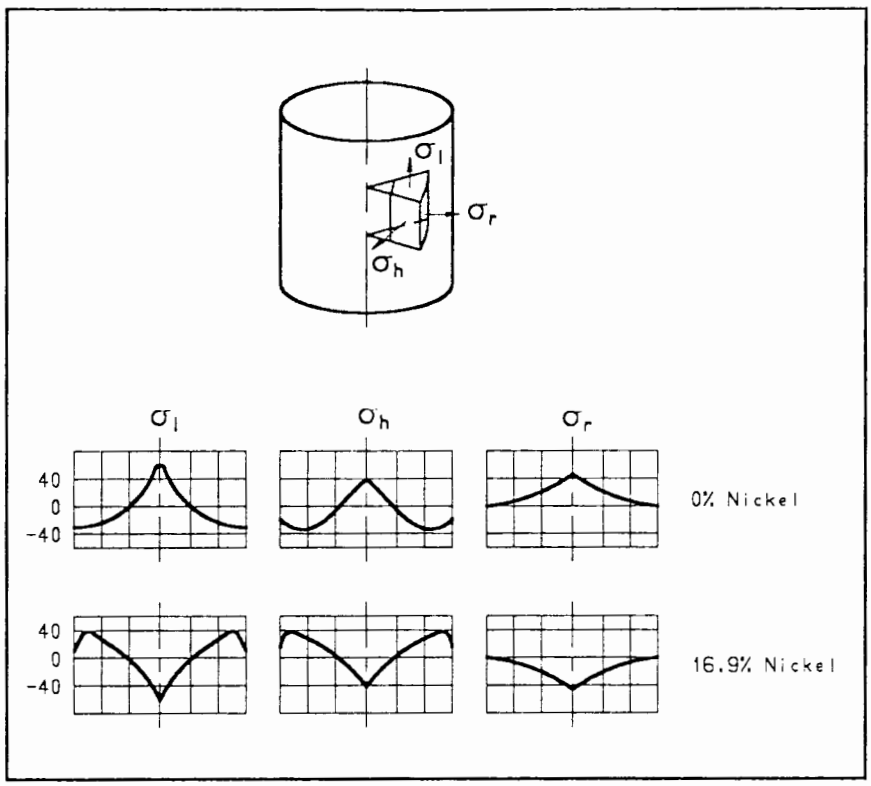

Fig 1.6 - Comparison of residual streses in water quenched bars - (a) nickel free and (b) 16.9% nickel steel. Normally materials contract upon cooling and a residual stress pattern varying from compression on the surface to tensile in the centre results. However steel also undergoes a phase change from austenite to ferrite and thus expands while cooling since ferrite is less dense than austenite. If the steel has a low concentration of alloying elements, this phase change occurs at such a high temperature that it does not influence the residual stress pattern; whereas certain alloying elements such as nickel cause the phase change to occur at lower temperatures and an opposite stress pattern to result.

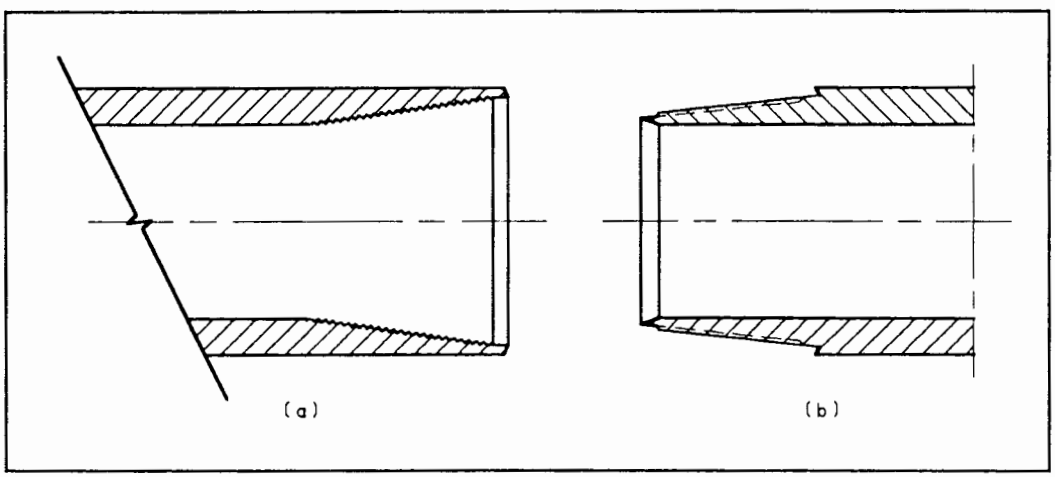

Fig 1.7 - Drill rod taper (a) and steel coupling (b) used to make a composite drill rod of the required length.

2. RESIDUAL STRESS MEASUREMENT TECHNIQUES

2.1 Introduction

In order to assess the potential effects of residual stress, a means of measuring them is required. Ideally this technique should be simple, accurate, reliable, inexpensive, portable and non-destructive. In the following sections, various techniques are discussed and assessed.

The presently available techniques can be classified into four groups. They are the following:

i. Diffraction techniques
ii. Stress sensitive techniques
iii. Cracking techniques
iv. Stress relaxation techniques

2.2 Diffraction Techniques

The techniques discussed in this section are:

i. X-ray diffraction
ii. Neutron diffraction

2.2.1 X-ray Diffraction

X-ray diffraction is one of the best known non-destructive techniques of residual stress measurement. This method is a modification of the well known principle of x-ray diffraction, in which constructive interference from the lattice planes in a crystal structure, results in a peak intensity of x-rays at certain diffraction angles (θ_x)[19] or scattering angle $(2\theta_x)$[77]. According to Bragg's law, this occurs when $\lambda = 2d_L.Sin(\theta_x)$, where d_L is the lattice spacing and λ is the characteristic x-ray wavelength[77] - see Fig 2.1[19]. The popularity of the technique stems from the relative ease with which the change in spacing of atomic planes can be measured

from the shifts of Bragg peaks in the diffraction pattern[19,41,48,77]. The atomic plane spacing may be considered as internal built-in strain gauges whose spacing is dependent on the local stress condition. This is illustrated in Fig 2.2 where it is shown that for material with its surface in compression, a change in the angle of tilt (ψ) results in a smaller value of lattice spacing (d_L) and subsequently the peak intensity occurs at a larger value of $2\theta_x$[19,77]. Stress is measured in the direction where the circle of tilt and specimen surface intersect, as illustrated in Fig 2.2(c)[77].

The relationship between stress and the change in interplanar spacing is written in terms of the stresses in the axial system of a specimen[77]. In other words, measurements made of interplanar spacing (d_L) along the normal to the diffracting planes L_3 (see Fig 2.3) are linked to the stresses in the specimen coordinate system W[77].

Stresses can be classified as either macroscopic or microscopic. Macroscopic stresses refer to those stresses arising from the movement of one macroscopic part of a body relative to another. Examples include machining and shot peening when regions near the surface are elongated plastically with respect to the bulk. Microscopic stresses refer to stresses arising from the differential deformation of a microscopic region (eg. a grain or second phase particle) compared to the rest of the material.

If it is assumed that there are only macroscopic stresses present in a material, it is implied that the stresses are constant under the beam being diffracted and that there are no stresses normal to the surface. The required residual stress equations for this case are written as follows[77]:

$$\frac{d_{\phi\psi} - d_o}{d_o} = \frac{S_2}{2} \sigma_\phi \sin^2\psi - S_1 (\sigma_{11} - \sigma_{22})$$

where: $d_{\phi\psi}$ = interplanar spacing measured when the specimen or incident beam is tilted by ψ - see Fig 2.3.

d_o = unstressed interplanar spacing.

ψ = angle of tilt of the incident beam with respect to the specimen.

σ_ϕ = stress in the ϕ direction - see Fig 2.3.

σ_{11} = stress in the W_1 direction.

σ_{22} = stress in the W_2 direction.

S_i = x-ray elastic constants.

The spacing (d_L) is linear versus $\sin^2\psi$, as illustrated in Fig 2.4(a), and the stresses can be obtained in the ϕ direction by tilting the specimen or incident beam by ψ and measuring d_L at each tilt[48,77]. The unstressed lattice parameter d_o is not necessary here and can be replaced by the stressed value[77].

If however, microstresses are required to be measured, then the process is not quite as straight forward, and so called ψ splitting occurs for positive and negative ψ - see Fig 2.4(b)[48,77]. Stresses normal to the surface cannot be assumed to be zero and the unstressed lattice parameter (d_o) is required[77]. Thought is required to be given to the measurement of d_o, since there is as yet no general method[77]. Fortunately considerable information can be obtained even without the d_o value, if hydrostatic and deviatoric stress components are considered[77].

Other possible results of d_L versus $\sin^2\psi$ are shown in Figs 2.4(c) and (d)[48,77]. These arise due to plastic or elastic stress inhomogeneity and differences between the tilt and diffractometer axis.

There are two practical methods of x-ray residual stress measurement which are employed:[77,78]

i. The diffractor method - This method has been referred to in the discussion so far. Accurate alignment is necessary here since specimen shifts as ψ varies can lead to large displacements of the measured peak. The disadvantages of this method are that the required diffractometers are generally not portable and the

regarded as a qualitative technique[12,82].

2.5.2 The Sach's Boring Out Technique

This method is only suitable for circular rods, large solid cylinders and thick walled tubes. In this method the specimen is first accurately mounted in a lathe[4,8,12,14,15] and a hole is then drilled up the centre if required. Thin annular layers of material are then successively removed from either the inner or outer surface. The initial dimensions are measured accurately and they are remeasured after each step in the machining process. From these measurements the residual stresses can be obtained.

The disadvantages of this method, other than its limited use are:

i. Specimens are assumed to have a uniform stress in the circumferential direction.

ii. The results are averaged over the direction in which the stress is measured.

iii. Residual stresses may well be induced due to the boring operation.

iv. It is a destructive technique.

2.5.3 The Successive Milling Technique

If for example material is milled away from one side of a bar shaped body containing tensile residual stresses at its surface and compressive residual stresses in the interior , the bar will bend away from the milled side, as shown in Fig 2.8[10,12]. Using strain gauges on the side opposite to the milled side, it is possible to measure the change in length of the side each time a layer of material is removed. The residual stresses in the different layers can be calculated from these measurements[12].

Although this is a reasonably reliable technique for measuring

the mean stress over a relatively large surface, only the mean uniaxial stresses are measured. Also there is a high risk of inducing residual stresses by the milling operation, the method is completely destructive, and is not portable.

2.5.4 The Trepanning or Ring Core Technique

In the trepanning or ring core technique, an annulus (i.e. trepan) is machined into a structure wall to isolate the surface of an island which is formed[38,39,78], as illustrated in Fig 2.9[39]. Relaxed strains which occur on the island are measured with a strain gauge rosette and the associated stresses and their directions are calculated from conventional elastic theory[78].

The disadvantages of this method are the following:

i. Mechanical machining of the island induces machining stresses which may seriously affect the results obtained. Air-abrasion, a nominally stress free drilling technique has been used but it is extremely slow[78].

ii. The minimum depth of the trepan required for full relaxation is approximately 1.2 times the island diameter. This would result in a typical depth of at least 12 mm, or greater, depending on the strain gauge rosette used, and this depth is too great for general use. Part depth trepanning has been used, but errors can be significant[78].

2.5.5 The Ring Splitting and Tongue Techniques

These techniques are suited to thin tubes. The ring splitting technique, may be used to determine circumferential/hoop stresses[4,8,14,15]. In order to perform this technique, a specimen is first cut from a tube and its outside diameter (in a plane perpendicular to an intended longitudinal cut) and thickness are measured. It is then slit longitudinally at one point. Next, either the change in diameter perpendicular to the plane of the cut or the distance between two previously scribed

lines on either side of the proposed cut is measured. From the measurement of change in diameter, the residual hoop stress can be calculated. A schematic of the process can be seen in Fig 2.10[8,10,14,15,83]. Stresses are assumed to vary linearly through the thickness of a specimen and to be constant on each circumferential plane[8]. In addition, they are also assumed to be unbalanced over the wall section, since only unbalanced forces between opposite walls will cause bending when a tube is slit[8].

The tongue technique may be used to determine longitudinal stresses. The method can be carried out in two similar ways:

i. A saw cut is made across the diameter of the tube, and the change in diameter is measured, as shown in Fig 2.11(a)[83].

ii. A tongue is cut parallel to the axis of the tube and the tip deflection is measured, as shown in Fig 2.11(b)[83].

The disadvantages of these methods are the following[8,14,15]:

i. They are destructive.

ii. The results are averaged over the length of the slit.

iii. Residual stresses may be induced by the cutting operation.

iv. Except for the cases where the residual stress distribution is uniform, the accuracy of these methods is low.

However the methods have the advantage of being quick and relatively simple and would be well suited to a production line operation if the inaccuracies could be tolerated.

2.5.6 The Deep Hole Drilling Technique

The deep hole drilling technique provides a full distribution of the three principal stresses in materials of up to about 0.25 metres thick[78]. All the information required is derived from a

3.2 mm hole, which is drilled through the thickness of the specimen, as shown in Fig 2.12(a). The hole must be measured every 2 mm of depth on 0, 45 and 90 degree axes, as shown in Fig 2.12(b). Using preferably stress free machining, a 10 mm diameter cylinder is then cored out, as shown in Fig 2.12(c). This relaxes the residual stresses acting on the 3.2 mm hole and consequently the hole changes shape. During the coring out procedure, the change in axial length should be measured continuously. After coring out, the hole is remeasured as before, as shown in Fig 2.12(d). From the measurements made, the three principal stresses and their directions can be determined[20].

While this technique allows the three principal stresses to be analysed completely, it is time consuming and it leaves a hole in a structure of about 20 mm in diameter.

2.5.7 The Crack Compliance Technique

The crack compliance technique involves the introduction of a crack with progressively increasing depth into a specimen, in order to release the residual stresses along the plane of the crack[84]. In practice, however, a crack is not easy to control so a slit of finite width is introduced using milling, electric discharge machining or electric discharge wire machining with wire as small as 25 μm diameter[84].

It uses the theory that the stresses and strains due to the introduction of a crack may be obtained by applying the existing stresses on the plane of the crack in the uncracked body, with sign reversed, to the faces of the crack[84]. This is demonstrated in Fig 2.13. Fig 2.13(a) shows an uncracked specimen containing residual stresses. In Fig 2.13(b) the introduction of a crack results in the production of strains and displacements. The addition of the crack closing stresses, Fig 2.13(c), to Fig 2.13(b) restores the configuration to the initial stress state shown in Fig 2.13(a). The case used for measurement is as shown in Fig 2.13(b). The stress distribution shown in Fig 2.13(c) can be found by placing strain gauges in

the vicinity of the crack, and consequently the residual stress distribution can be found[84].

This technique of residual stress measurement has been shown to compare well to x-ray methods and certain analytical computations[84]. It also has the advantage of being able to perform residual stress measurements in "difficult" areas and/or rapidly varying residual stress fields, such as at the toe of a fillet weld, where other methods are not well suited.

The main disadvantages of this technique are that cracks or slits are introduced into specimens or structures which may be difficult to remove[84]. Furthermore, the residual stress distribution can be affected by the choice of machining method used to cut the slit.

2.5.8 Centre Hole Drilling Techniques

The centre-hole drilling techniques are probably the most useful and widespread methods of surface residual stress measurement[26,43,57]. It can be used for laboratory and field work - on horizontal, vertical and overhead surfaces. A blind hole of approximately 1.4 mm to 2.0 mm depth and diameter is drilled into a specimen, in the centre of a three element strain gauge rosette[1-3,23,44,51,54,55,60,78], as illustrated in Fig 2.14(a)[23]. Since the hole can carry no stresses, its production in the stressed material causes a redistribution of strains to occur near the hole which can be detected by the strain gauges[2,3,26,51,53-55,60]. When the method was first developed by Mathar in 1934[16], extensometers were used. However, they proved to be inaccurate[17,24], and were replaced by bonded foil strain gauges once these were developed. Soete and Vancrombrugge[24] were the first researchers to use electrical resistance strain gauges[85], and subsequent researchers have also favoured them due to their many advantages - particularly accuracy if correctly used.

Even though this method can only really measure surface stresses, reasonable results on stresses varying with depth can

be obtained, by monitoring the change in strain as the hole is produced[17,25,26,67], or with the aid of finite element methods[26,27,29,31]. Furthermore, intelligent estimates can be made of stresses deeper in the material in this way. Varying surface stress fields can also be measured with the centre hole technique, as proposed by Kabiri[55], and Lu and Flavenot[25].

An important factor when using this technique is that the drilled hole must be "vertically" sided[3], unless the technique proposed by Tootoonian and Schajer[65] is used, where an inverse taper hole is drilled, as shown in Fig 2.14(b). By vertically sided it is meant that the hole walls should be parallel to the axis of the hole and perpendicular to the surface of the specimen being tested. Once the hole has been drilled, the principal residual stresses and their directions can be calculated from the relaxed strains[1-3,65]. When drilling inverse taper holes, different equation constants need to be used to the so called "conventional" method where vertically sided holes are required to be produced. Tootoonian and Schajer[65] recently proposed this modified hole drilling method, since more residual stress and strain can be relieved from a hole of this type than a hole drilled by conventional methods, thus increasing the sensitivity of the centre hole drilling technique. It must be noted that this taper hole method must be used with care, since the drilling process may induce plastic strains at the periphery of the hole, which can influence the measured results.

If the conventional hole drilling technique is used correctly, accuracy of around 8% can be achieved[3]. This technique is regarded as "semi-destructive"[23], since only a small hole is made, which can usually be tolerated, ground away or plugged[7]. Its disadvantage is that only partial relaxation is detected by the strain gauges. Therefore any errors in strain measurement and/or hole forming, can have significant effects on the accuracy of the predicted stress[2,65].

The hole may be drilled in a number of ways:

i. Low speed end mill - A hole is drilled with the aid of a hand drill and using a specially made cutter[23,38]. However this technique can result in high machining induced residual stresses[3,42-44].

ii. High speed drill - A drill bit is specially machined so that a cylindrically shaped hole can be drilled. The drill is usually powered by a high speed air turbine[40]. While this technique also induces residual stresses[3,43,44], they are lower than those produced using the end mill[42,43], especially if high speeds are maintained and cuts are small. Other problems are that the technique cannot be used reliably on hard materials[3,43], and once drilling starts, the rated speed of the turbine drops significantly, due to cutting and frictional resistance.

iii. Spark erosion - Bush and Kromer[44] have shown that the technique is not a stress free process[3]. It is also not portable and can destroy the strain gauge rosette.

iv. Electro-chemical machining - This technique is not easy to use. It may also interfere with the strain gauge readings[78], and is not portable[3].

v. Air-abrasion - An orbiting, tilted and eccentrically mounted nozzle is used here. A mixture of air and fine abrasive powder exits the nozzle at high pressure, eroding the specimen surface and forming a hole[3,38]. By adjusting the nozzle offset and tilt, a vertically sided hole of given diameter can be drilled[3]. As mentioned previously, this technique can be regarded as relatively stress free, due to the low inertia of the abrasive particles and any heat created during the drilling operation is eliminated by the cool jet of air.

A slight variation of this technique is that of using holographic interferometry instead of strain gauge rosettes, to

detect relaxed strains[57,67]. A small blind hole is drilled in a specimen containing residual stresses, as before, and the resulting stress relief gives rise to a fringe pattern. This resulting fringe pattern is then analysed using a "fringe counting" method. This technique was developed to overcome certain drawbacks of the "conventional" techniques previously discussed, such as hole alignment and the need for a smooth surface onto which strain gauge rosettes are required to be bonded[57,67]. However this technique is generally suitable only for laboratory work and specimen size in general could also be a problem due to the need for a vibration-isolated optical table as a work surface.

2.6 Proposed Choice of Residual Stress Measuring Technique

As mentioned previously, to assess the potential effects of residual stress, a means of measuring them is required which ideally is simple, proven, accurate, reliable, inexpensive, portable and non-destructive. Taking this into account, the AACH drilling technique was chosen for this thesis. Although it is not cheap to purchase an AACH drilling device, almost all of it was able to be fabricated and constructed at a relatively low cost, as described in Chapter 4.

It was also decided to determine whether the ring splitting technique could be used as a quick and reliable, if somewhat coarse method, of determining residual stresses in extruded aluminium tube; and hence whether a production run was operating within permissible limits.

2.7 Summary

This chapter has reviewed the various residual stress measurement techniques available. Many of them are inappropriate or expensive, and some have questionable accuracy. For the purpose of this thesis the techniques chosen to perform residual stress measurements, amongst the many methods examined, are the AACH drilling technique and the ring splitting technique. The AACH drilling technique was chosen due its many advantages, the

main ones being that it is reliable, induces negligible machining stresses and is relatively easy to use; while the ring splitting technique was chosen due to its simplicity and ease of use, particularly on the shop floor.

Since these techniques are of importance in this thesis, the next chapter has been devoted to their detailed description as well as the relevant theory.

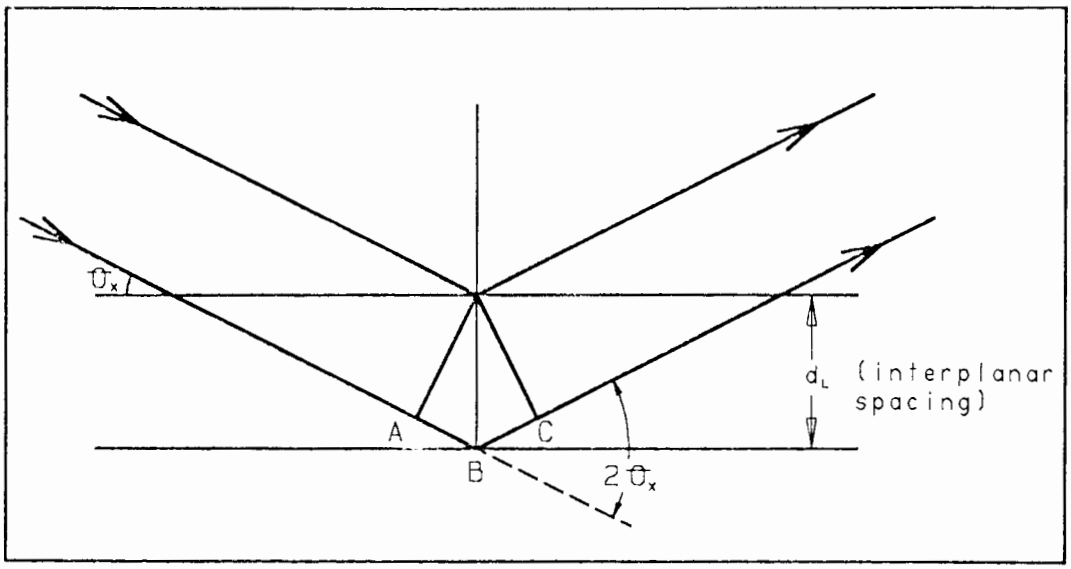

Fig 2.1 - Illustration of Bragg's law. For constructive inteference between diffracted x-ray beams (wavelength = λ), λ = AB + BC = $2d_L \cdot \sin(\theta_x)$.

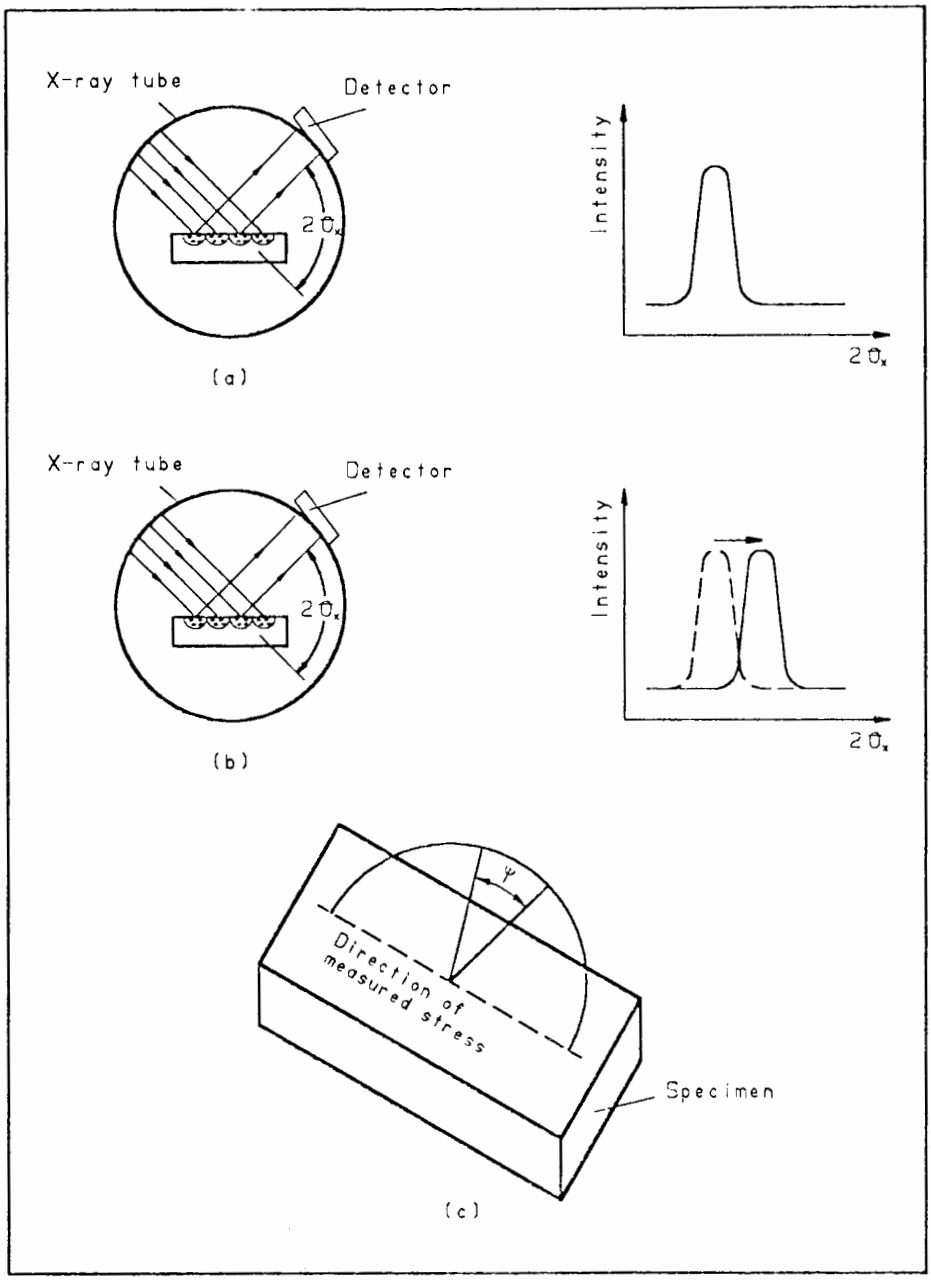

Fig 2.2 - Measurement of the effect of stress on lattice spacing d_L[77]. The incident beam diffracts rays of wavelength λ from planes parallel to the surface to satisfy Bragg's law (a). If the surface is in a state of compression, these planes are further apart than in the stress free state. Lattice spacing d_L is obtained from peak intensity versus scattering angle $2\theta_x$ and Bragg's law. After tilting (b), diffraction occurs from other grains (which are on the same planes) which in turn are closer spaced than in (a). The peak intensity therefore occurs at higher angles of $2\theta_x$. The stress is measured in a direction which is the intersection of the circle of tilt and the specimen surface (c).

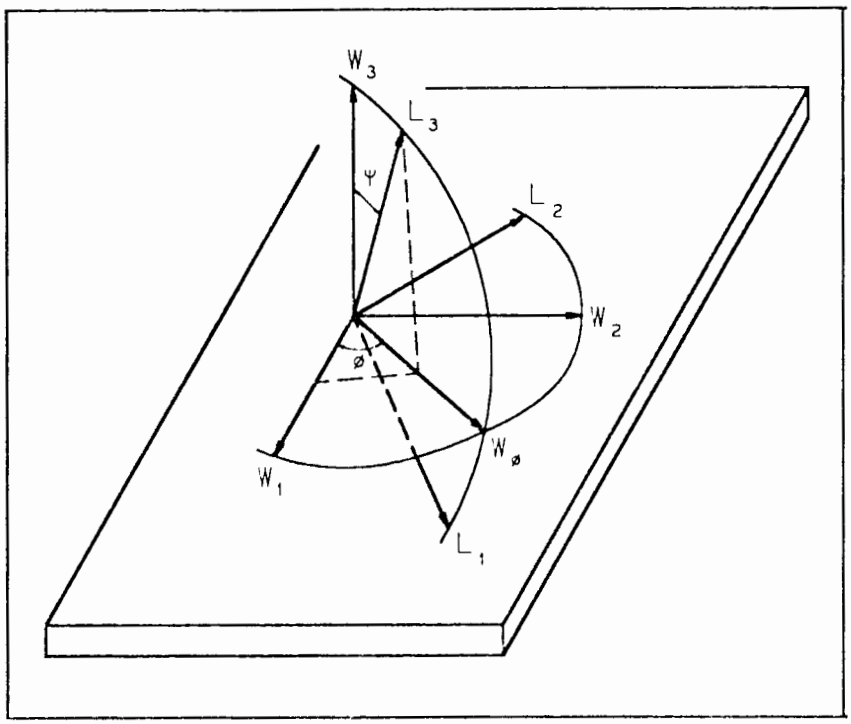

Fig 2.3 - The axial systems for the x-ray technique[77]. The W_i describe the sample, the L_i the measuring system. The lattice spacing (d) of planes perpendicular to L_3 are measured.

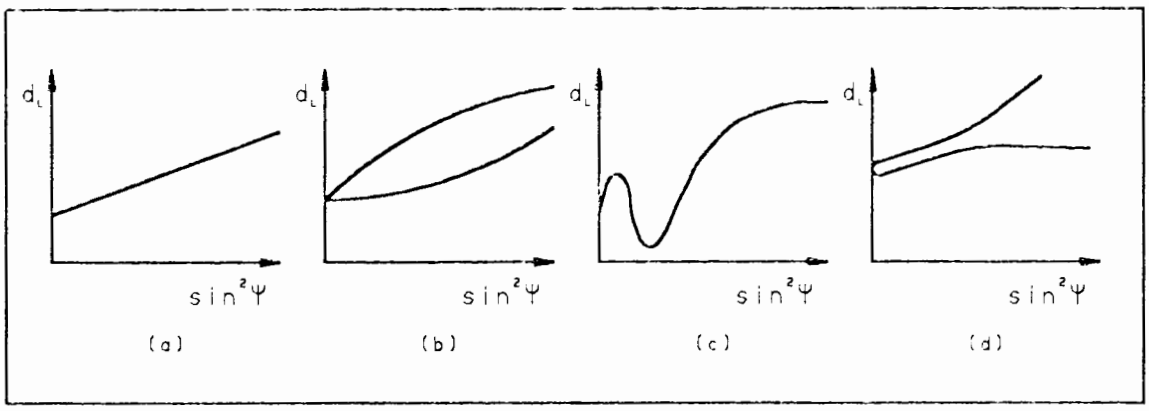

Fig 2.4 - Lattice spacing (d_L) versus $\sin^2\Psi$[77]. Graph (a) results from a biaxial stress state, graph (b) from Ψ splitting due to a triaxial stress system, graph (c) from oscillations due to plastic or elastic stress inhomogeneity, and graph (d) results if the tilt axis and diffractometer axis are not coincident.

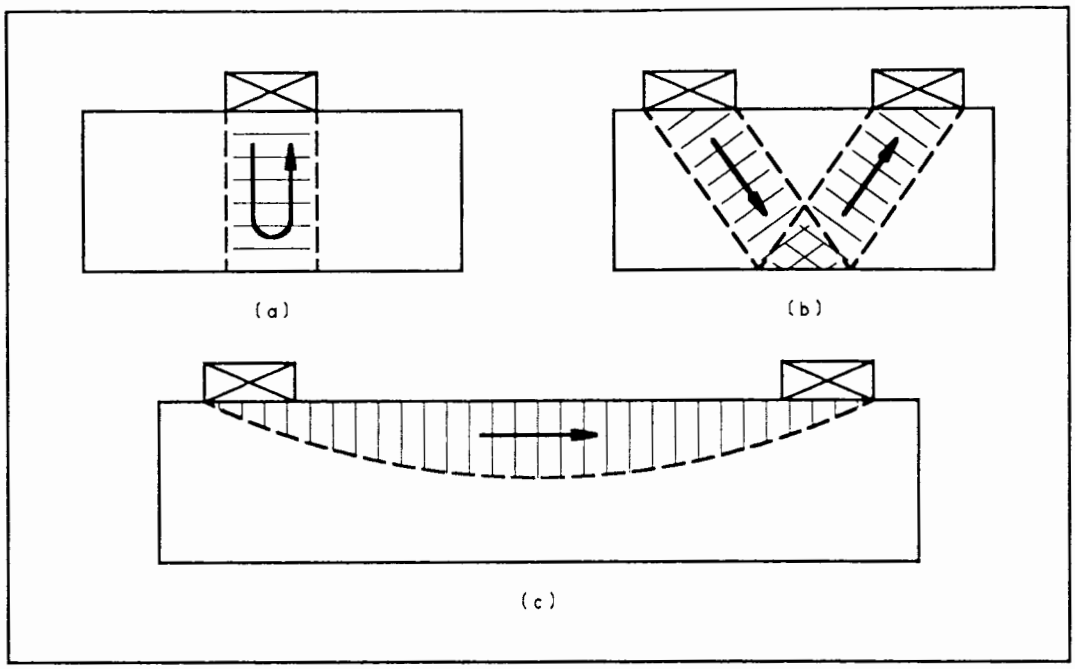

Fig 2.5 - Schematic view of accoustoelastic measurement configurations. The average stress is determined in the region through which the waves propagate, as indicated by the cross hatching[81].

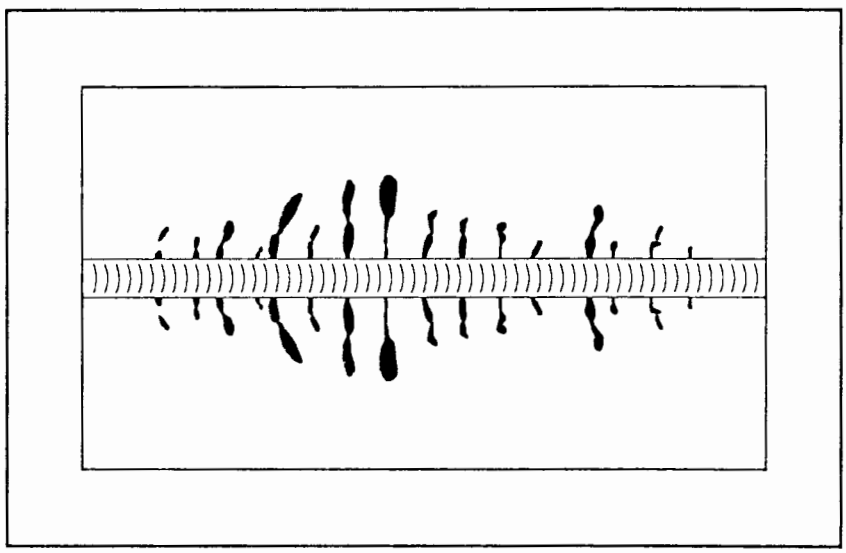

Fig 2.6 - Schematic of a hydrogen induced crack pattern in a simple butt joint. The pattern is produced by immersing specimens into an electrolyte and charging them with hydrogen by applying a d.c. current, using the specimen as the cathode and a set of lead strips as the anode. As can be seen, the hydrogen opens up bigger cracks in the middle which is consistent with Fig 1.3.

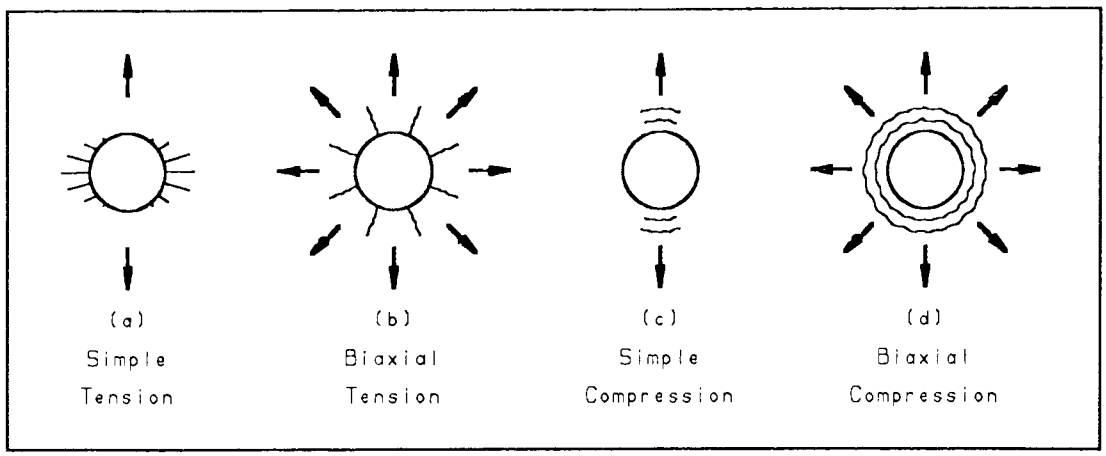

Fig 2.7 - Typical crack patterns obtained when using the brittle coating technique.

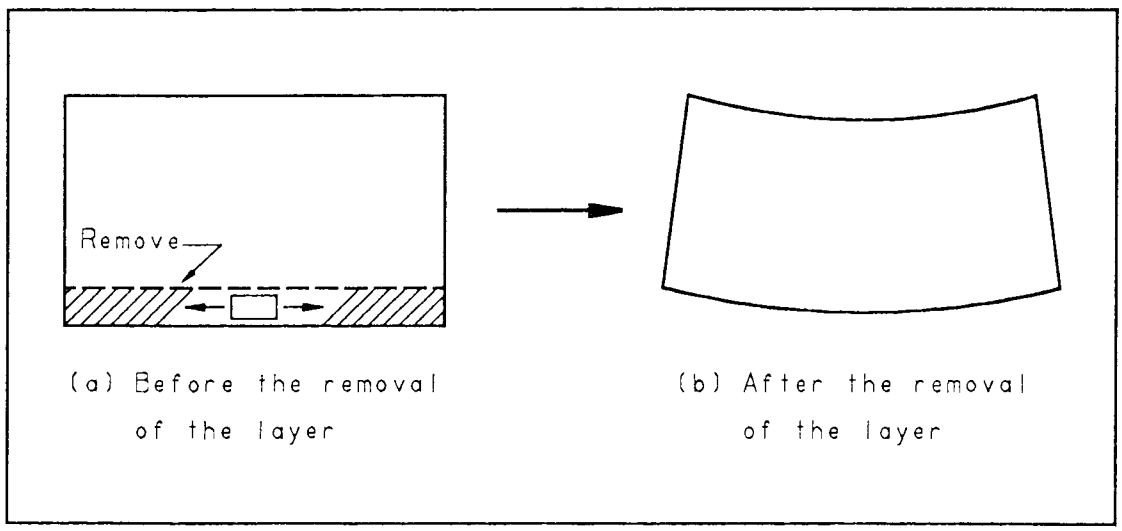

Fig 2.8 - The successive milling technique, where the removed layer carried tensile stresses. Thus when removed, the specimen exhibited concave bending.

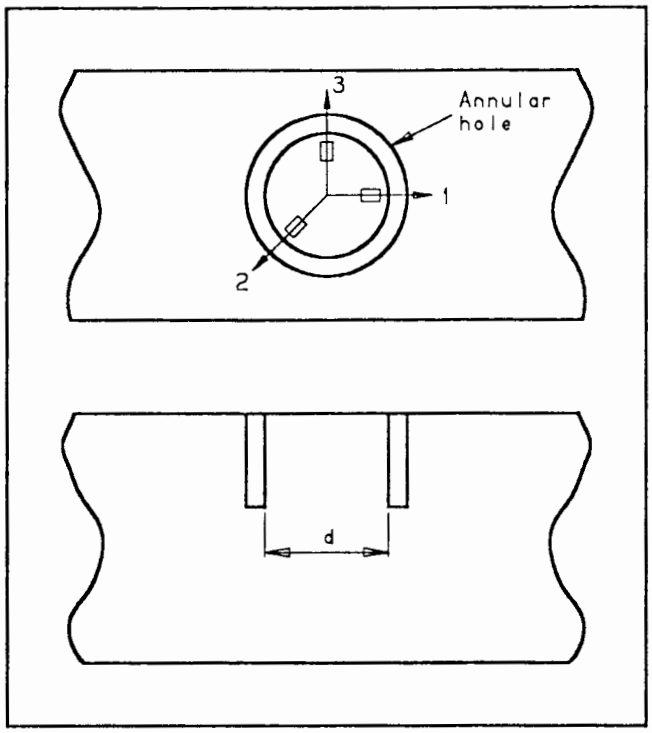

Fig 2.9 - Schematic of the trepanning technique. An annular hole is machined into a specimen to isolate an island which is formed. Residual stresses can be calculated from the relaxed strains detected by a strain gauge rosette.

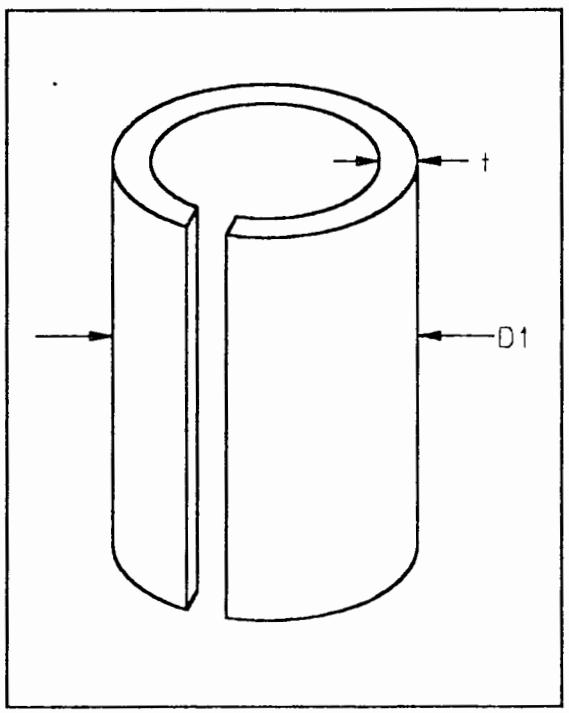

Fig 2.10 - The ring splitting technique, where D1 is the diameter after splitting and t is the tube thickness. The residual hoop stresses present in the tube can be calculated from the change in outside diameter after splitting.

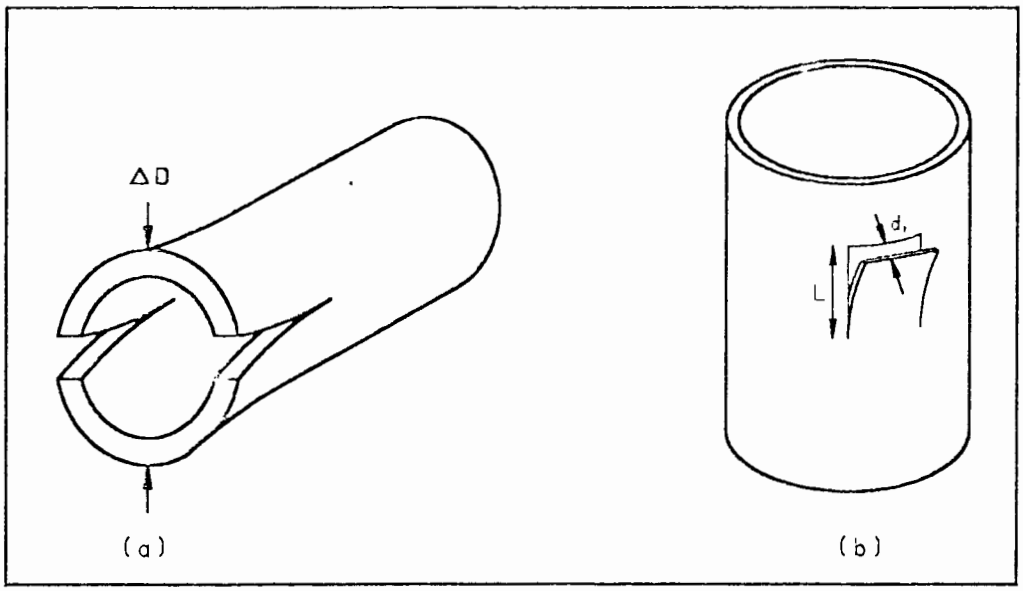

Fig 2.11 - The tongue technique, where ΔD is the change in diameter of the tube due to a longitudinal cut (a), and d, is the tip deflection of an axially cut tongue (b). From these values, longitudinal residual stresses can be calculated in tubes.

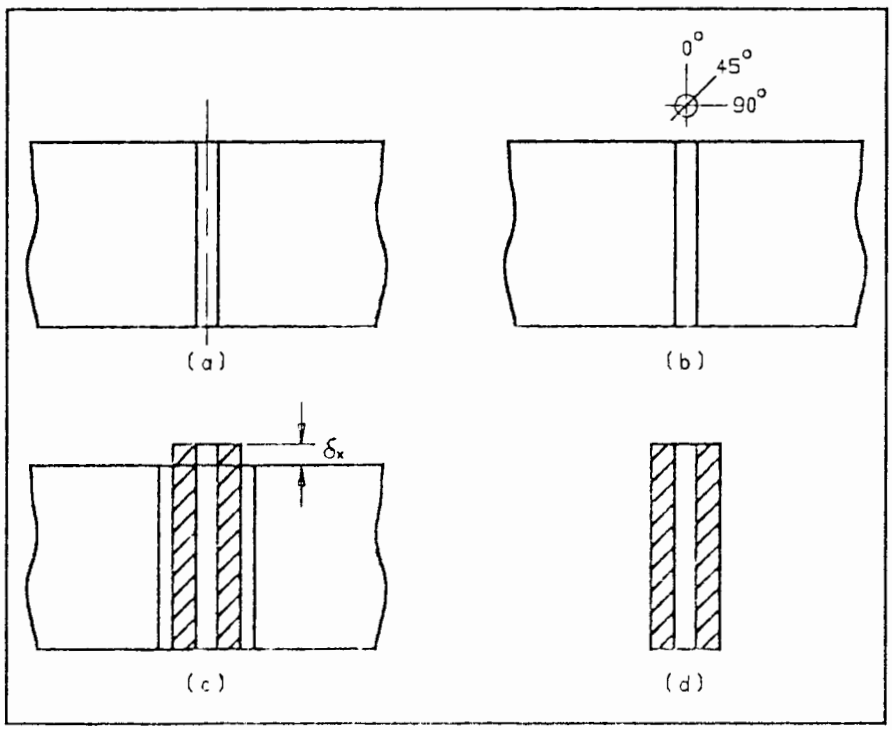

Fig 2.12 - The deep hole drilling technique. A hole of approximately 3.2 mm is drilled through a specimen (a), and its diameter is measured at 0 , 45 and 90° every 2mm of depth (b). A 10mm cylinder with the hole in its centre is then cored out (c). The change in axial length of the cylinder is continuously monitored. After coring the hole is measured as before (d). The three principal stresses can then be calculated from the measurements made.

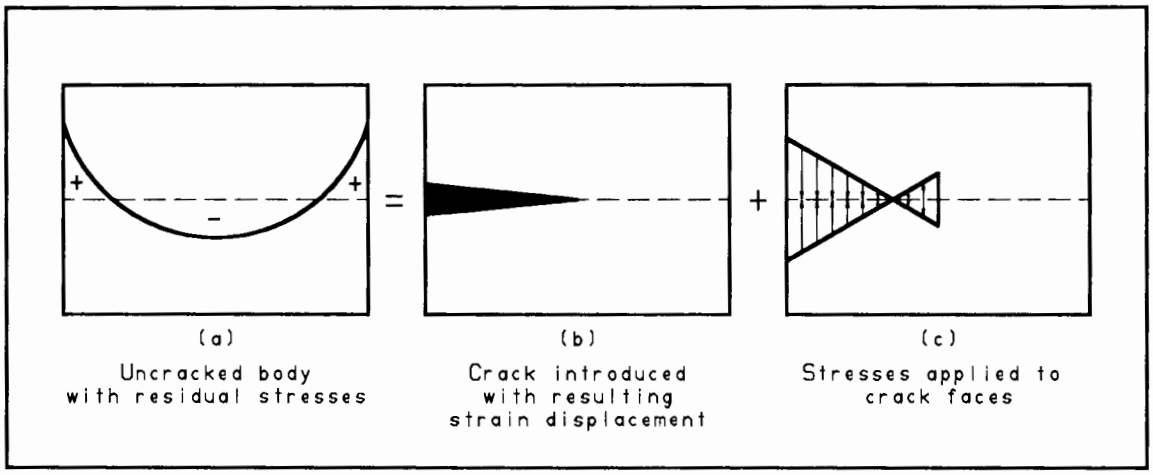

Fig 2.13 - The theoretical basis for the crack compliance method of residual stress measurement[64].

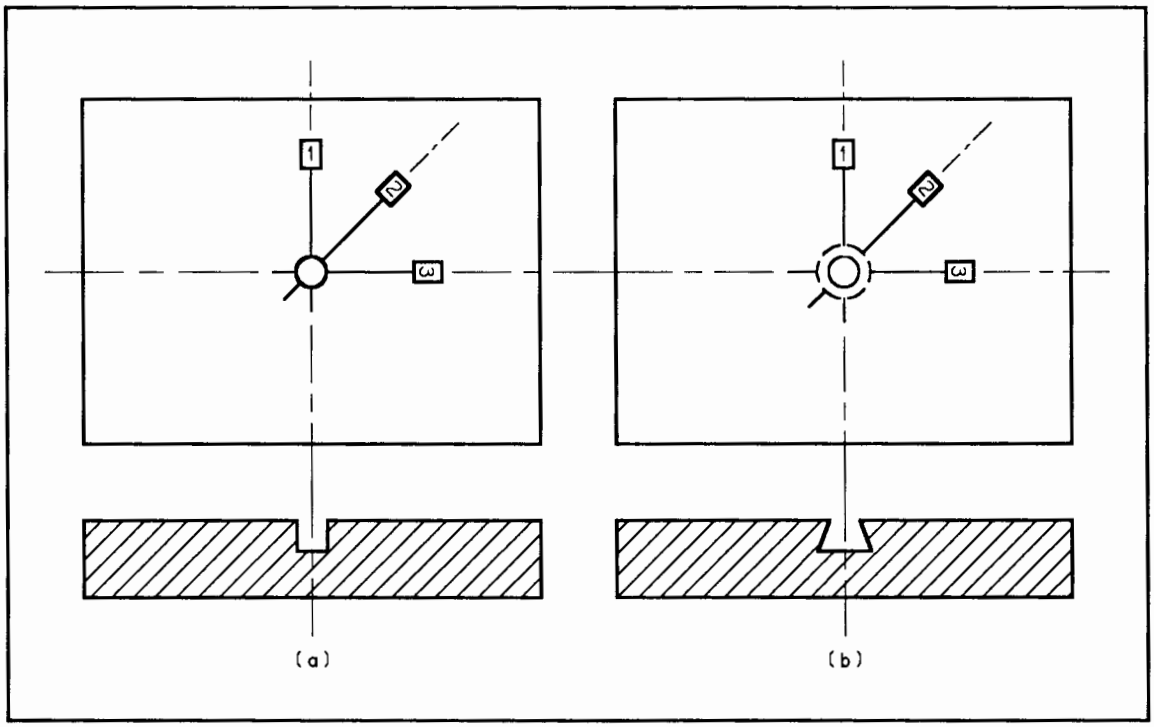

Fig 2.14 - The centre hole drilling technique showing hole location with respect to a strain gauge rosette. (a) shows the hole profile that most researchers who use this technique aim to drill, whereas (b) shows the profile recently proposed by Tootoonian and Schajer[65] which increases the sensitivity of the technique.

3. DESCRIPTION AND THEORY OF THE CHOSEN RESIDUAL STRESS MEASUREMENT TECHNIQUES

3.1 Introduction

Many methods of residual stress measurement were examined in the previous chapter. From them, two were chosen, namely the AACH drilling technique and the ring splitting technique. In this chapter these are discussed in greater detail.

3.2 The Air Abrasive Centre Hole Drilling Technique

As the name implies, this technique utilises a fine air abrasive stream to drill a hole in the centre of a 3-element strain gauge rosette, which is attached to a specimen. Refinements in strain gauge manufacturing techniques have made it possible to obtain strain gauge rosettes of very small dimensions. Therefore a hole of less than 2mm in depth and diameter[1,3,7,18,78] is sufficient for residual stress measurement. The technique has a significant advantage in its basic simplicity - it is quick and does not require an exceptional amount of skill. The main disadvantages are that the strain measuring device detects only a partial relaxation of the strains which occur when the hole is made[2]. As a result, strain gauge rosette manufacturers usually specify a range of hole sizes to be used with their rosettes. Since if the hole is too small, only a small percentage of the total strain is detected[3], and if the hole is too large, plasticity effects due to drilling could influence the strain gauges[3].

3.2.1 Analysis of the Technique

3.2.1.1 Principle of the Technique

If a hole is drilled in an infinite plane sheet of elastic isotropic material, which is subjected to a state of uniaxial stress, the radial stress at the edge of the hole must necessarily reduce to zero[2]. A redistribution of the stress will occur in the vicinity of the hole, since the hole can carry

no stresses. The radial stress in the direction of the load is shown schematically in Fig 3.1[2].

If a strain gauge is attached to the sheet before drilling, over a distance of 0.5d to 1.5d from the edge of the hole of diameter d, then as the hole is drilled the strain gauge will detect the strain associated with the reduction in stress shown by the cross-hatching in Fig 3.1[2]. This is related to the relaxation in stress at the edge of the hole. The relaxed strains measured by the strain gauges on the surface of the component are dependent upon the hole depth up to a certain point, beyond which further drilling does not significantly affect the strain. Schajer[26], Bathgate[22], Kelsey[17] and Rendler and Vigness[23] have reported that the maximum strain is released when the hole depth is equal to the hole diameter, whereas Micro-Measurements[86] and ASTM[87] specify that the hole depth should equal 1.2 times the hole diameter. As discussed in later chapters, for the experimental results presented in this thesis maximum strain relaxation was found to occur when the hole depth equalled the hole diameter.

In practice, stress fields are frequently biaxial, however the relaxation of the radial stresses will be of a form similar to the uniaxial case.

3.2.1.2 Required Hole Geometry and its Positioning

In order to obtain accurate results, it is important that the drilled hole has side walls which are normal to the test surface[3], i.e. for horizontal specimens - vertically sided walls. In addition the hole is to be cylindrically shaped, and its depth should be nominally equal to its diameter[17,22,23,26]. The optimum hole diameter is dependent on the type of strain-gauge rosette used. For a given strain-gauge rosette, the sensitivity and accuracy of the results increases with an increase in hole diameter[2] up to a point. This is due to the fact that the technique is only a partial relaxation technique. However the strain measurements are averaged across the diameter of the hole. The hole should be accurately

positioned in the centre of the 3-element strain-gauge rosette for best results[2,18,29,32,33,45]. This enables the strain-gauges to measure the same amount of relaxation relative to each other. Should the hole be off-centre, there are methods of taking this into account[32,33,45], as discussed in Section 3.2.2.4. It is however more time consuming to analyse the results.

3.2.1.3 Strain Gauge Rosettes and Strain Measuring Equipment

A variety of strain-gauge rosettes are available for the centre-hole drilling technique. The choice depends on the size of the hole to be drilled and the location of the measurement on the specimen. These rosettes consist of 3 elements typically oriented at 0°, 45° and 90° or 0°, 90° and 225° to each other, and have markings on them in order to facilitate the central targeting for location of where the hole is to be drilled. A few examples of available strain-gauge rosettes available from Micro-Measurements are shown in Fig 3.2[7]. Fig 3.2(a), type EA-XX-062RE, shows one of the original specially configured rosettes. Fig 3.2(b), type TEA-XX-062RK-120, shows an improvement on the design. The grid geometry is the same as the previous example, but it is easier to use and install. For example, the solder tabs have been brought to one side to simplify the lead wire routing and it is completely encapsulated with a polymide lamination to help protect the grid from damage whilst drilling. Fig 3.2(c), type CEA-XX-062UM-120, shows a configuration which resulted from a number of user requests which would enable a hole to be drilled adjacent to an obstruction[7], such as a weld bead or a protrusion in a specimen surface. BLH manufactures a strain gauge rosette, type FAER-03S-12-S6 EG, which is similar to that shown in Fig 3.2(c). This rosette was used for most the experimentation presented in this thesis, while a few measurements were performed with Micro-Measurements type TEA-06-062RK-120 rosette.

There is a wide choice of strain measuring instruments available. Points considered when making a choice were[1]:

i. A selection switch was needed, since there are three gauges which need to be connected simultaneously.

ii. For best overall accuracy a high quality instrument which has high resolution and good stability was required. This was because the technique is only a partial relaxation technique.

3.2.2 Measurement of Various Residual Stress Distributions

It is obvious that various residual stress distributions may occur, namely a uniform stress distribution, a non-uniform stress distribution in the plane of a specimen's surface and stress gradients varying with depth. Depending on the type of stress distribution present, the centre-hole drilling technique may need to be performed and/or analysed in different ways.

3.2.2.1 Uniform Stress Distribution

In this case, a hole of equal diameter and depth is drilled in the centre of a hole drilling 3-element strain-gauge rosette. The results of strain relaxation obtained from the strain measuring instrument are then used in the equations derived for the uniform stress distribution case in order to obtain the principal residual stresses and their directions.

The equations used for determining the principal residual stresses and their directions when a uniform residual stress distribution is assumed are derived by subtracting the biaxial stress solution for a thin plate from Kirsch's solution which is reported in Timoshenko's book[88]. As shown in Fig 3.3, this results in the stresses produced by a hole[21,29].

After some manipulation, as shown in Appendix A, the equations reduce to the following: (Note that the general case for a drilled hole is first given in Appendix A, and then it is simplified for the case of a centred hole.)

$$\sigma_{\frac{1}{2}} = -\frac{E}{2}\left(\frac{1}{K_1}\right)\left[\frac{\varepsilon_1 + \varepsilon_3}{1-\nu K_2/K_1}\right.$$

$$\left. \pm \frac{1}{1+\nu K_2/K_1}\sqrt{\left(\varepsilon_3 - \varepsilon_1\right)^2 + \left(\varepsilon_1 + \varepsilon_3 - 2\varepsilon_2\right)^2}\right] \quad \ldots \text{ eqn 3.1}$$

$$\alpha = \frac{1}{2}\tan^{-1}\left(\frac{\varepsilon_1 + \varepsilon_3 - 2\varepsilon_2}{\varepsilon_3 - \varepsilon_1}\right) \quad \ldots \text{ eqn 3.2}$$

Where: σ_1 = First principal stress

σ_2 = Second principal stress

ε_1 = Strain measured by the first strain gauge element

ε_2 = Strain measured by the second strain gauge element

ε_3 = Strain measured by the third strain gauge element

α = Angle of σ_1 from the first strain gauge element

$1/K_1$ = Calibration constant

$\nu K_2/K_1$ = Calibration constant

As regards notation, if α is positive as determined from the strain input data, then it is measured in the direction of the strain gauge rosette i.e. clockwise from strain gauge 1, as shown in Fig 3.4. Conversely, if α is negative, then it is measured in the counter direction of the rosette from strain gauge 1.

Equation 3.2 has two solutions in the range of $-90^\circ < \alpha < 90^\circ$, which can lead to confusion, as reported by Gupta[36] and Wang[33,37]. These two α solutions correspond with the direction of the two principal stresses. To determine the direction of σ_1, the signs of the numerator $(\varepsilon_1 + \varepsilon_3 - 2\varepsilon_2)$ and the denominator

($\varepsilon_3 - \varepsilon_1$) are ascertained, and the appropriate value of α is selected from Table 3.1[1].

As shown in the derivation of the equations (in Appendix A), the equation constants can be expressed either as A and B, or as $1/K_1$ and $\nu K_2/K_1$[2,23,29]. Constants A and B are dependent on material constants E (Young's modulus) and ν (Poisson's ratio), whereas $1/K_1$ and $\nu K_2/K_1$ can be regarded as independent of these material constants[2,23,29], since although still a function of ν, the dependence is very weak[29]. Schajer[29] has reported that finite element calculations have shown that for a hole of depth equal to diameter, K_1 varies within a 2 percent range and $\nu K_2/K_1$ varies from 0.27 to 0.32 for a range of ν from 0.25 to 0.35. If a uniaxial stress field is assumed, then $1/K_1$ and $\nu K_2/K_1$ conveniently reduce to the following[2], as shown in Appendix A:

$$\frac{1}{K_1} = \frac{\varepsilon_A}{\varepsilon'_A} \qquad \text{... eqn 3.3}$$

$$\nu K_2/K_1 = -\frac{\varepsilon'_T}{\varepsilon'_A} \qquad \text{... eqn 3.4}$$

Where: ε_A = Applied axial strain

ε'_A = Relaxed axial strain

ε'_T = Relaxed transverse strain

Beaney and Procter[1-3] have shown that $\nu K_2/K_1$ can be approximated as 0.3 or 0.33 and that $1/K_1$ is a function of hole diameter, for a given strain gauge rosette. These constants are given in Appendix B.

Thus when using the constants $1/K_1$ and $\nu K_2/K_1$, only one calibration is required for all elastic isotropic materials[2,23,29] for a given hole diameter. In fact, one need only look at the constants given by researchers such as Beaney[1,3] in order to determine these constants for a range of hole diameters.

3.2.2.2 Stress Gradients Varying with Depth

Various attempts have been made to determine residual stress variation with depth[5,17,22,24-31,46,68], which have been more or less successful. These include the incremental strain method, the average stress method, the power series method and the integral method.

The incremental strain method, introduced by Soete and Vancrombrugge[24], is still widely used today[26]. Kelsey[17] and Bathgate[22] developed the method further. It involves measuring the strain relaxations after successive small increments of hole depth. The stresses originally existing within each increment are then calculated by assuming that the incremental strain relaxations are only due to the stresses which existed within that increment. This assumption is however not valid and can lead to errors[26,27], since subsequent depth increments release strains from previous increments, in addition to strains released from the corresponding new increment, due to the effects of change in hole geometry. It is therefore possible for strain relaxations to increase even when the new hole depth increment is itself unstressed[26].

Nickola[46] proposed an average stress method, otherwise known as an equal weight solution, in order to overcome the theoretical shortcomings of the incremental strain method. It uses the concept of an equivalent uniform stress, which is equal to the uniform stress distribution within the hole depth that produces the same strain relaxation as the non-uniform stress distribution. The equivalent uniform stress is assumed to be equal to the average stress over the hole depth. This would only be true if the stresses at all depths contributed equally to the strain relaxations detected on the surface[26]. It is however found in practice that stresses in material closer to the surface have a larger effect on the measured strains than those further away[26].

Schajer[29] developed the power series method as an approximate yet theoretically accurate method of calculating non-uniform

stress fields from incremental strain data. It makes use of finite element calculations to compute series of coefficients, having power series variations with depth, corresponding to the strain responses when drilling. These strain responses are then used in a least-squares analysis of the measured relaxed strains. An advantage of the power series method is that the least-squares procedure provides a best fit curve through the measured strain data, whereas other methods give a stepped approximation of the inherent residual stresses. This averaging effect is especially effective when many hole depth increments are made. The method is however limited to smoothly varying stress fields[26]. This is due to only **average** stresses being determined from the top surface to any hole depth of interest, as pointed out by Shaw and Chen[30], and Flaman and Boag[31].

The integral method has been made practical by the use of finite element calculations as a calibration procedure. Initial developments of this method were made by Bijak-Zochowski[69], Niku-Lari et al[5], and Flaman and Manning[27], which were further developed by Schajer[26,68]. Although the procedure developed by Flaman and Manning is mathematically equivalent to Schajer's solution, the latter is easier to use. The integral method considers the contributions to the total measured strain relaxation by the stresses at all depths simultaneously[26,27], and is a viable and practical procedure for calculating stresses varying with depth[68]. It is best suited to the case where residual stresses vary sharply and where only a few hole depth increments are made.

All the methods discussed assume linearity of the specimen material. When residual stresses are greater than approximately 50 percent of yield stress, inaccuracies occur in the measured strains due to the local yielding at the stress concentration caused by the drilled hole[26]. Furthermore, Young's modulus (E) and Poisson's ratio (ν) are assumed constant throughout the material. This is not always correct as in the case of some case-hardened materials. However if depth variations of E and ν are known, then this problem can be overcome.

In this thesis, calculations of stress variations with hole depth were not attempted. The reason being that when using the AACH drilling technique, the desired hole geometry (i.e. a cylindrical hole with parallel sides) is only achieved once full hole depth has been reached due to the nature of the drilling process. However approximations of the stress variation through the thickness of the aluminium drill rods were made by performing measurements on the inside and outside surface of the rods, as well as on a plane perpendicular to the rods' axes (effectively the radius) in certain cases.

3.2.2.3 Non-uniform Surface Stress Distribution

Kabiri[55] suggested that since there is no means of determining how the stresses vary near the hole, except by drilling another hole; a new 5-element strain-gauge rosette should be manufactured and employed. Such a rosette is shown in Fig 3.5. His reasoning was that a linear stress field, as opposed to a uniform stress field, could then be assumed and analysed. The analysis presented by Kabiri is a complex and lengthy one. Furthermore, residual stresses are complex, so more than one reading would be needed anyway. It is felt that by using the standard 3-element strain-gauge rosette intelligently and by having a good understanding for the problem at hand, that it would not be necessary to use a special 5-element rosette.

Shaw and Chen[30] proposed a method of measuring stresses varying in all directions. However they also suggested that in order to obtain the residual stress distribution over the whole specimen, several strain gauge rosettes should be attached to the specimen at appropriate positions. Lu and Flavenot[25] suggested that chains of strain gauges could be used to measure the stress gradients in a plane, as shown in Fig 3.6. This configuration could also avoid plasticity effects due to the stress concentrations caused at drilled holes, and large stress fields, but is expensive in strain gauges.

3.2.2.4 Off-centred Hole in an Uniform Residual Stress Field

If a hole is drilled so that its centre is not coincident with the centre of the strain gauge rosette (i.e. the hole is eccentric), then the strain gauge elements will detect different amounts of strain relative to one another. In essence the strain gauge element closest to the hole will detect a disproportionately high strain reading which is more a function of eccentricity than the true residual stress state in the material. Attempts have been made to produce methods of calculating principal residual stresses and their directions when this occurs.

Sandifer and Bowie[32] developed a solution which is complex and requires an iterative procedure to solve. Tieu[47] also investigated this problem and presented a direct method to evaluate the principal residual stresses and their directions. However the relations are complex. Wang[33] developed a simpler solution and suggested that there are errors in the solutions presented by Sandifer and Bowie[32], and Tieu[47].

The derivation of the residual stress equations for the case of an off-centred hole are shown in Appendix A.

3.3 The Ring Splitting Technique

Simple methods can be used for the determination of residual stresses in thin wall tubing if the stresses consist of high tensile stresses at the one surface and high compressive stresses at the other surface[15]. The measurement of residual hoop stresses in thin walled cylinders may be estimated by the ring splitting method, which involves splitting a hollow cylindrical specimen in the longitudinal direction, as shown in Fig 2.10[4,8,10,14,15,83].

3.3.1 Analysis of the Technique

As with other mechanical methods, this method is based on the fundamental phenomenon that the removal of part of a stressed

body causes both the cut out piece and the remainder to experience elastic strain[15]. When using the ring splitting technique, this elastic strain results in the cut tube either opening (if the hoop stresses are on average effectively tensile), or closing (if the hoop stresses are on average effectively compressive). The residual stresses are assumed to vary linearly through the wall thickness of the tube[8,10] and to be consistent on each horizontal plane parallel to the cut[8], even though they may be complex in nature. Beam theory is used to derive the residual stress equation , as shown in Appendix A, which is the following:

$$\sigma_h = \frac{E\ t}{1 - \nu^2} \times \left(\frac{1}{D_0} - \frac{1}{D_1} \right) \qquad \ldots \text{ eqn } 3.5$$

Where: σ_h = Residual hoop stress

E = Young's modulus

ν = Poisson's ratio

t = Wall thickness

D_0 = Outside diameter before ring splitting

D_1 = Outside diameter after ring splitting

Sachs and Espey[15] reported that an ideal tube specimen used in the ring splitting technique requires its length to be at least three times its diameter, and that a specimen with a length of two diameters could yield at least 95% of the maximum deflection. They reasoned that the probable source of the effect of length on deflection is the presence of longitudinal stress in the tube which is released by the cutting operation.

Another factor which can influence the deflection is the cutting operation which plastically deforms the metal at a certain depth from the cut and relieves the stress within this layer of metal[15]. This effect can be small, but the relieved stresses will not give rise to any corresponding measurable deformation of the object. The cutting operation can also induce residual stresses in a component both from machining induced stress as

well as because of temperature effects, and thus affect the initial residual stress field. Furthermore, residual stresses are triaxial in nature, but strain is only measured in one plane.

Due to the assumptions and drawbacks of this technique, measured residual stresses are often lower than their true value. This is particularly so if residual stresses are high[15]. The technique must thus be used with extreme caution and should not be relied upon when accurate values of residual stress are required. However the technique is useful for comparative purposes, for example relative levels of locked-in stresses in variously processed but otherwise identical products can be assessed.

3.4 Summary

Detailed discussions of the AACH drilling technique and the ring splitting technique have been presented in this chapter. Now that the principles of the AACH drilling technique have been discussed, it is in order to attempt a design of such a drilling device and its accessories, so that it can be used for experimentation. This is presented in the next chapter.

(e1 + e3) - 2e2	e3 - e1	Range of alpha
Less than zero	Less than zero	-90 < alpha < -45
Less than zero	Greater than zero	-45 < alpha < 0
Greater than zero	Less than zero	0 < alpha < 45
Greater than zero	Greater than zero	45 < alpha < 90

Table 3.1 - Range of values of principal stress directions (ref 1). The correct values of alpha are found by noting the signs of the expressions used to calculate it. This formulation is only applicable to 0, 45, 90 or 0, 90, 225 degree rosettes.

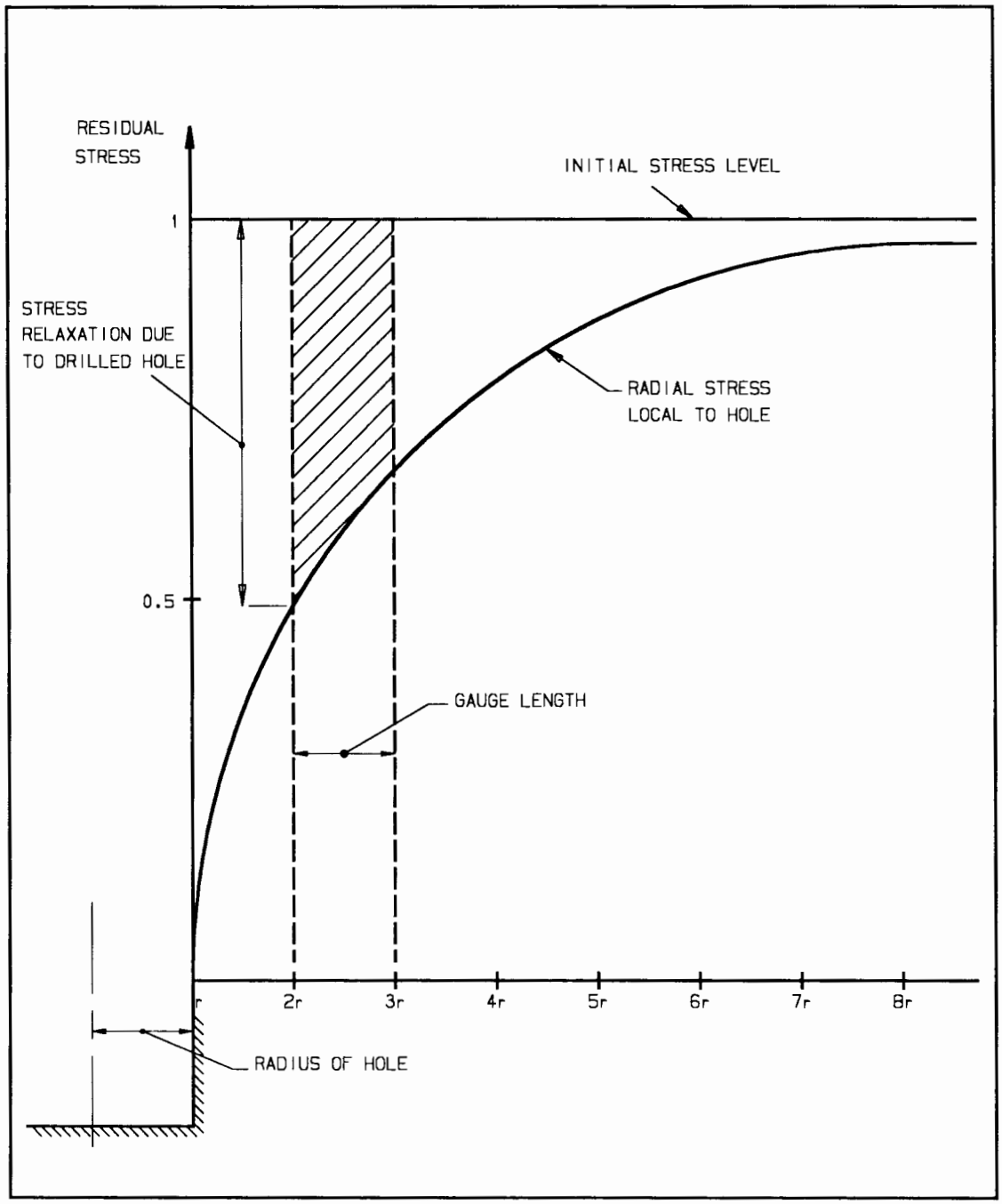

Fig 3.1 - Principle of the centre hole drilling technique. If a hole is drilled in an infinite sheet of elastic isotropic material which is subjected to a state of uniaxial stress, then a redistribution of stress occurs in the vicinity of the hole. An attached strain gauge rosette will detect a certain amount of stress relaxation due to the drilled hole as indicated by the cross hatched area.

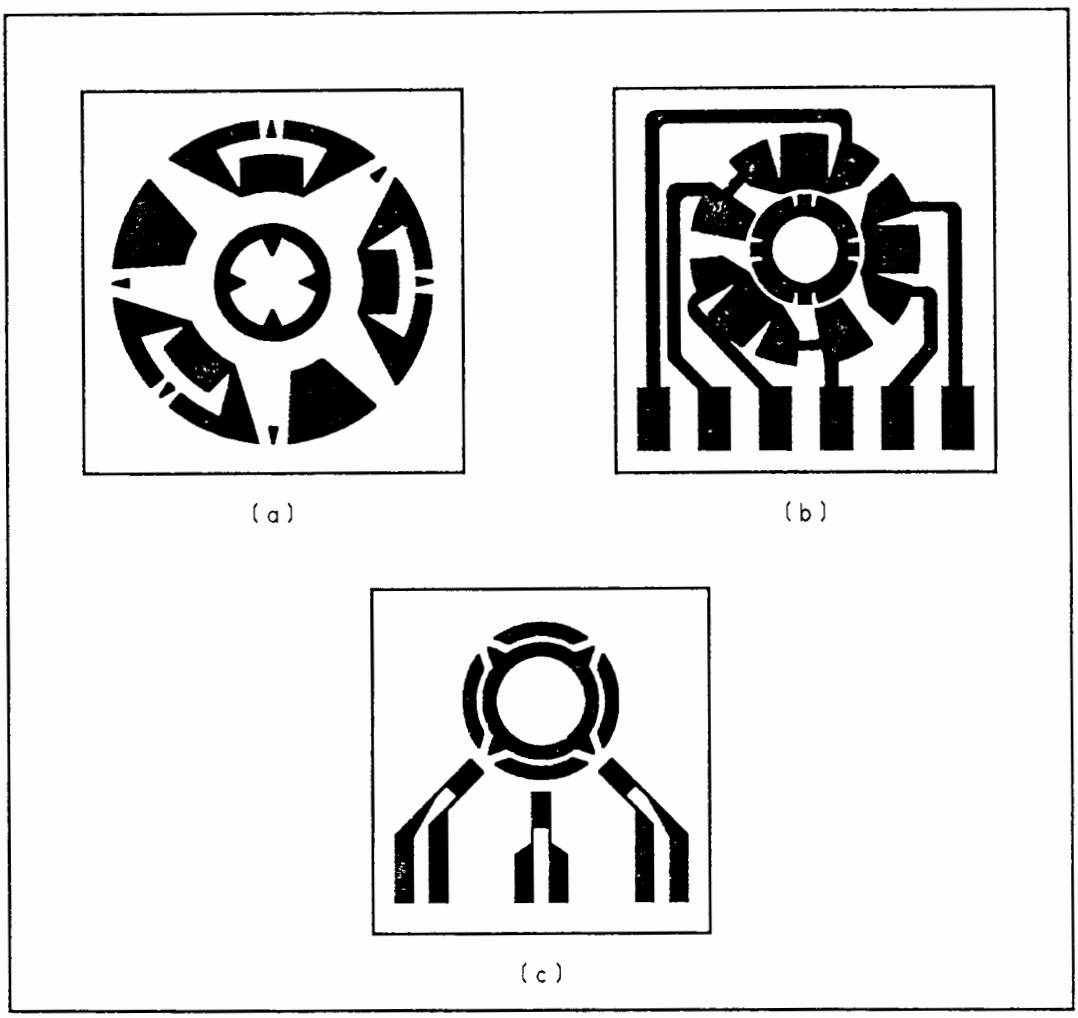

Fig 3.2 – Various centre hole drilling strain gauge rosettes, manufactured by Micro-Measurements and BLH. Type (a) shows one of the earlier rosettes developed, while type (b) shows an improved version. Type (c) was developed so that strain gauges could be placed near obstructions such as weld beads.

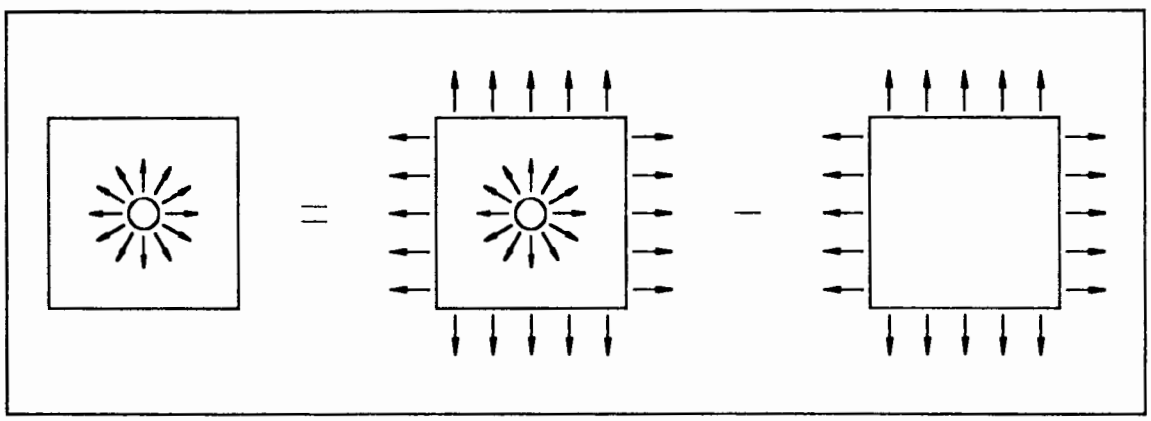

Fig 3.3 – Relieved stresses due to a hole drilled in a uniform residual stress field are derived by subtracting the biaxial stress solution for a thin plate from Kirsch's[88] solution.

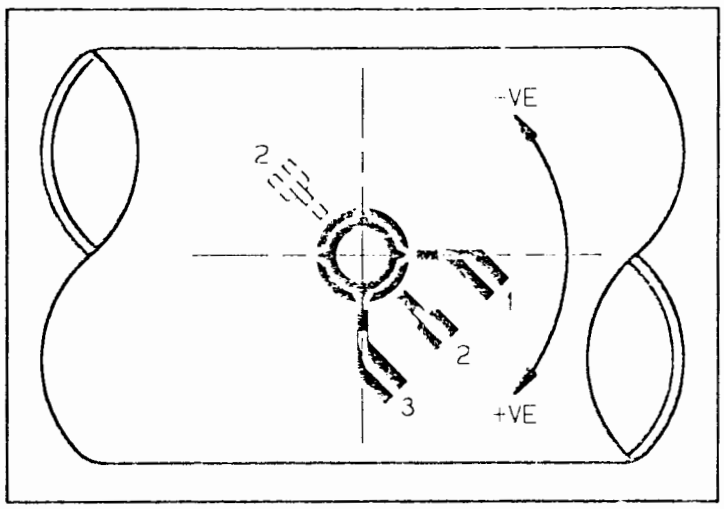

Fig 3.4 - Direction of α. If α is calculated to be positive, then it is measured clockwise in the direction of the strain gauge rosette. Conversely if α is negative, then it is measured anti-clockwise in the counter direction of the strain gauge rosette.

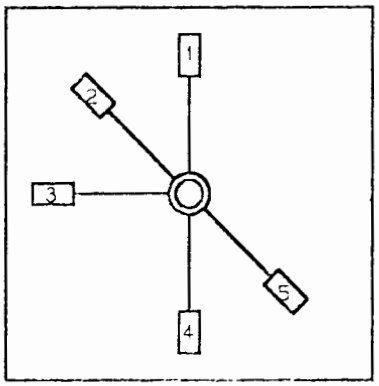

Fig 3.5 - Kabiri's[55] proposed 5 element strain gauge rosette for the measurement of a varying surface stress field.

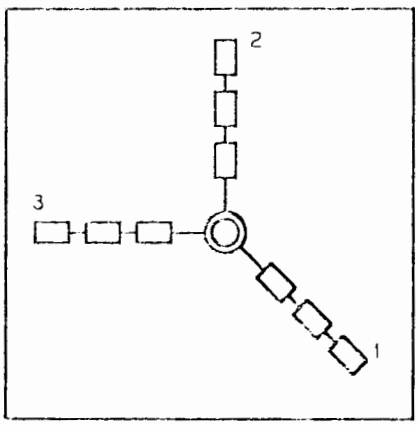

Fig 3.6 - Lu and Flavenol's[25] proposed strain gauge configuration to measure surface stress gradients, avoiding plasticity effects.

4. DESIGN OF THE AIR ABRASIVE CENTRE HOLE DRILLING DEVICE

4.1 Introduction

The previous chapters have examined the various techniques used to measure residual stress. Also examined was the theoretical detail of the two techniques chosen for residual stress measurement of extruded aluminium (7075-T6) drill rods, namely the AACH drilling technique and the ring splitting technique. This chapter is concerned with the detailed design of the AACH drilling device. In order to design the device, it is necessary to assess the tasks and functions it is required to perform. Therefore the design philosophy of the system is discussed first followed by the detailed design of the system. Finally, in this chapter, problems and modifications of the design are presented.

The principle of the design was similar to a unit designed by Beaney and Procter[1-3]. The design presented in this chapter attempts to create an inexpensive working model, where the components are manufactured locally with the exception of a few which were obtained from Procter in the U.K.

4.2 Design Philosophy

Before commencing the initial design, it was necessary to take the objectives of the drilling device into account. They are discussed in the following sections and included the following:

i. Hole positioning and measuring.
ii. Hole geometry.
iii. Vacuum extraction.
iv. Control and adjustment.
v. Air and powder supply.

4.2.1 Hole Positioning and Measurement

As mentioned in the previous chapter, a hole was required to be drilled in the centre of a strain gauge rosette. Once this had

been done, its diameter was required to be measured so that the correct value of $1/K_1$ could be chosen in order to determine the magnitudes of the residual stresses. In order to fulfil the positioning and measurement functions of the AACH drilling device, an optical unit compatible with a drilling unit was proposed. The extent of their compatibility was that they would both be able to be secured in a common guide bush. A test specimen could thus be accurately positioned beneath the guide bush with the aid of the optical unit and thereafter a hole drilled in the desired position with minimum deviation by replacing the optical unit with the drilling unit in the guide bush.

In order to achieve its requirements, the proposed optical unit was to consist primarily of an eyepiece mounted in a micrometer head with both fixed and movable cross hairs (in a manner similar to a conventional Vickers hardness indenter), an objective lens to focus on a strain gauge rosette or a drilled hole, and a ring illuminator to facilitate viewing through the optical unit. The preliminary design is shown in Fig 4.1.

4.2.2 Hole Geometry

As mentioned in the previous chapter, drilled holes were required to have vertical sides for greatest accuracy if one were to use the conventional mathematical derivations[2,3,23] as opposed to tapered hole derivations[65]. By vertical, it is meant that the sides must be parallel and normal to the work surface. Since work surfaces are usually horizontal, sides will be referred to as vertical in future. To enable these holes to be drilled accurately, standard 0.46 mm sapphire nozzles were used which could be replaced when worn by the abrasive powder. For best results and low nozzle wear, the ideal nozzle to work surface distance is 1.5 mm[1].

When drilling a hole, if the nozzle were to be held stationary and perpendicular to the work surface, then a hole with the section approximately as shown in Fig 4.2(a) would result. As can be seen, it is far from ideal with non-vertical sides.

However if the nozzle were to be slightly tilted, a hole with one vertical side could be produced as shown in Fig 4.2(b). In addition, if the nozzle were to be given a certain offset and orbited, a vertically sided hole of chosen diameter could be drilled. This concept is illustrated in Fig 4.2(c).

4.2.3 Vacuum Extraction

Some form of vacuum extraction was necessary since the fine abrasive powder used for the drilling operation (nominally 50 μm aluminium oxide) would cause rapid wear when in contact with moving parts. Powder as well as abraded specimen particles in the work area could have also interfered with the drilling action, as the work area would be cluttered with debris. In order to prevent strain gauge rosettes from being damaged by the debris in the work area, they were coated with a protective coating - Micro-Measurements M-Coat B. This was effective since the air-alumina stream was aimed at the centre of a strain gauge rosette and not directly at the strain gauge elements. Therefore the coating needed only to provide protection against rebounding particles which would have lost most their momentum due to their low mass.

Excessive particles in the atmosphere could have also created a health hazard and affected breathing, as well as the performance and reliability of the electronic components, particularly the strain gauge amplifier and the associated recording equipment.

4.2.4 Control and Adjustment

For efficient operation, air pressure, powder quantity and nozzle orbiting speed needed to be suitably controlled. An SS White Airbrasive model K machine[89] was obtained to control air pressure and to regulate powder delivery. Nozzle orbiting was controlled by placing a potentiometer in series with an electric motor, used to drive the drilling unit. The drilling unit was also to be used to control the nozzle offset and tilt, so that the required vertically sided hole of the required dimensions could be drilled, as outlined in Section 4.2.2.

Based on the above considerations a preliminary outline of the drilling unit was conceived, as shown in Fig 4.3.

4.2.5 Air and Powder Supply

Air could be obtained from virtually any source that could provide a pressure of at least 5.5 bar (80 psi). In addition to the pressure regulator on the SS White Airbrasive machine, an additional pressure regulator with an air filter was recommended, so that moisture could be prevented from entering the air-powder stream and causing possible clogging of the system. Abrasive powder was introduced into the air stream via a mixing chamber in the SS White Airbrasive machine, which was located on top of a vibrator device. By regulating the amount of vibration, the quantity of powder in the air stream was controlled.

4.3 Proposed Design Outline

The design of the air abrasive drilling device was divided into four main constituents, namely:

i. The optical unit.
ii. The drilling unit.
iii. A guide bush fixture.
iv. Auxiliary components.

These constituents are discussed in detail in the following sections, with component drawings at the end of the chapter and in the appendices.

4.4 Detailed Design of the AACH Drilling Device

This section follows the format as set out in the design outline in the previous section. All detailed descriptions of the design will refer directly to the drawings shown in Appendices C to F. Key components referred to in the text have their component numbers written after them in square brackets. This component

number refers to the assembly drawings given at the end of the chapter as well as in the appropriate appendix which is mentioned at the beginning of the section.

It should be noted that almost all the components of the air abrasive drilling device were manufactured from 431 stainless steel to reduce corrosion and to keep all fine threads free from corrosion and other chemical contaminants.

4.4.1 Optical Unit

The component numbers given in square brackets in this section and the following sub-sections refer to Fig 4.4 and to the drawings in Appendix C.

The optical unit shown in Fig 4.5 was a critical component in the functioning of the system. The drilling unit was extremely dependent upon the accuracy of its alignment capabilities. It was used both before and after the drilling process for both the setting up of the drill location and subsequent hole measurement. Its functions are listed as follows:

Prior to drilling:	Positioning of guide bush relative to the strain gauge rosettes.
After drilling:	Measurement of hole diameter.
	Measurement of hole depth.
	Measurement of any hole eccentricity with respect to the centre of the strain gauge rosettes.
	Assessment of any hole taper.

4.4.1.1 Optics and Magnification

The optical facility was designed to work as a precision microscope. The eyepiece and objective lens were kept at a fixed distance apart so that magnification remained constant. The lenses are detailed overleaf.

CBS Objective: 50 x magnification, focal length = 25 mm

Cooke micrometer eyepiece: 15 x magnification

The objective lens was attached to the optical tube [8] by means of a matching thread on the lower side of the tube. The optical tube was positioned by eight grub screws [11], which both secured it and allowed for its adjustment.

4.4.1.2 Focusing Mechanism

The principle used for the focusing of the optical unit was based on keeping the two lenses a fixed distance apart. The focusing adjuster [2] was threaded with a fine 0.5mm pitch thread for vertical adjustment of the optical adapter [3]. The optical adapter had a grub screw in it which acted as a locating pin in the key way machined in the optical tube holder [1]. This served as a guide when adjusting focus and ensured that the optical adapter did not rotate. The circlip [12] kept the optical tube holder in position.

4.4.1.3 Ring Illuminator

The illumination ring [7] consisted of a series of small light bulbs equi-spaced around the circumference of a plastic ring. It was pressed into the lower section of the optical tube holder, and allowed for clearer vision of an object below the objective lens. The wiring from this component passed between the optical tube holder [1] and the optical tube [8] and out to the control box via a small hole in the optical tube holder [1].

4.4.2 Drilling Unit

The component numbers given in this section and the following sub-sections refer to Fig 4.6 and to the drawings in Appendix D. The drilling unit, shown in Fig 4.7 was a highly compact precision instrument. It consisted of many small components with close tolerances, so that consistently well drilled holes could be produced. Key components of the design are discussed in the

technique is generally restricted to small specimens due to the size limitations on specimen holders.

ii. The parallel beam method - This method obviates the need for focussing corrections and accurate specimen alignment, and is the basis for various commercial portable stress analysers. A disadvantage of this method is its low intensity x-ray beam which necessitates longer exposure times.

For the x-ray system, the following are general points of importance:

i. This method has the great advantage of being truly non-destructive[19,66,77], unless residual stress information below the surface is required, in which case successive layers of material need to be removed[66].

ii. Diffracted peaks from different phases in complex materials are accessible, which allows strains to be examined in each of these if necessary[77].

iii. Due to their low energy, x-rays only penetrate a few microns into a specimen, so only the stresses at the very surface are measured[19,66]. Therefore the sample surface must be smooth and surface preparation of the sample is extremely important. (eg. cleaning by abrasive methods will change the stress pattern.) Indeed local machining or surface treatments can completely swamp or mask the underlying residual stresses[19]. In order to obtain any information below the surface, successive layers of material need to be removed. So for full stress variation with depth measurement, x-ray diffraction is destructive[66].

iv. Measurements can only be performed on x-ray diffracting materials[66].

v. Pronounced textural effects and/or coarse grain size can give misleading results.

vi. The cost of the equipment is comparatively high.

Thus x-ray diffraction can be a useful non-destructive technique for evaluating residual surface stresses and can give accurate results if used correctly. However the method is far from straight forward, and is expensive. Also, proper care must be taken both with practical techniques and with interpretation.

2.2.2 Neutron Diffraction

Neutron diffraction works on the same principle as x-ray diffraction[13,49,50,66]. However neutrons have more energy, and therefore penetration in steel can be achieved up to 40 mm[78]. Measured strains are averaged within a sampling volume, which can be as small as 1 mm cube[66]. The technique therefore has the great advantage of being non-destructive even when residual stress measurements are required below the surface[66].

This technique has, however, the following disadvantages:

i. Measurements can only be performed on neutron diffracting materials[66].

ii. A neutron source is needed and this is not always readily available[66,78].

iii. The job must be taken to the reactor which limits the job size and prevents portability of the technique[78].

iv. The test facility is relatively costly and there are often time constraints on such equipment[66,78].

v. Long exposure times of the test specimens to neutron radiation are necessary[66].

vi. There can be a large uncertainty (±50 MPa.) associated with the technique. This is acceptable when large magnitudes of residual stresses are measured (eg. 300±50 MPa), but if small magnitudes of residual stress are measured, they will be difficult to interpret (eg. 30±50 MPa)[78].

2.3 Stress Sensitive Techniques

When stresses exist in metals, some of the physical or

mechanical properties are changed[12] and it is sometimes possible to determine residual stresses by measuring these properties. Stress sensitive techniques discussed in the following sections include the following:

i. Magnetic techniques
ii. Ultrasonic techniques
iii. Hardness techniques

2.3.1 Magnetic Techniques

Micromagnetic quantities based on the Barkhausen noise phenomenon (the signal created from the forced movement of Bloch walls), are used to measure residual stresses[79,80]. Bloch walls separate adjacent magnetic domains which have different local magnetisation directions[79,80]. The movement of the Bloch walls, and therefore the amount of Barkhausen noise, is directly related to energy barriers due to local stresses[79,80].

The technique has the advantage of being non-destructive, and quick to analyse and process residual stresses. However it relies upon a second order effect, can only be used on magnetic materials and is limited to a depth of around 0.2 mm[78] since the Barkhausen noise is damped in the material due to the depth through which it has to pass.

2.3.2 Ultrasonic Techniques

The velocity and attenuation of sound waves in a metal specimen varies linearly with the average stress through which the waves propagate[12,81]. Since shorter waves are able to penetrate deeper into metals, ultrasonic waves are more suitable than ordinary audio sound waves. These waves are transmitted and received by transducers placed on a specimen's surface. A variety of experimental configurations can be utilised as shown in Fig 2.5. The configurations shown in Figs 2.5(a) and (b) allow an average through thickness stress to be detected, whereas the configuration shown in Fig 2.5(c) detects the average stress in a surface layer[81].

This technique has a good all round potential[78], its main advantages being that it is non-destructive and easy to use. Unfortunately it also relies on a second order effect. Temperature variations and microstructural effects can influence wave velocity and thus affect the accuracy of the results[78,81]. Precise time measurements are also required, and it is a relatively developmental averaging technique[78,81].

2.3.3 Hardness Techniques

The state of surface residual stresses influence the compressive yield strength obtained when a small hard ball is gently pressed on the smooth surface of the specimen to be studied[12]. While increasing the load, a relationship between the load and electrical resistance of the contact point is obtained. This can be used to obtain the surface value of the residual stress. However this technique lacks accuracy, especially when variable metallurgy and microstructure exists, and is still in the laboratory stage[12].

2.4 Cracking Techniques

Another group of techniques developed to determine residual stresses involves the close observation of crack development in a specimen due to stress. The cracks can be induced by two methods:

i. Hydrogen induced cracking
ii. Stress corrosion cracking

2.4.1 Hydrogen Induced Cracking Technique

In this process specimens are immersed in an electrolyte and charged with hydrogen by applying a dc current, using the specimen as the cathode and a set of lead strips as the anode[12]. Various different crack patterns result which are related to a residual stress distribution. An example of this can be seen in Fig 2.6[12]. This technique has the disadvantages of being destructive, time consuming, and only gives qualitative

as opposed to quantitative results.

2.4.2 Stress Corrosion Cracking Technique

In this case specimens are boiled in an aggressive (corrosive) environment[12]. The method is similar to the hydrogen induced cracking technique, and similar crack patterns develop. This technique is also destructive and time consuming, and also only gives qualitative results.

2.5 Stress Relaxation Techniques

The stress relaxation techniques are based upon the principle that while unloading, strains are elastic, even if the material has been plastically deformed. Therefore it is possible to determine the residual stress without knowing the loading history of the material. Summarised in the following sections are various methods of performing this technique. They are the following:

i. The brittle coating technique
ii. The Sach's boring out technique
iii. The successive milling technique
iv. The trepanning or ring core technique
v. The ring splitting and tongue techniques
vi. The deep hole drilling technique
vii. The crack compliance technique
viii. The centre hole drilling techniques

Before discussing these techniques, some general comments regarding sectioning methods should be made[78]. All the techniques that will be discussed require cutting, slicing or machining of some form without the introduction of spurious strains or induced machining stresses. The only truly stress free methods of material removal appear to be electro-chemical machining and chemical etching. Air-abrasion techniques can also be regarded as relatively stress free[3,46] due to the low

inertia of the tiny abrasive particles, and any heat generated is rapidly cooled by the jet of air, as discussed later in the chapter. However this method is best suited to centre hole drilling techniques.

Electro-chemical machining can remove large volumes of material, but it is not always easy to use. Chemical etching is very slow and can have a deleterious effect on strain measuring devices - eg. bonded strain gauges, unless properly protected. Therefore its use is limited and as a result machining is generally restricted to conventional cutting, filing, etc... using light cuts to minimise machining stress, which are time consuming. It must be noted that machining is a big problem when using hard materials such as rail steels or stainless steels, due to their high work hardening rates, and is virtually impossible for tungsten carbide cobalt materials.

2.5.1 The Brittle Coating Technique

When using this technique, the measuring point and its surrounding areas are coated with a brittle lacquer[12]. A small hole (eg. 3.2 mm diameter and depth) is then drilled at the measuring point[82] and cracks are produced, due to stress relaxation, in the lacquer, as shown in Fig 2.7[9,12,82]. If the residual stress is extremely high, the pattern will form immediately upon drilling. However if the stresses are low, it may be necessary to cool the lacquer slightly to bring out the pattern. Care must be taken not to allow the lacquer to cool too much since crazing of the lacquer can occur. From the direction and distribution of the cracks, it is possible to determine the direction of the main stresses, since they are perpendicular to the direction of the cracks. This technique is preferably a laboratory technique, but it can also be used for field measurements if the atmosphere is dry[12].

Advantages of this technique are that little damage is done to the specimen and rapid determination of the direction of the principal stresses together with an approximate indication of their magnitude is possible[12]. However it should only be

following sub-sections.

4.4.2.1 Air Tube

The air tube [8] was an adjustable brass tube through which the air abrasive mixture flowed. It was press fitted into the air tube housing [6] and included a nylon sleeve pressed onto its top section which provided a cone shaped running fit for the inlet tube [7].

4.4.2.2 Air Tube Housing

The air tube housing [6] was located inside the running tube [21]. It was tilted and offset by adjustment screws, located in the grub screw collar [15] and offset gimble [26] respectively, to create the required hole profile when drilling. The adapter [5] was press fitted onto the top of the tube so as to form one rigid component.

4.4.2.3 Running Tube

The running tube [21] was the rotational (ie. orbiting) component of the drill. It slid into the air bearing bush [24] and was lightly lubricated with oil when drilling. It was driven by a timing belt-pulley system - its speed being adjustable from a control box to allow for best results when drilling a hole.

The tube was perforated with a series of holes. There were four holes in the lower section to allow for nozzle offset and four holes in the top section which allowed for tilt adjustment of the air tube housing [6]. The eight holes located above the keyway were designed for vacuum extraction. Abrasive particles were sucked from the work area through these holes, and out through the vacuum tube attached to the vacuum housing.

4.4.2.4 Sapphire Nozzle

The sapphire nozzle [22] was an imported component from SS White Industries in the USA - part number 353-1942x, which has been

designed specifically for the air abrasive drilling application. It had an internal diameter of 0.46mm and had to be handled with care as it was extremely delicate.

Nozzles were monitored for wear, as a worn nozzle resulted in a badly drilled hole. Effects of nozzle wear could usually be noticed by a fuzzy appearance of the hole when viewing it through the optical unit[1]. Nozzles were typically able to drill approximately 100 holes before replacement was required.

4.4.2.5 Supply Head and Stabilizer

The supply head [4] was threaded onto the adapter [5] and thus secured the inlet tube [7]. It was loosely fitted to the adapter so that the inlet tube could remain stationary while the drilling unit was orbiting. If the supply head was tightened too firmly, then the rubber tube carrying the air abrasive stream from the SS White machine became twisted and entangled. The stabilizing unit helped to avoid this happening. It consisted of the following:

- a stabilizer rod [28] - the other end of the stabilizer arm fitted around it.
- a stabilizer arm [29] - this held the inlet tube with a grub screw.
- a stabilizer base [30] - this is not shown here to avoid cluttering and can be seen in the parts drawings of Appendix D. It was attached to the belt casing lid [9] and the stabilizing rod was attached to it.

4.4.2.6 Vacuum Extraction and Sealing

As mentioned previously, there was a necessity for a vacuum extraction unit. This was achieved by placing the vacuum shroud [2] over the work surface and connecting a domestic vacuum cleaner to the vacuum outlet tube. Debris was sucked from the work surface, and passed between the running tube [21] and the

air tube housing [6] and through the vacuum holes in the running tube [21]. The vacuum housing [16] had two o-rings [20] on its inside. They created a seal between the running tube [21] and the vacuum housing [16] so that no abrasive particles were able to come into contact with moving parts.

A seal was created on top of the running tube by placing a neoprene seal [14] over the opening and clamping it down with an end washer [13], which was secured with a fastening nut [27].

4.4.2.7 Offset and Tilt Adjustment Facility

The offset adjustment facility consisted of two grub screws threaded through opposite sides of the offset gimble [26], which was held centrally at the bottom of the running tube [21]. The grub screws were thus able to hold the air tube housing [6] in any position (within the gimble), thereby allowing for the adjustment of the nozzle offset, as shown in Fig 4.8

The tilt adjustment facility consisted of four equi-spaced screws, threaded through the grub screw collar [15]. They supported the top of the air tube housing [6], and by their careful adjustment in the same plane as the nozzle offset, the correct tilt could be achieved in order to create a vertically sided hole, as outlined in Section 4.2.2.

4.4.2.8 The Drive System

A drive system was required in the design so that the running tube [21] could be orbited (or rotated), once the correct tilt and offset had been set, so that the desired hole could be drilled. It consisted of an adapted Black and Decker cordless screwdriver motor (2.4 V, 24 rpm), two pulleys [18][19] and a timing belt [23]. The motor speed was controlled by a potentiometer which was located in a control box.

4.4.3 Guide Bush Fixture

The component numbers given in this section and the following

sub-sections refer to Fig 4.6 and to the drawings in Appendix D.

The guide bush was an extremely important feature of the unit. It remained in a fixed position providing a universal bush fixture for both the optical and drilling units, so that any specimen could be carefully aligned before drilling.

The guide bush fixture [1] was threaded with a 0.5mm pitch thread so that the optical and drilling units could be firmly attached by means of screwing on a securing ring [3] common to both. Similar thread also allowed for the fine adjustment of the guide bush in the guide clamp [25]. Furthermore the guide clamp was attached to a stand as shown in Fig 4.5 and Fig 4.7. As can be seen, a cross-vice supported on a wooden disc was placed on a base plate. This enabled the strain gauge rosettes attached to specimens to be carefully positioned under the guide bush with the aid of the optical unit. The wooden disc had a brass bush protruding from its centre, which was located in a drilled hole in the base plate to allow for a clamped specimen to be rotated. Once in the correct position, the disc was prevented from rotating by two clamps positioned on either side of it. The cross-vice was bolted to the wooden disc and possessed locking nuts to prevent further movement once a strain gauge rosette had been positioned.

4.4.3.1 Vacuum Shroud

A bayonet fitting was machined on opposite sides of the guide bush [1] so as to incorporate the vacuum shroud [2] during the drilling process. As mentioned previously, this enabled the abrasive particles used for drilling to be extracted so that effective, hazard free drilling could be achieved.

4.4.3.2 Air Bearing

The air bearing [24] was incorporated in the guide bush design so as to ensure accuracy of the optical unit when using it to align the fixed strain gauge rosettes with the optic axis (and axis of rotation) and hence with the drilled holes. It also

facilitated the measurement of the diameter, depth and taper of the drilled holes. Air required for its operation was tapped off the same compressed air supply used by the drilling unit. The air was introduced through a copper nozzle, which was pressed into the side of the guide bush housing, and passed through the air bearing orifices so as to keep the optical unit centred in the guide bush.

The air bearing was employed solely for the optical unit. A light coating of oil was applied to it when using the drilling unit so that there was lubrication between the metal contact surfaces. The oil was wiped off immediately after the removal of the drilling unit from the guide bush. The top surface of the air bearing bush provided a flat surface on which the optical and drilling units could be positioned.

4.4.4 Auxiliary Components

Auxiliary components required for the operation and calibration of the optical and drilling units include the following :

- Pneumatics and pneumatic circuit.
- Nozzle alignment and optical calibration jig.
- Stand.

4.4.4.1 Pneumatics and Pneumatic circuit

Any compressed air supply that could deliver a pressure of at least 5.5 bar was suitable for the operation of the unit. Since residual stress measurements to be taken with the unit were to be performed in a laboratory, it was decided to make use of the compressed air line used by the mechanical engineering workshop. As dry air was required to prevent clogging of the abrasive particles, a Festo pressure regulator with a filter and moisture trap (type LFR 1/8-8-0, series 3478, EDV Nr 10578) was placed in the pneumatic circuit, as shown in Fig 4.9.

Next a T-piece was placed in the circuit, with valves on its branches, so that air could be directed either to the SS White

machine, when drilling, or to the air bearing, when using the optical unit. Reference 89 provides a description of the pneumatic circuit of the SS White machine.

4.4.4.2 Nozzle Alignment and Optical Calibration Jig

The component numbers given in this section refer to drawings in Appendix E and Fig 4.10.

An additional item which was required for the design was the nozzle alignment and optical calibration jig, which enabled the optical unit to be centred and the correct nozzle offset to be set.

In order to achieve this, an alignment jig similar to an elongated v-block [1] was designed. A v-block holder [4] was designed to be screwed into the bottom of the v-block [1] so that the device could be held in a vice. Since the running tube of the drilling unit and the optical tube holder of the optical unit were designed to have the same outer diameter, the correct nozzle offset was achieved by clamping them on either side of the v-block [1], with the aid of the securing block [2] and securing plate [3], so that the nozzle tip was in focus when viewing it through the optical unit. By adjustment of the appropriate grub screws, the nozzle could be offset the desired amount. The amount of offset was measured with the micrometer head of the optical unit.

In order to centre the optics, an alignment cylinder [5] was designed. The cylinder had the same diameter as the optical tube holder (of the optical unit) and had an edge in the centre of one of its ends on which the optics could be focused and centered.

It was noted however that due to lack of stiffness of the stand and slight inaccuracies in the drilling and optical units, the alignment cylinder did not allow for a strain gauged specimen to be accurately positioned below the guide bush. This problem and its solution together with other problems encountered are

discussed in Section 4.5.

4.4.4.3 Stand

The component numbers given in this section refer to drawings in Appendix E and Fig 4.11.

The stand consisted primarily of a base plate [1], support plate [3], and a shaft [4]. Its function was to hold the optical and drilling units at a certain distance above the work surface. It can also be seen in Fig 4.5 and Fig 4.7.

4.5 Problems and Modifications of the Initial Design

As with most designs, certain problems were encountered when initially testing the units as well as during later stages. These are discussed below, with drawings in Appendix F.

4.5.1 Slipping of the Air Tube

Due to the high pressure required by the system, it was found initially that the air tube, [8] of Fig 4.6, slipped within the air tube housing, [6] of Fig 4.6. This was obviously unacceptable, because apart from rendering the system inoperative, the sapphire nozzles could be crushed. The problem was overcome by machining flats on the nut of the air tube, [2] of Appendix F, and tapping a hole in the air tube housing, [1] of Appendix F. Thus the air tube could be held in place by a grub screw, screwed through the air tube housing.

4.5.2 Seating of the Inlet Tube

With the bottom end of the inlet tube, [7] of Fig 4.6, being conical as well as the nylon insert of the air tube, [8] of Fig 4.6, on which it rested, bad seating could occur which led to excessive leakage of abrasive particles. To resolve this problem, the conical end of the inlet tube was rounded, [3] of Appendix F, so that better seating could be obtained.

4.5.3 Unscrewing of the Supply Head

As the supply head, [4] of Fig 4.6, was loosely tightened to the air tube housing, [6] of Fig 4.6, in such a way that the inlet tube, [7] of Fig 4.6, would not be clamped, it was found that the supply head had a tendency to unscrew during the drilling operation. This problem was rectified by securing it with a lock nut, [31] of Fig 4.12, added above the fastening nut, as can be seen in this figure.

4.5.4 Jamming of the Inlet Tube

When using fine particles, it was extremely difficult to maintain a dust free environment, due to leakages and imperfect vacuum extraction. As a result, it was found that the inlet tube, [7] of Fig 4.6, occasionally jammed, even though it was only lightly held between the inlet tube and the supply head. To help overcome this problem, thin teflon washers, [32] of Fig 4.12, were made to fit on either side of the collar of the inlet tube.

4.5.5 Misalignment of Adjusting Screws

Upon assembly of the drilling unit, it was found that the nozzle offset adjustment screws and the tilt adjustment screws were not in the same plane. This would lead to obvious difficulties when attempting to create the correct hole profile. This problem was easily rectified by removing some material from the bottom of the air tube housing, [1] of Appendix F.

4.5.6 Frictional Effects Due to the O-rings

It was found that the o-rings, [20] of Fig 4.6 created more resistance than was expected on the running tube, [21] of Fig 4.6. By replacing them with lip seals the problem was overcome and the running tube was able to run with little resistance.

4.5.7 Moments Exerted on the Running Tube

Even though the timing belt, [23] of Fig 4.6, was not fitted tightly over the pulleys, [18] and [19] of Fig 4.6, it was found that it exerted a noticeable moment on the running tube, [21] of Fig 4.6. As a result the running tube tilted against the spigotted collar, which created problems during the operation of the drilling unit. These problems were at first undetected, but with use, the running tube was found to seize occasionally. This problem was temporarily overcome by slightly increasing the internal diameter of the spigotted collar, [12] of Fig 4.6, and placing a nylon bush between it and the running tube.

4.5.8 Lack of Stiffness of the System

Due to the slight lack of stiffness of the stand arrangement and possible misalignment errors in the design, it was found that the drilled hole was not always located correctly, even though the optical unit was perfectly centred. As explained later in Chapter 5 (in calibration procedures), this problem was overcome by specifying a specific orientation of the optical and drilling units in the guide bush, and centering the optical unit on a drilled hole. Also, a retort stand was provided to hold the vacuum hose, from the vacuum extraction unit, as it created a moment, and hence deflection, on the system due to its weight.

4.5.9 Tilt Adjustment of the Air Tube Housing

The air tube housing, [6] of Fig 4.6 was cylindrical where the tilt adjusting screws tightened against it. This would make it difficult to have control over the amount of tilt of the system, due to there not being a common reference surface once the air tube housing was tilted. Also, the tilt adjustment screws had flat ends, which did not provide a satisfactory contact point. To overcome this problem, flats were machined on the air tube housing, [1] of Appendix F, and the ends of the tilt adjustment screws, [4] of Appendix F, were rounded.

4.6 Summary

In this chapter, the requirements of the AACH drilling device were analysed. Based on this, the design was undertaken with the assistance of C.S.Clarke[90]. This was followed by a discussion of problems and modifications of the initial design which were encountered upon initial testing of the system. Fig 4.13 shows the setup of the AACH drilling equipment, with the drilling unit held in the guide bush and the other components placed around it. In the next chapter, experimental details and the test programme are discussed.

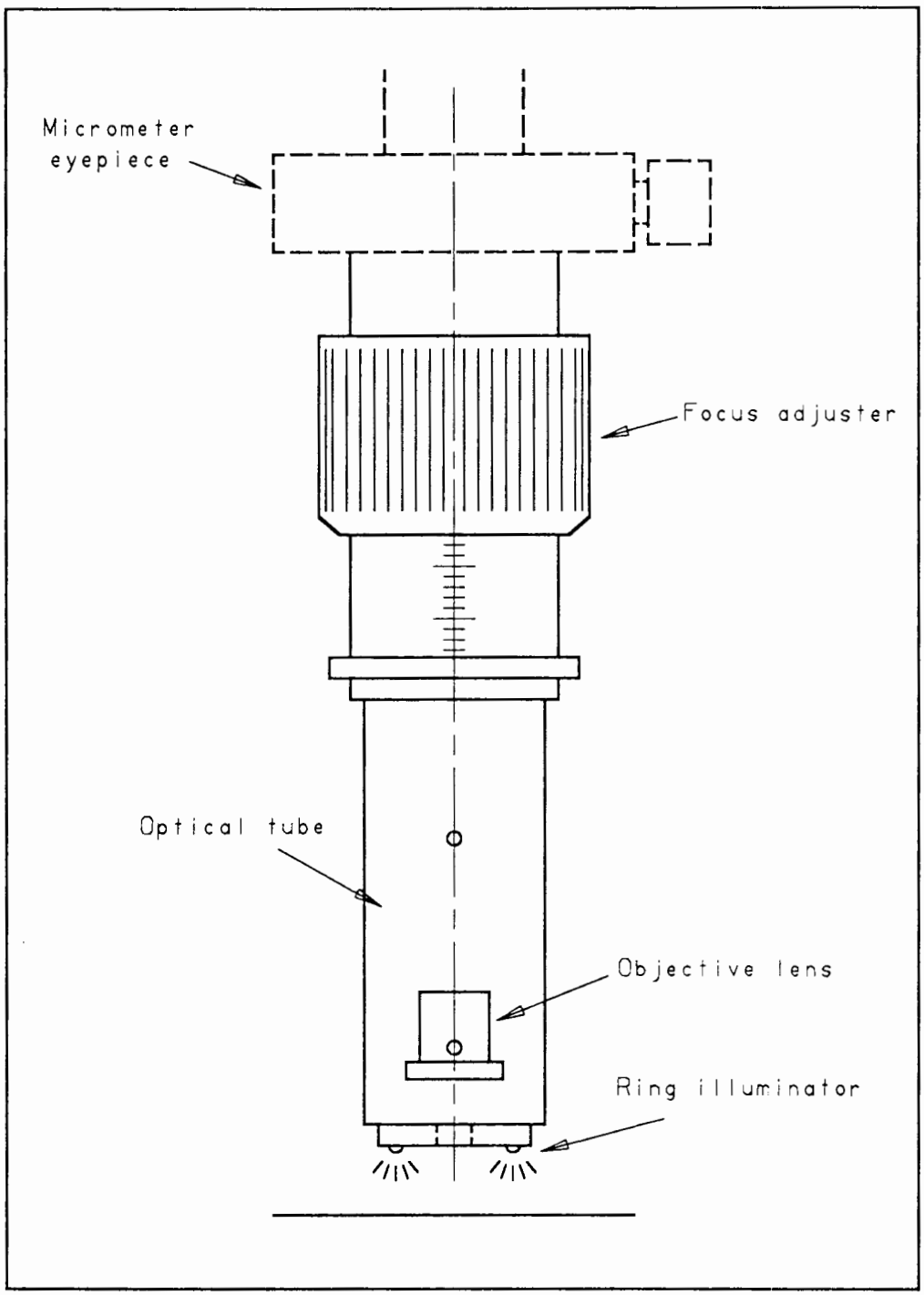

Fig 4.1 - The preliminary design of the optical unit.

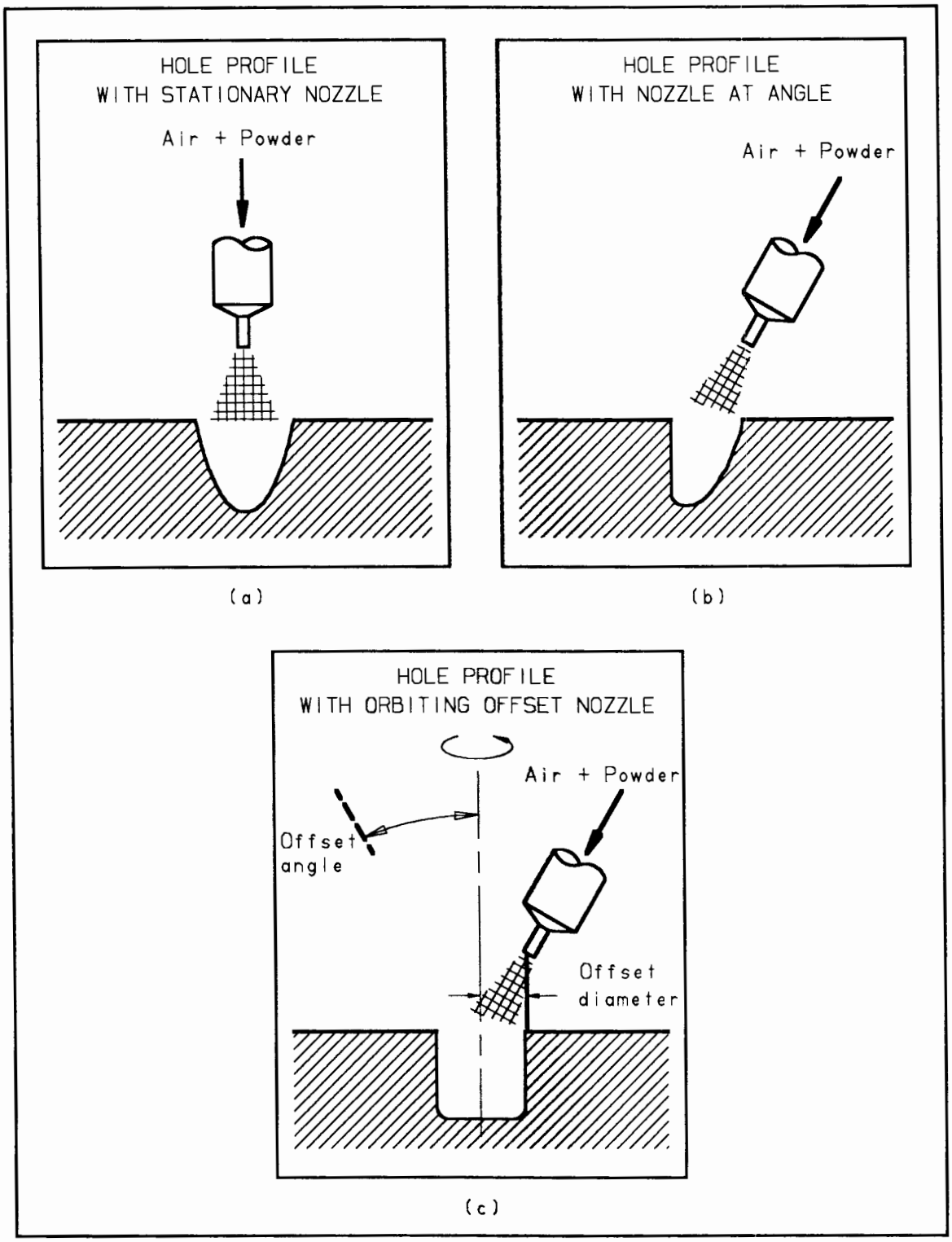

Fig 4.2 - Various hole profiles for different nozzle orientations. If a nozzle was held vertical (a), then an unacceptable tapered hole was produced. By tilting the nozzle (b), it was possible to produce a hole with one "vertical" side. By tilting and offsetting the nozzle and allowing it to orbit (c), it was possible to produce the required hole geometry.

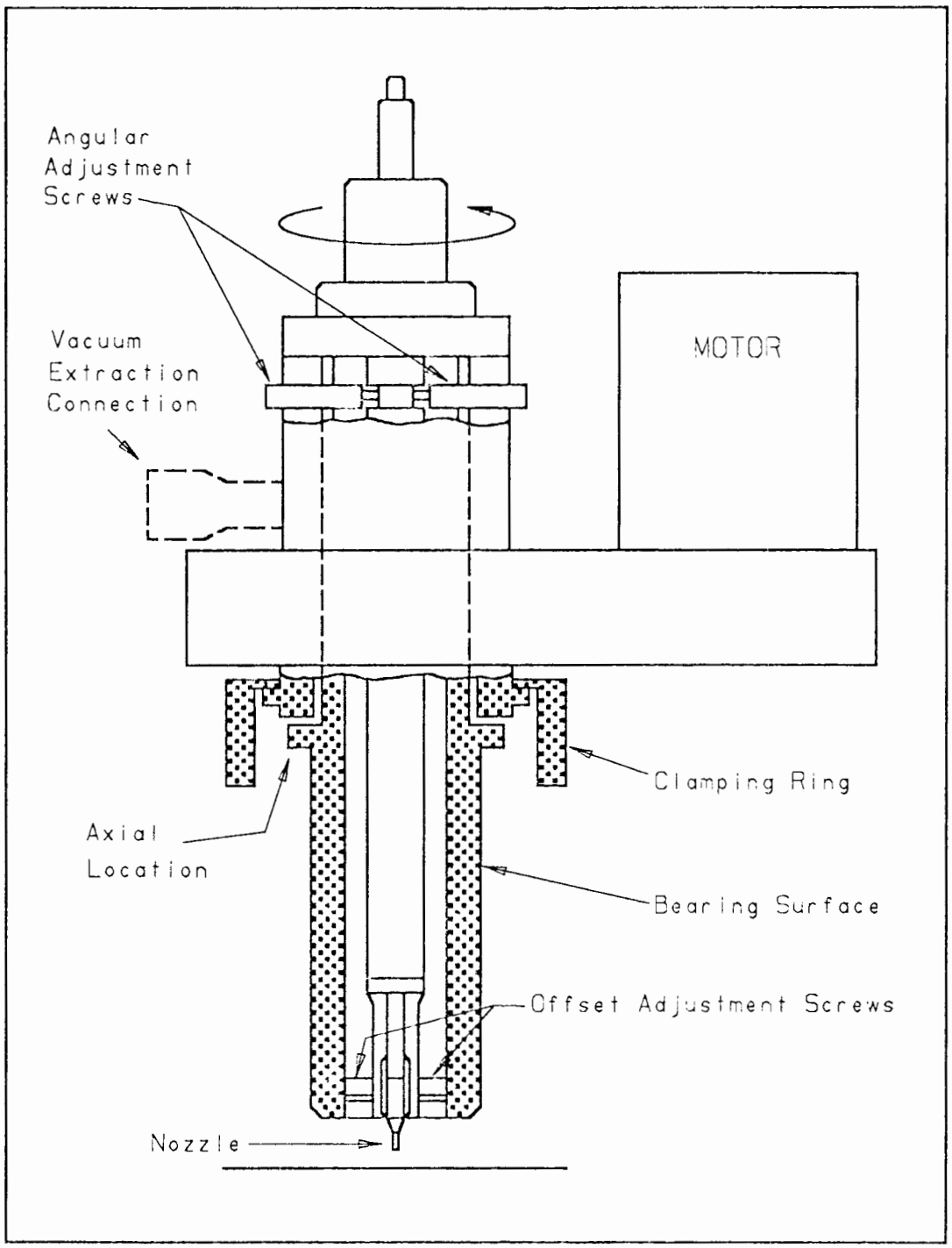

Fig 4.3 - The preliminary design of the drilling unit.

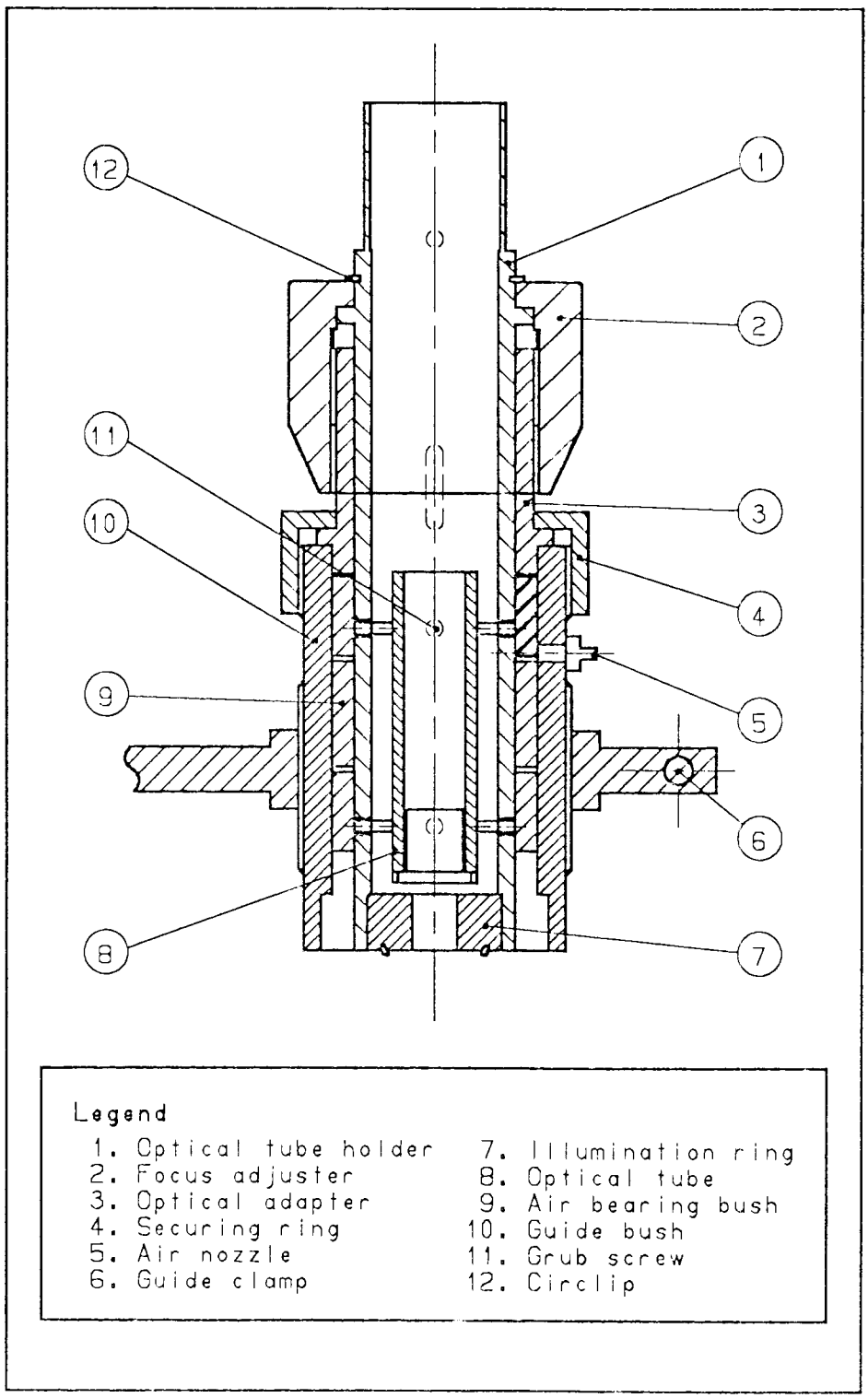

Fig 4.4 – Assembly drawing of the optical unit (but without the removable Vickers hardness type eyepiece).

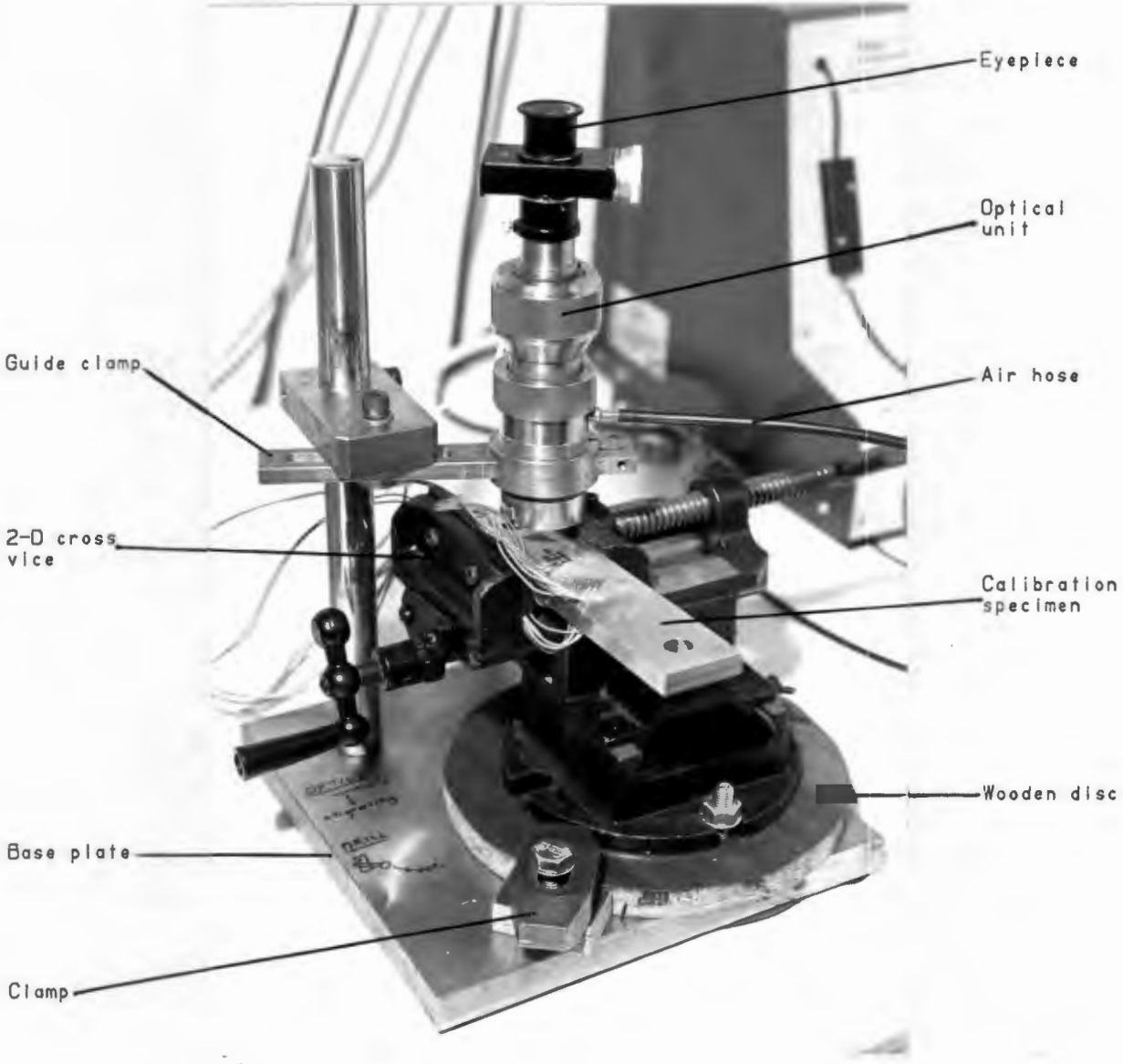

Fig 4.5 - Photograph of the optical unit. Note, from the top, the optical unit, which is held in the guide clamp, can be seen. Beneath it is a calibration specimen which is held in a 2-D cross vice, so that it can be accurately positioned below the optical unit. The cross vice in turn is secured to a wooden disc, which is able to rotate. Beneath the wooden disc is the base plate on which the recommended orientation of the optical unit and guide clamp can be seen, in order to compensate for misalignment effects.

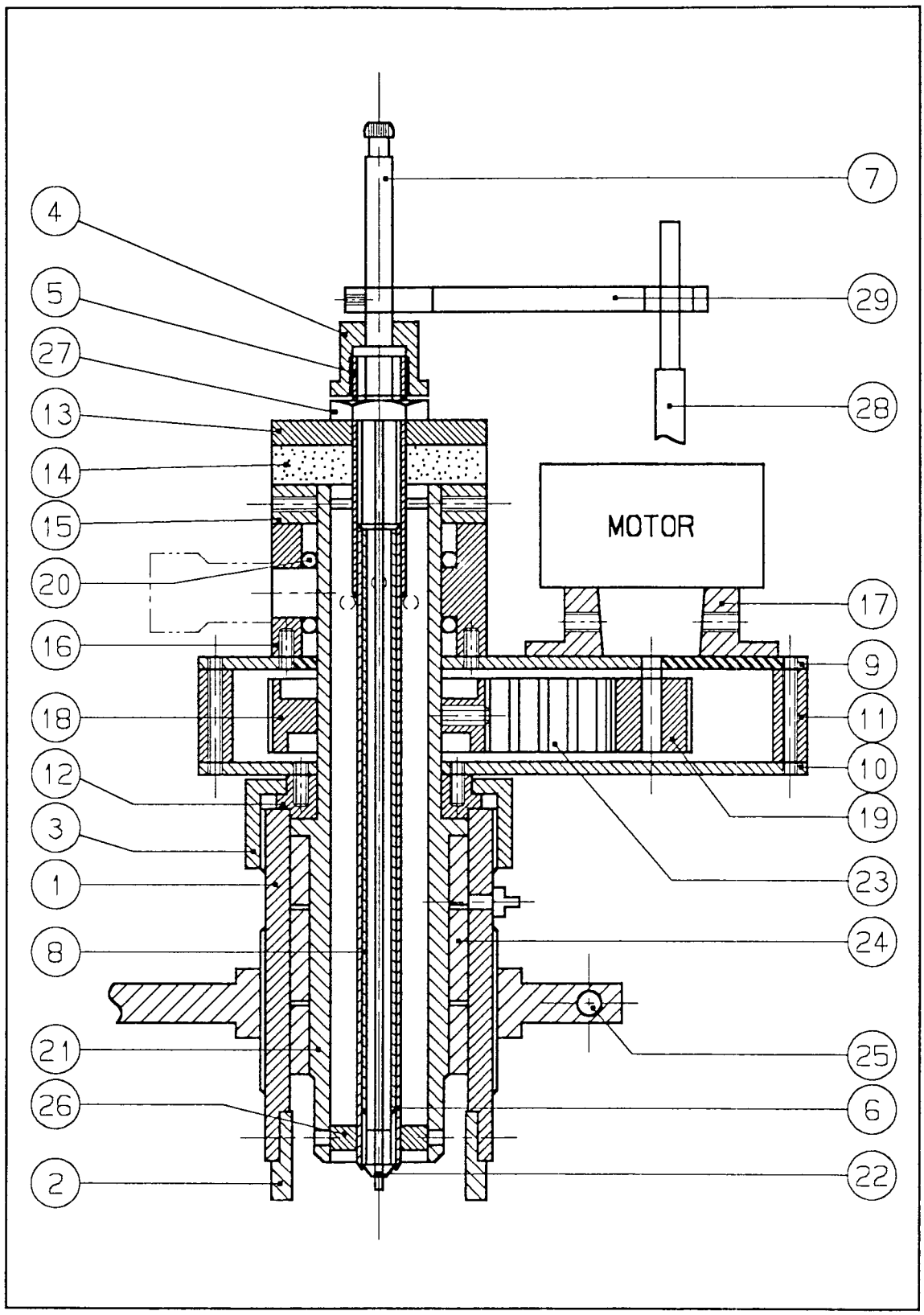

Fig 4.6 - Assembly drawing of the drilling unit.

Note: The legend is overleaf.

Legend for Fig 4.6.

1. Guide bush
2. Vacuum shroud
3. Securing ring
4. Supply head
5. Adapter
6. Air tube housing
7. Inlet tube
8. Air tube
9. Belt casing lid
10. Belt casing bottom
11. Belt casing wall
12. Spigotted collar
13. End washer
14. Seal
15. Grub screw collar
16. Vacuum housing
17. Motor mounting
18. Timing belt pulley
19. Timing belt pulley
20. O-ring
21. Running tube
22. Sapphire nozzle
23. Timing belt
24. Air bearing bush
25. Guide clamp
26. Offset gimble
27. Fastening nut
28. Stabilizer rod
29. Stabilizer arm
30. Stabilizer base (not shown)

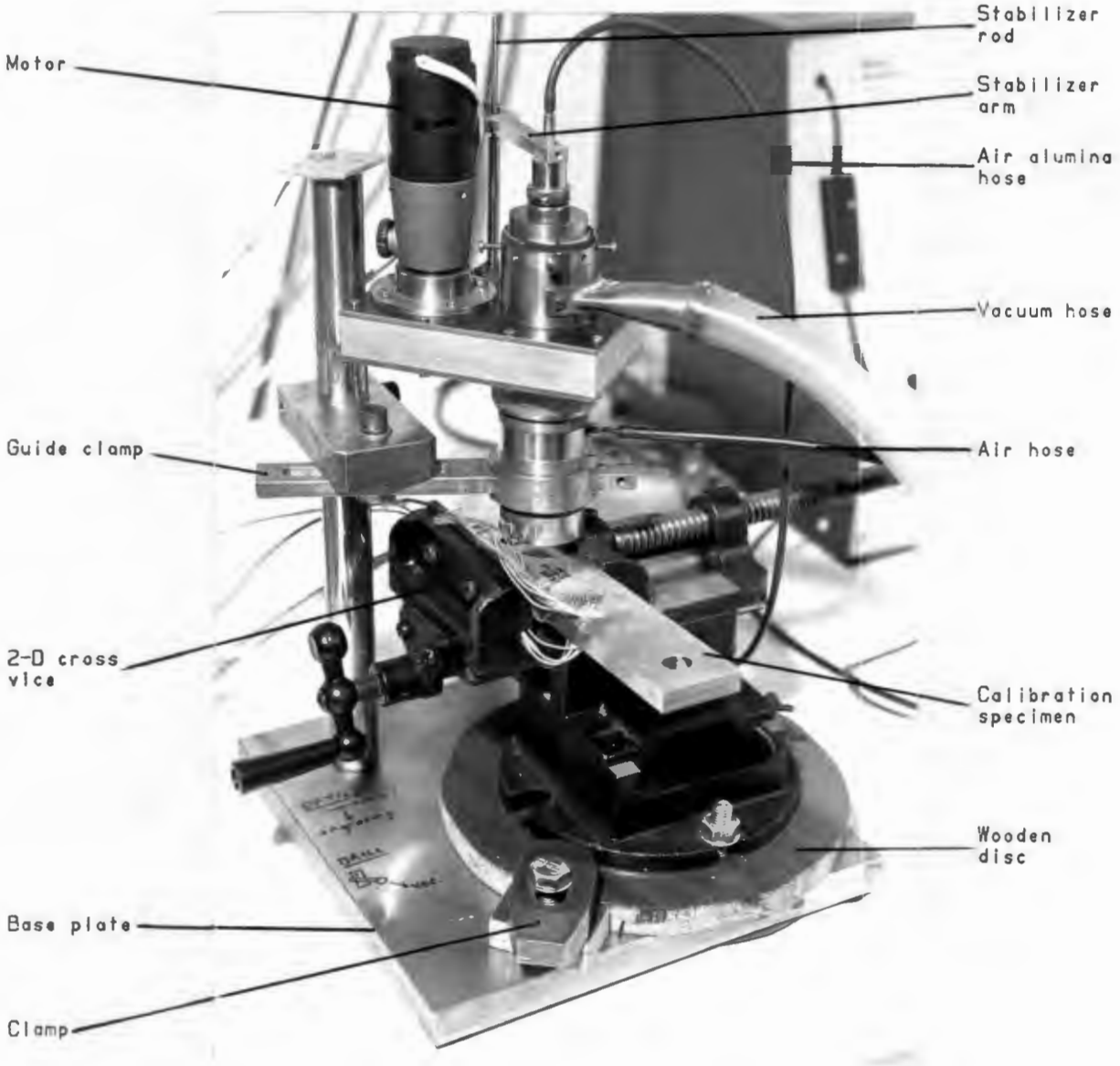

Fig 4.7 - Photograph of the drilling unit. Note, from the top, the drilling unit can be seen held in the guide bush with the air-alumina and vacuum hoses connected to it. The rest of the components in the photograph are as in Fig 4.5.

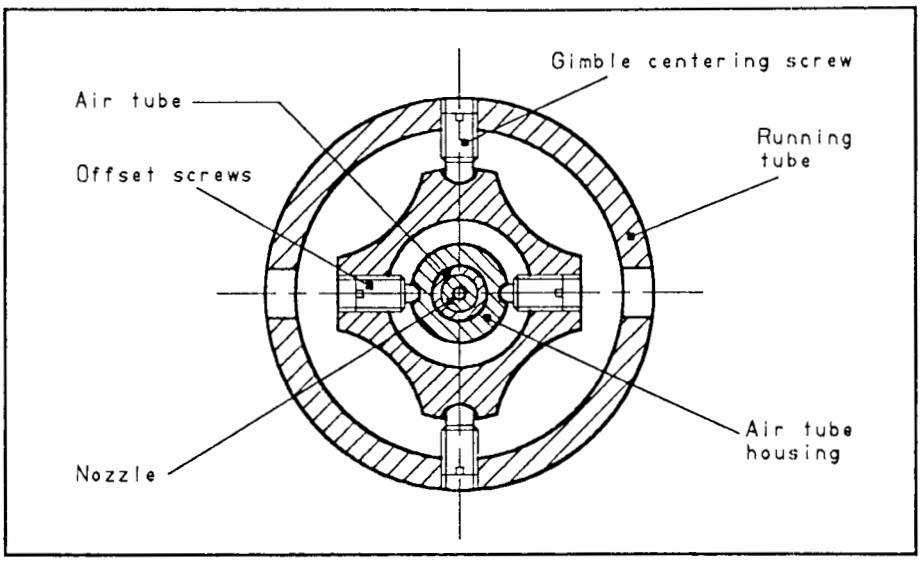

Fig 4.8 - Bottom view of the offset adjustment facility. The offset screws were used to offset the air tube housing (and thus nozzle) the required amount. Tilt adjustment was required to be made in the same direction as the offset adjustment - horizontal in this figure.

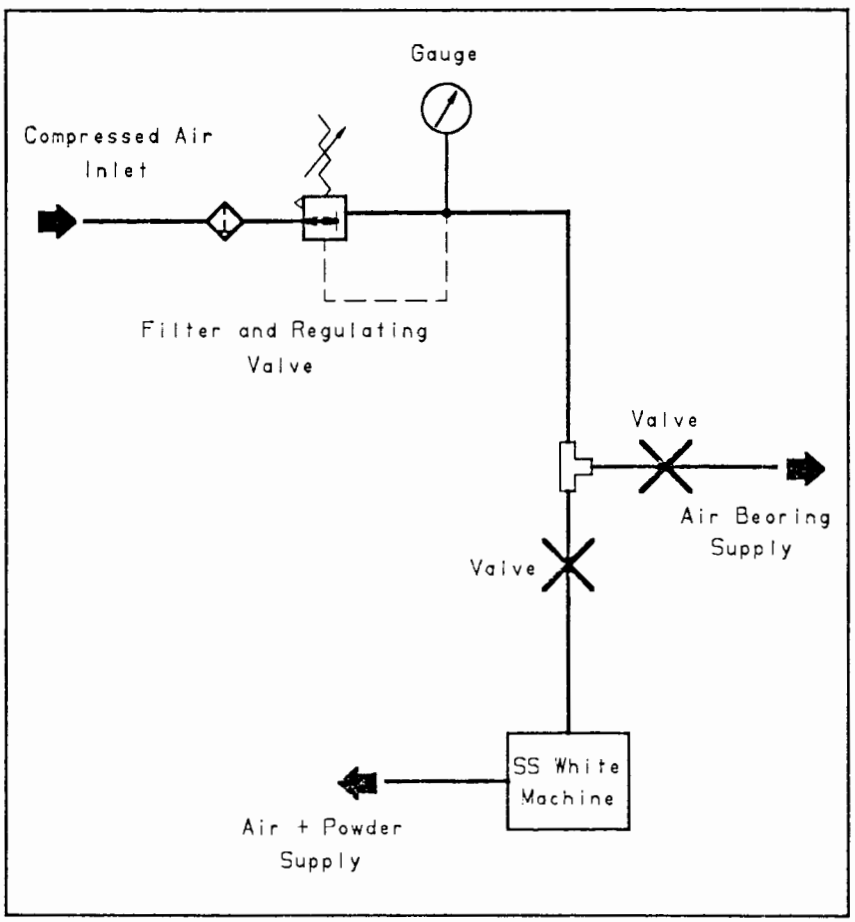

Fig 4.9 - The pneumatic circuit.

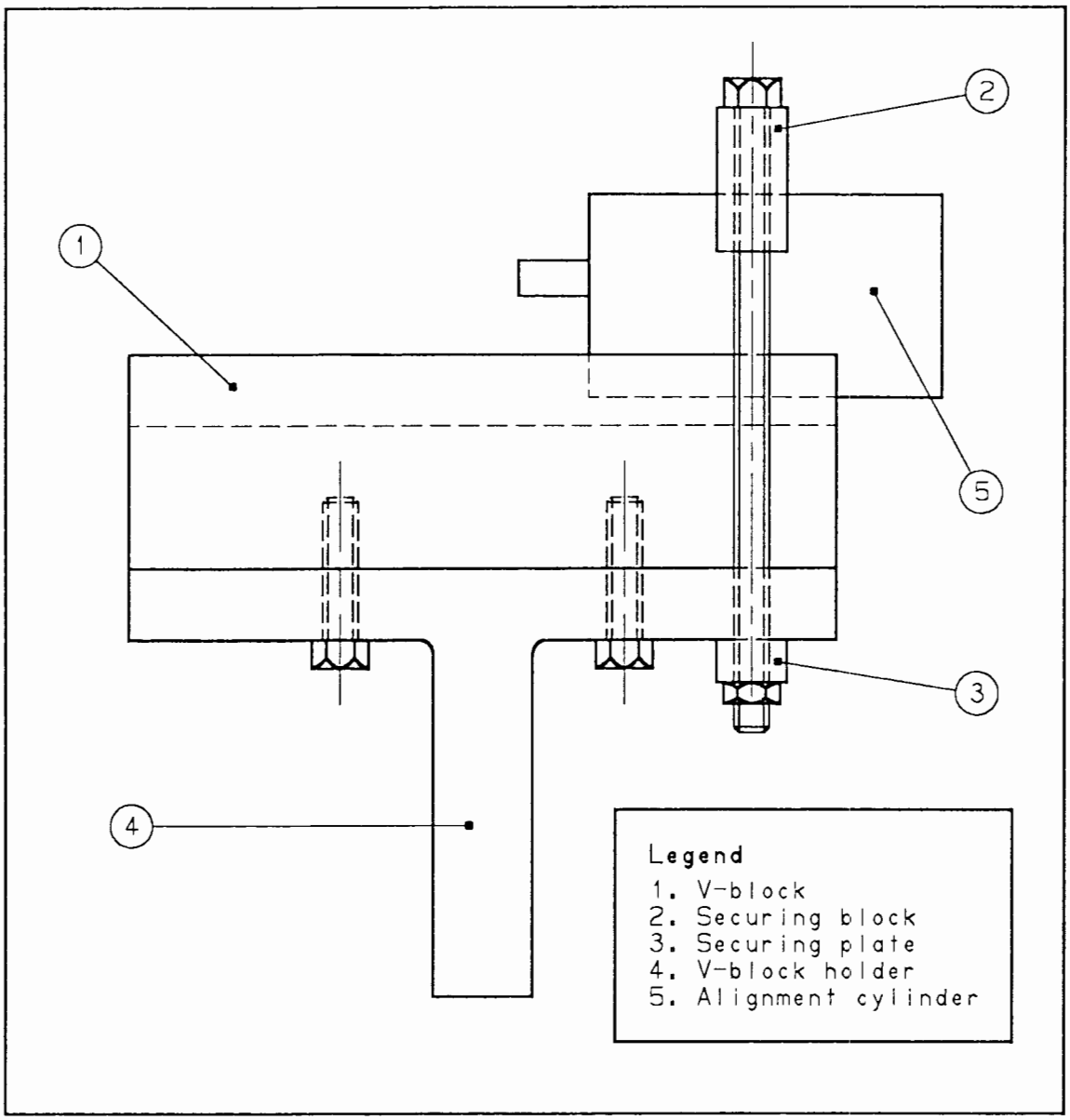

Fig 4.10 - The alignment jig with the alignment cylinder which was intended to be used for centering the optical unit.

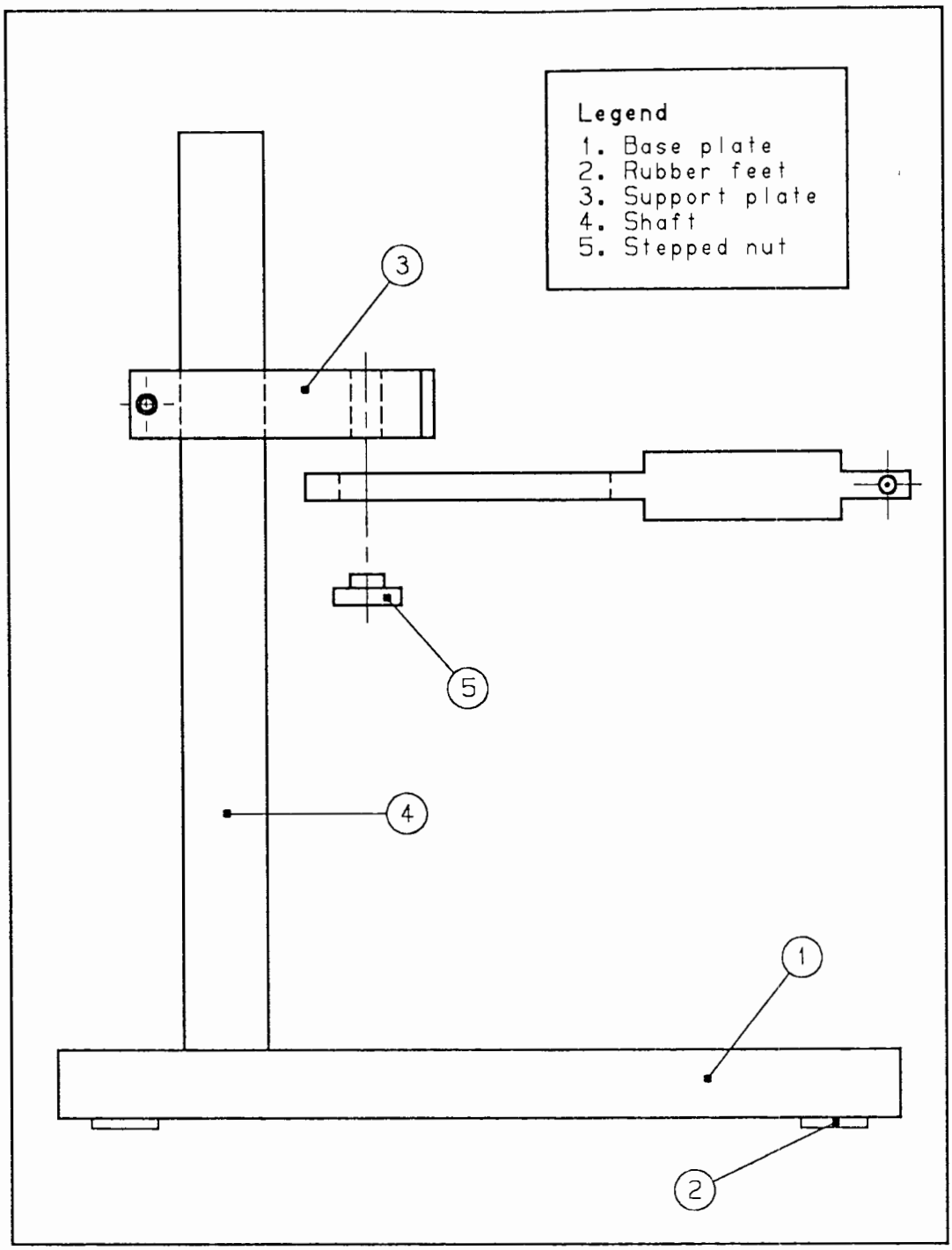

Fig 4.11 - The stand arrangement used to hold the optical and drilling units.

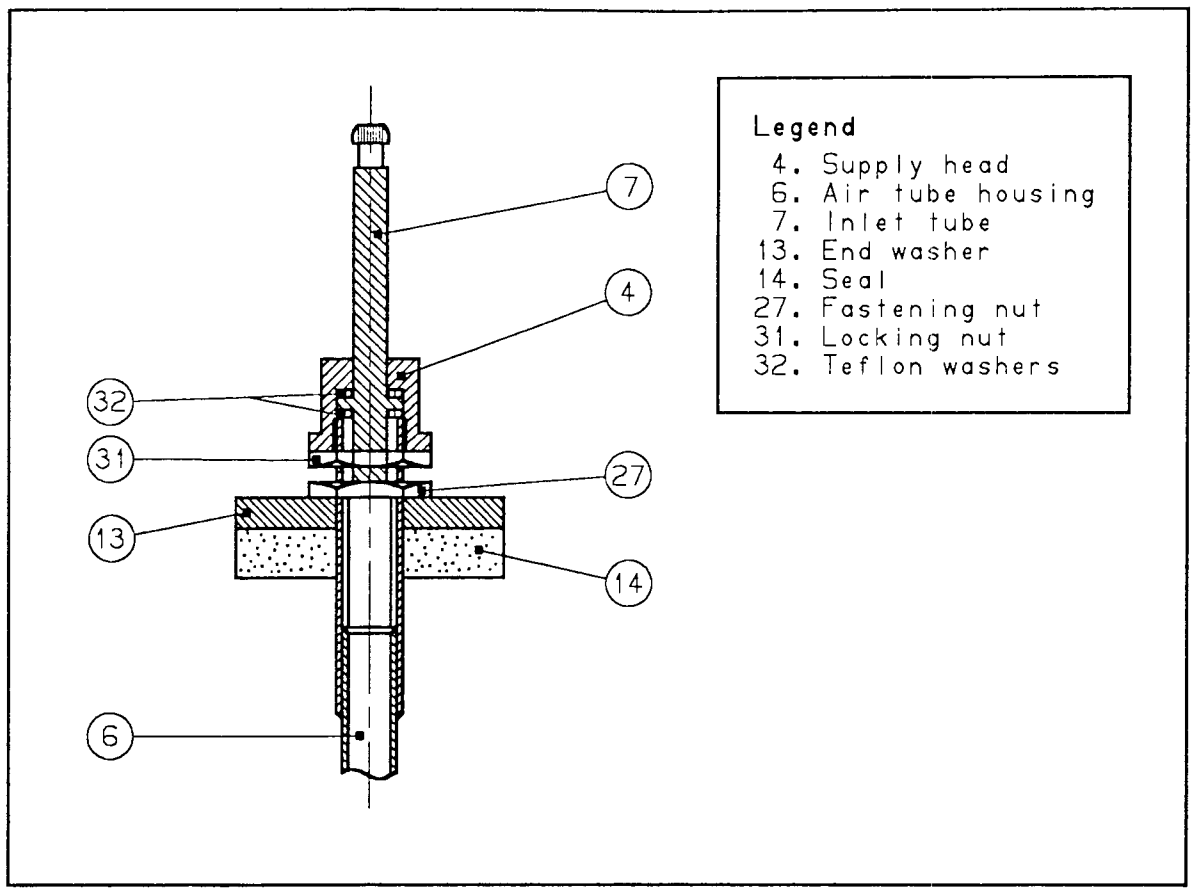

Fig 4.12 - Modifications to the top end of the drilling unit. A lock nut (31) was added to prevent the supply head (4) from loosening. Teflon washers (32) were added on either side of the inlet tube collar (7) to prevent it from jamming. Note that non-sequential numbering has been used so that the numbers correspond with those in other drawings.

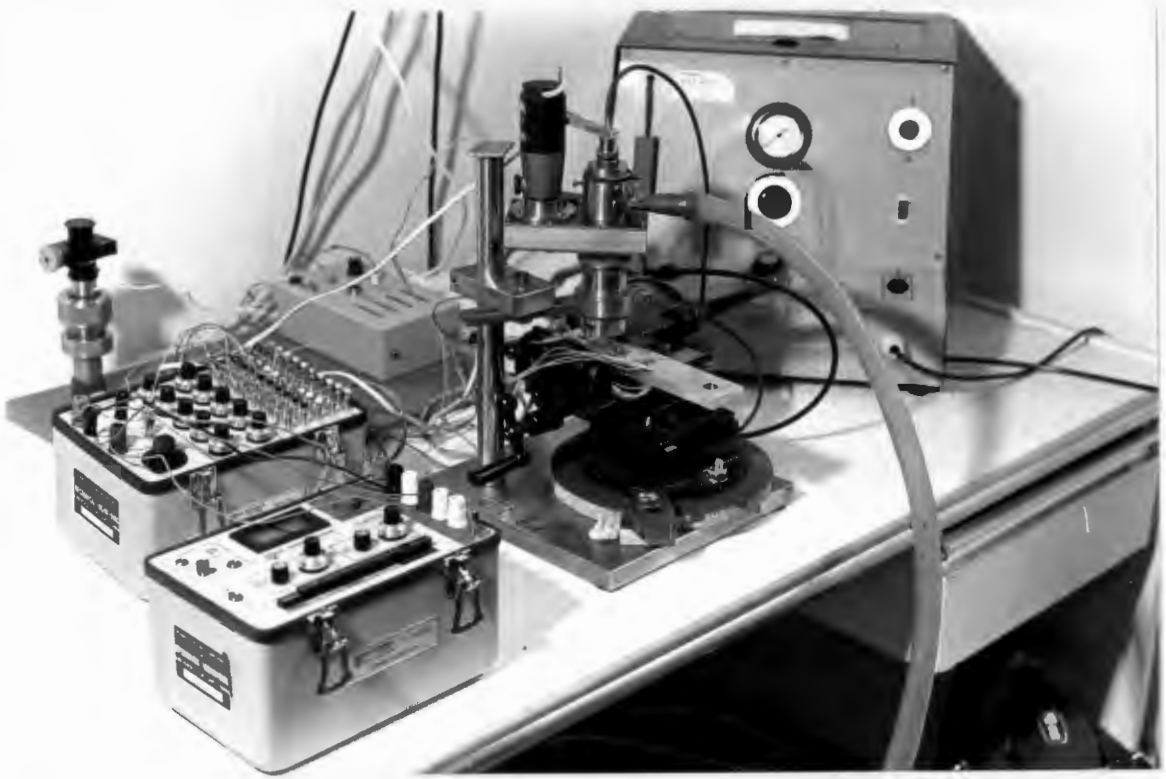

Fig 4.13 – Setup of the AACH drilling rig. In the centre of the photograph, the drilling unit can be seen in the stand arrangement. Around it (from the lower left corner in a clockwise direction) are the strain gauge amplifier and ten channel selector switch, the optical unit in the background, the electrical control box and the SS White Airbrasive Model K machine.

5. EXPERIMENTAL DETAILS

5.1 Introduction

After design and fabrication of the facility, calibration of the system was required. Test procedures were also required to be established and the necessary equipment acquired in order to perform a typical AACH measurement, as well as a typical ring splitting residual stress measurement. Also presented in this chapter is a discussion of the specimen drill rods that were provided by Hulett Aluminium as well as the specific test programme that was conducted when analysing the residual stresses present in these rods.

5.2 The Air Abrasive Centre Hole Drilling Device

The AACH drilling device was described in the previous chapter. The optical and drilling units were designed so that they would both be able to be located in the guide bush so that the facility could be aligned to a "target" strain gauge rosette before drilling the required hole in it. As mentioned previously the air bearing was only used (i.e. supplied with pressurised air) when using the optical unit, so that the optical unit could be centred in the guide bush. When using the drilling unit, the air bearing was lightly lubricated with oil in order to prevent frictional effects. Thereafter the oil was immediately removed from its surface so as to prevent particles or debris adhering to the oil and consequently damaging the air bearing and drilling unit surfaces in subsequent use.

5.3 Calibration of the Air Abrasive Centre Hole Drilling Device

5.3.1 The Optical Unit

There were two particular features that needed to be calibrated on the optical unit - magnification and centering.

5.3.1.1 Magnification

The optical unit was calibrated with the aid of an etched graticule. The etching consisted of a 1 mm line divided into 0.01 mm divisions. The optical unit was focused on the graticule, and by rotating the crosshair micrometer, the adjustable crosshair was shifted across the 1 mm etching. The reading on the micrometer thus corresponded to a 1 mm object size. The process was repeated ten times, and the results are shown in Table 5.1.

As can be seen, the optical unit had a magnification of 3.702 ± 0.006. This process was repeated and checked intermittently during experimentation, with no significant change.

5.3.1.2 Centering of the Optical Unit

Since the drilling unit was heavier than the optical unit, it caused a larger deflection of the guide clamp (part 6 in Appendix C and part 25 in Appendix D) due to a cantilever effect. As a result it was found that even though the optical unit was perfectly centered using the optical calibration jig, slightly off-centred holes were produced. This problem was easily overcome by a small alignment adjustment of the optical unit which compensated for the hole offset. The nett effect was that targets focused on by the optical unit, for example the centre of a strain gauge rosette, could be precisely drilled by the drilling unit, with no further significant offset. By maintaining a specified orientation of the optical unit when using it in the guide bush, this slight misalignment of the optical axis would not affect the optical unit's aiming capability.

The above procedures were carried out and found to work well. Furthermore, the misalignment of the optical axis did not affect the other functions of the optical unit, namely hole depth and diameter measurement, since only its focusing abilities were

required for these tasks. An orientation was also specified for the drilling unit when it was to be used in the guide bush since it had an eccentric centre of gravity with respect to the guide bush and could thus create a varying cantilever effect if used in different orientations. This orientation together with the one specified for the optical unit was marked on the base plate as can be seen in Fig 4.5 and Fig 4.7.

5.3.2 The Drilling Unit

There are three features related to hole dimensions - diameter, depth and wall angle - which were needed to be calibrated with the aid of the drilling unit.

5.3.2.1 Hole Diameter

The hole diameter is affected by the nozzle offset, which could be adjusted by the grub screws located in the offset gimble. It is also slightly affected by the tilt of the air tube. Therefore when comparing hole sizes for given nozzle offsets, it is implied that the tilt has been adjusted so that the desired vertically sided hole was obtained.

Due to the minor adjustments of the optical unit the following method was used when adjusting the nozzle offset. The drilling unit was secured on the one end of the alignment jig with a PVC clamp, as shown in Fig 5.1, so that a specially marked angular adjustment screw was in a horizontal position. This ensured that the nozzle would be offset in the correct plane. The optical unit was secured on the opposite side of the v-block with a PVC clamp, as shown in Fig 5.1, with the depth engraving on the "optical tube" and crosshair micrometer collinear with the specially marked angular adjustment screw. The drill nozzle was then offset the required distance in the opposite direction of the specially marked angular adjustment screw, with the aid of the crosshairs in the eye-piece. Table 5.2 relates the approximate hole diameters with a given nozzle offset, as determined experimentally.

5.3.2.2 Hole Depth

The depth of the hole was mainly governed by elapsed drilling time. It is also affected by the hole diameter, pressure, powder flow and the type of material to be drilled. If the pressure and powder flow settings were set as recommended, ie. 5.5 bar and 6.5 - 6.75 respectively, then for a hole size of approximately 1.5 mm in diameter and depth in aluminium, a drilling time of approximately 5 minutes was required.

Several holes were required to be drilled in some scrap material of the type to be used for performing residual stress measurements before attempting to drill into any test specimens or components. This gave the operator the ability to refine the drilling time required and ensured more consistency and hence better results.

5.3.2.3 Wall Angle

Once the nozzle offset was fixed, the angle of the hole wall depended on the tilt of the air tube ([8] of Fig 4.6).

i. Notation

A positive or negative number is used to describe the amount of tilt of the air tube. The magnitude of the number indicates the number of half revolutions through which the angular adjustment screws needed to be turned to offset the air tube from its centred position. The sign indicates the direction of tilt relative to the nozzle offset. This is more clearly explained in Fig 5.2. Configuration (a) shows the air tube perfectly centred in the drilling unit with zero tilt and zero nozzle offset. If the nozzle were then offset, as shown in configuration (b), the tilt would still be regarded as zero, since the top of the air tube is still in the central position which is a useful point of reference. By offsetting the top of the air tube in the same direction as the nozzle offset relative to the axis of orbiting rotation, as shown in configuration (c), the tilt would be regarded as

positive. Tilting in the opposite direction would give negative tilt as shown in configuration (d). Table 5.3 shows how the value of tilt (measured in degrees) compares to the tilt notation used.

ii. Tilt variation

Before performing the calibration experiment for hole wall angle as a function of the tilt of the air tube, some thought was given to the various optional configurations in which the combination of tilt and nozzle offset could possibly produce holes with vertical walls. This is shown in Fig 5.3. As can be seen, if there is negative tilt for a given nozzle offset, then it may well be possible to form the desired hole. If there is a positive tilt, it is not possible to produce the desired hole if the air tube is tilted past the vertical position and the abrasive stream does not cross the axis of rotation as shown in Fig 5.3(b). However for other configurations, as shown in Figs 5.3(a) and (c), the required hole profile may be obtained.

When tilt was calibrated, a number of holes were drilled with a given nozzle offset and varying tilt so that the desired vertically sided hole could be obtained. The offset was chosen so that the correctly drilled hole would have a diameter of approximately 1.5 mm. There were two methods employed to determine the wall angle of the holes. The first method, which was a somewhat qualitative one, involved using the optical unit to scan the hole side walls from top to bottom. This was achieved by focusing on the top of the hole and slowly adjusting the focus until the bottom of the hole could be seen. Tapered sides were noticed due to their illumination by the ring illuminator, located at the bottom of the optical unit, as an infocus annular surface, rather like a confocal microscope.

The second method, which was a quantitative and more rigorous approach, involved sectioning the holes. This was achieved by milling followed by local polishing of the drilled specimens.

If the milling technique alone was chosen, care was taken to avoid deformation of the hole, and/or the formation of burrs on the sectioned edge. This milling approach, correctly undertaken, was used in a series of tests to evaluate wall angle and taper effects. After sectioning, the sectioned holes were viewed through a Mitutoyo profile projector and the slope of the hole walls was measured. The results of this calibration are given in Fig 5.4. It was found that the best results were generally obtained when the value of tilt was between 0 and -1. (It must be remembered that a tilt of 0 does not indicate that the drilling rod is vertical, since as shown in Fig 5.2 the value of tilt is relative to the axis of rotation and not nozzle offset.)

5.3.3 Evaluation of the Equation Constants

The residual stress equations derived in Appendix A are rewritten below:

$$\sigma_{\frac{1}{2}} = -\frac{E}{2}\left(\frac{1}{K_1}\right)\left[\frac{\varepsilon_1 + \varepsilon_3}{1-\nu K_2/K_1} \pm \frac{1}{1+\nu K_2/K_1}\sqrt{\left(\varepsilon_3 - \varepsilon_1\right)^2 + \left(\varepsilon_1 + \varepsilon_3 - 2\varepsilon_2\right)^2}\right] \quad \text{... eqn 5.1}$$

$$\alpha = \frac{1}{2}\tan^{-1}\left(\frac{\varepsilon_1 + \varepsilon_3 - 2\varepsilon_2}{\varepsilon_3 - \varepsilon_1}\right) \quad \text{... eqn 5.2}$$

As can be seen, the constants $1/K_1$ and $\nu K_2/K_1$ needed to be evaluated. Since it was difficult to induce a known residual stress in a material, the constants were found by applying a known uniaxial stress field to a calibration specimen, thus simulating a known residual stress field. The reason for using a uniaxial stress field was that, as shown in Appendix A, the equation constants conveniently reduce to the following under this condition:

$$\frac{1}{K_1} = \frac{\varepsilon_A}{\varepsilon'_A} \quad \text{... eqn 5.3}$$

$$\frac{\nu K_2}{K_1} = -\frac{\varepsilon'_T}{\varepsilon'_A} \quad \text{... eqn 5.4}$$

where: ε_A = applied axial strain

ε'_A = relaxed axial strain

ε'_T = relaxed transverse strain

Since it was not known whether any residual stresses were present in the calibration specimen, the following method, which is similar to that used by previous researchers[2,18,22,23,25,35,44] was followed:

i. An aluminium bar was loaded axially to various load levels within the elastic limit using an ESH servohydraulic testing machine. (Stresses needed to be kept below $0.3\sigma_y$ in order to prevent plasticity effects due to the hole which was to be drilled.) The corresponding strains under these loads were recorded.

ii. The specimen was unloaded and holes were drilled in the centre of the attached strain gauge rosettes.

iii. The calibration specimen was located back in the test rig, the strain gauge readings were reset to zero and the specimen was reloaded to the previous load levels with the corresponding strains again being recorded.

iv. The relaxed strains were calculated by subtracting the strains obtained in step (iii) from those obtained in step (i).

By using this method, any inherent residual stresses in the calibration specimen, such as rolled in stresses, were effectively cancelled out. It should be noted that a half bridge configuration for strain readings was used with 1/4 bridge active gauge and a dummy gauge on the specimen to compensate for

thermal effects. A photograph of the specimen and the experimental rig can be seen in Fig 5.5(a) and (b).

Two of these calibration experiments were performed. From the strains obtained in each experiment, the following constants were derived from the slopes of the appropriate graphs needed to describe them:

i. Young's Modulus (E): This was obtained from the slope of the graph of load before hole drilling versus axial strain.

ii. Poisson's Ratio (ν): This was obtained from the slope of the graph of transverse strain versus axial strain before hole drilling.

iii. $1/K_1$: This was obtained from the slope of the graph of relaxed axial strain versus axial strain before hole drilling.

iv. $\nu K_2/K_1$: This was obtained from the slope of the graph of relaxed transverse strain versus relaxed axial strain.

E and ν were checked against the values quoted by Hulett Aluminium, 71.5 ± 0.5 GPa and 0.33 respectively, to see if they were comparable, while the constants $1/K_1$ and $\nu K_2/K_1$ were compared to their documented CEGB values[1]. In addition to deriving these constants, stresses were recalculated using the relaxed strains substituted in the residual stress equations. For these calculations, the derived equation constants as well as the documented constants were used (for comparison sake) and the results were compared to the applied stresses.

For the first of the two calibration experiments an aluminium bar similar to that shown in Fig 5.5(a) and (b) and of dimension 191 mm x 40.3 mm x 10.02 mm, was used as a calibration specimen. Two hole drilling strain gauge rosettes were initially, perhaps naively, attached to one of its sides so that consistency of the

strain readings could be monitored. (After the experiment it was thought that the strain gauge rosettes should rather be placed on opposite sides to check for any bending.) The calibration specimen was loaded in load control in the servohydraulic machine, as this was more accurate. Slight hysteresis was evident from the load versus strain plot obtained from the load cell, and this was attributed to slight bending of the specimen.

The applied loads together with the strains recorded both before and after hole drilling can be seen in Table 5.4, and Table 5.5 respectively. From these results, the relaxed strains were calculated for the various loading conditions as shown in Table 5.6. From this data the constants E, ν, $1/K_1$ and $\nu K_2/K_1$ were calculated for both strain gauge rosettes, as described previously in this section, and the results are summarised below. The required graphs are shown in Fig 5.6 to Fig 5.15.

Strain gauge rosette #1:

$E = 77.9 \pm 2.0$ GPa

$\nu = 0.306 \pm 0.005$

$1/K_1 = 1.955 \pm 0.043$

$\nu K_2/K_1 = 0.282 \pm 0.024$

Strain gauge rosette #2:

$E = 76.4 \pm 0.5$ GPa

$\nu = 0.296 \pm 0.002$

$\frac{1}{K_1} = 2.207 \pm 0.007$

$\nu K_2/K_1 = 0.272 \pm 0.004$

As can be seen from the graphs, the plots generally intercept the y-axis close to zero. The results for Young's Modulus and Poisson's Ratio correlate to the values quoted by Hulett Aluminium to within 8% and 12% respectively. The holes drilled in the centre of strain gauge rosettes #1 and #2 had average diameters of 1.625 mm and 1,637 mm respectively. Therefore the values according to CEGB[1] for $1/K_1$ are 2.001 and 1.979 respectively. Thus the experimental error for this constant was within 5% of the CEGB[1] value. For the strain gauge rosette type used for the experiment (BLH type FAER-03S-12-SX-EG) the documented CEGB[1] value of $\nu K_2/K_1$ is 0.33. Thus the experimental error for this constant was within 20%. While this would appear

to be a poor result, it must be noted that the residual stress equations are not particularly sensitive to this constant[2], as will be discussed later in Chapter 6. Beaney and Procter[2] have also reported that the resulting error in the maximum numerical principal stress is in any case less than half the error in the constant.

The average recalculated stresses obtained using the derived constants are shown in Table 5.7 and Fig 5.14. The stresses were averaged to take into account any possibility of bending that might have occurred. As can be seen, the results were generally within 5% of the applied values. In fact, the error was as low as approximately 1% for the higher stress values. The values of the second principal stress agreed well with the expected value of zero, since a uniaxial stress was applied. However the values of angle α (alpha) were larger than their expected result of zero. The stresses were also recalculated using the documented constants for comparison sake, as mentioned previously. These are shown in Table 5.8 and Fig 5.15. These results are very close to the results obtained using the derived constants, and thus have similar errors.

Based on the results obtained, it was decided that the calibration experiment was reasonably accurate and that the constants derived compared well with their documented values. However it was decided to re-perform the experiment to check repeatability and to try to compensate for the slight bending effect. An aluminium bar with a cross-sectional area of 750 mm^2 was used with a hole drilling strain gauge rosette attached to each face. Two linear strain gauges were attached axially close to the rosettes, as shown in Figs 5.5(a) and (b). This would allow for the consistency of the strain gauge readings to be checked as well as any bending of the calibration specimen to be detected and eliminated, since as mentioned previously, it was suspected that bending could have affected the results of the first calibration experiment. In an effort to reduce or eliminate any bending effects, the calibration specimen was machined as accurately as possible. Also when placing it in the test rig, spacers were used to align it as accurately as

possible.

During experimentation, strain gauge rosette #2 became problematic. Furthermore it was found that the calibration specimen showed signs of bending. This was indicated by differing recorded strain values on the linear strain gauges on either side of the calibration specimen. In an effort to compensate for bending, the strains obtained for the remaining hole drilling strain gauge rosette were multiplied by a correction factor obtained by summing the results of the two linear strain gauges, divided by twice the value of the linear strain gauge reading on the corresponding side of the strain gauge rosette. The results of the experiment are shown in Appendix G in Tables G.1 to G.7 and Figs G.1 to G.6 and are summarised below:

Strain gauge rosette #1:

$E = 75.4 \pm 0.3$ GPa

$\nu = 0.312 \pm 0.007$

$1/K_1 = 2.350 \pm 0.027$

$\nu K_2/K_1 = 0.386 \pm 0.020$

As can be seen from the graphs, the plots intercept the y-axis closer to zero than in the case of the first calibration experiment (comparing Figs G.1 to G.6 with Figs 5.6 to 5.15). Therefore the incorporation of the strain correction factors to compensate for the effect of bending was considered successful. The results for Young's Modulus and Poisson's Ratio again correlated well with the values quoted by Hulett Aluminium - this time within 6%. The drilled hole had an average diameter of 1.514 mm, which corresponded in a CEGB[1] value of $1/K_1$ of 2.281. Therefore the experimental error of $1/K_1$ was within 3% of the CEGB[1] value. A similar hole drilling strain gauge rosette was used to that in the previous experiment, giving $\nu K_2/K_1$ a CEGB[1] value of 0.33. Thus the experimental error for this constant was within 15%. As discussed previously, this correlation is not as severe as might be expected, since the error in maximum numerical principal stress is less than half the error in this constant[2]. The recalculated stresses were within 5% of the applied stresses for the higher values, while

the values of the second principal stress were close to zero as expected, since a uniaxial stress was applied. For this experiment, the values of the angle α (alpha) were also close to zero as expected for the same reason.

On the whole it was thought that the calibration experiments were successful in showing that the documented CEGB[1] calibration constants could be used, even though the entire range of hole sizes was not covered. These documented values[1] are shown in Appendix B. The first sheet is for BLH strain gauge rosettes - type FAER-03S-12-SX-EG or similar and the second sheet for Micro-Measurement strain gauge rosettes - type EA-XX-062RE-120 . As discussed, by taking possible bending effects into account in the second calibration experiment, more accurate results were obtained.

5.4 Description and Classification of the Drill Rods and Specimens

As mentioned previously in Chapter 1 residual stress measurements were conducted on various extruded aluminium drill rods provided by Hulett Aluminium. These rods had each undergone similar but slightly different production processes which will be discussed in Section 5.4.2. Also discussed under this section (5.4) is the drill rod classification, the specimen identification method used and the different types of specimens used for experimentation.

5.4.1 Drill Rod Classification

Six aluminium drill rods (alloy 7075-T6, of length between 1.7 m and 2.6 m, diameter of approximately 70 mm and wall thickness of approximately 9.6 mm) were supplied by Hulett Aluminium for residual stress measurement. The first four had undergone a so called "old route" of processing, the fifth - a so called "stretch route" of processing and the sixth - a so called "new route" of processing. (These processing routes will be discussed fully in the next section.) It was decided to reclassify a representative sample of the rods for ease of identification as shown in Table 5.9.

5.4.2. Processing Details of the Aluminium Drill Rods

As mentioned in the previous section, residual stresses in aluminium drill rods from three different processing routes were required to be analysed. These routes together with their sequential processes[91] are shown in Table 5.10. These processes are described as follows[91,92]:

- Extrude Bloom: This was a hot seamless extrusion process. Billets of 380 mm or 430 mm length and 203 mm diameter were predrilled to a 57 mm bore and preheated to 410°C prior to extrusion. The cross sectional dimensions of the extruded blooms were nominally 74.00 mm OD and 52.50 mm ID.

- Anneal: This heat treatment process softened the extruded blooms to facilitate subsequent cold drawing. The blooms were heated to 350±10°C and maintained at this temperature for 2 hours. The blooms were then slowly cooled at a rate of 15°C/hour to a temperature of 250°C, afterwhich they were removed from the furnace and allowed to cool in air to room temperature.

- Tag and Draw: The drawing process was a cold working process and was capable of maintaining tighter tolerances than the hot working extrusion process. It involved pulling the extruded bloom through a draw die and over a draw bulb, which both formed and reduced the bloom to the required dimensions of nominally 70.00 mm OD and 51.00 mm ID. Since the resultant OD was always smaller than the blooms' OD, the end of the blooms were swagged/tagged to assist in the pulling of the bloom through the draw dies. This basically involved crimping the ends of the blooms. After drawing, the tagged ends were cut and discarded.

- Solution Heat Treat: This was the first stage in the strengthening of the 7075 aluminium alloy. It involved taking the hardening phase $MgZn_2$ into solid solution.

The rods were heated to a temperature of 465±5°C and maintained at this temperature for 1 hour. Thereafter they were water quenched in a water bath of temperature between 25°C and 37°C.

- Reel: The reel process involved straightening the rods through a series of rollers orientated at 45° to one another in a three dimensional fashion.

- Control Stretch: Rods were stretched longitudinally by subjecting them to an axial load slightly in excess of their proof stress. This resulted in an increase in length of 1.5% to 3%.

- Cut: The rods were cut to length.

- Age: This was the second stage of strengthening the 7075 aluminium alloy. It involved the precipitation of the hardening phase $MgZn_2$. The rods were heated to a temperature of 105±5°C and maintained at this temperature for 8 hours. They were then further heated to a temperature of 135±5°C and maintained at this temperature for 16 hours. This resulted in a T6 temper designation of the rods.

The percentage composition of the alloying elements of the 7075 aluminium alloy is shown in Table 5.11. (Single figures indicate maximum content.)

The "old route" was the original method used by Hulett Aluminium to manufacture the drill rods. Hulett Aluminium proposed the "new route" and the stretch route" in an effort to reduce any inherent residual stresses induced during the manufacture of the drill rods. As can be seen from Table 5.10, the "new route" differed from the "old route" in the sequence of the processes. The "stretch route" differed from the "old route" by replacing the reeler operation with a controlled stretch, since it was thought that the reeler process induced the most fabrication residual stresses.

Before sending the rods for analysis, Hulett Aluminium had performed some simple tests on offcuts from the rods and reported that the "stretch route" had in fact induced a small compressive residual stress in the rods whereas the "new route" had only lowered the residual stresses slightly compared to the "old route". However they mentioned that if needed they would prefer to opt for the "new route" as the controlled stretch in the "stretch route" was expensive to incorporate in their production line. Hulett Aluminium further reported that the mechanical properties (i.e. proof stress, UTS and elongation) of the drill rods produced by the "stretch route" and the "new route" were within specification. From the trials they had performed, the average values of proof stress and UTS had in fact improved for these routes compared to the "old route" as shown in Table 5.12.

5.4.3 Specimen Types and Identification

In order to keep a record of the results, specimens from the drill rods had to be clearly marked and identified. Before analysing the residual stresses in the rods, sections were marked out along their length with a permanent marker, with length approximately equal to the diameter of the rods (approximately 70 mm). These sections were numbered sequentially, with the reference letter of the rod following this number (eg. 1A, 2A ...), and were used to cut specimens from the rods.

When referring to specimens with length equal to diameter, the identification code of the section from which it was cut was used (eg. 1A, 8E, 14F ...). When referring to specimens of length equal to two or three times diameter, all section numbers together with the rods' reference letter was used. For example a specimen of length equal to twice its diameter cut from sections 17 and 18 of rod E, was referred to as specimen 17,18E. A specimen of length equal to three times its diameter cut from sections 3, 4 and 5 of rod F, was referred to as 3,4,5F.

The curvature of the rods was then established. This was done by

placing the ends of the rods on rollers and rotating them slowly while taking readings from a clock gauge placed at predetermined positions along the length of the rods, as shown in Fig 5.16. Half the difference between the maximum and minimum readings of the clock gauge indicated the amount of initial curvature or distortion of the rods at a particular point. The location of these readings also showed the top and bottom points of the curve. It was found that the top and bottom points of the bend were almost collinear in all cases. In other words, the rods approximated the shape of an arc as shown graphically in Fig 5.17 for rod A.

A "clock face" was then marked on the rods with 12 o'clock being at the top of the bend when looking along the length of the rod from specimen 1 onwards as shown in Fig 5.18. When specimens were cut from the drill rods, this clock face notation was marked on each specimen so that their relative orientation could be monitored. Various specimen types were used for both the AACH drilling and ring splitting techniques, as shown in Fig 5.19 and Fig 5.20 respectively. The three different specimens shown in Fig 5.19 which were used for the AACH drilling technique were employed as follows:

i. The specimen shown in (a) was used for measuring the residual stress on the inner surface of the rods. As can be seen a portion of the rod was cut away to enable a strain gauge rosette to be attached to the specimen and to allow for the drilling device to be positioned so that a hole could be drilled in the centre of the strain gauge rosette. Specimens of this type had a length equal to three times diameter, so that when cutting out the required portion, relieved residual stresses in the area of the strain gauge rosette were kept to a minimum. The specimen shown in Fig 5.19(a) has had its ends cut off so that they could be used for further analysis (ie. it was three times longer when the AACH residual stress measurement was performed.)

ii. The specimen shown in (b) was used for measuring residual

stress on the outer surface of the rods. Specimens used for this purpose were cut from the previously marked sections with length equal to diameter. This length was sufficient to ensure that the stress relaxation caused by the drilled hole was representative of the residual stress in the rod and was not influenced by the residual stress induced by specimen cutting operation.

iii. The specimen shown in (c) was used for measuring residual stress on a plane perpendicular to the rod axis, effectively on the radius or mid-wall thickness of the rods. These specimens were cut from previous specimens which had been analysed. They were required to be cut carefully using a band saw with a coarse toothed blade with a slow cutting speed and slow feed so as to minimise any induced residual stress due to the cutting operation.

Most of the specimens used for the air abrasive centre hole drilling technique were of the type shown in Fig 5.19(b) as it was generally found that the residual stress pattern varied from highly tensile in a hoop direction on the outside surface to compressive on the inside surface, with the exception of rod E. It was thought that these high tensile stresses were more likely to be responsible for any premature failure of the drill rods than the comparatively lower compressive residual stresses. The other types of specimens were used mainly to determine the residual stress distribution through the thickness of the drill rods.

The three specimens shown in Fig 5.20 were used for the ring splitting technique. These specimens (a), (b) and (c) had length to diameter ratios of 2, 3 and 1 respectively. These three lengths were used since it was decided to confirm the advice given by Sachs and Espey[15] that a tube of length equal to three times its diameter should ideally be used due to longitudinal stresses being released by the ring splitting operation. It was, however, found that the specimens of length equal to diameter yielded results close to and sometimes exceeding those for specimens of length equal to three times

diameter. As a result the majority of ring splitting specimens had length equal to diameter. It was found when using the air abrasive centre hole drilling technique that the longitudinal residual stresses were much lower than the circumferential (or hoop) residual stresses and therefore the effect of specimen length, when using the ring splitting technique, probably did not play an important role.

5.5 The Air Abrasive Centre Hole Drilling Test Procedure

The test procedure for an air abrasive centre hole test can be roughly divided into four sections, namely equipment check, setting up, testing and data acquisition, and data processing. In order to report how the test procedure was carried out, a typical test conducted on the outer diameter of specimen 8A at the 12 o'clock position will be discussed. It is assumed that the necessary components had been calibrated.

5.5.1 Equipment Required for the Air Abrasive Centre Hole Drilling Technique

Before carrying out a residual stress measurement, it was necessary to check that all the required equipment was available. The main items on the equipment list comprised of the following:

- Air abrasive centre hole drilling unit
- Air abrasive centre hole optical unit
- Guide bush and stand arrangement
- 2 dimensional cross-vice
- SS White Airbrasive machine model K
- Alumina (50 μm - 70 μm particle size)
- Hole drilling three element strain gauge rosettes
- Strain gauge amplifier
- Ten channel selector switch
- Strain gauge cement
- Strain gauge protective coating (Micro-Measurement M-Coat was used)
- Alcohol

- Fine grit sandpaper
- Electrical wire suitable to be connected to the strain gauge rosettes
- Soldering iron and solder
- Multimeter
- Oil
- Vacuum source
- Air filter and regulator
- Stop watch
- Tape
- Retort stand
- Feeler gauge

5.5.2 Setting up for the Test

After it had been ascertained that all the equipment required was available, the setting up procedure could begin. First specimens had to be prepared by cutting them from the rods and attaching hole drilling strain gauge rosettes in the desired locations. The orientation of the strain gauge rosettes were as shown in Fig 5.21. For residual stress measurements performed on the outside surface of the rods, strain gauge element 1 was aligned parallel to the axis of the rods, as shown in Fig 5.21(a). Whereas for residual stress measurements performed on the inside surface of the rods, strain gauge element 2 was aligned parallel to the axis of the rods, as shown in Fig 5.21(b). For residual stress measurements performed on the radius of the rods, strain gauge element 2 was aligned with the radial direction of the rods, as shown in Fig 5.21(c). Electrical wires were then soldered to the strain gauge rosettes and the resistance of the strain gauges as well as the possibility of any short circuits were checked. Thereafter a protective coating was applied to the strain gauge rosettes to prevent them being damaged by rebounding particles in the work area, during hole drilling.

Next a test specimen was accurately positioned below the guide bush as follows:

- The air pressure was regulated to zero on the first air pressure regulator, located before the T-piece - see Fig 4.9.
- The alumina powder level in the mixing chamber of the SS White Airbrasive machine was checked.
- The guide clamp and support plate were orientated as shown in the sketch on the base plate - see Fig 4.5 and 4.7.
- The guide bush was cleaned.
- The specimen was placed in the cross vice approximately in position below the guide bush.
- A dummy gauge was placed in the vicinity of the test specimen to compensate for thermal effects.
- The strain gauge rosette was connected to the ten channel selector switch, which in turn with the dummy gauge was connected to the strain gauge amplifier.
- The drilling unit was secured in the guide bush in the orientation sketched on the base plate (see Fig 4.7) and the nozzle tip distance to the specimen was adjusted to 0.5 mm, by rotating the guide bush in the guide clamp.
- The drilling unit was replaced with the optical unit in the guide bush, ensuring that the orientation was as indicated in the sketch on the base plate - see Fig 4.5.
- The air bearing bush was connected to the pneumatic circuit.
- The air pressure was regulated to six bar on the first air pressure regulator and the valve to the air bearing bush was opened.
- The ring illuminator was turned on.
- The strain gauge rosette, attached to the test specimen, was accurately positioned below the guide bush with the aid of the cross vice while viewing it through the optical unit. (See Section 4.2.1 for further details.)
- The air bearing valve was closed and the optical unit was replaced with the drilling unit, in its correct orientation, in the guide bush.

- The nozzle tip distance was checked and adjusted if necessary. If it required adjusting, then the strain gauge rosette had to be checked for alignment as described previously.
- The drilling unit was removed from the guide bush and the air bearing bush was lightly lubricated with oil.
- The drilling unit was again placed in the guide bush in its correct orientation.
- The SS White Airbrasive machine was turned on and the valve to it was opened. The pressure regulator on the SS White Airbrasive machine was adjusted to 5.5 bar.
- The vibrator control on the SS White Airbrasive machine was set to 6.5 - 6.75 units.
- Checks for blockages and flow problems in the air-alumina stream were conducted by inserting the air-alumina tube from the SS White Airbrasive machine in the vacuum hose and actuating the foot switch of the SS White Airbrasive machine. By doing this it could easily be seen whether the air-alumina stream was hindered in any way.
- The vacuum hose was connected to the vacuum tube as shown in Fig 4.13. Note that a retort stand was used to hold the vacuum hose close to the vacuum tube and tape was used to seal the gap between them so that the vacuum hose did not pull down on the drilling unit causing small deflections and thus cause the hole to be drilled in the incorrect position. It is not however shown in Fig 4.13 in an attempt to prevent cluttering of the photograph.
- The drilling unit was connected to the pneumatic circuit by connecting the air-alumina tube from the SS White Airbrasive machine to the air inlet tube.
- The vacuum shroud was lowered onto the test specimen and any openings were sealed.

5.5.3 Testing and Data Acquisition

Once the setting up for the test was completed, testing could begin. The points below follow on from the previous section.

- The strain gauge readings on the strain gauge amplifier were zeroed.
- The drilling unit was set in motion and the motor speed was adjusted so that the running parts of the drilling unit were orbiting at a speed of 3 to 4 rpm.
- The vacuum unit was turned on.
- The foot switch of the SS White Airbrasive machine was depressed while simultaneously starting the stop watch.
- The rotation of the drilling unit and the air-alumina flow were constantly monitored during the drilling operation.
- Strain readings were taken after every minute without stopping the drilling unit, as a form of monitoring progress.
- After the predetermined hole drilling time of approximately 5 minutes, the air-alumina stream and the drill unit were stopped and the vacuum unit was turned off.
- The pressure release valve of the SS White unit was depressed so that any remaining pressure in the unit could be released.
- The final strains were recorded.
- The drilling unit was removed from the guide bush.
- The guide bush was thoroughly cleaned and any remaining debris was removed.
- The optical unit was inserted in the guide bush.
- The valve to the SS White Airbrasive machine was closed and the valve to the air bearing bush was opened.
- The hole depth was inspected. If the hole was not deep enough, then the drilling unit would have to be re-inserted in the guide bush in order to continue drilling until the required hole depth was reached, as set out in the previous steps.
- The hole diameter was measured three times at different angles and these values were recorded.

- The hole depth was measured twice and these values were recorded.
- Any taper effects of the hole were inspected and recorded.

For this specific test specimen, 8A at the 12 o'clock position, the results shown in Table 5.13 were recorded:

5.5.4 Data Processing

From the results of measured hole diameter, the sensitivity constant $1/K_1$ was found to be 2.084 mm using the table shown in Appendix B for the BLH strain gauge rosette. $\nu K_2/K_1 = 0.33$ for this rosette, as shown in the same table. These constants together with the final strains were substituted in the equations 5.1 and 5.2, which are rewritten below, in order to find the principal residual stresses and their directions. The value of E was taken as 71.5 ± 0.5 GPa, as quoted by Hulett Aluminium.

$$\sigma_{\frac{1}{2}} = -\frac{E}{2}\left(\frac{1}{K_1}\right)\left[\frac{\varepsilon_1 + \varepsilon_3}{1-\nu K_2/K_1} \pm \frac{1}{1+\nu K_2/K_1}\sqrt{\left(\varepsilon_3 - \varepsilon_1\right)^2 + \left(\varepsilon_1 + \varepsilon_3 - 2\varepsilon_2\right)^2}\right]$$

$$\alpha = \frac{1}{2}\tan^{-1}\left(\frac{\varepsilon_1 + \varepsilon_3 - 2\varepsilon_2}{\varepsilon_3 - \varepsilon_1}\right)$$

$\therefore$ $\sigma_1 = 82.7 \pm 8.3$ MPa

$\sigma_2 = 16.9 \pm 1.7$ MPa

$\alpha = -82.7^\circ$

From these results the hoop longitudinal and shear residual stresses were calculated so that the hoop stress values could be compared to the results when using the ring splitting method. These values were calculated to be:

σ_{hoop} = 81.6 ± 8.2 MPa

σ_{long} = 18.0 ± 1.8 MPa

σ_{shear} = 8.3 ± 0.8 MPa

5.6 The Ring Splitting Test Procedure

The ring splitting test procedure that was conducted consisted of a few basic steps. As mentioned previously this was one of its attractive features. A test specimen was first cut to size (either one, two or three times its diameter - i.e. 70 mm, 140 mm or 210 mm) unless this had previously been done. Thereafter the following steps were followed:

- The outer diameter of the specimen was measured at least ten times (depending on its length), perpendicular to the plane of the intended cut, with a micrometer.
- The inner diameter of the specimen was measured at least ten times (depending on its length), perpendicular to the plane of the intended cut, with a micrometer.
- The tube was split at the predetermined position using either a band saw or a power saw. A coarse toothed blade running at a slow speed and a slow feed was used so as to minimise induced residual stresses and heat generation.
- The outer diameter was then measured at least ten times (depending on specimen length), perpendicular to the plane of the cut with a micrometer.
- From the measurements, the residual hoop stress was obtained using the formula derived in Appendix A, which is rewritten below:

$$\sigma_h = \frac{E\ t}{1 - \nu^2} \times \left(\frac{1}{D_o} - \frac{1}{D_1} \right)$$

where: σ_h = Hoop stress

E = Young's Modulus

t = Rod thickness

ν = Poisson's ratio

D_o = Outer rod diameter prior to ring splitting

D_1 = Outer rod diameter after ring splitting

For the specific case of specimen 8A at the 6 o'clock position, which was previously discussed from a hole drilling viewpoint as an example, results of such ring splitting are shown in Table 5.14

During the first few ring splitting tests, longitudinal strain measurements were taken periodically after the specimen had been split in order to establish whether there were any temperature effects due to heat created in the specimen during the cutting operation. In order to achieve this, four linear strain gauges had been attached longitudinally to the specimen at the 12, 3, 6 and 9 o'clock positions, prior to the ring splitting operation. However the results indicated negligible longitudinal strain changes, so the exercise was not pursued. It was also not certain whether the low recorded strains could have been due to the drifting of the strain measuring equipment.

As mentioned previously, the ring splitting technique is an averaging technique, whereas the AACH drilling technique is a local one. Therefore it was not surprising to find that the result obtained from ring splitting was less than that obtained from the AACH drilling technique (i.e. 69.4 MPa cf 82.7 MPa). This matter will be discussed in greater detail later in the results and discussion chapter.

5.7 The Test Programme

The length and diameter of the rods were first measured. Next the curvature of the rods was determined and sections were marked out along their length as described in Section 5.4.3. For rod A the following experiment was conducted to determine whether any residual longitudinal stresses were released when the tube was cut. From the curve describing the curvature of rod

A (see Fig 5.17) three points of interest, where the change in bending appeared to be the largest, were identified. These points corresponded approximately to the 1/4, 1/2 and 3/4 points along the rod. It was thought that the largest residual stress might exist at these points - analogous to an arched bow. Linear strain gauges were therefore placed at the 12 o'clock and 6 o'clock positions at these points when first cutting the rod, so that any relieved residual stresses could be measured. However strain readings were small, generally less than 10 $\mu\varepsilon$, and as a result this process was not repeated.

Next a dimensional analysis of the rods was conducted according to the procedure outlined in Section 5.4.3. Air abrasive centre hole drilling tests followed near the 1/4, 1/2 and 3/4 points of the rods at the 12, 3, 6 and 9 o'clock positions on the outer diameter to try get an understanding of how the residual stress varied along the length of the rods.

Rod A was received first for testing and was manufactured according to the "old route". Since Hulett Aluminium had received complaints about rods manufactured according to this route, it was decided to determine the residual stress at various other points along the rod, as will be discussed in the next chapter, in order to gain a better understanding of how the residual stress varied along its length. A measurement was conducted on the inside surface of the rod near the centre, so as to try understand how the residual stresses varied through the wall thickness of the rod.

Rod E, which was manufactured according to the "stretch route", had additional measurements conducted on its inside surface as well as its mid-wall thickness, near its centre. Rod F, manufactured according to the "new route", had additional measurements conducted on its internal diameter as well as its mid-wall thickness near its 1/4 and 3/4 points. These measurements were also undertaken so as to try understand how the residual stress varied through their wall thicknesses.

Following the air abrasive centre hole drilling tests, a large

selection of specimens, especially those adjacent to, and including, the specimens that had been tested according to the air abrasive centre hole drilling technique were used to perform ring splitting residual stress measurements. This was done so that the two methods used to measure residual stress could be compared as well as to gain further insight of how the residual stress varied along the length of the rods.

The test programme is summarised in Table 5.15 for easy reference.

5.8 Summary

In this chapter a description of the air abrasive centre hole drilling equipment was given. Its calibration together with the calibration of the residual stress equation constants were presented. This was followed by the classification of the drill rods, a description of their processing details and a discussion of the specimen types used for residual stress measurement and their identification. The test procedures used for the air abrasive centre hole drilling technique and the ring splitting technique were described next, followed by a description of the test programme used to analyse the residual stresses of the rods.

In the next chapter, the results and discussion of the rod dimensional analyses and residual stress measurements obtained from both techniques, using the procedures described in this chapter, will be presented.

Micrometer Reading		
Initial	Final	Fin-Init
0.781	4.482	3.701
0.555	4.268	3.713
0.049	3.749	3.700
0.635	4.336	3.701
0.647	4.342	3.695
0.389	4.080	3.691
0.333	4.037	3.704
0.942	4.642	3.700
0.939	4.648	3.709
0.021	3.723	3.702
Average =		3.702
Standard dev =		0.006

Table 5.1 - Calibration results of the optical unit.

Nozzle Offset (mm)	Hole Diameter (mm)
0.554	2
0.425	1.6

Table 5.2 - Nozzle offset versus hole diameter.

Tilt Units	Angle to vertical (Degrees)
-6	-0.84
-5	-0.73
-4	-0.62
-3	-0.51
-2	-0.40
-1	-0.28
0	-0.17
1	-0.06
2	0.05
3	0.16
4	0.27
5	0.38
6	0.49

Table 5.3 - Comparison of tilt values to angle from vertical. A negative angle indicates that the tube is tilted away from the nozzle offset of the drilling unit, whereas a positive angle indicates that the tube is tilted in the opposite direction.

MICRO-STRAINS BEFORE HOLE						
LOAD	SGR 1			SGR 2		
(kN)	AXIAL	45 DEG	90 DEG	AXIAL	45 DEG	90 DEG
10	319	173	-95	314	183	-91
10	333	173	-96	314	183	-92
10	278	136	-87	327	174	-94
10	280	139	-86	329	173	-92
20	652	299	-192	637	313	-187
20	656	299	-191	638	313	-188
20	606	276	-185	650	314	-189
20	608	279	-185	652	314	-188
30	939	420	-283	967	445	-283
30	940	420	-284	967	444	-284
30	924	417	-287	969	445	-285
30	931	419	-286	970	446	-284

Table 5.4 - Strains recorded during the first calibration experiment before hole drilling.

MICRO-STRAINS AFTER HOLE						
LOAD	SGR 1			SGR 2		
(kN)	AXIAL	45 DEG	90 DEG	AXIAL	45 DEG	90 DEG
10	180	72	-64	126	54	-45
10	183	74	-61	127	54	-43
10	176	68	-51	132	59	-44
10	178	68	-51	133	59	-45
20	335	138	-116	293	118	-99
20	337	136	-114	293	117	-99
20	334	130	-101	299	121	-97
20	335	130	-100	298	121	-98
30	489	200	-166	456	177	-151
30	490	199	-164	456	176	-149
30	492	191	-150	459	181	-148
30	492	191	-150	459	181	-149

Table 5.5 - Strains recorded during the first calibration experiment after hole drilling.

RELAXED MICRO-STRAINS (BEFORE HOLE - AFTER HOLE)						
LOAD	SGR 1			SGR 2		
(kN)	AXIAL	45 DEG	90 DEG	AXIAL	45 DEG	90 DEG
10	139	101	-31	188	129	-46
10	150	99	-35	187	129	-49
10	102	68	-36	195	115	-50
10	102	71	-35	196	114	-47
20	317	161	-76	344	195	-88
20	319	163	-77	345	196	-89
20	272	146	-84	351	193	-92
20	273	149	-85	354	193	-90
30	450	220	-117	511	268	-132
30	450	221	-120	511	268	-135
30	432	226	-137	510	264	-137
30	439	228	-136	511	265	-135

Table 5.6 - Relaxed strains calculated for the first calibration experiment.

RECALCULATED AVERAGE STRESSES (MPa) USING DERIVED CONSTANTS			
APPLIED	SGR 1 + SGR 2		
STRESS	SIG(1)	SIG(2)	ALPHA
24.8	27.0	-0.4	13.8
24.8	27.5	-0.6	12.8
24.8	23.7	-1.3	11.5
24.8	23.9	-0.9	11.7
49.5	52.1	0.7	7.2
49.5	52.3	0.6	7.3
49.5	48.8	-1.3	8.1
49.5	49.1	-1.1	8.1
74.3	75.1	0.5	6.1
74.3	75.0	-0.0	6.3
74.3	73.3	-2.3	7.2
74.3	73.9	-1.8	7.1

Table 5.7 - Average recalculated stresses using expeimentally derived constants for the first calibration experiment.

RECALCULATED AVERAGE STRESSES (MPa) USING TABULATED CONSTANTS			
APPLIED	SGR 1 + SGR 2		
STRESSE	SIG(1)	SIG(2)	ALPHA
24.8	27.4	1.2	13.8
24.8	27.9	1.0	12.8
24.8	23.9	0.1	11.5
24.8	24.1	0.5	11.7
49.5	53.1	3.8	7.2
49.5	53.3	3.7	7.3
49.5	49.5	1.6	8.1
49.5	49.9	1.8	8.1
74.3	76.5	5.0	6.1
74.3	76.3	4.5	6.3
74.3	74.4	2.0	7.2
74.3	75.1	2.5	7.1

Table 5.8 - Average recalculated stresses using tabulated constants for the first calibration experiment.

Hulett's Reference	Author's Reference
Sample #34 - Old Route	A
Sample #2 - Stretch Route	E
Sample #47 - New Route	F

Table 5.9 - Drill rod classification. For ease of identification, the drill rods were reclassified as shown.

Step No.	A Old Route	E Stretch Route	F New Route
1	Extrude bloom	Extrude bloom	Extrude bloom
2	Anneal	Anneal	Anneal
3	Tag	Tag	Tag
4	Draw	Draw	Solution heat treat
5	Solution heat treat	Solution heat treat	Reel
6	Reel	Control Stretch	Draw
7	Cut	Cut	Reel
8	Age	Age	Cut
9	---	---	Age

Table 5.10 - The sequential processes of the three different processing routes.

Alloy	Si	Fe	Cu	Mn	Mg	Cr	Zn	Ti	Others
Min %	-	-	1.2	-	2.1	-	5.1	-	-
Max %	0.40	0.50	2.0	0.3	2.9	0.28	6.1	0.20	0.15

Table 5.11 - The percentage composition of the alloying elements of the 7075 aluminium alloy.

	Proof Stress (MPa)	UTS (MPa)	Elongation %
Old Route	496.4 +/- 1.1	545.6 +/- 2.6	12.6 +/- 1.1
Stretch Route	505.0 +/- 7.4	551.4 +/- 3.2	14.2 +/- 1.6
New Route	536.8 +/- 4.6	575.4 +/- 6.4	10.4 +/- 0.9

Table 5.12 - Mechanical properties of a sample batch of the drill rods from the three different processing routes.

SPECIMEN 8A			
Drill Time (min)	Micro-strain 12 o'clock		
	G1	G2	G3
0	0	0	0
1	-33	-90	-175
2	-20	-133	-285
3	-2	-152	-406
4	30	-160	-460
5	40	-160	-495
6	60	-150	-508
Avg hole dia =			1.589
Avg hole depth =			1.585

Table 5.13 - AACH drilling results for specimen 8A at the 12 o'clock position. G1, G2, and G3 refer to strain gauge elements 1, 2 and 3 respectively.

SPECIMEN 8A - CUT AT 6 O'CLOCK			
Reading	OD0	ID0	OD1
1	70.020	50.945	70.645
2	70.025	50.946	70.440
3	70.029	50.960	70.435
4	70.035	50.958	70.439
5	70.018	50.950	70.455
6	70.027	50.948	70.482
7	70.038	50.944	70.464
8	70.012	50.955	70.455
9	70.015	50.971	70.432
10	70.028	50.995	70.478
Av Dia.	70.025	50.957	70.473
Av Thk.	9.534		
Calculated Stress =			69.4 MPa
Variance =			9.4 MPa

Table 5.14 - Ring splitting results for specimen 8A cut at the 6 o'clock position.

TEST PROGRAMME		
Pre-evaluation	AACH Drilling Technique	Ring Splitting Technique
Measure dimensions	Check equipment	Measure ODo, IDo
Measure bending	Set up	Split / Cut
Mark specimens	Acquire data	Measure OD1
	Process data	Process data

Table 5.15 - Test programme matrix.

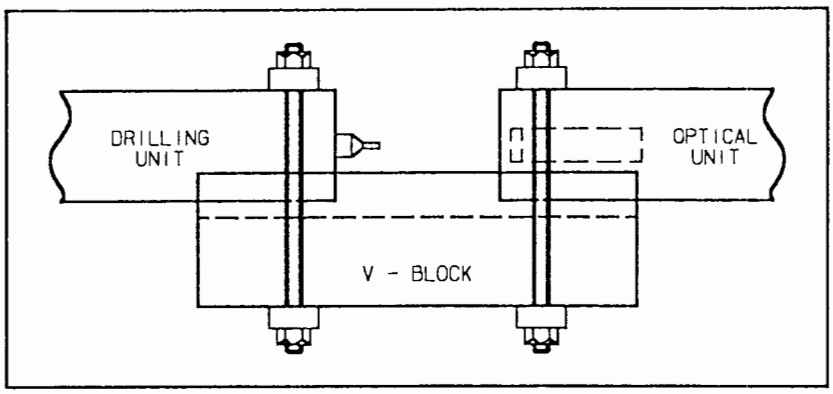

Fig 5.1 - Setting of the nozzle offset. The drilling and optical units were placed on opposite ends of the v-block. The nozzle was then offset the required distance with the aid of the micrometer eyepiece of the optical unit.

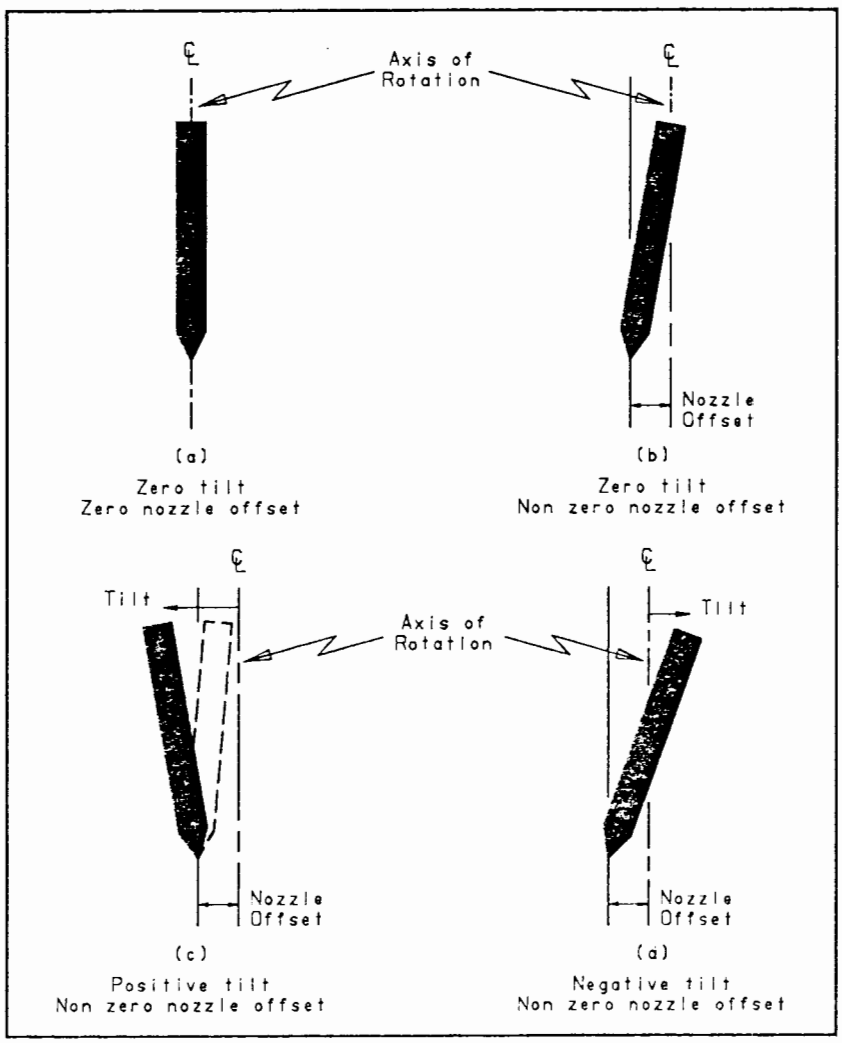

Fig 5.2 - Tilt notation. Configuration (a) shows the position where nozzle offset and tilt are both zero. If the nozzle is then offset, then the tilt will still be zero (b). By offsetting the top of the air tube (in the same plane as the nozzle offset), positve tilt can be achieved by moving in the same direction as the nozzle offset (c) and negative tilt, by moving in the opposite direction to the nozzle offset (d).

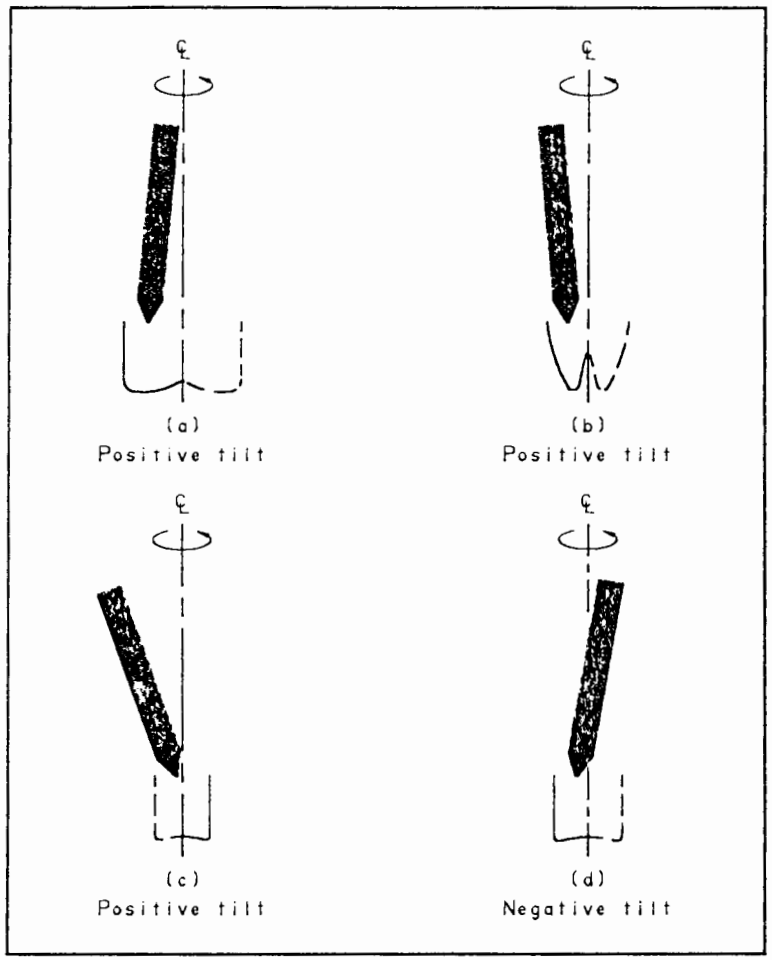

Fig 5.3 - Nozzle offset and tilt combinations. Various nozzle offset and tilt combinations were considered in order to determine how it might be possible to drill the required vertically sided hole. With the exception of case (b), most configurations provide this possibility. The solid line of the hole represents the direct impact of the alumina particles in the positions shown.

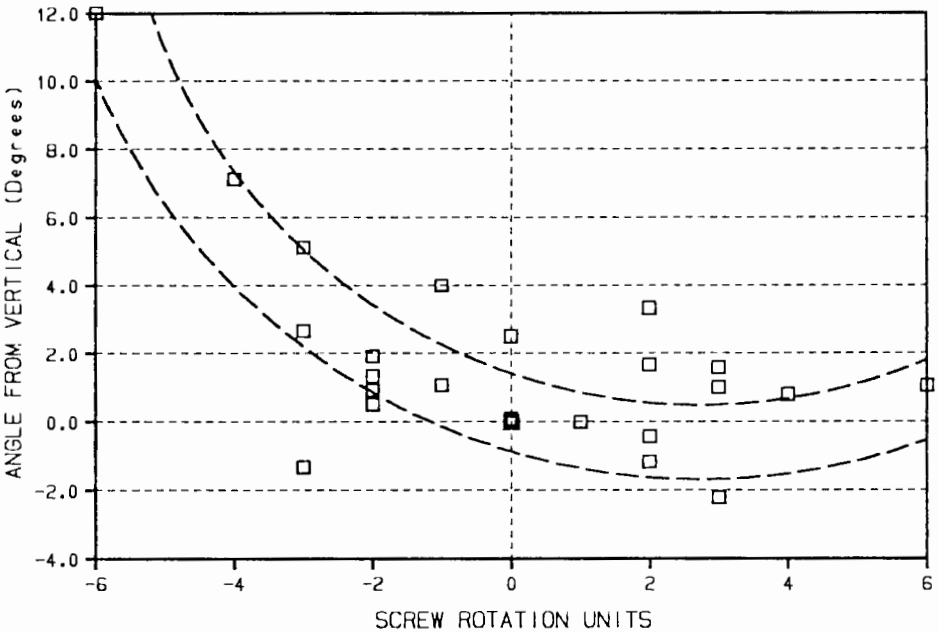

Fig 5.4 - Graph of hole wall angle versus tilt of the air tube of the drilling unit. Tilt units are the number of half screw rotations of the angular adjustment screws. The sign of the tilt indicates the direction of tilt as defined in secion 5.3.2.3.

Fig 5.5(a) - Photograph of a calibration specimen in the experimental rig.

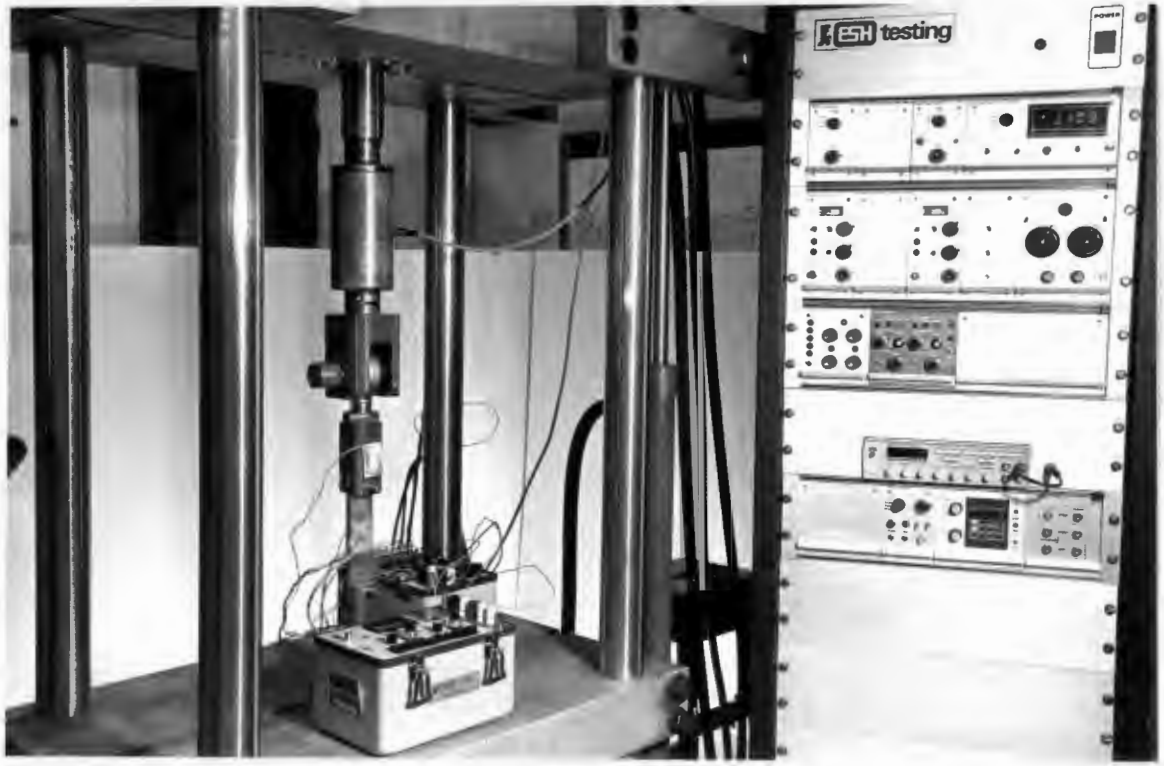

Fig 5.5(b) - Photograph of a calibration specimen together with the ESH servonydraulic testing machine.

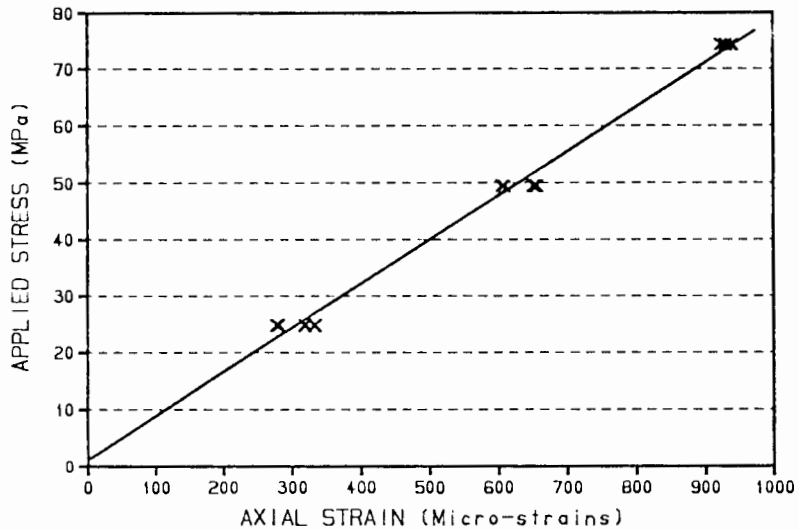

Fig 5.6 - Graph of stress-strain data using strain gauge rosette #1 for the first calibration experiment, from which Young's Modulus could be determined.

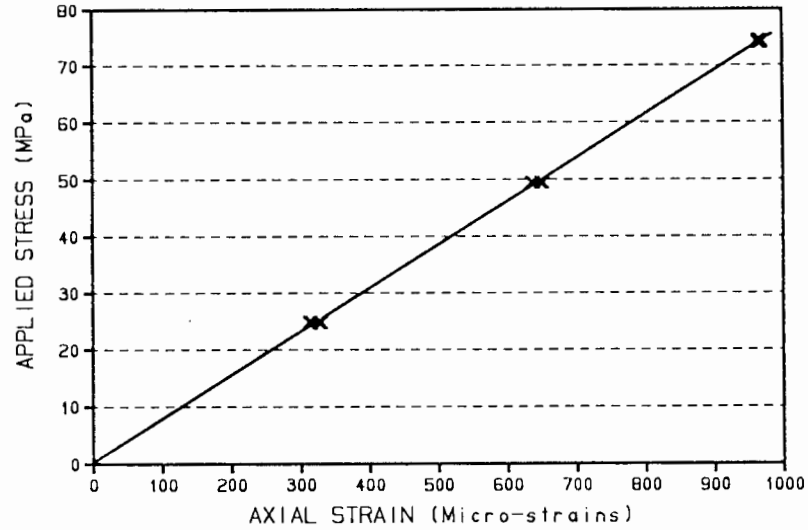

Fig 5.7 - Graph of stress-strain data using strain gauge rosette #2 for the first calibration experiment, from which Young's Modulus could be determined.

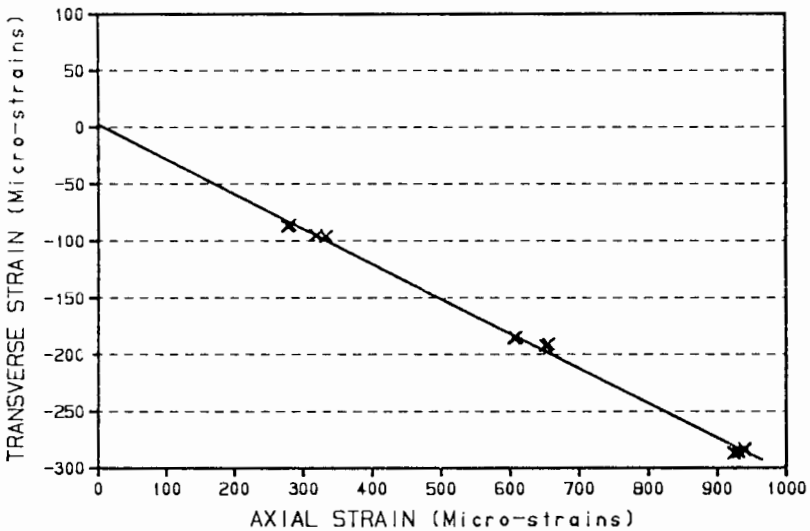

Fig 5.8 - Graph of transverse and axial strains using strain gauge rosette #1 for the first calibration experiment, from which Poisson's Ratio could be determined.

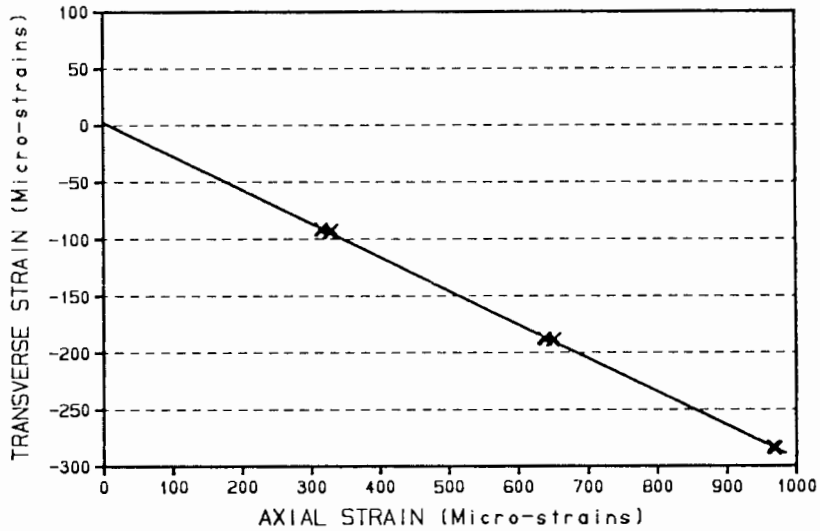

Fig 5.9 - Graph of transverse and axial strains using strain gauge rosette #2 for the first calibration experiment, from which Poisson's Ratio could be determined.

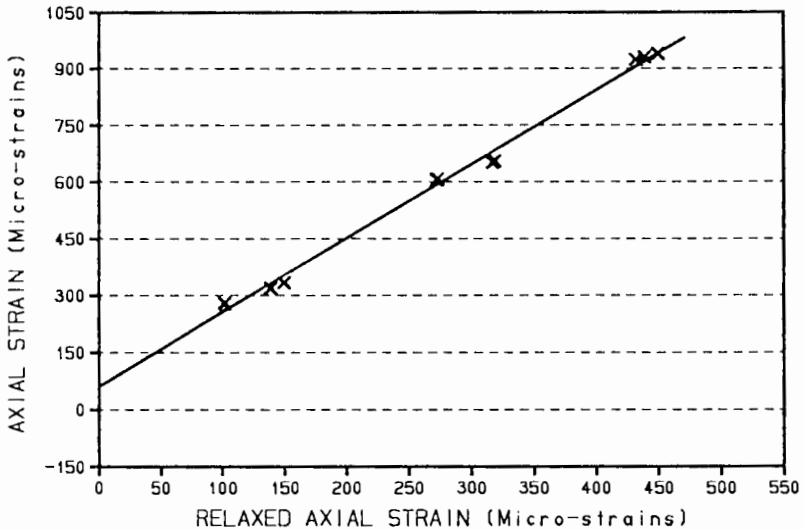

Fig 5.10 - Graph of axial and relaxed axial strains using strain gauge rosette #1 for the first calibration experiment, from which 1/K1 could be determined.

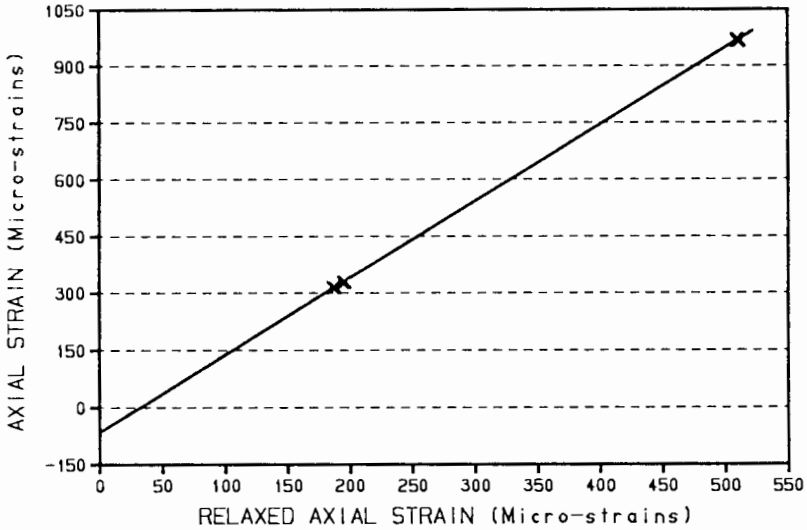

Fig 5.11 - Graph of axial and relaxed axial strains using strain gauge rosette #2 for the first calibration experiment, from which 1/K1 could be determined.

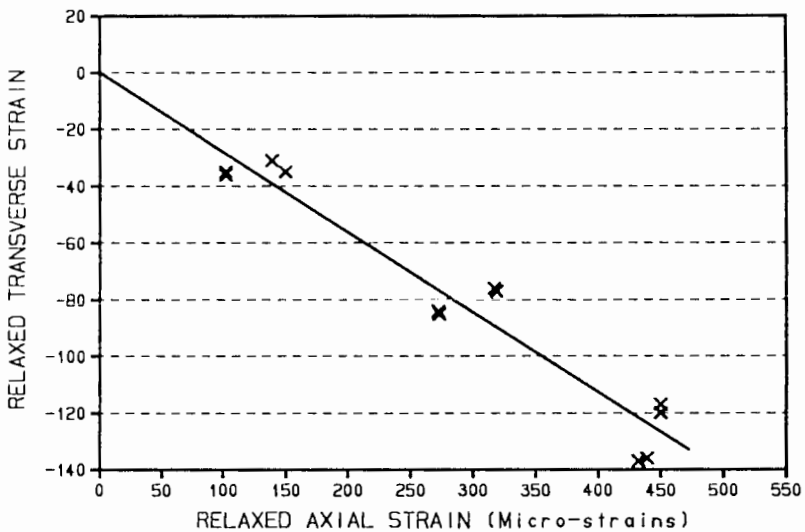

Fig 5.12 - Graph of relaxed axial and transverse strains using strain gauge rosette #1 for the first calibration experiment, from which vK2/K1 could be determined.

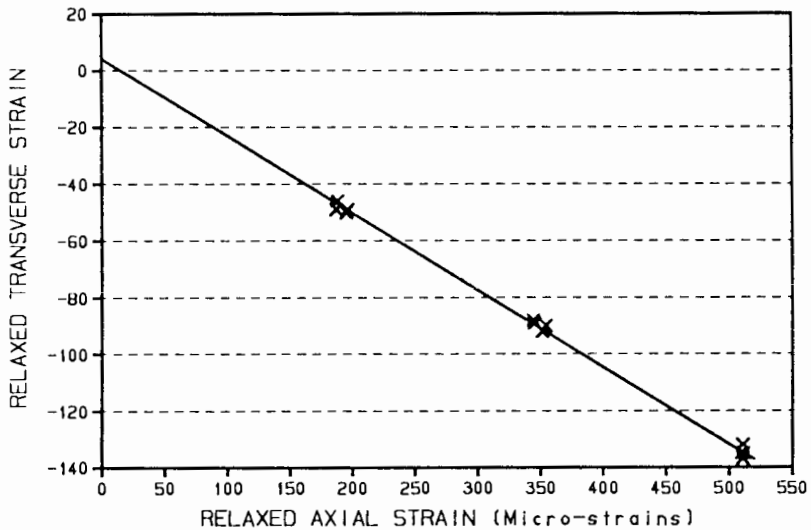

Fig 5.13 - Graph of relaxed axial and transverse strains using strain gauge rosette #2 for the first calibration experiment, from which vK2/K1 could be determined.

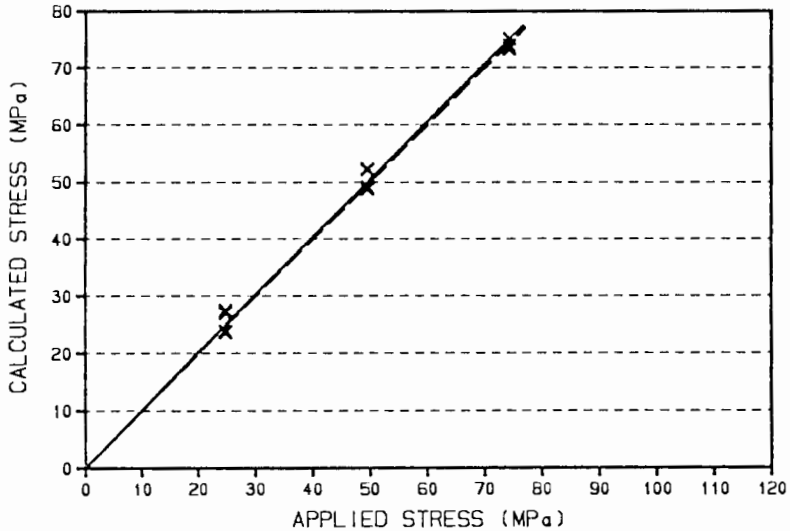

Fig 5.14 - Graph of the average calculated relaxed stresses versus the applied stresses using the derived constants for the first calibration experiment. The dashed line represents equal stresses on both axes.

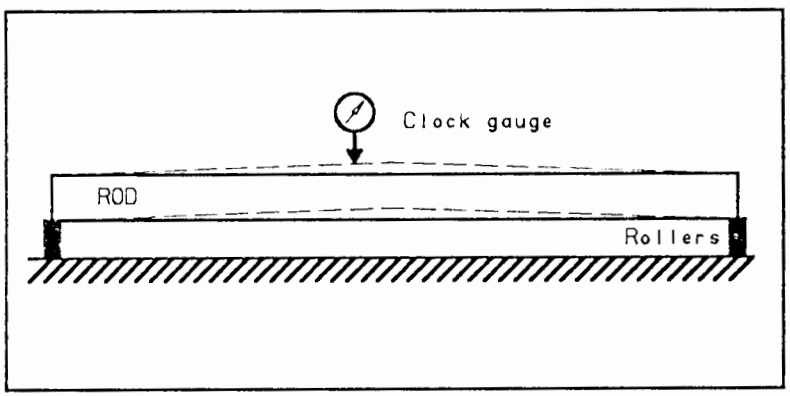

Fig 5.16 - Measurement of rod distortion bending. Rods were placed with their ends on rollers and rotated, while their distortion was measured with a clock gauge.

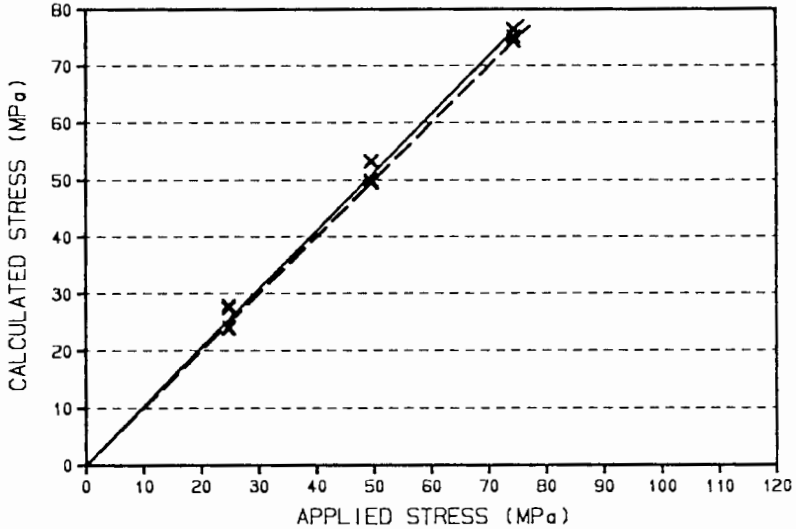

Fig 5.15 - Graph of the average calculated relaxed stresses versus the applied stresses using the CEGB[1] constants for the first calibration experiment. The dashed line represents equal stresses on both axes.

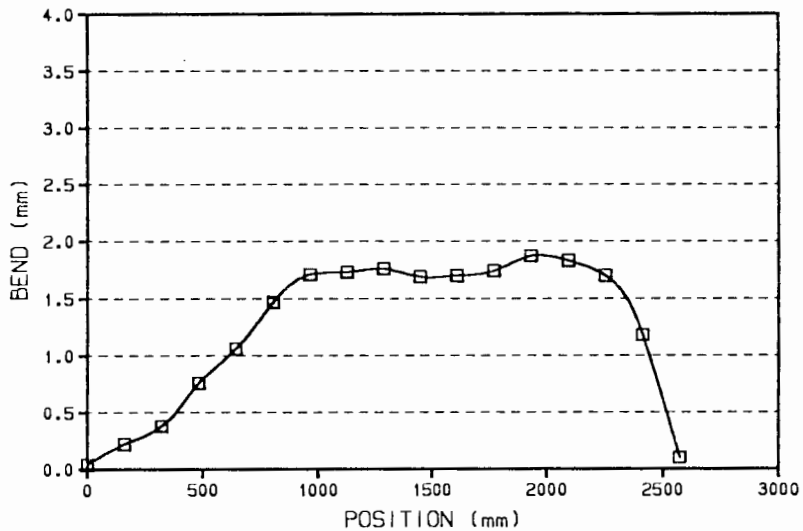

Fig 5.17 - Bending deflection curve of rod A.

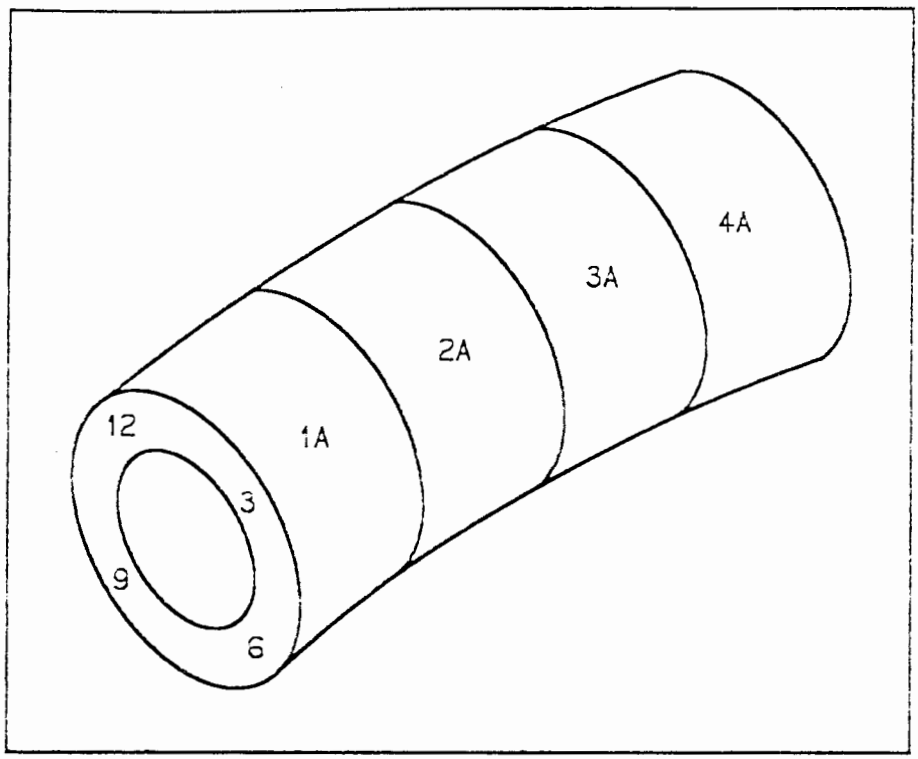

Fig 5.18 – Notation of specimen identification and orientation. The 12 o'clock and 6 o'clock positions are marked at the top and bottom of the curve of the rod respectively.

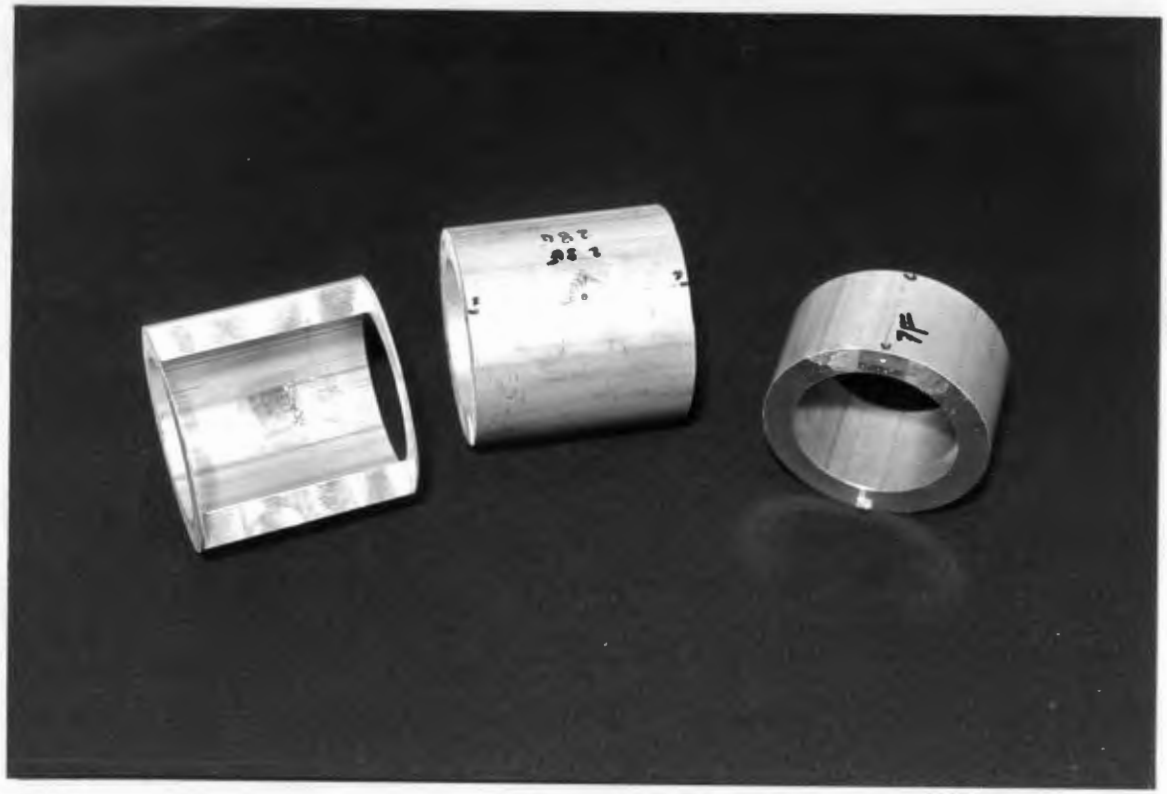

(a) (b) (c)

Fig 5.19 - Various specimens used for the AACH drilling technique. Specimen (a) was used for inner surface residual stress measurements, specimen (b) for outer surface residual stress measurements and specimen (c) for mid wall thickness residual stress measurements.

(a) (b) (c)

Fig 5.20 – Various specimens used for the ring splitting technique. Specimens with length to diameter ratios of one (c), two (a) and three (b) were chosen to determine whether specimen length would influence the residual stress results.

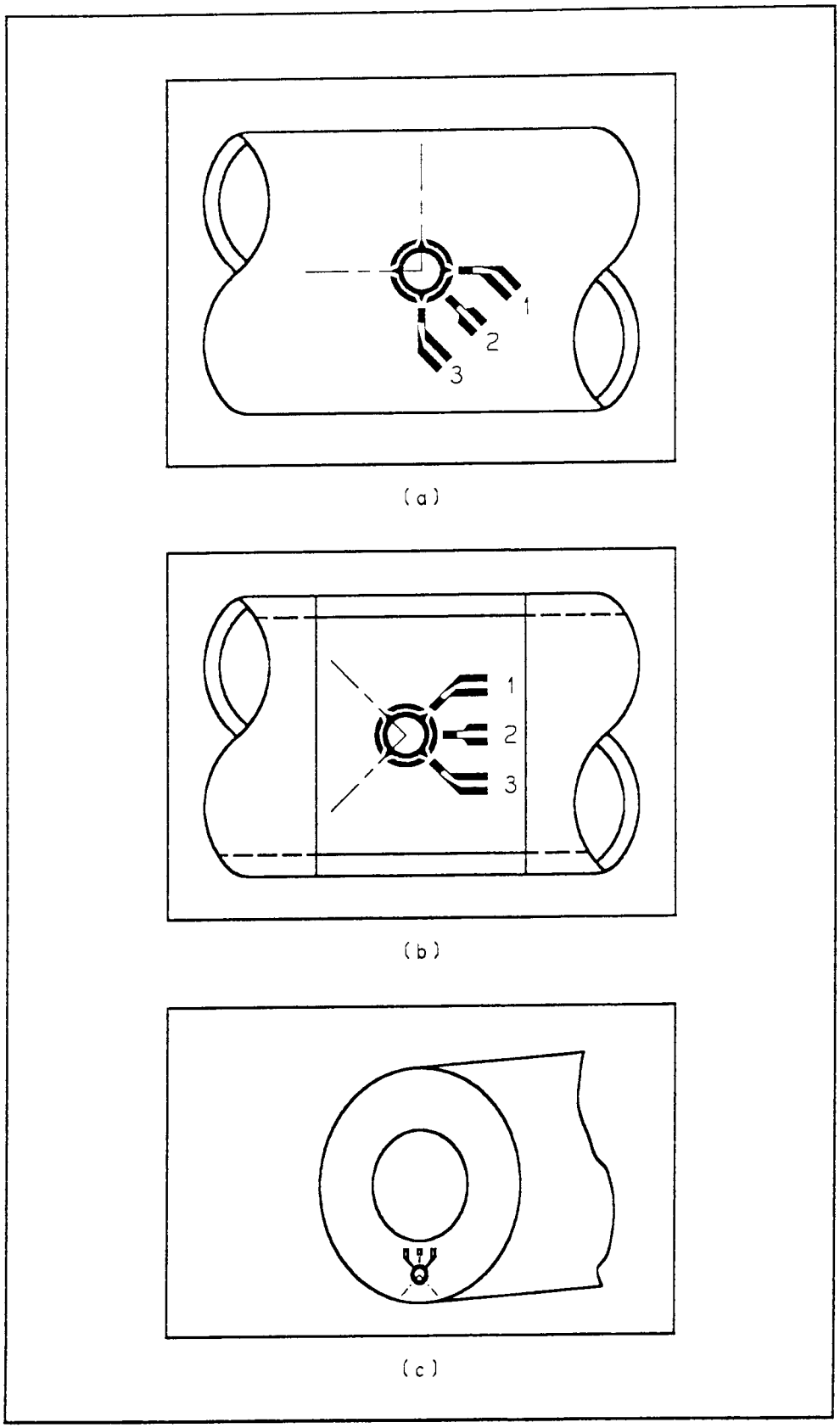

Fig 5.21 - Strain gauge rosette orientations for outer surface, inner surface and mid wall thickness residual stress measurements are shown in (a), (b) and (c) respectively.

6. RESULTS AND DISCUSSION

6.1 Introduction

Once the design and calibration of the AACH drilling device had been completed and the test programme defined, the experimental programme was undertaken. The residual stresses due to fabrication of three drill rods, which had undergone similar but slightly different processing routes, as discussed in the previous chapter, were analysed using the AACH drilling technique and the ring splitting technique. The results yielded by these two techniques are presented in this chapter, together with relevant comparison and discussion, as well as an evaluation of the errors induced with the AACH drilling technique. Some of the experimentation, particularly for rod A, was performed with the assistance of da Silva Pauleta[93].

6.2 Geometric Characteristics

The dimensions of the drill rods which were measured prior to experimentation are shown in Table 6.1. As can be seen only a two thirds length of drill rod of type F ("new route") was provided for residual stress measurement.

The curvature, ie. bending deflection, of the rods is shown in Fig 6.1 which shows a comparison of the curvature of the three rods. As mentioned previously, it was found that the points of both maximum and minimum curvature measured along the length of the rods were almost collinear - ie. the rods approximated the shape of an arched bow. Rods A and E, which had approximately the same length, had similar curvature with local maximums near the 1/4 and 3/4 points and a local minimum near the 1/2 point. The graph for rod F also exhibits a local maximum near its 1/4 point, and from the shape of the graph it seems possible that if it were the same length as rod A and rod E that it would also have another local maximum near its 3/4 point and a local minimum near its 1/2 point, thus having the same shape as rods A and E.

This similarity in curvature patterns appeared to indicate a trend in the production and subsequent straightening processes. It was conjectured that the residual stress distribution pattern in the rods may be related to the induced curvature of the rods. However further analysis was required before this could be concluded.

As can be seen from the comparison of rod curvature in Fig 6.1, the maximum curvature of rod A is almost four times that of rods E and F; while the maximum curvature of rod F is only slightly larger than that for rod E and might have been larger, possibly reaching a maximum of approximately 1 mm, had it been longer. These differences in maximum curvature were not surprising since, as shown in Table 5.10, rod F was straightened through the series of reels on two different occasions compared to the one occasion for rod A, and rod E was straightened by means of a controlled stretch with an axial load slightly in excess of the drill rod proof stress.

6.3 Longitudinal Strains due to Cutting

The results of strain relaxation (measured in micro-strains) of rod A resulting from cutting it in half and then into quarters are shown in Table 6.2. As mentioned previously, it was thought that large residual stresses might exist at the points of maximum curvature of the rods, and that when cutting the rods, springback would possibly occur about these points due to out of balance longitudinal residual stresses - analogous to an arched bow. The sectioning test conducted on rod A to test this did not yield any significant springback or substantial relieved longitudinal strains. It was therefore decided not to undertake such tests on future drill rods.

6.4 Results of the AACH Drilling Technique

The detailed results of the residual stress measurements using the AACH drilling technique are shown in Appendix H in Tables H.1 to H.14, H.15 to H.26 H.27 to H.40 for rods A, E and F respectively. These tables include data of relieved strain

versus time as well as data of final strains, principal stresses and their directions, hoop stresses, longitudinal stresses, shear stresses, hole dimensions and $1/K_1$, versus circumferential position on various specimens. The hoop, longitudinal and shear stresses were calculated from the principal stresses using the following equations:

$$\sigma_H = \frac{\sigma_1 + \sigma_2}{2} - \frac{\sigma_1 - \sigma_2}{2}\cos(2\theta) \quad \ldots \text{ eqn 6.1}$$

$$\sigma_L = \frac{\sigma_1 + \sigma_2}{2} + \frac{\sigma_1 - \sigma_2}{2}\cos(2\theta) \quad \ldots \text{ eqn 6.2}$$

$$\tau = - \frac{\sigma_1 - \sigma_2}{2}\sin(2\theta) \quad \ldots \text{ eqn 6.3}$$

where θ = angle between the longitudinal direction of rods and σ_1.

The errors associated with the AACH drilling results are not given here as their determination is complex. They are dependent on various aspects which include: hole misalignment, hole geometry (eg. wall taper and rounding), accuracy of hole diameter measurement, and the accuracy of the assumption that $\nu K_2/K_1$ can be assumed constant. Instead, the errors are discussed fully in Section 6.7, where it is shown that there is a confidence in the reported results to within approximately 6%.

Before commencing the discussion of the AACH drilling results, certain points are restated to assist in interpretation:

i. When performing residual stress measurements on the outside surface of the rods, strain gauge rosettes were orientated with the first strain gauge element in the longitudinal direction of the rods (see Fig 5.21).

ii. When performing residual stress measurements on the inside surface of the rods, strain gauge rosettes were orientated with the second strain gauge element in the longitudinal direction of the rods (see Fig 5.21).

iii. When performing residual stress measurements on the a plane normal to the axis of the rods, strain gauge rosettes were orientated with the second strain gauge element in the radial direction of the rods (see Fig 5.21).

iv. By definition α is the angle between the first strain gauge element and the direction of the maximum principal stress measured in the direction of the strain gauge rosette (see Fig 3.4).

6.4.1 Rod A - "Old Route"

Rod A was manufactured according to a so called "old route" which included the following sequential processes: extrusion, annealing, drawing, tagging, solution heat treatment, straightening through a series of reels, cutting and ageing. This is discussed in detail in Section 5.4.2.

6.4.1.1 Residual Stress Measurement on the Outside Surface

Various measures of residual stress on the outer surface of rod A are discussed below under appropriate headings.

i. Maximum Principal Stress (σ_1)

Rod A was found to have the second highest measured residual stress on its outer surface. The stress was found to be 136.9 MPa acting in a direction of -78.7° to the longitudinal direction in specimen 8A at the 6 o'clock position, as can be seen in Fig 6.2. The average measured value of σ_1 in rod A was 85.6 MPa, and may be considered to act predominantly in (or close to) the circumferential direction, since the magnitude of α was typically between 75° and 90°, with the exception of one instance - specimen 18A at the 9 o'clock position (see Tables H.1 - H.14). This was expected due to the nature of the extrusion process - a billet is forced over a mandrel and stretches in the circumferential direction when moving outwards radially.

ii. Minimum Principal Stress (σ_2)

The minimum measured residual stress in rod A was found to be -13.2 MPa acting in a direction of -148.5° in specimen 18A at the 9 o'clock position as can be seen in Fig 6.3. The average measured value of σ_2 in rod A was 28.9 MPa. The results of σ_2 exhibit similar trends to σ_1 in terms of the locations of its maximum and minimum values, as well as variation along the length of rod A - see Fig 6.2 and 6.3. This consistency with σ_1 was of interest when considering the stress flow direction which is discussed below.

iii. Stress Flow Direction

If σ_2 were equal to σ_1 then it would be clear that a uniform residual stress field, equal in all directions, was present. The principal stresses are however unequal. Therefore in order to recognize where the residual stresses existed, ie. the stress flow direction, σ_1 and σ_2 were combined by vector addition. The magnitude of the resultant stress was not of importance here, since it is not meaningful. Instead, its direction was sought in order to gain insight into the stress flow direction pattern.

The stress flow directions for rod A are shown in Table 6.3. From the results, a bar graph (Fig 6.4) of the distribution of the stress flow directions was made to see whether the results predominated around a certain value. This was expected due to the consistency in the variation of σ_2 with respect to σ_1. As can be seen in Fig 6.4, this was the case with an average value of 62° ± 9.4° to the longitudinal direction of the rod. What is of interest here is that when the drill rods were received from Hulett Aluminium, a spiral pattern along the length of the rod, which was apparently caused by the reels during the straightening process, could be seen. This spiral was also angled at approximately 62° to the longitudinal direction of rod A. It was thus conjectured that the spiraling of the reels over the rods during the straightening process had an

influence on the residual stress pattern.

With this in mind, it was decided to check whether there was any "periodicity" of the stresses along rod A. Using the three specimens 8A, 18A and 27A, where the residual stress distribution around the circumference was reasonably well known, the required period of the spiral was calculated between the positions of the maximum principal stresses at these points, by dividing the distance between them by the number of spiral revolutions observed. The result was compared to the period of the spiral measured on the rod of approximately 117 mm. This is shown in Table 6.4, and as can be seen from the limited results, there is evidence of periodicity.

iv. Longitudinal Stress

The longitudinal stresses were calculated using eqn 6.2 and their distribution along rod A is shown in Fig 6.5. As can be seen that there is a trend for the highest value of σ_L measured in a specimen to occur at the bottom of the curve exhibited by rod A - ie. at the 6 o'clock position, while the lowest value of σ_L occurred at the top of the bend - ie. at the 12 o'clock position. This is more clearly illustrated in Figs 6.6 and 6.7. This trend can be explained as follows: before straightening, the rods were more bent than after straightening. By bending the rods to a straighter position in the straightening process, the superimposed stress state at the 6 o'clock position would be tensile and conversely compressive at the 12 o'clock position. This concept is illustrated simply in Fig 6.8.

Fig 6.9 shows the average longitudinal stress around the circumference of various specimens plotted as a function of distance. The results were averaged around the circumference to take into account bending effects. As can be seen, these stresses are approximately constant along the length of the rod. This was expected due to the nature of the extrusion and drawing processes, where the outer

surface of the rods are stressed evenly during manufacture.

6.4.1.2 Residual Stress Measurement on the Inside Surface

A residual stress measurement was performed on the inner surface of specimen 15,16,17A at the 3 o'clock position to gain insight into how the residual stresses varied through the wall thickness of rod A. A maximum compressive value of -50.2 MPa acting in a direction of 67° to the longitudinal direction (see Table H.14) was measured at this point.

An aperture was required to be cut into the drill rod wall as discussed in Section 5.4.3 and illustrated in Fig 5.19. To determine the effects of the aperture on the residual stress distribution in the rods, a ring splitting type analysis was performed. The change in rod diameter was noted after the aperture had been machined and was used to estimate approximately the level of any relieved stress. Table 6.5 shows that a stress of 1.3 MPa was relieved, which is low compared to the residual stresses present in the drill rod. It was therefore decided that this method for inner residual stress measurement was sound, due to the negligible relieved stresses resulting from the machining of the required aperture.

6.4.1.3 Stress Gradient

The stress gradient in rod A varied from tensile on the outer surface to compressive on the inner surface. The magnitude of the tensile stress being larger than that of the compressive stress. It was expected that there should be a sign change in the stresses for the equilibrium of forces through the thickness of the rod, and that the magnitude of the outer stress should be larger since the outer layers of the rod are required to stretch more during the extrusion process. Although an understanding of the stress gradient has been obtained, it is not however precisely known how the stresses varied.

6.4.2 Rod E - "Stretch Route"

Rod E was manufactured according to a so called "stretch route" which included the following sequential processes: extrusion, annealing, tagging, drawing, solution heat treatment, straightening by means of a controlled stretch, cutting and ageing. This is described in detail in Section 5.4.2.

6.4.2.1 Residual Stress Measurement on the Outside Surface

Various measures of residual stress on the outer surface of rod E are discussed below under appropriate headings. The minimum principal stress will be discussed first since it has the highest magnitude of the two principal stresses, unlike rods A and F.

i. Minimum Principal Stress (σ_2)

The largest compressive residual stress measured in rod E was found to be -39.6 MPa in specimen 27,28,29E at the 6 o'clock position. The average value of σ_2 is -22 MPa as can be seen in Fig 6.10. The results of α (see Tables H.15 - H.26), which is the angle between the first strain gauge element and the direction of σ_1, are effectively randomly distributed throughout all 360°, indicative of a nominally equibiaxial stress field. This is in all probability due to the controlled stretch used to straighten the rods, where a load slightly in excess of the aluminium 7075 alloy proof stress was applied, which reoriented and redistributed the residual stresses in rod E.

ii. Maximum Principal Stress (σ_1)

Rod E was found to have the lowest σ_1 magnitude of -1.3 MPa acting in a direction of -5.3° to the longitudinal direction in specimen 8,9,10E at the 12 o'clock position, as can be seen in Fig 6.11. The average value of σ_1 in rod E is -13.2 MPa. As in the case of σ_2, σ_1 decreased on average along the length of rod E. However σ_1 did not show

the same trend of stress variation around the circumference of rod E at various points along the rod as σ_2. This added further evidence to the concept that the stress field was effectively equibiaxial as a result of the stretch process, with no preferred location around the circumference of maximum or minimum stress - in effect a "randomness".

iii. Stress Flow

A similar analysis was performed for rod E as in the case of rod A, in order to determine the stress flow directions. The results are shown in Table 6.6 and Fig 6.4. As can be seen, the results are approximately randomly distributed over the whole angular range, with an average value of 38.7 ± 19.5° to the longitudinal direction of rod E.

iv. Longitudinal Stress

Fig 6.12 shows the variation of the longitudinal stress along the length of rod E, calculated from eqn 6.2. Average longitudinal stresses are shown in Fig 6.9 (as in the case of rod A) to take into account any bending effects. As can be seen, the stress distribution is fairly constant as was expected due to the nature of the extrusion and drawing processes and subsequent straightening process.

6.4.2.2 Residual Stress Measurement on the Inside Surface and Mid-wall Thickness

Two additional residual stress measurements were performed on rod E to determine the residual stress variation through the wall thickness. A measurement on the inside surface was conducted on specimen 17,18,19E at the 12 o'clock position. A further measurement was conducted on specimen 19E on a plane perpendicular to the axis of the rod, at a mid-wall position on a so called "radius" (after it had been detached from specimen 17,18,19E). This radial measurement was conducted at a distance of 3.3 mm from the outer surface of specimen 19E at the 12 o'clock position.

A maximum tensile stress of 6.8 MPa acting in a direction of -86.6° to the longitudinal direction was measured on the inside surface of rod E. A maximum compressive stress of -37.0 MPa acting in a direction of -55.9° to the radial direction was measured on the mid-wall thickness of rod E. These results are detailed in Tables H.25 and H.26 respectively.

6.4.2.3 Stress Gradient

The stress gradient in rod E varied from compressive on the outside surface to higher compressive value 3.3 mm in from the outside, to tensile through the wall thickness. The magnitudes of the compressive stresses are larger than that of the tensile stress. Again it was expected that there should be a sign change in the stresses for the equilibrium of forces through the thickness of the rod, but the relatively high stress magnitudes on the radius was not.

6.4.3 Rod F - "New Route"

Rod F was manufactured according to a so called "new route" which included the following sequential processes: extrusion, annealing, tagging, solution heat treatment, straightening through a series of reels, drawing, straightening again through a series of reels, cutting and ageing. This is discussed in detail in Section 5.4.2. Due to the similarity in the manufacturing processes of rods A and F, the results for these rods have similar trends.

6.4.3.1 Residual Stress Measurement on the Outside Surface

Various measures of residual stress on the outer surface of rod F are discussed below under appropriate headings.

i. Maximum Principal Stress (σ_1)

Rod F was found to have the highest measured residual stress on its outside surface. It was found to be a tensile, nominally hoop stress, of 215.2 MPa acting in a

direction of -88.6° to the longitudinal direction in specimen 19,20,21F at the 6 o'clock position, as can be seen in Fig 6.13. The average value of σ_1 was 121.9 MPa, and as in the case of rod A, σ_1 acted predominantly in the circumferential direction of rod F.

ii. Minimum Principal Stress (σ_2)

The minimum measured residual stress in rod F was 7.6 MPa acting in a direction of 26.9° to the longitudinal direction in specimen 5,6,7F at the 6 o'clock position, as can be seen in Fig 6.14. The average value of σ_2 in rod F was 50.9 MPa. As with rod A, σ_2 exhibited similar trends to σ_1 in terms of the location of maximum and minimum values.

iii. Stress Flow Direction

Similar results of stress flow were obtained for rod F to rod A, with the stress flow oriented at approximately 62° to the longitudinal direction of rod F, as can be seen in Table 6.7 and Fig 6.4. Rod F also had similar spiral patterns to rod A, apparently caused by the reels during the straightening process. Furthermore, there is also evidence of periodicity in σ_1, (see Table 6.4). The consistency of these results with rod A further led to the belief that the straightening process for these rods has an influence on the residual stress pattern.

iv. Longitudinal Stress

Fig 6.15 shows the longitudinal stress variations along the length of rod F, calculated using eqn 6.2. As can be seen more clearly in Fig 6.6, the maximum values of σ_L tended to exist at the 6 o'clock position, consistent with rod A. However there is no trend in the location of the minimum values of σ_L for rod F. The average longitudinal stresses calculated using eqn 6.2 along rod F were approximately constant, as shown in Fig 6.9. As with the other rods, this was expected due to the nature of the extrusion and drawing

processes.

6.4.3.2 Residual Stress Measurement on the Inside Surface and Mid-wall Thickness

Four additional residual stress measurements were conducted on rod F to determine the residual stress gradient through the wall thickness. These included two inside surface measurements on specimens 5,6,7F and 19,20,21F at the 6 o'clock positions, as well as two mid-wall thickness, so called "radius" measurements on specimens 7F and 21F at the 6 o'clock positions. The measurements on the "radius" of rod F (ie. a plane perpendicular to the rod axis) were conducted 3.3 mm in from the outer surface, as in the case of rod E. The results are detailed in Tables H.33 - H.40. It can be seen that maximum compressive inner surface residual stresses of -53.7 MPa at 27.1° to the longitudinal direction and -107.4 MPa in the longitudinal direction were measured, and that maximum tensile "radius" residual stresses on the radius of 48.9 MPa at -81° to the radial direction and 56.1 MPa at -79.4° to the radial direction were measured.

6.4.3.3 Stress Gradient

The stress gradient of rod F varied from tensile on the outer surface to compressive on the inner surface. The two measurements performed on the "radius" gave an indication of stress variation through the wall thickness as shown in Table 6.8. As can be seen in Fig 6.16, the stresses decrease through the wall thickness in an almost linear fashion. However, residual stress values between these points are not known. The change in sign was once again expected for equilibrium of forces through the thickness of the rod. The decrease in residual stress through the wall thickness seemed more likely in contrast to the results of rod E.

6.5 Results of the Ring Splitting Technique

The detailed results of the residual stress measurements using

the ring splitting technique for rods A, E and F are shown in Appendix I in Tables I.1 - I.15, I.16 - I.27 and I.28 - I.41 respectively. These tables include data of initial outer and inner diameters, outer diameters after ring splitting, wall thicknesses, residual stresses and their associated errors. The errors reported in the results are due to diameter measurement errors and variations. A conventional Kline and McClintock[94] error analysis yielded on average approximately a 10% error for this aspect.

As can be seen in the tables in Appendix I, different specimen lengths were used to check whether specimen length had any influence on the results. It was found, however, that this was not the case.

6.5.1 Rod A - "Old Route"

The results of the ring splitting stresses for Rod A are shown in Fig 6.17. A maximum tensile hoop stress of 76.6 ± 11.3 MPa was measured in specimen 33A, while an average value of 59.4 MPa was obtained over the length of the rod. In general the stresses appeared to fluctuate around the average stress along the rod.

6.5.2 Rod E - "Stretch Route"

The results of the ring splitting stresses for rod E are shown in Fig 6.18. A maximum compressive hoop stress of -31.7 ± 3.3 MPa was measured in specimen 36E, while an average value of -17.9 MPa was obtained. In general the stresses appeared to increase in magnitude along the rod.

6.5.3 Rod F - "New Route"

The results of the ring splitting stresses for rod F are shown in Fig 6.19. A maximum tensile stress of 101.9 ± 16.6 MPa was measured in specimen 22,23F, while an average hoop stress of 76.9 MPa was obtained. In general the stresses appeared to fluctuate around the average stress along the rod, as in the case of rod A.

6.6 Comparison of Results Between the AACH Drilling and Ring Splitting Techniques

Graphs of residual hoop stresses obtained from the AACH drilling and ring splitting techniques are shown in Figs 6.20 - 6.22 for rods A, E and F respectively. As can be seen, trends were similar. If the AACH hoop stresses were tensile then so were the ring splitting stresses and vice versa. Furthermore, the magnitude of the ring splitting results are mostly lower in magnitude than the AACH results. This is due to the ring splitting technique being an averaging technique, whereas the AACH drilling technique is a localised one with the stresses averaged over the drilled hole.

The hoop residual stresses measured using the two techniques were compared where the stress gradient through the rod thickness was known. As mentioned previously, when using the ring splitting technique, the stresses are assumed to vary linearly through the wall thickness, and to be constant on each circumferential plane. They are further assumed to be unbalanced over the wall section, since only unbalanced forces between opposite walls will cause bending when the tube is slit[8]. By using these assumptions at the places of known stress gradient, the stresses were compared by separating an assumed linearly varying stress field, found from the AACH drilling technique, into a bending component and a pure membrane or "force" component, as illustrated in Fig 6.23. Where possible, stress results for the AACH drilling technique were averaged around the circumference to correspond with assumptions of the ring splitting technique.

The results for the points of interest are tabulated and compared in Table 6.9. Only the results for the outer and inner surfaces from the AACH drilling technique are used when calculating the stress gradient, to approximate it as a linear variation. Table 6.9 shows that the ring splitting results compare reasonably well to the bending component of the hoop residual stress from the AACH drilling technique, with variances between 10% and 30%. Furthermore the membrane components of the

AACH drilling technique are approximately one third of the AACH bending component, and therefore the ring splitting stresses too, with the exception of specimen 19,20,21F. If this trend is assumed to be correct, then it would appear that the ring splitting results are approximately 75% of the average AACH hoop stresses around the circumference of the rods on the outer surface. Using this hypothesis, AACH and ring splitting hoop stresses are compared at all points where more than one AACH residual stress measurement was made, as shown in Table 6.10. For the data obtained, the average variance in this hypothesis is 13.8%.

6.7 Error Analysis of the Air Abrasive Centre Hole Drilling Technique.

From the calibration experiments, it was determined that this technique could be used with a confidence of 5% error. In the following sections, an analytical approach will be taken where by all possible errors in each step of experimentation are considered.

6.7.1 Induced Stresses due to Machining

As mentioned previously, there are various methods of hole drilling for the centre hole technique such as low speed milling, high speed drilling etc. Air abrasion was chosen since unlike other methods, it induces minimal machining stresses. This is due to the low inertia of the abrasive particles, and any heat generated is quickly cooled by the air stream. Although no direct measure of AACH machining induced stresses was undertaken in this study, Beaney[3] reported AACH machining induced strains of less than 5 microstrains, which if applicable in this case, would represent an error of typically 1%.

6.7.2 Hole Misalignment

Beaney and Procter[2,18] reported that a 0.013 mm mis-positioning of a 1.575 mm hole with respect to the strain gauges gives a 2% error in predicted stress. This is however

applicable to a strain gauge rosette which has a target to strain gauge distance of 2.565 mm. The BLH strain gauge rosettes used for almost all of the present experimental work has a target to strain gauge distance of 1.754 mm. Using ratios it can be determined that for the former strain gauge rosette a 0.5% (0.013/2.565 x 100) misalignment gives rise to this 2% error. Most of the holes drilled had a diameter of approximately 1.575 mm. Therefore for the BLH strain gauge rosettes a 0.009 mm (0.5% x 1.754) misalignment would also give rise to a 2% error.

When measuring misalignment of the holes after drilling, it was found that the majority of holes had a misalignment error of less than 10 μm which would imply an error of approximately 2%.

6.7.3 Hole Diameter Measurement

Hole diameter measurement has a direct influence on the constant $1/K_1$ tabulated in Appendix B. Since almost all the residual stress measurements were conducted using a BLH strain gauge rosette, errors for this rosette will be assessed here. In Section 5.3.1.1 it was shown that the optical unit has a magnification of 3.702 ± 0.006. This gives rise to a 0.16% (0.006/3.702 x 100) error. If an average hole size of 1.575 mm is considered, a 0.16% error could imply that the hole was actually 1.578 mm. From Appendix B, the $1/K_1$ values are 2.121 for a 1.575 mm hole and 2.115 for a 1.578 mm hole. Since the calculated residual stresses are directly proportional to $1/K_1$, this discrepancy gives rise to a 0.2% error in the calculated residual stress.

6.7.4 Hole Geometry

Beaney[3] considered various hole geometries, namely: a squared hole, a tapered hole, a tapered hole rounded at the bottom and a tapered hole rounded at the bottom as well as the top - see Fig 6.24. He reported that a tapered hole is less sensitive than a squared hole (i.e. $1/K_1$ is slightly greater) and rounding of the bottom more so; but rounding the top in addition to this produces an increase in sensitivity. As can be seen the larger

the hole diameter, the less effect geometry has on $1/K_1$. Beaney showed that for holes larger than 1.8 mm (in a strain gauge rosette of 2.565 mm target to strain gauge distance - equivalent to a 1.23 mm hole in the BLH strain gauge rosettes mainly used) the effects of taper can be ignored. However rounding of the hole needed to be taken into account. As can be seen in Fig 6.25(a) - 6.25(c), which are considered to be the "worst" holes formed during experimentation, rounding was a problem. From Fig 6.24 a 5% error can be evaluated by noting the error found for large holes and remembering that this graph was produced from holes drilled in a larger strain gauge rosette than were used for experimentation presented in this thesis.

For the better drilled holes, as shown in Fig 6.25(d), the hole geometry error can be found to be approximately 2% from Fig 6.24. Here rounding of the bottom affects accuracy, but taper and rounding of the top are negligible.

6.7.5 Plasticity Effects

When a hole is produced in a residual stress field which is greater than one third of the yield stress of the material in which it is present, plasticity effects arise due to the stress concentration caused by the hole. This effect occurred only in one of the residual stress measurements, specimen 19,20,21F at the 6 o'clock position, and as a result was not considered when evaluating the overall error.

6.7.6 Error from $\nu K_2/K_1$

Beaney and Procter[2] reported that $\nu K_2/K_1$ can be assumed to be a constant value of 0.3 for Micro-Measurements strain gauge rosettes - type EA-XX-062RE-120, and 0.33 for BLH strain gauge rosettes - type FAER-03S-12-SX EG or similar. They further reported that the scatter in this assumption was approximately 12% and that the resulting error in the maximum numerical principal stress is less than half the error in the constant. The overall error varies from approximately -2.76% when the system is in pure shear to approximately 5.16% as the system

changes to equal biaxial tension, as can be seen in Fig 6.26. From the present AACH drilling results, it can be seen that the ratio of $\sigma_{max} : \sigma_{min}$ is rarely above 0.5. Therefore from Fig 6.26 the error in maximum numerical principal stress is 0.26% for 1% error in $\nu K_2/K_1$. But from the above, the scatter in assuming a constant value of $\nu K_2/K_1$ can be as high as approximately 12%. So the error in principal stress from $\nu K_2/K_1$ is approximately 3%.

6.7.7 Total Error

From the discussion thus far, the various errors are summarised below:

Induced machining stresses	1 %
Hole misalignment	2 %
Hole diameter measurement	0.2 %
Hole geometry	5 %
Plasticity effects	~ 0 %
$\nu K_2/K_1$ error	3 %

As a worst condition, these percentage errors could simply be added, yielding 11.2%. However this is unnecessarily conservative and an error summation analysis that is more realistic yields 6.2%.

This error is considered to be the maximum error obtained for at least 90% of the air abrasive centre hole drilling measurements performed. In fact most measurements were considered to have greater accuracy than this figure, which is comparable with the error found during calibration.

6.8 Summary Discussion

In this chapter thus far, the results of residual stress measurements made using the AACH drilling and ring splitting techniques have been discussed and compared. This formed part of the investigation conducted into the failure of 7075-T6 aluminium drill rods manufactured by Hulett Aluminium, which

were perceived to fail in service by their clients. Hulett Aluminium thought, however, that the problem was due to bad handling rather than due to manufacture. From the results, it can be determined whether residual stress contributed significantly to failure by superimposing the service loads on the residual stress distribution.

6.8.1 Shortcomings

The main shortcoming of the residual stress measurement was that due to the high cost of the strain gauge rosettes and the length of the drill rods, limited measurements were made in an effort to optimise strain gauge rosette utilisation. Comprehensive measurements were conducted at the 1/4, 1/2 and 3/4 points of each rod. From these measurements, stress trends were found and comparisons were made, both on individual rods and between them.

6.8.2 Comparison of Drill Rods A, E and F

Before experimentation commenced, geometric similarities were noticed between the drill rods. Their bending deflection curves had similar shapes (taking into account that rod F was shorter than rods A and E), but had different magnitudes, as can be seen in Fig 6.1. This difference in magnitude was thought to be due to the different straightening methods employed to straighten the rods. In Section 6.2, it was conjectured that the residual stress pattern may be related to the bending deflection or curvature of the rods. There is not enough data to confirm this with the results from the AACH drilling technique, but various trends which are discussed shortly give evidence of this residual stress-curvature relationship. If one, however, considers the results of the ring splitting technique, which lack accuracy but serve as a good means of comparison, then it can be seen in Fig 6.17 - 6.19 that there is evidence of stress peaks and dips around the 1/4, 1/2 and 3/4 points of the rods, which coincide with the points of local maximums and minimums in bending deflection of the rods. Further analysis of the manufacturing routes is however required to determine what causes the bending deflections.

Due to the similarity in the manufacturing processes of rods A and F, their results are also similar and show consistency. Whereas rod E yields quite different results with not many trends. The results are summarised in Table 6.11 where maximum, minimum and average values of σ_1, σ_2, σ_h and σ_l on the outer surface of the drill rods from the AACH drilling technique and values of σ_h from the ring splitting technique are given. Rod F has the highest measured residual stress, followed by rod A, on their outer surfaces. In contrast, Rod E has compressive residual stresses on its outer diameter, with magnitudes smaller than the stresses in rods A and F. As mentioned previously, stresses on the inside surfaces of the rods are smaller in magnitude and opposite in sign to the stresses measured on the outside surfaces.

Further similarities between rods A and F (but not rod E), are that σ_1 acts close to the circumferential direction and σ_2 close to the longitudinal direction (see results in Appendix H), the maximum longitudinal stresses predominate at the 6 o'clock position (see Fig 6.6), the stress flow directions predominate at 62° to the longitudinal direction of the rods which coincides with the spiral of the straightening process (see Fig 6.4), and there was evidence of periodicity in the stresses (see Table 6.4). The last three points give strong evidence that the reels used for straightening the rods influence the residual stress distribution in two ways: (i) by bending the rods from a large "arch" to a smaller "arch", (ii) by spiraling along the length of the rods. If this is correct, then it may explain why the stresses in rod F are higher than those in rod A, since it was passed through the reels on two separate occasions.

Rod E differs from the above in that the stress distribution and direction exhibited no preferred direction, and was effectively random. Therefore none of the above trends were exhibited. This is assumed to be due to the straightening process, which comprised of an axial stretch slightly in excess of the 0.2% proof stress. The stresses are thought to have been redistributed and reoriented so that nominally equibiaxial stress fields resulted.

Other trends exhibited by all three rods are that they have constant average longitudinal stresses along their length. Also the ring splitting results are approximately equal to the bending component and three times the membrane component of the average AACH residual hoop stresses, and resultantly 75% of the total average AACH residual hoop stresses.

6.8.3 Contribution of Residual Stress to Drill Rod Failure

Now that the residual stresses in the three drill rods have been analysed, the question of whether it was the cause of any failures needs to be answered. Problems were experienced with rods manufactured according to the so called "old route", therefore the results of rod A are examined here. Some high residual stresses were measured in rod A, for example 136.9 MPa in specimen 8A at the 6 o'clock positions. However, on average the stresses were much lower - see Table 6.11, and it would depend on the service loads whether these stresses are regarded as unacceptably high. It had been reported that environmentally assisted crack growth (corrosion fatigue but not stress corrosion cracking (SCC)) occurred at the first engaged thread (see Fig 1.7) of some drill rods[74], which is near the centre of the rod wall thickness. If the stress gradient of rod A is considered (ie. 106.7 MPa on the outer surface and -51.43 MPa on the inner surface), it can be reasoned that the stresses in this area are low. However it is not known how the machining of the thread at the end of the drill rods affected the residual stress distribution, since no threaded samples were provided. It is nonetheless felt that the problem was more probably one of the threaded couplers (which connect the drill rods) being overtorqued[74], or bad handling aspects, rather than excessively high stresses in manufacture. Had this been the case, there would have been vast numbers of pipe failures (from SCC) and this was not the case! Indeed pipe failures were remarkably rare[74].

If residual stress is however considered to be a problem, then it is recommended that the "stretch route" be used to manufacture the drill rods, even though the stretch may be

expensive to incorporate into the production line process. The advantages of the stretch route are that the induced residual stress are low and compressive which is favourable especially when superimposed by the service loads.

Rod	Average Length	Average O.D.	Average I.D.
A	2572.5	70.04	50.98
E	2581.0	69.92	50.94
F	1745.0	69.85	50.85

Table 6.1 - Drill rod dimensions (mm) measured before experimentatiom.

Position	Distance (mm)	Relieved strains	
		1/2 cut	1/4 cut
12	708.7	0.0	10.0
o'clock	1030.5	0.0	1.5
side	1981.8	3.0	
6	700.0	-2.0	10.0
o'clock	1020.9	1.5	3.0
side	1982.4	4.0	

Table 6.2 - Relieved longitudinal strains due to cutting of drill rod A.

SPEC NO.	POSITION o'clock	SIG(1) MPa	SIG(2) MPa	ANGLE Degrees
2A	6	71.1	8.1	78.0
8A	12	82.7	17.0	-71.1
8A	3	87.0	21.9	73.9
8A	6	136.9	74.2	-50.3
8A	9	88.5	42.2	-60.7
14A	3	99.0	50.3	-58.9
18A	12	66.3	9.8	-81.0
18A	3	106.7	56.8	-55.0
18A	6	80.3	39.2	54.3
18A	9	90.8	-13.2	66.8
27A	12	65.1	11.4	-66.4
27A	3	63.9	31.8	-51.9
27A	6	105.8	59.5	58.2
27A	9	66.0	16.8	-68.4
30A	6	73.8	26.0	-66.4

Table 6.3 - Stress flow directions for rod A.

DRILL ROD	ROD A			ROD F
FROM	8A 6 o'cl	18A 3 o'cl	8A 6 o'cl	5,6,7F 3 o'cl
TO	18A 3 o'cl	27A 6 o'cl	27A 6 o'cl	19,20,21F 6 o'cl
DISTANCE	700 mm	630 mm	1330 mm	980 mm
REVS	5.75	5.25	11	8.25
PERIOD	121 mm	120 mm	120 mm	118 mm

Table 6.4 - Periodicity of stresses for rods A and F.

SECTION 15,16,17A - ROOF CUT			
Reading	OD0	ID0	OD1
1	70.077	51.118	70.134
2	70.066	51.104	70.136
3	70.078	50.081	70.138
4	70.076	50.047	70.126
5	70.078	50.032	70.092
Ave Dia	70.075	51.037	70.084
Ave Thk	9.519		
Calculated Stress =			1.4 MPa
Error =			3.4 MPa

Table 6.5 - Ring split stress released due to cutting of a hole for inside surface measurements.

SPEC NO.	POSITION o'clock	SIG(1) MPa	SIG(2) MPa	ANGLE Degrees
8,9,10E	12	-1.3	-8.8	76.1
8,9,10E	3	-14.6	-19.9	-26.3
8,9,10E	6	-9.4	-20.2	54.3
8,9,10E	9	-14.0	-21.0	4.0
17,18,19E	12	-6.0	-18.9	34.3
17,18,19E	3	-12.2	-25.1	62.5
19E	6	-9.0	-10.0	-25.6
19E	9	-4.3	-10.5	20.2
27,28,29E	12	-13.4	-30.9	58.2
27,28,29E	3	-27.9	-31.1	33.4
27,28,29E	6	-24.5	-39.6	-38.4
27,28,29E	9	-22.0	-27.5	-31.5

Table 6.6 - Stress flow directions for rod E.

SPEC NO.	POSITION o'clock	SIG(1) MPa	SIG(2) MPa	ANGLE Degrees
5,6,7F	12	93.1	49.9	-60.8
5,6,7F	3	153.5	85.9	59.2
5,6,7F	6	138.5	7.6	-82.7
5,6,7F	9	87.6	22.2	-48.9
12,13,14F	12	88.5	42.7	-55.0
12,13,14F	6	151.2	52.5	62.6
19,20,21F	12	93.2	46.3	-53.5
19,20,21F	3	104.8	53.8	57.2
19,20,21F	6	215.2	118.3	-59.8
19,20,21F	9	93.4	30.3	-50.1

Table 6.7 - Stress flow directions for rod F.

Specimen	O.D.	Mid-wall	I.D.
5,6,7F	138.5	48.9	-53.7
19,20,21F	215.2	56.1	-107.4

Table 6.8 - Stress (MPa) variations through the wall thickness of rod F at the 6 o'clock position.

Spec. No.	AACH Stress Results (MPa)				Ring Split (MPa)
	Outer Surface	Inner Surface	Membran Cpt	Bend Cpt	
18A	78.5	-40.7	18.9	59.6	53.9
17,18,19E	-13.4	6.8	-3.3	-10.1	-13.5
5,6,7F	114.6	-54.8	31.4	83.2	67.4
19,20,21F	123.9	-107.5	9.5	117.0	81.4

Table 6.9 - Comparison of hoop stresses between the AACH drilling and ring splitting techniques.

Note: For spec 18A the inner surface stress was taken from adjacent specimen 15,16,17A.

Spec. No.	Average AACH	75% AACH	Ring Split	Variance %
8A	97.8	73.4	66.5	9.4
18A	78.5	58.8	53.9	8.3
27A	74.0	55.5	59.3	6.4
8,9,10E	-14.9	-11.2	-6.6	41.1
17,18,19E	-13.4	-10.1	-13.5	25.2
27,28,29E	-31.6	-23.7	18.0	24.1
5,6,7F	114.6	86.0	67.1	22.0
12,13,14F	118.2	88.7	91.3	2.9
19,20,21F	123.9	92.9	81.4	12.4
Average Variance =				13.8

Table 6.10 - Comparison of ring splitting to AACH hoop stress results.

Stress		Rod A	Rod E	Rod F
Maximum	Max	136.9	-1.3	215.2
Principal	Min	63.9	-27.9	87.6
(MPa)	Avg	85.6	-13.3	121.9
Minimum	Max	74.2	-8.8	118.3
Principal	Min	-13.2	-39.6	7.6
(MPa)	Avg	28.9	-22	50.9
Hoop	Max	134.5	-4.3	215.1
(MPa)	Min	62.1	-37.9	74.3
	Avg	82.9	-19.9	116.6
Long	Max	76.6	-1.3	118.4
(MPa)	Min	9.8	-28.1	8.3
	Avg	32.8	-15.3	52.6
Ring	Max	76.6	-7.3	101.9
Split	Min	47.6	-31.7	53.2
(MPa)	Avg	59.4	-17.9	76.9

Table 6.11 - Summary of residual stresses on the outer surface of the drill rods.

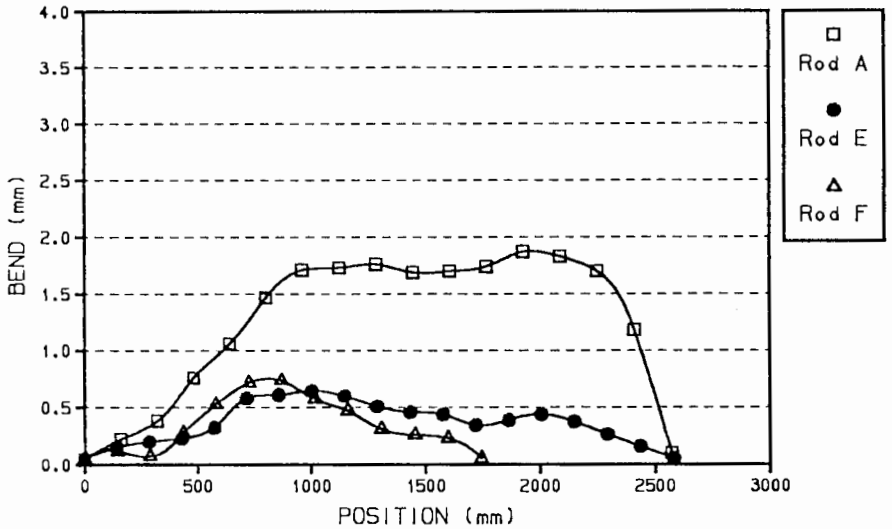

Fig 6.1 - Comparison of the bending deflections of the three drill rods.

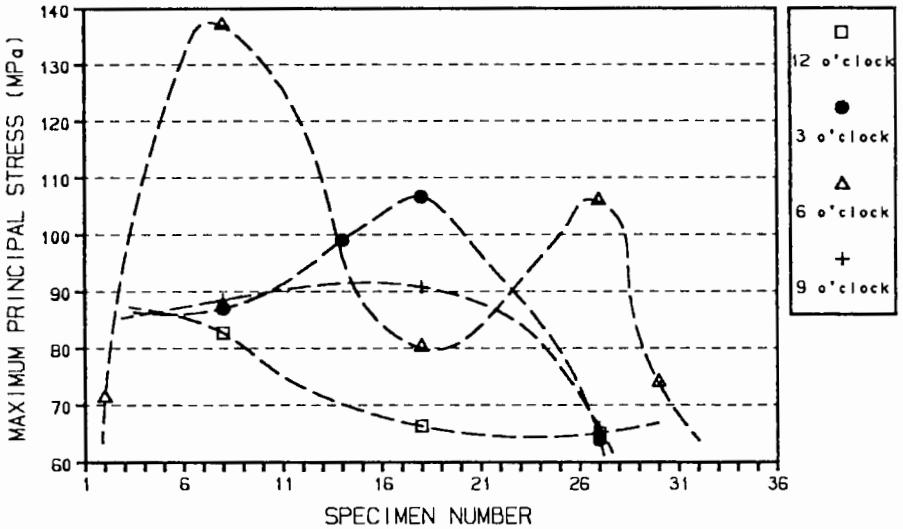

Fig 6.2 - Maximum AACH principal stresses as a function of distance along the length of rod A.

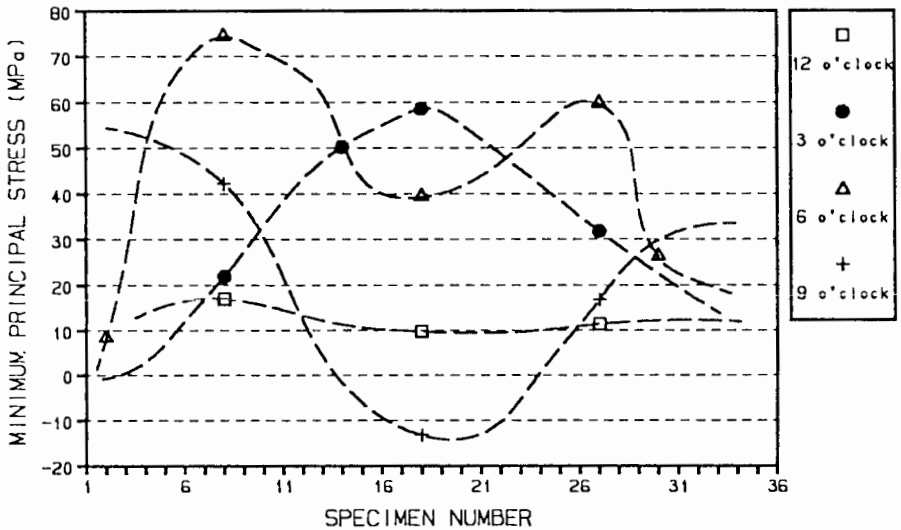

Fig 6.3 - Minimum AACH principal stresses as a function of distance along the length of rod A.

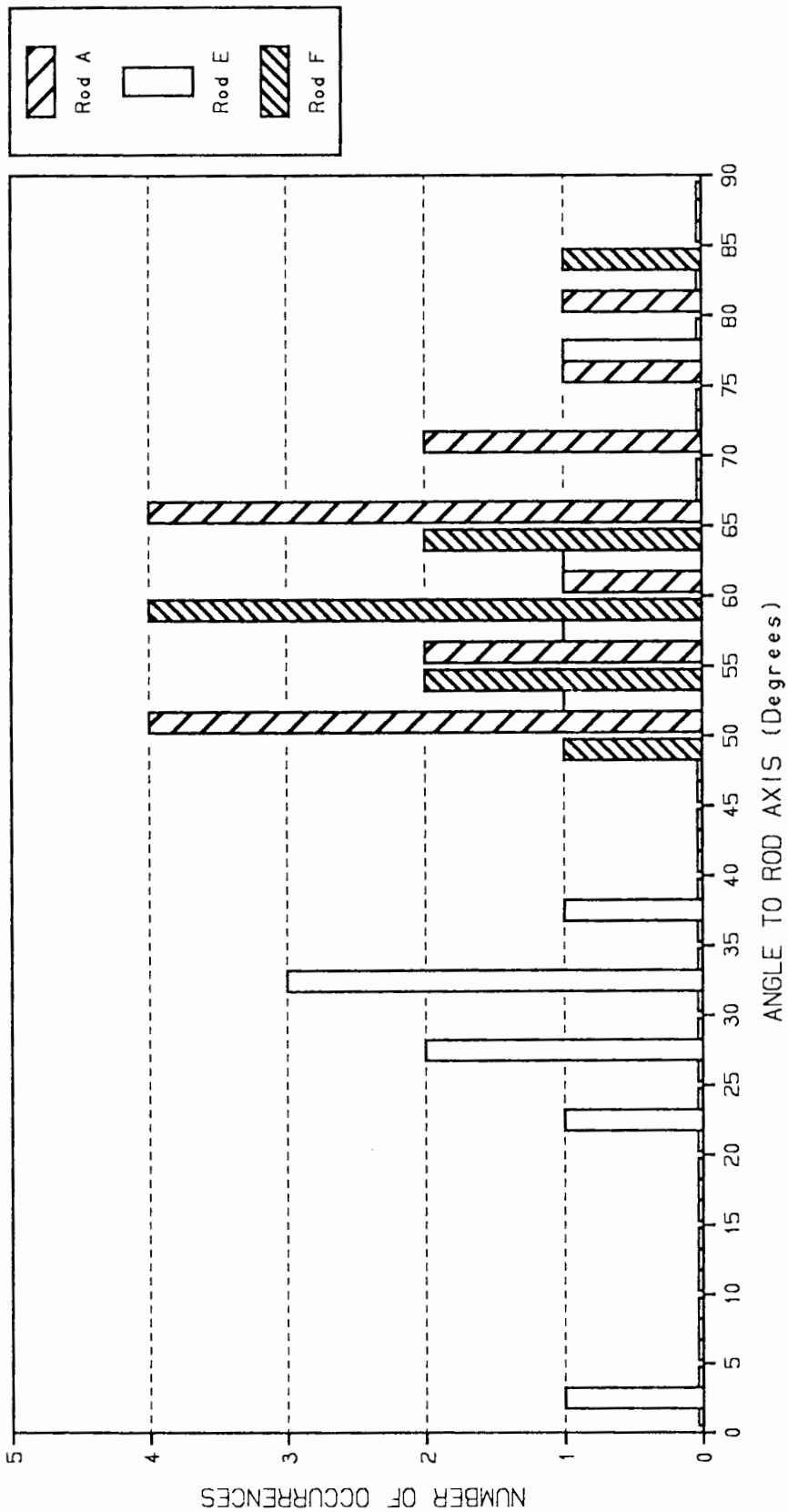

Fig 6.4 – Distribution of the stress flow directions in the drill rods.

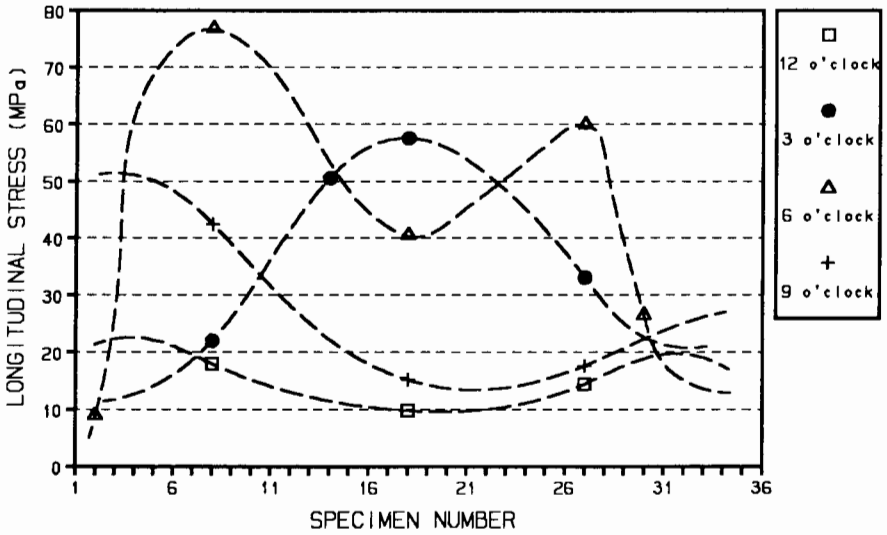

Fig 6.5 - Longitudinal AACH stresses as a function of distance along the length of rod A.

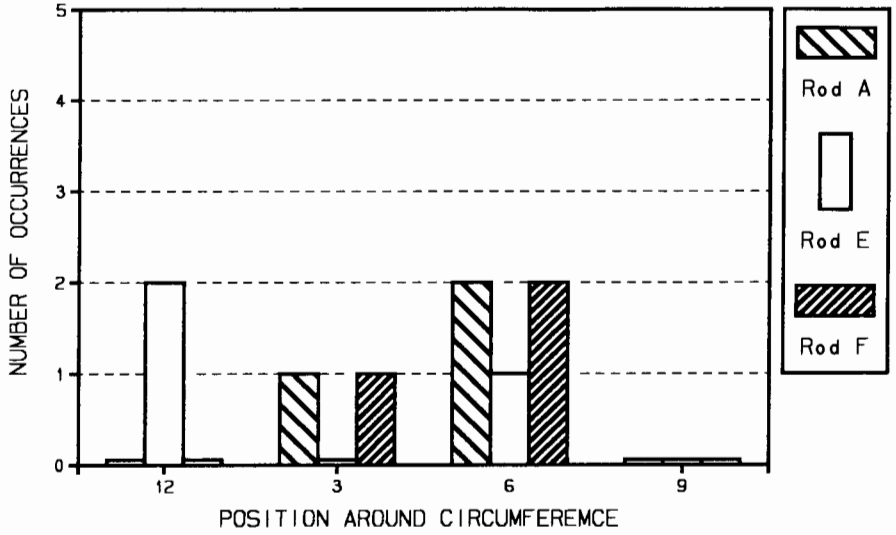

Fig 6.6 - Distribution of the maximum longitudinal stresses around the circumference of the rods.

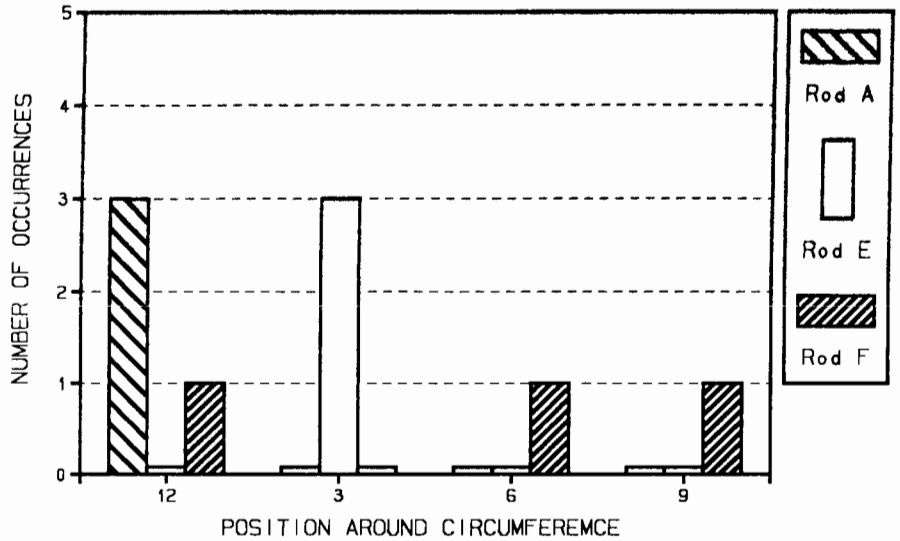

Fig 6.7 - Distribution of the minimum longitudinal stresses around the circumference of the rods.

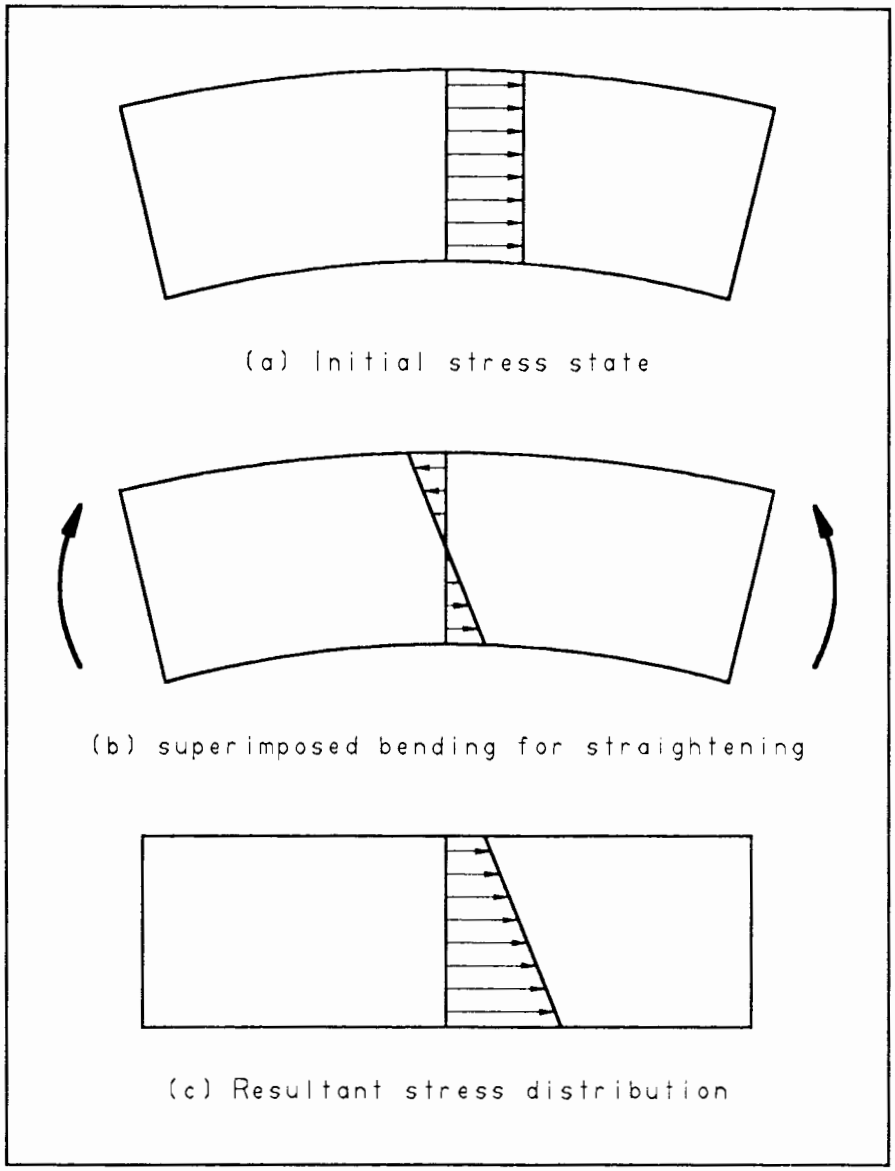

Fig 6.8 - The effect of straightening bent drill rods on longitudinal stresses.

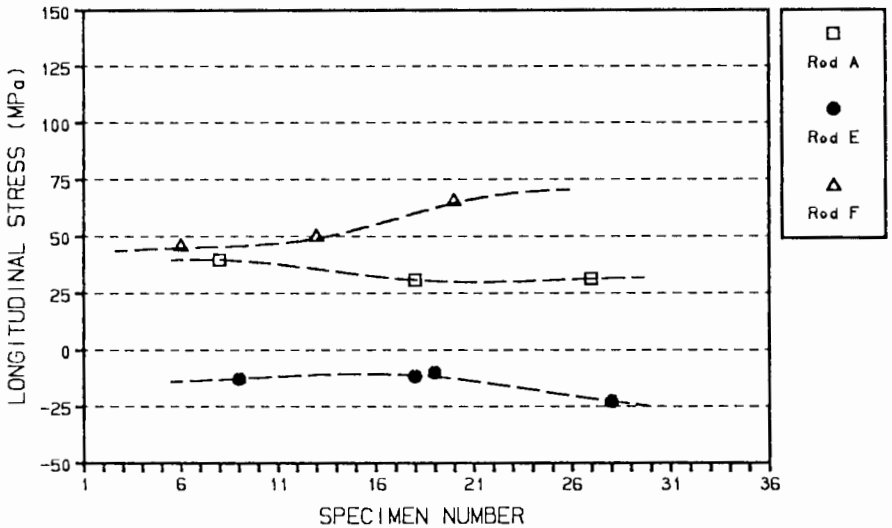

Fig 6.9 - Average longitudinal AACH stress distribution as a function of distance along the length of the rods.

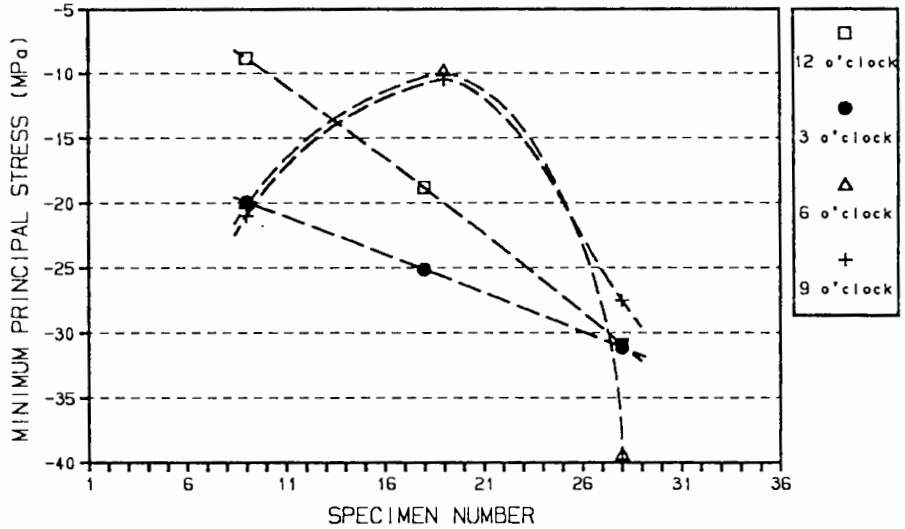

Fig 6.10 - Minimum AACH principal stresses as a function of distance along the length of rod E.

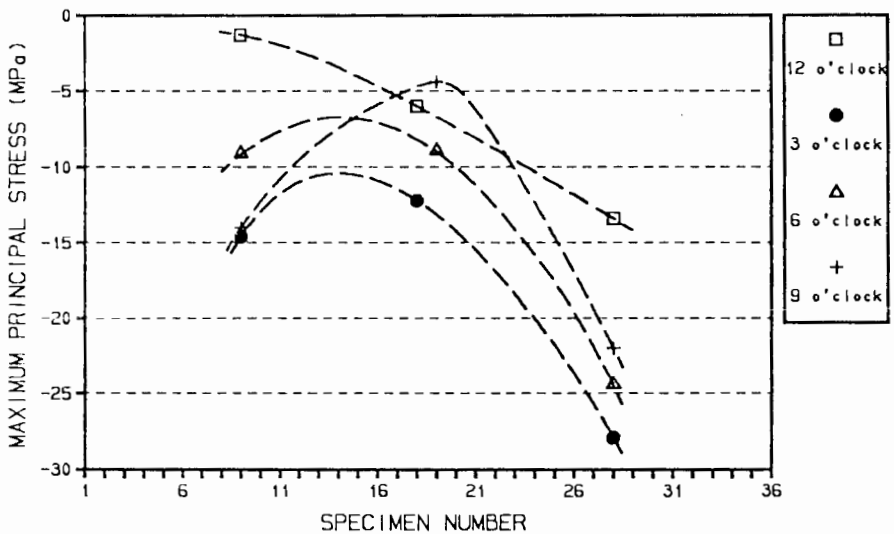

Fig 6.11 - Maximum AACH principal stresses as a function of distance along the length of rod E.

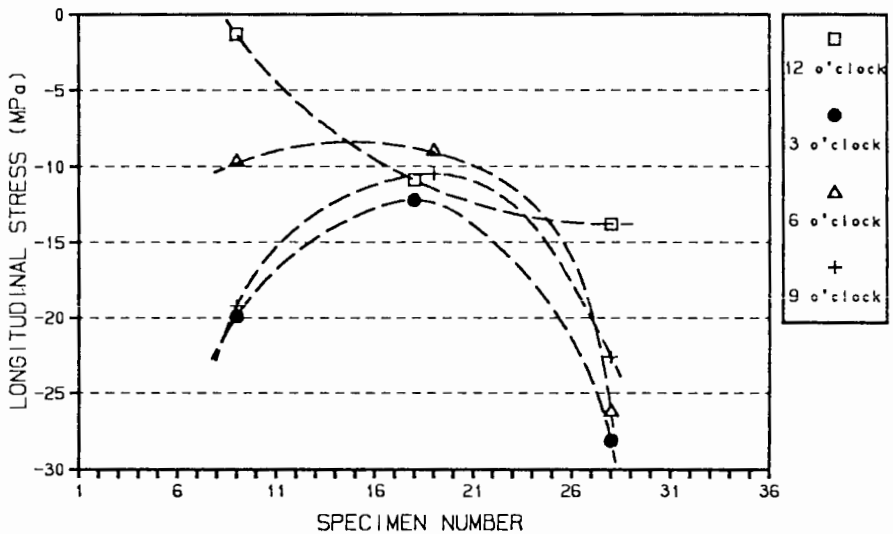

Fig 6.12 - Longitudinal AACH stresses as a function of distance along the length of rod E.

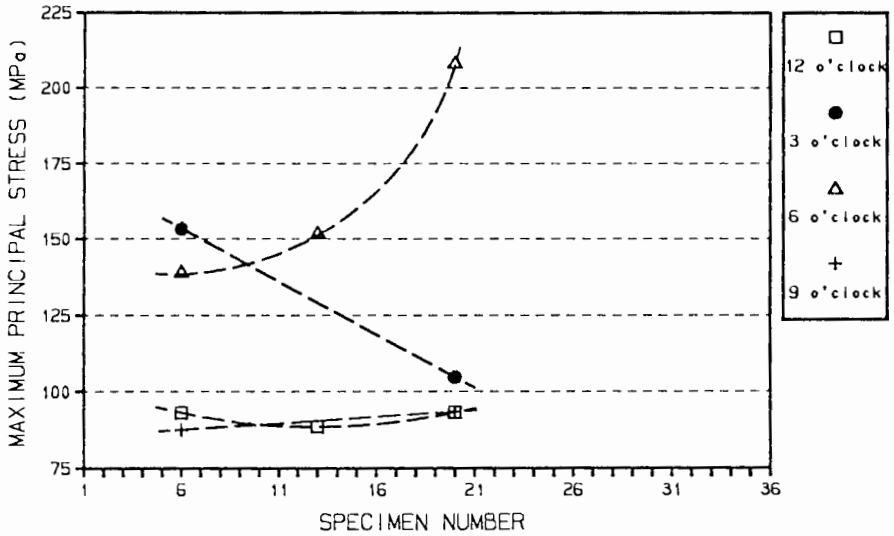

Fig 6.13 - Maximum AACH principal stresses as a function of distance along the length of rod F.

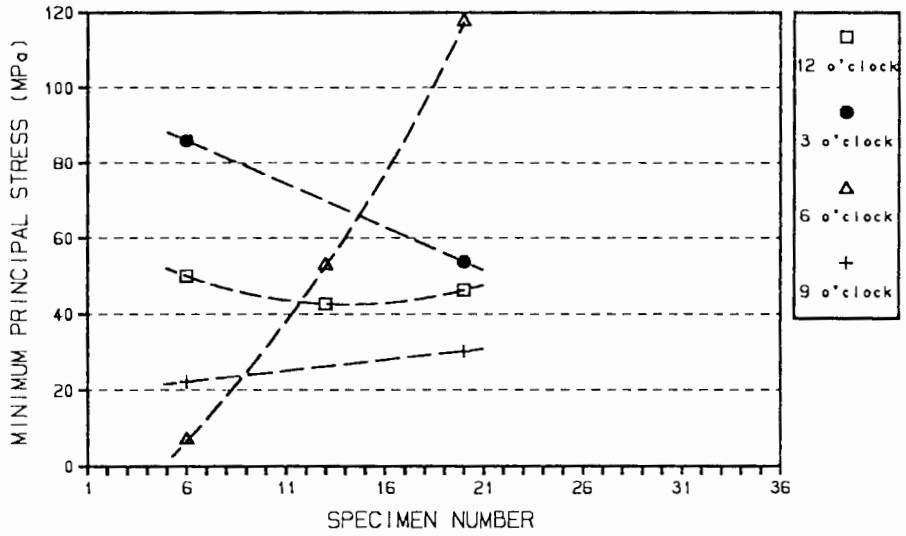

Fig 6.14 - Minimum AACH principal stresses as a function of distance along the length of rod F.

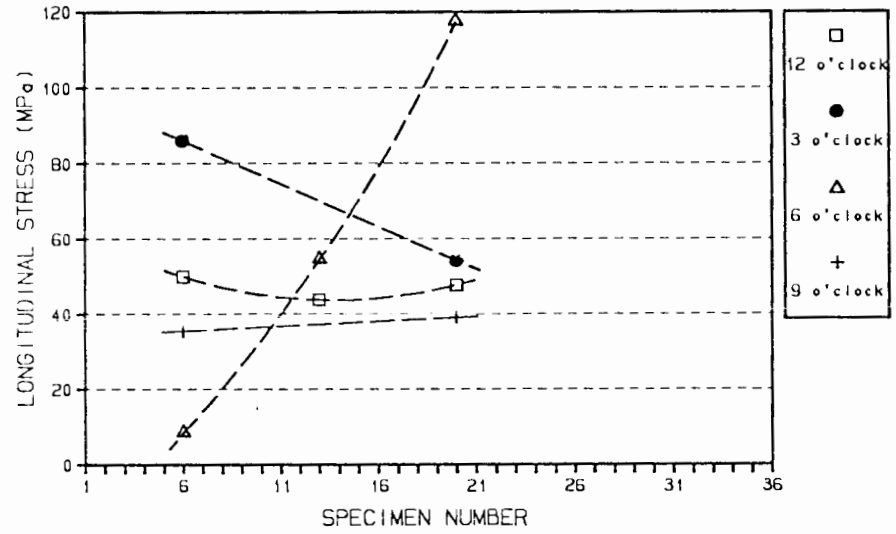

Fig 6.15 - Longitudinal AACH stresses as a function of distance along the length of rod F.

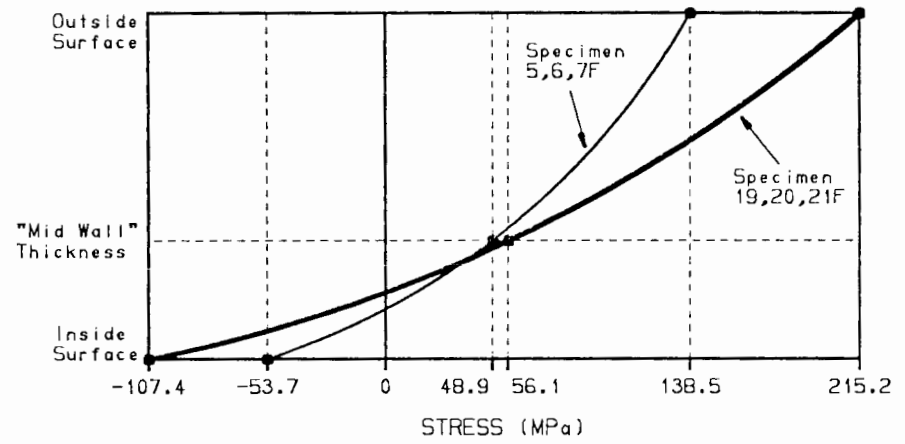

Fig 6.16 - Stress gradient through the wall thickness of rod F.

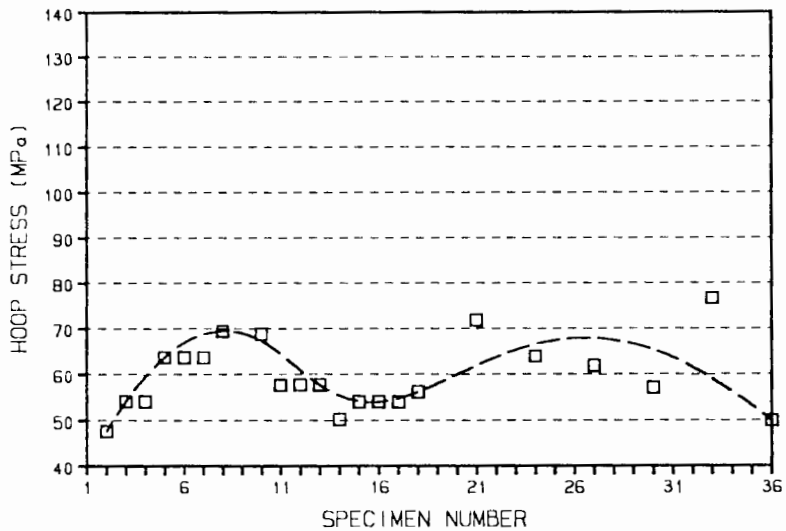

Fig 6.17 - Ring splitting hoop stresses as a function of distance along the length of rod A.

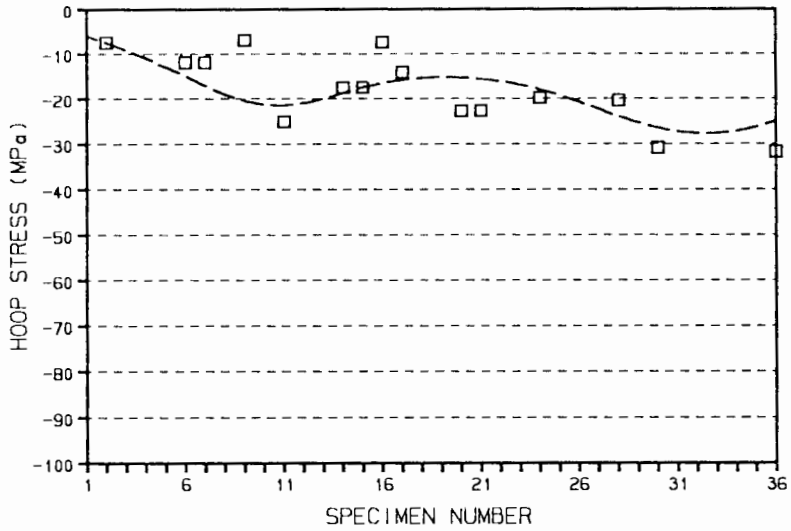

Fig 6.18 - Ring splitting hoop stresses as a function of distance along the length of rod E.

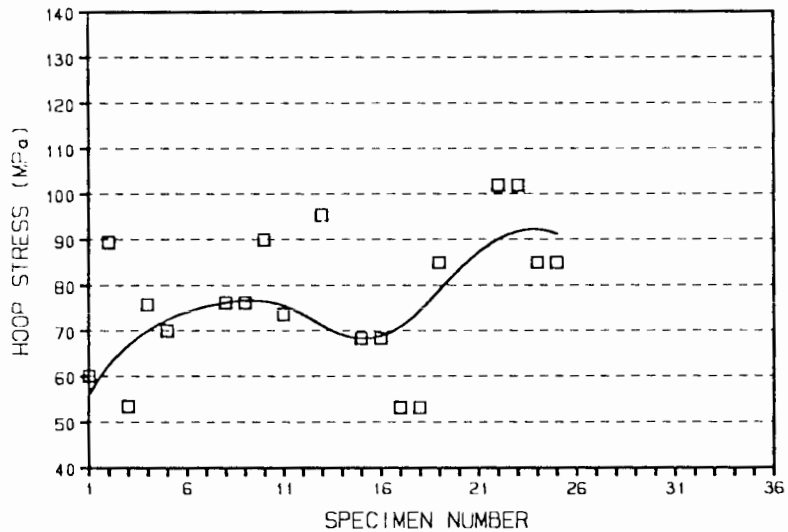

Fig 6.19 - Ring splitting hoop stresses as a function of distance along the length of rod F.

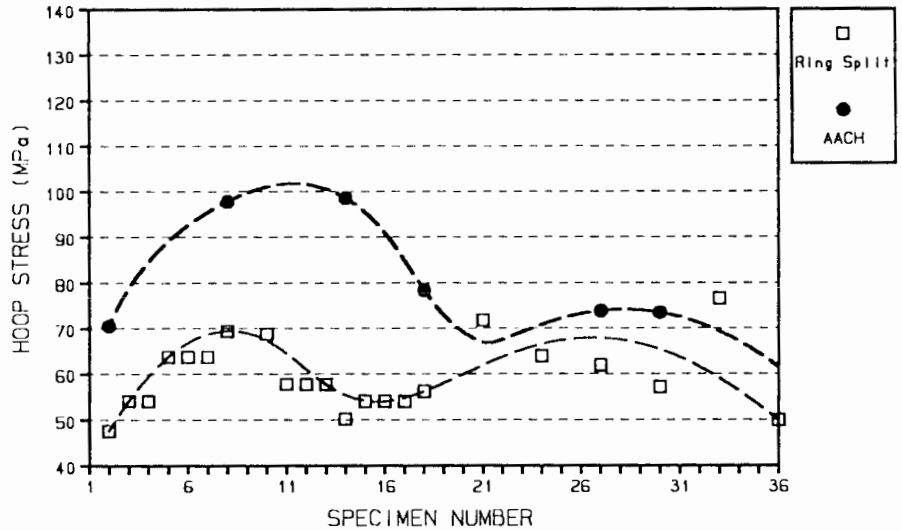

Fig 6.20 - Comparison of average AACH and ring splitting hoop stresses for rod A.

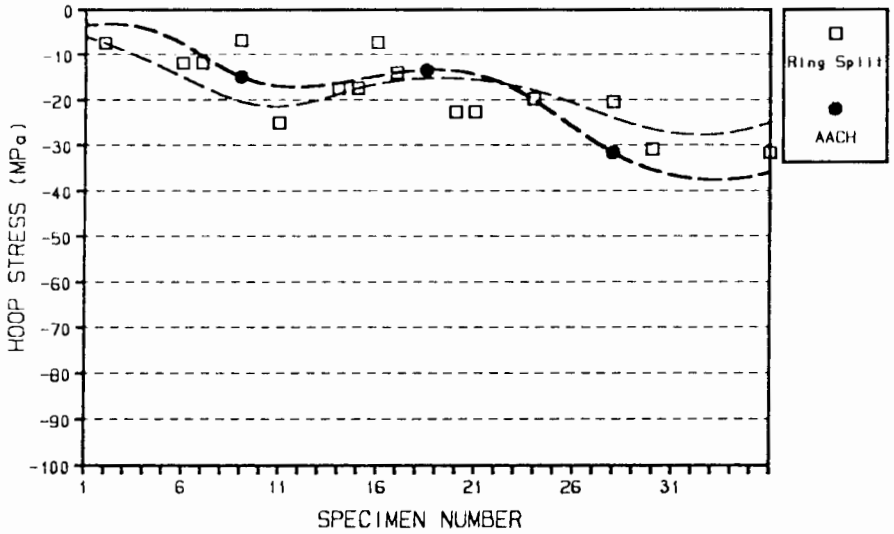

Fig 6.21 - Comparison of average AACH and ring splitting hoop stresses for rod E.

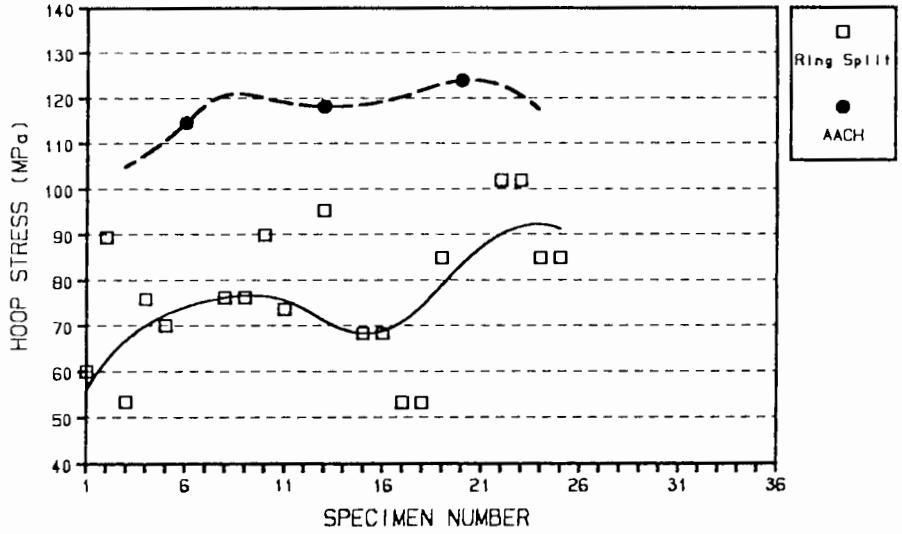

Fig 6.22 - Comparison of average AACH and ring splitting hoop stresses for rod F.

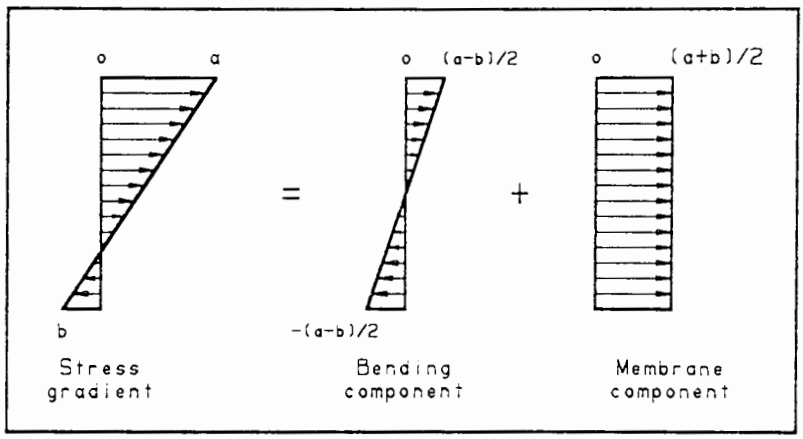

Fig 6.23 - Components of a linearly varying stress gradient.

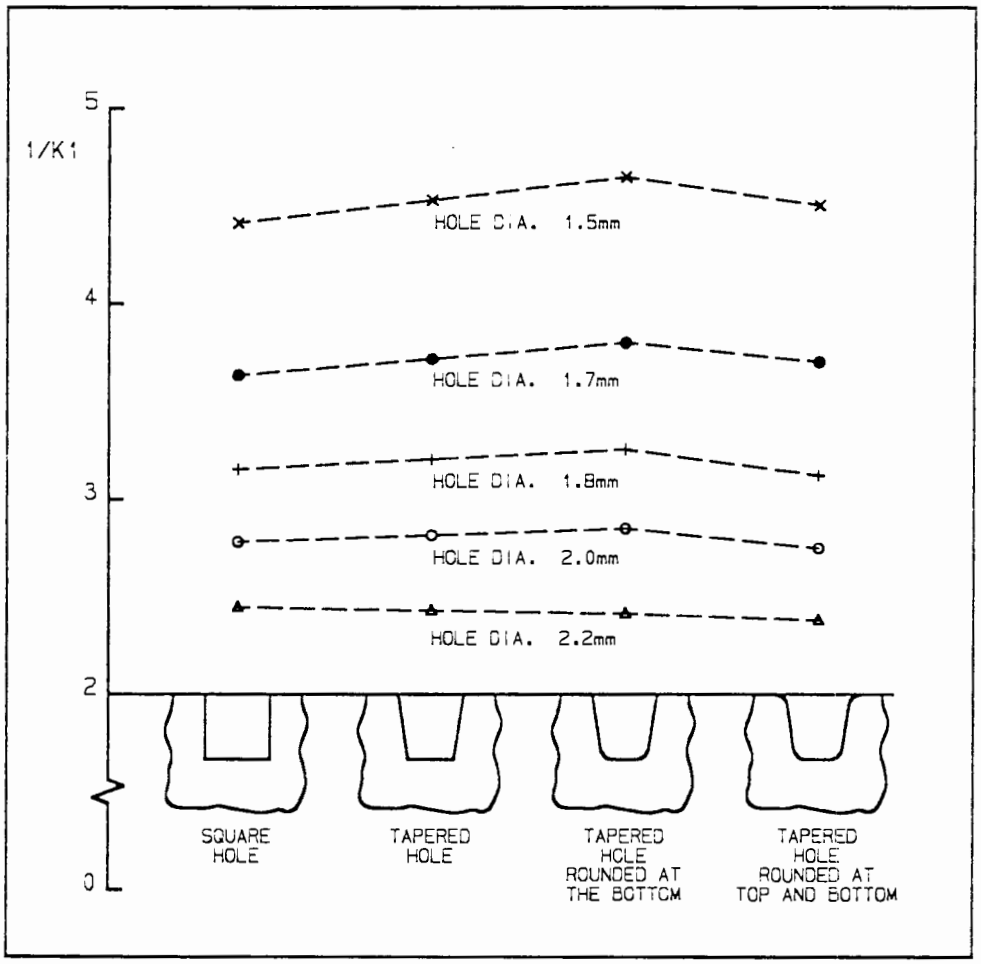

Fig 6.24 - Effect on 1/K1 of change in hole geometry[3].

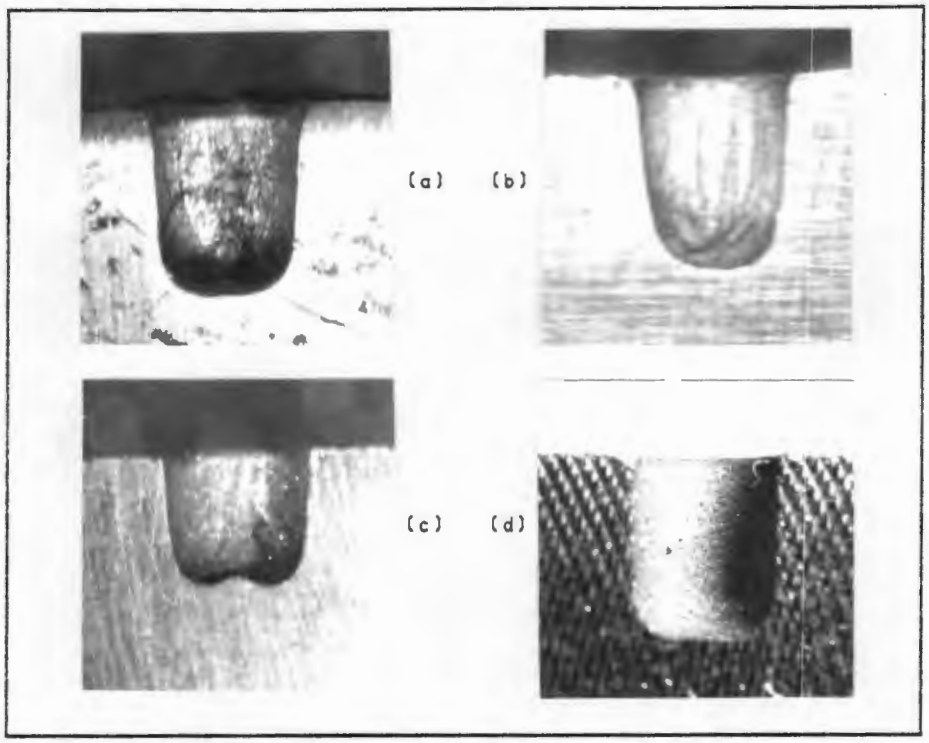

Fig 6.25 - Various hole profiles obtained while using the air abrasive centre hole technique.

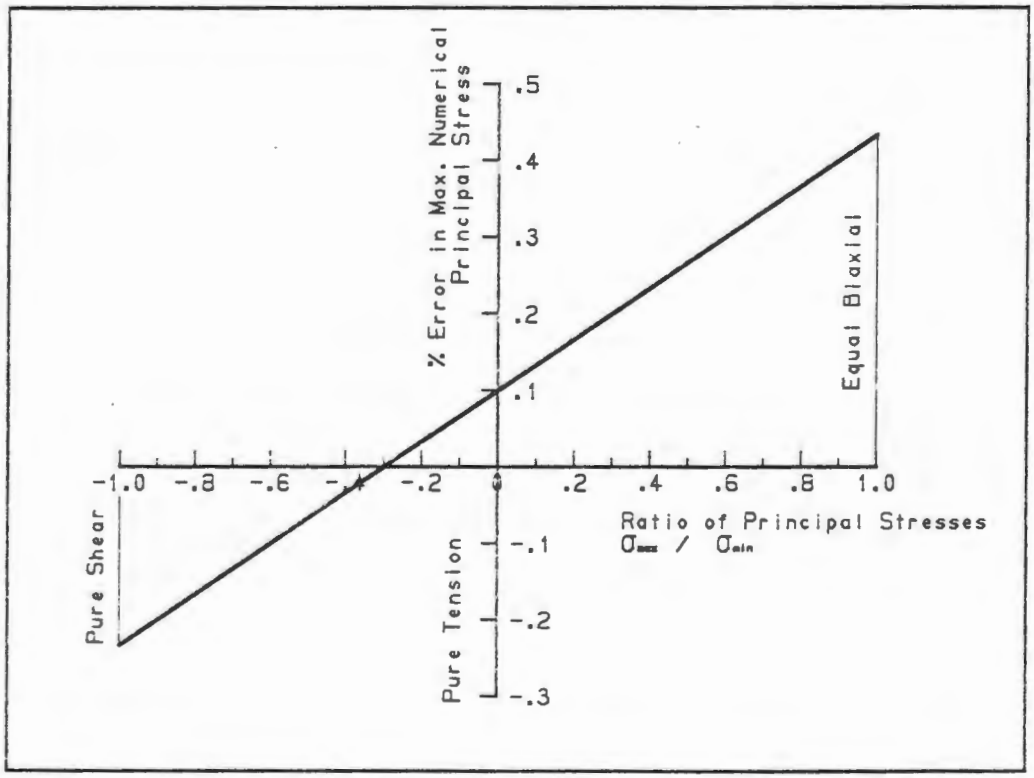

Fig 6.26 - Error in maximum numerical principal stress for a 1% error in $vK2/K1$ [2].

7. CONCLUSIONS AND RECOMMENDATIONS

7.1 Introduction

In this thesis a variety of residual stress measurement techniques have been investigated, from which the air abrasive centre hole (AACH) drilling technique was chosen to perform accurate residual stress measurements. In addition, it was decided to use the ring splitting technique to compare the results of a quick and easy technique to a reliable one, when examining the residual stresses in extruded aluminium drill rods. The equipment necessary to perform the AACH drilling technique was then designed, manufactured and calibrated, so that holes of around 1.5 mm diameter (and depth) and of the required profile could be drilled, allowing accurate residual stress measurements to be obtained. Thereafter residual stresses were measured in aluminium drill rods from three similar but slightly different manufacturing processes, using both the AACH and ring splitting techniques. The results obtained were then analysed and compared in order to establish trends in the residual stress distributions, the possible cause of the residual stresses arising during manufacture and whether the presence of residual stresses in the drill rods was responsible for their failure.

7.2 Conclusions

The conclusions drawn can be divided into (i) those pertaining to the residual stress measurement techniques - investigation and design, and (ii) those pertaining to the results of testing of the drill rods.

7.2.1 Residual Stress Measurement Techniques - Investigation and Design

The following conclusions can be drawn here:

i. An AACH drilling device was designed and built based on a similar system due to Beaney and Procter[1-3].

ii. The AACH drilling technique can be used as an accurate

and reliable method of residual stress measurement. It was used to measure residual stress values within an accuracy of approximately 6%.

iii. When using the AACH drilling technique, a "squared" hole of a depth equal to diameter was regarded as providing best results.

iv. With respect to the specific test facility that was built, the following parameters were applied in order to drill a hole approximately 1.5 mm in depth and diameter: a nozzle offset of 0.425 mm, a tilt of between 0 and -1 (-0.17° to -0.28°), a 5.5 bar air pressure, a 6 to 6.5 vibrator setting and a drilling time of 4 to 5 minutes.

v. The ring splitting technique is suitable as a simple shop floor method of residual stress measurement in extruded rods.

7.2.2 Testing and Results

Additional conclusions that can be drawn are the following:

vi. Tests were conducted on sample aluminium (7075 - T6 alloy) drill rods, supplied by Hulett Aluminium, to measure inherent residual stresses (σ_1, σ_2, σ_H, σ_L) using the AACH drilling and ring splitting techniques.

vii. The principal findings of these tests are listed below:

- The highest residual stresses were found on the outer surfaces of rod F ("new route"), followed by rod A ("old route") with tensile values of 215.2 and 136.9 MPa respectively. Rod E ("stretch route") had the lowest residual stresses and these were opposite in sign (ie. compressive), with the most compressive value of -39.6 MPa.
- Stress reversal existed through the wall thickness of the rods, with a "maximum" inside surface stress value of -51.3 MPa, 6.8 MPa and -58.8 MPa for rods A, E and F respectively.
- For rods A and F, σ_1 was aligned predominantly in the hoop or circumferential direction; whereas for rod E,

σ_1 acted more biaxially, or in effectively randomly distributed directions.

- The stress flow direction in rods A and F predominated at approximately 62° to their longitudinal direction, which coincided with a spiral presumably caused by the straightening process when the rods were passed through a series of reels. Furthermore, there was evidence of periodicity in the stresses in rods A and F arising from this spiralling effect. Rod E, however, did not exhibit these trends presumably since it was straightened by means of an axial stretch.
- The maximum values of σ_L measured around the circumferences of rods A and F were generally found at the 6 o'clock position (ie. the bottom of their slight initial bend) and the minimum values of these stresses, at the 12 o'clock position (ie. the top of their initial bend). Rod E did not show this trend due to the equal equi-biaxial stresses induced by the axial stretch at most points.
- The average longitudinal stresses along the length of the rods were approximately constant.
- The residual stresses measured using the ring splitting technique followed the trend in variation along the length of the rods exhibited by the AACH drilling results, however they were lower in magnitude.
- The ring splitting results can be compared well to the AACH drilling results. The ring splitting results were approximately equal to the bending component, three times the membrane component and therefore three quarters of the AACH hoop stress results.
- The maxima and minima in the initial bending deflection curves of the rods corresponded well to the peaks and dips in the respective ring splitting stress distributions along the rods.
- There was further evidence of the correlations between the initial bending deflection curves of rod A and F and their respective residual stress distributions.

- From the careful but necessarily limited number of residual stress tests undertaken, residual stress was not regarded as the cause of drill rod failure.

7.3 Recommendations

Based on the findings and conclusions of this report, the following recommendations can be made:

i. The AACH drilling technique can be used as an accurate and reliable method of residual stress measurement.

ii. The ring splitting technique can be used as a quick and easy method of determining approximate residual stresses in extruded drill rods.

iii. The "Stretch Route" (rod E) should be used to manufacture future drill rods, despite the cost implications, if residual stress is considered a problem by Hulett Aluminium.

iv. Hulett Aluminium can use the ring splitting technique to determine hoop residual stresses in drill rods, since if the results are multiplied by a factor of approximately 4/3, then the hoop residual stresses (which are approximately equal to the maximum principal residual stresses) on the outer surface can be approximated with an average error of 13.8%

v. The lack of stiffness of the AACH drilling system should be rectified for ease of use, otherwise the optical and drill units should be used consistent with the orientation marked on the base plate.

vi. The securing ring on the drilling and optical units should incorporate a form of quick release to facilitate the securing and removing of these units to and from the guide bush, thereby speeding up this presently tedious task.

vii. Strain gauge rosettes should include short wires attached to the terminals of each strain gauge element, thereby facilitating the set-up procedure for AACH drilling

tests.

viii. Practice holes should be drilled in scrap material, similar to that to be tested, before conducting tests in order to optimise the variables (ie. drilling time, air pressure etc). This will ensure consistency and better results.

LIST OF REFERENCES

1. Beaney E M, Instuction Manual for the CEGB Air Abrasive System for Measuring Residual Stresses, 1986.

2. Beaney E M and Procter E, 'A Critical Evaluation of the Centre Hole Technique for the Measurement of Residual Stresses,' Strain, 10 (1974), pp. 7-14.

3. Beaney E M, 'Accurate Measurements of Residual Stress on any Steel Using the Centre Hole Method,' Strain, 12 (1976), pp. 99-106.

4. Johnson W and Mellor P B, Plasticity for Mechanical Engineers, London, D. Van Nostrandt Company Ltd, 1962, pp. 206-208.

5. Niku-Lari A, Lu J and Flavenot J F, 'Measurement of Residual Stress Distribution by the Incremental Hole-Drilling Method,' Experimental Mechanics, 25 (1985), pp. 175-185.

6. Sadat A B and Bailey J A, 'Residual Stress in Turned AISI 4340 Steel,' Experimental Mechanics, 27 (1987), pp. 80-85.

7. Perry C C, 'Residual Stress...the Nemesis of the Liberty Bell,' Epsilonics, December (1983), pp. 10-11.

8. Polakowski N H, Strength and Structure of Engineering Materials, New Jersey, 1966, pp. 458-484.

9. Tokarcik A G and Polzin M H, 'Quantitative Evaluation of Residual Stresses by the Stress Coat Drilling Technique,' Experimental Stress Analysis, 9 (1952) pp. 195-207.

10. Baldwin W M, 'Residual Stresses in Metals,' Edgar Marsburg Lecture, June (1949), pp. 539-583.

11. Israeli A and Papiar R, 'Residual Stress Profile in Machined Parts,' ASTM Journal of Testing and Evaluation, November (1981), pp. 348-353.

12. Masubuchi K, Analysisis of Welded Structures, Great Britain, Pergamon Press, 1980, pp. 112-136.

13. Albertini G et al, 'Residual Stress Measurements in Welded Steel Fe510D,' Proceedings of the Fourth International Conference on Residual Stresses, SEM, June (1994), pp. 959-963.

14. Ford H, 'Mechanical Methods for the Measurement of Internal Stresses,' Symposium of Internal Stresses in Metals and Alloys, (1948), pp. 3-11.

15. Sachs G and Espey G, 'The Measurement of Residual Stresses in Metals,' The Iron Age, September (1941), pp. 63-71.

16. Mathar J, 'Determination of Internal Stresses by Measuring the Deformation Around a Drilled Hole,' Transactions of the American Society of Mechanical Engineers, 56 (1934), pp. 249-254.

17. Kelsey R A, 'Measuring Non-uniform Residual Stresses by the Hole Drilling Method,' Proceedings of the Society for Experimental Stress Analysis, 14 (1956), pp. 181-194.

18. Bynum J E, 'Modifications to the Hole Drilling Technique of Measuring Residual Stresses for Improved Accuracy and Reliability,' Experimental Mechanics, 21 (1981), pp. 21-33.

19. Bentley A P, 'Measurement of Residual Stress by X-Ray Diffraction,' Short Course on Residual Stress Measurement, Strain Society of South Africa, 24 November 1987.

20. Procter E, Beaney E M and Mitchell D H, 'Deep Hole Residual Stress Measurement,' Short Course on Residual Stress Measurement, Strain Society of South Africa, 24 November 1987.

21. Kabiri M, 'Towards More Accurate Residual Stress Measurement by the Hole Drilling Method: Analysis of Relieved-Strain Coefficients,' Experimental Mechanics, 26 (1986), pp. 14-21.

22. Bathgate R G, 'Measurement of Non-Uniform Bi-Axial Stresses by the Hole Drilling Method,' Strain, 4 (1968), pp. 20-29.

23. Rendler N J and Vigness I, 'Hole Drilling Strain Gage Method of Measuring Residual Stresses,' Experimental Mechanics, 6 (1966), pp. 577-586.

24. Soete W and Vancrombrugge R, 'An Industrial Method for the Determination of Residual Stresses,' Proceedings for the Society of Experimental Stress Analysis, 8 (1950), pp. 17-28.

25. Lu J and Flavenot J F, 'Applications of the Incremental Hole Drilling Method for Measurement of Residual Stress Distribution,' Experimental Techniques, 13 (1989), pp. 18-24.

26. Schajer G S, 'Measurement of Non-uniform Residual Stress Using the Hole Drilling Method. Part I - Stress Calculation Procedures,' ASME Journal of Engineering Materials and Technology, 110 (1988), pp. 338-342.

27. Flaman M T and Manning B H, 'Determination of Residual Stress Variation with Depth by the Hole Drilling Method,' Experimental Mechanics, 25 (1985), pp. 205-207.

28. Flaman M T, Mills B E and Boag J M, 'Analysis of Stress Variation with Depth Measurement Procedures for the Centre Hole Method of Residual Stress Measurement,' Experimental Techniques, 11 (1987), pp. 35-37.

29. Schajer G S, 'Application of Finite Element Calculations to Residual Stress Measurements,' ASME Journal of Engineering Materials and Technology, 103 (1981), pp. 157-163.

30. Shaw D and Chen H Y, 'A Finite Element Technique to Analyze the Data Measured by the Hole Drilling Method,' Experimental Mechanics, 30 (1990), pp. 120-123.

31. Flaman M T and Boag J M, 'Comparison of Residual Stress Variation with Depth Analysis Techniques for the Hole Drilling Method,' Experimental Mechanics, 30 (1990), pp. 352-355.

32. Sandifer J P and Bowie G E, 'Residual Stress Measurement by the Blind Hole Method with an Off-Centred Hole,' Experimental Mechanics, 18 (1978), pp. 173-179.

33. Wang J, 'Measurement of Residual Stress by the Hole Drilling Method: General Stress-Strain Relationship and its Solution,' Experimental Mechanics, 28 (1988), pp. 355-358.

34. Owens A, 'Application of Residual Stress Techniques in the Determination of In-situ Load in Reinforcement Bars,' Experimental Techniques, 12 (1988), pp. 23-27.

35. Rao G J, Sankar K R and Narayanan R, 'Determination of Calibration Constants for Hole Drilling Technique Using Special Strain Gage Rosette,' Journal of Testing and Evaluation, 14 (1986), pp. 207-212.

36. Gupta B P, 'Hole Drilling Technique: Modifications in the Analysis of Residual Stresses,' Experimental Mechanics, 13 (1973), pp. 45-48.

37. Wang J, 'Measurement of Residual Stress by the Hole Drilling Method: on the Direction of Maximum Residual Stress,' Experimental Mechanics, 28 (1988), pp. 24-26.

38. Witt F, Lee F and Rider W, 'A Comparison of Residual Stress Measurements Using Blind Hole, Abrasive Jet and Trepan-Ring Methods,' Experimental Techniques, 7 (1983), pp. 41-44.

39. Misra A and Peterson H A, 'Examination of the Ring Method for Determination of Residual Stress,' Experimental Mechanics, 21 (1981) pp. 268-272.

40. Shenker M I, 'Experimental Techniques for the Determination of Residual Stresses by the Blind-Hole High-Speed Air-Turbine Method,' Short Course on Residual Stress Measurement, Strain Society of South Africa, 24 November 1987.

41. Macherauch E, 'X-Ray Stress Analysis,' Experimental Mechanics, 6 (1966) pp. 140-153.

42. Flaman M T, 'Brief Investigation of Induced Drilling Stresses in the Centre-Hole Method of Residual-Stress Measurement,' Experimental Mechanics, 22 (1982), pp. 26-30.

43. Flaman M T and Herring J A, 'Comparison of Four Hole Producing Techniques for the Centre-Hole Residual-Stress Measurement Method,' Experimental Techniques, 9 (1985), pp. 30-32.

44. Bush A J and Kromer F J, 'Simplification of the Hole-Drilling Method of Residual Stress Measurement,' ISA Transactions, 12 (1973), pp. 249-259.

45. Wang J, 'Refined Analysis of the Relieved Strain Coefficient for the Off-Centre Hole-Drilling Case,' Experimental Mechanics, 30 (1990), pp. 367-371.

46. Nickola W E, 'Practical Subsurface Residual Stress Evaluation by the Hole-Drilling Method,' Proceedings of the Spring Conference on Experimental Mechanics, June (1986), pp. 47-58.

47. Tieu A K, 'A Direct Method to Evaluate Hole Alignment Error in Residual Stress Measurement,' Experimental Mechanics, 25 (1985), pp. 43-47.

48. Peck C A, 'Practical Aspects of Residual Stress Measurement by X-Ray Diffraction,' Proceedings of ASM Conference on Residual Stress in Design, Process and Material Selection, April (1987), pp. 7-9.

49. Prask H J and Choi C S, 'Residual Stress Measurements in Armament System Components by Means of Neutron Diffraction,' Proceedings of ASM Conference on Residual Stress in Design, Process and Material Selection, April (1987), pp. 21-26.

50. Smith D J et al, 'Neutron Diffraction Measurements of Residual Stress and Plastic Deformation in an Aluminium Alloy Weld,' Journal of Strain Analysis, 23 (1988), pp. 201-211.

51. Boag J M, Flaman M T and Herring J A, 'Consideration of Using the Hole Drilling Method for Measuring Residual Stress in Engineering Components,' Proceedings of ASM Conference on Residual Stress in Design, Process and Material Selection, April (1987), pp. 1-6.

52. Schwaighofer J, 'Determination of Residual Stress on the Surface of Structural Parts,' Experimental Mechanics, 4 (1964), pp. 54-56.

53. Dini J W, Benedetti G A and Johnson H R, 'Residual Stress in Thick Electrodeposits of a Nickel-Cobalt Alloy,' Experimental Mechanics, 16 (1976), pp. 56-60.

54. Nawwar A M, McLachlan K and Shewchuck J, 'A Modified Hole Drilling Technique for Determining Residual Stresses in Thin Plates,' Experimental Mechanics, 16 (1976), pp. 226-232.

55. Kabiri M, 'Measurement of Residual Stress by the Hole Drilling Method: Influences of Transverse Sensitivity of the Gages and Relieved Strain Coefficients,' Experimental Mechanics, 24 (1984), pp. 252-257.

56. Durez J and Bazergui A, 'Through-thickness Measurement of Residual Stress in Thin Tubes,' Experimental Mechanics, 23 (1983), pp. 211-217.

57. Nelson D V and McCrichard J T, 'Residual Stress Determination Through Combined Use of Holographic Interferometry and Blind Hole Drilling,' Experimental Mechanics, 26 (1986), pp. 371-378.

58. Niku-Lari A, 'Residual Stresses and Surface Finish in Shot-Peened Components and Materials,' Experimental Techniques, 7 (1983), pp. 30-36.

59. Niku-Lari A, 'Influence of Residual Stresses by Shot-Peening Upon the Fatigue Life of Materials,' Experimental Techniques, 7 (1983), pp. 21-25.

60. Koshti A and Egle D M, 'An Alternate Technique for Implementing Centre Hole Drilling/Residual Stress Measurements,' Experimental Techniques, 9 (1985), pp. 28-30.

61. Chakravarti A P, Nawwar A M and Stringer D C, 'Residual-Stress Distribution as a Result of Flame-Straightening Procedure, ' Experimental Techniques, 12 (1988), pp. 19-21.

62. Throop J F, 'Fracture Mechanics Analysis of the Effects of Residual Stress on Fatigue Life,' ASTM Journal of Testing and Evaluation, 9 (1983), pp. 75-78.

63. Nawwar A M and Shewchuk J, 'The Effect of Preload on Fatigue Strength of Residually Stressed Specimens,' Experimental Mechanics, 23 (1983), pp. 409-413.

64. Eigenmann B, Schulze V and Vöhringer O, 'Surface Residual Stress Relaxation in Steels by Thermal or Mechanical Treatment,' Proceedings of the Fourth International Conference on Residual Stresses, SEM, June (1994), pp. 598-607.

65. Tootoonian M and Schajer G S , 'Enhanced Sensitivity Residual Stress Measurements Using Taper Hole Drilling,' Proceedings of the Fourth International Conference on Residual Stresses, SEM, June (1994), pp. 52-62.

66. Fathallah R et al, 'Comparison of Residual Stresses Determined by X-ray Diffraction, Neutron Diffraction and the Hole Drilling Method in Aerospace Shot Peened Materials,' Proceedings of the Fourth International Conference on Residual Stresses, SEM, June (1994), pp. 834-843.

67. Nelson D V, Fuchs E A and Makino A, 'An Overview of the Holographic-Hole Drilling Technique for Residual Stress Measurement,' Proceedings of the Fourth International Conference on Residual Stresses, SEM, June (1994), pp. 63-72.

68. Schajer G S, 'Measurement of Non-Uniform Residual Stresses Using the Hole Drilling Method. Part II - Practical Application of the Integral Method,' ASME Journal of Engineering Materials and Technology, 110 (1988), pp. 344-349.

69. Bijak-Zochowski M, 'A Semi-Destructive Method of Measuring Residual Stresses,' VDI-Berichte, 313 (1978), pp. 469-476.

70. Wilks M D B, Nowell D and Hills D A, 'The Influence of Residual Stress on Crack Growth Rate,' Proceedings of the Fourth International Conference on Residual Stresses, SEM, June (1994), pp. 1238-1245.

71. Ragozin Y I and Polianin I V, 'A New Express Method of Residual Stress Relief in Metals and Ceramics,' Proceedings of the Fourth International Conference on Residual Stresses, SEM, June (1994), pp. 926-931.

72. Nakagiri A et al, 'The Residual Stress Relief Under Mechanical Vibrations and Subsequent Dimensional Change in Copper and Brass,' Proceedings of the Fourth International Conference on Residual Stresses, SEM, June (1994), pp. 1300-1305.

73. Ashby M F and Jones D R H, Engineering Materials 2: An Introduction to Microstructures, Processing and Design, Great Britain, Pergamon Press, 1986, pp. 75-78.

74. Harty B D, 'Technical Assistance Report No. HTA 90/10 CT,' Hulett Aluminium Internal Report, May (1990).

75. Tait R B, 'LEFM Fracture Toughness Measurement of 7075 Aluminium Alloy Drill Rod Materials,' Department of Mechanical Engineering, University of Cape Town, April (1991).

76. Tait R B, 'Failure of 7075 Drill Rods - Review of Report HTA 90/10 May 1990,' Department of Mechanical Engineering, University of Cape Town, June (1990).

77. Cohen J B, 'The Non-Destructive Measurement of Residual Stresses Via Diffraction,' Proceedings of the Fourth International Conference on Residual Stresses, SEM, June (1994), pp. 1-13.

78. Procter E, 'History and Background of Residual Stress Measurement Techniques,' Short Course on Residual Stress Measurement, Strain Society of South Africa, 24 November 1987.

79. Wobker H G, Karpuschowski B and Regent C, 'Quality Control of Residual Stresses on Ground Workpieces with Micromagnetic Techniques,' Proceedings of the Fourth International Conference on Residual Stresses, SEM, June (1994), pp. 424-433.

80. Ruud C O, DiMascio P S and Yavelak J J, 'Comparison of Three Residual Stress Measurement Methods on a Mild Steel Bar,' Experimental Mechanics, 25 (1985), pp. 338-343.

81. Bruce Thompson R, 'An Overview of Ultrasonic Measurement Techniques,' Proceedings of the Fourth International Conference on Residual Stresses, SEM, June (1994), pp. 97-111.

82. Gadd C W, 'Residual Stress Indications in Brittle Lacquer,' Experimental Stress Analysis, 4 (1946), pp. 74-77.

83. Harty B and Hurd T, Discussion February 1991.

84. Cheng W and Finnie I, 'An Overview of the Crack Compliance Method for Residual Stress Measurement,' Proceedings of the Fourth International Conference on Residual Stresses, SEM, June (1994), pp. 449-458.

85. Terblanche E, Marquardt A E and Greeff B, 'Residual Stress Determination Techniques,' Short Course on Residual Stress Measurement, Strain Society of South Africa, 24 November 1987.

86. Micro-Measurement Strain Gauge Rosette TEA-06-062RK-120 Leaflet.

87. American Society for Testing and Materials, 'Standard Test Method for Determining Residual Stresses by the Hole-Drilling Strain-Gage Method,' ASTM Standard E837-89, (1989).

88. Timoshenko S P and Goodier J N, Theory of Elasticity, 2nd ed., New York, McGraw-Hill, 1951, p.80.

89. S S White, Industrial Abrasive Unit Model K - Service Manual.

90 Clarke C S, Air Abrasive Hole Drilling Device, Final year MEC410 Thesis project, University of Cape Town, 1990.

91. Harty B and Hurd T, Hulett Aluminium, Discussion 4 November 1991.

92. Moodlyar R, Hulett Aluminium, Discussion 26 September 1994.

93. Da Silva Pauleta G, Air Abrasive Centre Hole Drilling, Final year MEC410 Thesis project, University of Cape Town, 1991.

94. Kline S J and McClintock F A, 'Describing uncertainties in single sample experiments,' Mechanical Engineering, 3 (1953).

APPENDIX A

EQUATION DERIVATIONS

A.1 The Air Abrasive Centre Hole Drilling Technique

Consider the centre drawing of Fig 3.3 where a thin plate with a small hole drilled in it is under a state of uniform biaxial state of stress. This state of stress has been solved theoretically by G. Kirsch for an infinite plate, as reported in Timoshenko's book[88]. If the stress state of the plate, before the hole is drilled, is subtracted form Kirsch's solution, the result will be as shown in the left drawing of Fig 3.3. This state of stress is of interest, since it produces the strains measured by the strain gauges as a hole is drilled. It can be calculated as follows with reference to Fig A.1[33]:

$$\sigma_u = \frac{\sigma_1 + \sigma_2}{2}\left[1 - \left(\frac{r_h}{R_i}\right)^2\right] + \frac{\sigma_1 - \sigma_2}{2}\left[1 - 4\left(\frac{r_h}{R_i}\right)^2 + 3\left(\frac{r_h}{R_i}\right)^4\right]\cos 2\gamma_i - \left[\frac{\sigma_1 + \sigma_2}{2} + \frac{\sigma_1 - \sigma_2}{2}\cos 2\gamma_i\right]$$

$$\sigma_v = \frac{\sigma_1 + \sigma_2}{2}\left[1 + \left(\frac{r_h}{R_i}\right)^2\right] + \frac{\sigma_1 - \sigma_2}{2}\left[-1 - 3\left(\frac{r_h}{R_i}\right)^4\right]\cos 2\gamma_i - \left[\frac{\sigma_1 + \sigma_2}{2} - \frac{\sigma_1 - \sigma_2}{2}\cos 2\gamma_i\right]$$

$$\sigma_{uv} = + \frac{\sigma_1 - \sigma_2}{2}\left[-1 - 2\left(\frac{r_h}{R_i}\right)^2 + 3\left(\frac{r_h}{R_i}\right)^4\right]\sin 2\gamma_i - \left[- \frac{\sigma_1 - \sigma_2}{2}\sin 2\gamma_i\right]$$

$$\therefore \sigma_u = -\frac{X}{2} r_i^2 - \frac{Y}{2}\left(3r_i^4 - 4r_i^2\right)\cos 2\gamma_i \qquad \text{...eqn A.1(a)}$$

$$\therefore \sigma_v = \frac{X}{2} r_i^2 - \frac{Y}{2}\left(3r_i^4\right)\cos 2\gamma_i \qquad \text{...eqn A.1(b)}$$

$$\therefore \sigma_{uv} = -\frac{Y}{2}\left(2r_i^2 - 3r_i^4\right)\sin 2\gamma_i \qquad \text{...eqn A.1(c)}$$

where:

$$\left.\begin{aligned} r_i &= \frac{r_h}{R_i} \\ X &= \sigma_1 + \sigma_2 \\ Y &= \sigma_1 - \sigma_2 \end{aligned}\right\} \qquad \text{...eqn A.2}$$

The relieved stress components in the direction of u' and v' are:

$$\sigma_{u'} = \frac{1}{2}\left(\sigma_u + \sigma_v\right) + \frac{1}{2}\left(\sigma_u - \sigma_v\right)\cos 2\phi_i + \sigma_{uv}\sin 2\phi_i$$

...eqn A.3(a)

$$\sigma_{v'} = \frac{1}{2}\left(\sigma_u + \sigma_v\right) - \frac{1}{2}\left(\sigma_u - \sigma_v\right)\cos 2\phi_i - \sigma_{uv}\sin 2\phi_i$$

...eqn A.3(b)

By Hooke's law, the relieved strain in the longitudinal direction of gauge i is:

$$\varepsilon_i = \frac{\sigma_{u'} - \nu\sigma_{v'}}{E} \qquad \text{...eqn A.4}$$

Furthermore from Fig A.1, it can be seen that:

$$\gamma_i = \theta_i - \alpha \qquad \text{...eqn A.5}$$

Substituting eqn A.1 into eqn A.3, it can be found that:

$$\sigma_{u'} = -\frac{X}{2}r_i^2\cos 2\phi_i - Yr_i^2\cos 2\gamma_i - Y\left(r_i^2 - \frac{3}{2}r_i^4\right)\left(\cos 2\gamma_i\cos 2\phi_i + \sin 2\gamma_i\sin 2\phi_i\right)$$

...eqn A.6(a)

$$\sigma_{v'} = \frac{X}{2} r_i^2 \cos 2\phi_i - Y r_i^2 \cos 2\gamma_i + Y \left(r_i^2 - \frac{3}{2} r_i^4 \right) \left(\cos 2\gamma_i \cos 2\phi_i + \sin 2\gamma_i \sin 2\phi_i \right)$$

...eqn A.6(b)

Substituting eqn A.6 into eqn A.4 and considering eqn A.5, the strain relaxation in gauge i is:

$$\varepsilon_i = \left\{ - \frac{X}{2} (1 + \nu) r_i^2 \cos 2\phi_i - Y (1 - \nu) r_i^2 \cos 2(\theta_i - \alpha) - Y (1 + \nu) r_i^2 \left(1 - \frac{3}{2} r_i^2 \right) \left[\cos 2(\theta_i - \alpha) \cos 2\phi_i + \sin 2(\theta_i - \alpha) \sin 2\phi_i \right] \right\} \Big/ E$$

...eqn A.7

In order to resolve the direction angle of maximum residual stress form eqn A.7, the following trigonometric relations are used:

$$\cos 2(\theta_i - \alpha) = \cos 2\theta_i \cos 2\alpha + \sin 2\theta_i \sin 2\alpha \qquad \text{...eqn A.8}$$

$$\cos 2(\theta_i - \alpha) \cos 2\phi_i + \sin 2(\theta_i - \alpha) \sin 2\phi_i =$$

$$\cos 2(\theta_i - \alpha - \phi_i) =$$

$$\cos 2(\theta_i - \phi_i - \alpha) =$$

$$\cos 2(\theta_i - \phi_i) \cos 2\alpha + \sin 2(\theta_i - \phi_i) \sin 2\alpha$$

...eqn A.9

Substitute eqn A.8 and eqn A.9 into eqn A.7:

$$\varepsilon_i = \left[- \frac{(1 + \nu)}{2E} r_i^2 \cos 2\phi_i \right] + \left[- \frac{(1 - \nu)}{E} r_i^2 \cos 2\theta_i - \frac{(1 + \nu)}{E} r_i^2 \left(1 - \right. \right.$$

$$\frac{3}{2} r_i^2 \Big) \cos 2(\theta_i - \phi_i) \Big] Y \cos 2\alpha +$$

$$\Big[- \frac{(1 - \nu)}{E} r_i^2 \sin 2\theta_i - \frac{(1 + \nu)}{E} r_i^2 \Big(1 -$$

$$\frac{3}{2} r_i^2 \Big) \sin 2(\theta_i - \phi_i) \Big] Y \sin 2\alpha \qquad \text{...eqn A.10}$$

Consequently the strain relaxation in gauge i is the following:

$$\varepsilon_i = A_i X + B_i Y \cos 2\alpha + C_i Y \sin 2\alpha \qquad \text{...eqn A.11}$$

where:

$$A_i = - \frac{(1 + \nu)}{2E} r_i^2 \cos 2\phi_i \qquad \text{...eqn A.12(a)}$$

$$B_i = - \frac{1}{E} \Big[(1 - \nu) r_i^2 \cos 2\theta_i + (1 + \nu) r_i^2 \Big(1 - \frac{3}{2} r_i^2 \Big) \cos 2(\theta_i - \phi_i) \Big] \qquad \text{...eqn A.12(b)}$$

$$C_i = - \frac{1}{E} \Big[(1 - \nu) r_i^2 \sin 2\theta_i + (1 + \nu) r_i^2 \Big(1 - \frac{3}{2} r_i^2 \Big) \sin 2(\theta_i - \phi_i) \Big] \qquad \text{...eqn A.12(c)}$$

If the relieved strains ε_1 , ε_2 and ε_3 of three arbitrarily placed gauges - 1, 2, 3 - are measured and assuming that the strain at the centre of the gauges approximate the average strains obtained over the gauge area, eqn A.11 can be rewritten as the following:

$$\begin{bmatrix} A_1 & B_1 & C_1 \\ A_2 & B_2 & C_2 \\ A_3 & B_3 & C_3 \end{bmatrix} \begin{Bmatrix} X \\ Y \cos 2\alpha \\ Y \sin 2\alpha \end{Bmatrix} = \begin{Bmatrix} \varepsilon_1 \\ \varepsilon_2 \\ \varepsilon_3 \end{Bmatrix} \qquad \text{...eqn A.13}$$

Let D , D_X, D_{YC} and D_{YS} be the determinants of eqn A.13 as follows:

$$D = \begin{vmatrix} A_1 & B_1 & C_1 \\ A_2 & B_2 & C_2 \\ A_3 & B_3 & C_3 \end{vmatrix} \quad \text{...eqn A.14}$$

$$D_X = \begin{vmatrix} \varepsilon_1 & B_1 & C_1 \\ \varepsilon_2 & B_2 & C_2 \\ \varepsilon_3 & B_3 & C_3 \end{vmatrix} \quad \text{...eqn A.15}$$

$$D_{YC} = \begin{vmatrix} A_1 & \varepsilon_1 & C_1 \\ A_2 & \varepsilon_2 & C_2 \\ A_3 & \varepsilon_3 & C_3 \end{vmatrix} \quad \text{...eqn A.16}$$

$$D_{YS} = \begin{vmatrix} A_1 & B_1 & \varepsilon_1 \\ A_2 & B_2 & \varepsilon_2 \\ A_3 & B_3 & \varepsilon_3 \end{vmatrix} \quad \text{...eqn A.17}$$

Then solving equation A.12:

$$X = \frac{D_X}{D} \quad \text{...eqn A.18}$$

$$Y \cos 2\alpha = \frac{D_{YC}}{D} \quad \text{...eqn A.19}$$

$$Y \sin 2\alpha = \frac{D_{YS}}{D} \quad \text{...eqn A.20}$$

because $Y \geq 0$, from eqn A.19 and eqn A.20 it can be found that:

$$Y = \frac{\sqrt{\left(D_{YC}\right)^2 + \left(D_{YC}\right)^2}}{|\ D\ |} \quad \text{...eqn A.21}$$

From equations A.2, A.18 and A.21, the solution of the principal relieved stresses can be obtained:

$$\sigma_{1,2} = \frac{1}{2}\left[\frac{D_X}{D} \pm \frac{\sqrt{\left(D_{YC}\right)^2 + \left(D_{YC}\right)^2}}{|\ D\ |}\right] \qquad \text{...eqn A.22}$$

From equations A.19 and A.20, it can be found that:

$$\tan 2\alpha = \frac{D_{YS}}{D_{YC}} \qquad \text{...eqn A.23}$$

As there are multiple solutions of equation A.23 for α, it will not necessarily give the correct direction of σ_1. In order to determine the correct value of α, eqn A.19 and eqn A.23 should be considered simultaneously. From eqn A.23:

$$2\alpha' = \tan^{-1}\left(\frac{D_{YS}}{D_{YC}}\right) \qquad \text{...eqn A.24}$$

where $2\alpha'$ is the principal value of the arctangent function, i.e. $-90^\circ < 2\alpha' < 90^\circ$ is either in quadrant I or IV. From eqn A.19 it can be seen that the sign of cos 2α must agree with that of $D_{YC}/\ D$, since $Y \geq 0$. Thus if $D_{YC}/\ D \geq 0$, then cos $2\alpha \geq 0$ and 2α is also in quadrants I or IV. This agrees with the range of the principal value of $2\alpha'$, i.e. $2\alpha = 2\alpha'$. Conversely, if $D_{YC}/\ D < 0$, the $2\alpha < 0$ and 2α is in quadrant II or III, which is 180° from therange of the principal value of $2\alpha'$, i.e. $2\alpha = 2\alpha' + 180^\circ$.

The above discussion indicates that in determining the direction of σ_1 , the ratio $D_{YC}/\ D$ should be used as a judging condition. The criterion then is:

$$\text{if } D_{YC}/\ D \geq 0, \text{ then } \alpha = \frac{1}{2}\tan^{-1}\left(\frac{D_{YS}}{D_{YC}}\right) \qquad \text{...eqn A.25(a)}$$

$$\text{if } D_{YC}/\ D \geq 0, \text{ then } \alpha = \frac{1}{2}\tan^{-1}\left(\frac{D_{YS}}{D_{YC}}\right) + 90^\circ \qquad \text{...eqn A.25(b)}$$

Equations A.24, A.25 and A.26 are effective to the off-centre and centre hole drilling cases when using a rectangular strain

gauge rosette.

A.1.1 Off-centred Hole

For the off-centred case (see Fig A.2), the values of R_i , θ_i and ϕ_i can be calculated as follows:

$$R_i = \sqrt{\left(R \sin \xi_i - e \sin \beta \right)^2 + \left(R \cos \xi_i - e \cos \beta \right)^2}$$

$$\theta_i = \tan^{-1} \left(\frac{R \sin \xi_i - e \sin \beta}{R \cos \xi_i - e \cos \beta} \right)$$

$$\phi_i = \xi_i - \theta_i$$

After determining these values for i = 1,2,3, the principal relaxed stresses and their directions can be found from equations A.12, A.14 - A.17, A.22 and A.25.

A.1.2 Centred Hole

For the centred hole drilling case, as shown in Fig A.3, the hole-gauge geometries are the following:

$$\theta_1 = 0^\circ$$

$$\theta_2 = 45^\circ$$

$$\theta_3 = 90^\circ$$

$$\phi_1 = \phi_2 = \phi_3 = 0^\circ$$

$$R_i = R$$

$$r_i = r = \frac{r_h}{R}$$

Substituting the above into eqn A.12, the matrix of the coefficients of eqn A.13 can be found to be:

$$\begin{bmatrix} A & B & 0 \\ A & 0 & B \\ A & -B & 0 \end{bmatrix}$$

where: $A = -\frac{(1 + \nu)\ r^2}{2E}$

$$B = -\frac{2r^2\ [\ 1 - 3(1 + \nu)r^2/4\ ]}{E}$$

Eqn A.13 then becomes the following:

$\varepsilon_1 = AX + BY \cos 2\alpha$ ...eqn A.26(a)

$\varepsilon_2 = AX + BY \sin 2\alpha$ ...eqn A.26(b)

$\varepsilon_3 = AX - BY \cos 2\alpha$ ...eqn A.26(c)

Substituting eqn A.26 into equations A.14 - A.17, A.22 and A.23, the principal relieved stresses can be found to be the following:

$$\sigma_{1,2} = \frac{1}{4}\left[\frac{\varepsilon_1 + \varepsilon_3}{A} \pm \frac{\sqrt{(\varepsilon_3 - \varepsilon_1)^2 + (\varepsilon_1 + \varepsilon_3 - 2\varepsilon_2)^2}}{|\ B\ |} \right]$$

...eqn A.27(a)

The direction of σ_1 is:

$$\text{if } (\varepsilon_1 - \varepsilon_3) \leq 0, \text{ then } \alpha = \frac{1}{2}\tan^{-1}\left[\frac{\varepsilon_1 + \varepsilon_3 - 2\varepsilon_2}{\varepsilon_3 - \varepsilon_1} \right]$$

...eqn A.27(b)

$$\text{if } (\varepsilon_1 - \varepsilon_3) > 0, \text{ then } \alpha = \frac{1}{2}\tan^{-1}\left[\frac{\varepsilon_1 + \varepsilon_3 - 2\varepsilon_2}{\varepsilon_3 - \varepsilon_1} \right] + 90^\circ$$

...eqn A.27(c)

The constants A and B contain the material constants E and ν. If these material constants were separately stated, then the relaxed stress equations would apply to any elastic, isotropic material[23]. The material constants may be separated from the constants A and B by using a different approach than that taken previously: the maximum and minimum radial strains, as measured about the hole, can be expressed in terms of the principal stresses and the material constants, provided the proper proportionality constants are included as follows[23]:

$$\varepsilon_{max} = \frac{K_1}{E}\sigma_1 - \frac{\nu K_2}{E}\sigma_2 \qquad \text{...eqn A.28}$$

$$\varepsilon_{min} = \frac{K_1}{E}\sigma_2 - \frac{\nu K_2}{E}\sigma_1 \qquad \text{...eqn A.29}$$

If it assumed for the moment that the direction of the principal stresses are known, then the strain measuring system can be aligned with its x-axis coincident with the direction of maximum principal stress (i.e. $\alpha = 0$). For this condition, the strain ε_1 equals ε_{max} of eqn A.28 and ε_3 equals ε_{min} of eqn A.29. Under these conditions, with $\alpha = 0$, eqn A.27 can be solved for the measured strains, with solutions as follows:

$$\varepsilon_{max} = (A + B)\,\sigma_1 + (A - B)\,\sigma_2 \qquad \text{...eqn A.30}$$

$$\varepsilon_{min} = (A + B)\,\sigma_2 + (A - B)\,\sigma_1 \qquad \text{...eqn A.31}$$

Comparing eqn A.28 and eqn A.30, or eqn A.29 and eqn A.31, it becomes evident that:

$$A + B = \frac{K_1}{E}$$

$$A - B = -\frac{\nu K_2}{E}$$

$$\therefore \quad A = \frac{1}{2E}\left(K_1 - \nu K_2\right)$$

and $B = \frac{1}{2E}\left(K_1 + \nu K_2 \right)$

Taking into account that the sign of the residual stress present in a component will be opposite to the measured relaxed strains, the residual stress equations can be rewritten as:

$$\sigma_1 = -\frac{E}{2}\left(\frac{1}{K_1}\right)\left[\frac{\varepsilon_1 + \varepsilon_3}{1 - \nu K_2/K_1} - \frac{\sqrt{(\varepsilon_3 - \varepsilon_1)^2 + (\varepsilon_1 + \varepsilon_3 - 2\varepsilon_2)^2}}{1 + \nu K_2/K_1}\right] \quad \text{...eqn A.32}$$

$$\sigma_2 = -\frac{E}{2}\left(\frac{1}{K_1}\right)\left[\frac{\varepsilon_1 + \varepsilon_3}{1 - \nu K_2/K_1} + \frac{\sqrt{(\varepsilon_3 - \varepsilon_1)^2 + (\varepsilon_1 + \varepsilon_3 - 2\varepsilon_2)^2}}{1 + \nu K_2/K_1}\right] \quad \text{...eqn A.33}$$

$$\alpha = \frac{1}{2}\tan^{-1}\left[\frac{\varepsilon_1 + \varepsilon_3 - 2\varepsilon_2}{\varepsilon_3 - \varepsilon_1}\right] \quad \text{,,,eqn A.34}$$

Note: α can be calculated as before or by using Table 3.1

A.1.3 Solution of $1/K_1$ and $\nu K_2/K_1$

If a stress state of uniaxial tension[2] is considered with the x-axis of the strain gauge rosette coincident with the direction of the maximum principal stress, then the following stress and strain values are applicable:

$\sigma_1 = E\,\varepsilon_1$

$\sigma_2 = 0$

$$\alpha = 0$$

$$\varepsilon_1 = \varepsilon'_A$$

$$\varepsilon_3 = \varepsilon'_T$$

If $\alpha = 0$, then from eqn A.34:

$$\varepsilon_1 + \varepsilon_3 - 2\varepsilon_2 = 0 \qquad \text{...eqn A.35}$$

Since $\sigma_2 = 0$, substituting eqn A.34 into eqn A.33 yields the following:

$$\frac{\varepsilon_1 + \varepsilon_3}{1 - \nu K_2/K_1} + \frac{\varepsilon_3 - \varepsilon_1}{1 - \nu K_2/K_1} = 0$$

$$\therefore \quad \boxed{\frac{\nu K_2}{K_1} = -\frac{\varepsilon'_T}{\varepsilon'_A}} \qquad \text{...eqn A.36}$$

Substitute eqn A.35 into eqn A.32:

$$\sigma_1 = -\frac{E}{2}\left(\frac{1}{K_1}\right)\left[\frac{\varepsilon_1 + \varepsilon_3}{1 - \nu K_2/K_1} - \frac{\varepsilon_3 - \varepsilon_1}{1 + \nu K_2/K_1}\right] \qquad \text{...eqn A.37}$$

Substituting the values of ε_1 and ε_3 , and eqn A.36 into eqn A.37, it can be shown that:

$$\boxed{\frac{1}{K_1} = -\frac{\varepsilon_A}{\varepsilon'_A}} \qquad \text{...eqn A.38}$$

A.2 The Ring Splitting Technique

From beam theory, the bending moment released when splitting is:

$$M = E' I K$$

where: $$K = \frac{1}{R_o} - \frac{1}{R_1} = \frac{2}{D_o} - \frac{2}{D_1}$$

$$E' = \frac{E}{1 - \nu^2}$$

The factor of $1-\nu^2$ is used to calculate E' since the tube deflects under a condition of plain strain[8]. This is as a result of the tube being too rigid to bend longitudinally if subjected to a circumferential bending moment[15].

$$\therefore M = \frac{E\ I}{1 - \nu^2} \left(\frac{2}{D_o} - \frac{2}{D_1} \right)$$

Also from beam theory:

$$\sigma = \frac{M\ y}{I}$$

$$\therefore \sigma = \frac{E}{1 - \nu^2} \left(\frac{2}{D_o} - \frac{2}{D_1} \right) y$$

For this technique, stresses are assumed to vary linearly through the thickness of the tube or rod. As a result, the neutral axis can be assumed to be at the centre of the tube thickness and y thus varies from -t/2 to t/2.

$$\therefore \boxed{\sigma_{max} = \frac{E\ t}{1 - \nu^2} \left(\frac{D_1 - D_o}{D_o\ D_1} \right)} \quad \text{...eqn A.39}$$

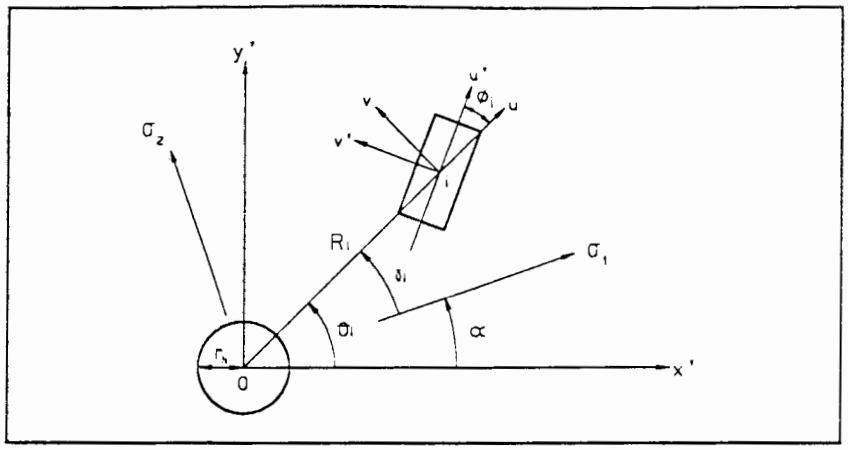

Fig A.1 - Reference coordinate and hole gauge geometries.

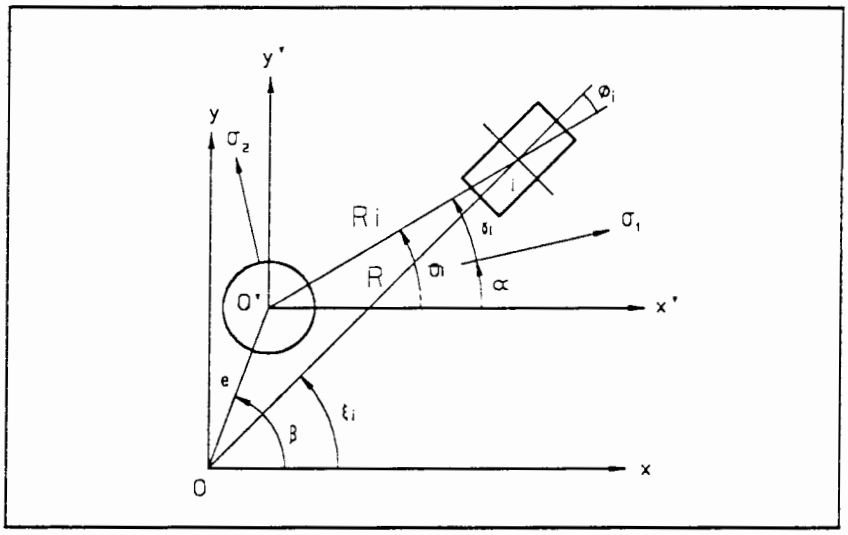

Fig A.2 - Hole gauge geometries of off-centre hole drilling case.

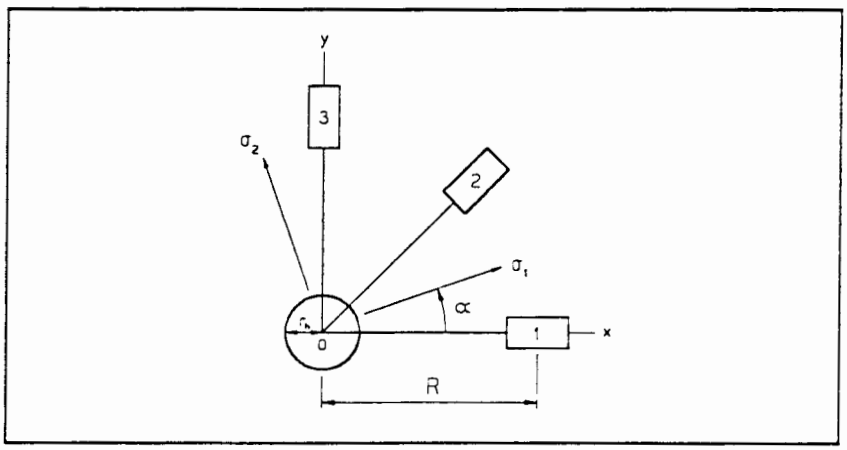

Fig A.3 - Centre hole drilling case.

APPENDIX B

EQUATION CONSTANTS

BLH GAUGES FAER-03S-12-SX EG

(CALCULATED USING vK2/K1 = 0.33)

DIAM (INS)	0	1	2	3	4	5	6	7	8	9
0.055	2.649	2.640	2.631	2.622	2.613	2.604	2.595	2.587	2.578	2.570
0.056	2.561	2.552	2.544	2.536	2.527	2.519	2.511	2.502	2.494	2.486
0.057	2.478	2.470	2.462	2.454	2.446	2.438	2.430	2.422	2.414	2.407
0.058	2.399	2.391	2.384	2.376	2.369	2.361	2.354	2.346	2.339	2.331
0.059	2.324	2.317	2.310	2.302	2.295	2.288	2.281	2.274	2.267	2.260
0.060	2.253	2.246	2.239	2.232	2.226	2.219	2.212	2.205	2.199	2.192
0.061	2.185	2.179	2.172	2.166	2.159	2.153	2.146	2.140	2.134	2.127
0.062	2.121	2.115	2.109	2.102	2.096	2.090	2.084	2.078	2.072	2.066
0.063	2.060	2.054	2.048	2.042	2.036	2.030	2.024	2.019	2.013	2.007
0.064	2.001	1.996	1.990	1.984	1.979	1.973	1.968	1.962	1.957	1.951
0.065	1.946	1.940	1.935	1.930	1.924	1.919	1.914	1.908	1.903	1.898
0.066	1.893	1.887	1.882	1.877	1.872	1.867	1.862	1.857	1.852	1.847
0.067	1.842	1.837	1.832	1.827	1.822	1.817	1.813	1.808	1.803	1.798
0.068	1.793	1.789	1.784	1.779	1.775	1.770	1.765	1.761	1.756	1.752
0.069	1.747	1.743	1.738	1.734	1.729	1.725	1.720	1.715	1.711	1.707

Table B.1 - Hole drilling constants 1/K1 for BLH strain gauge rosettes.

MM GAUGES EA-XX-062RE-120

(CALCULATED USING vK2/K1 = 0.3)

DIAM (INS)	0	1	2	3	4	5	6	7	8	9
0.060	4.710	4.695	4.680	4.665	4.650	4.635	4.621	4.606	4.591	4.577
0.061	4.562	4.548	4.534	4.520	4.505	4.491	4.477	4.463	4.449	4.436
0.062	4.422	4.408	4.395	4.381	4.367	4.354	4.341	4.327	4.314	4.301
0.063	4.288	4.275	4.262	4.249	4.236	4.223	4.210	4.198	4.185	4.173
0.064	4.160	4.148	4.135	4.123	4.111	4.098	4.086	4.074	4.062	4.050
0.065	4.038	4.026	4.015	4.003	3.991	3.979	3.968	3.956	3.945	3.933
0.066	3.922	3.911	3.899	3.888	3.877	3.866	3.855	3.844	3.833	3.822
0.067	3.811	3.800	3.789	3.778	3.768	3.757	3.746	3.736	3.725	3.715
0.068	3.704	3.694	3.684	3.674	3.663	3.653	3.643	3.633	3.623	3.613
0.069	3.603	3.593	3.583	3.573	3.563	3.544	3.544	3.534	3.525	3.515
0.070	3.505	3.496	3.486	3.477	3.468	3.458	3.449	3.440	3.431	3.421
0.071	3.412	3.403	3.394	3.385	3.376	3.367	3.358	3.349	3.340	3.332
0.072	3.323	3.314	3.305	3.297	3.288	3.280	3.271	3.262	3.254	3.246
0.073	3.237	3.229	3.220	3.212	3.204	3.196	3.187	3.179	3.171	3.163
0.074	3.155	3.147	3.139	3.131	3.123	3.115	3.107	3.099	3.091	3.084
0.075	3.076	3.068	3.060	3.053	3.045	3.038	3.030	3.022	3.015	3.008
0.076	3.000	2.993	2.985	2.978	2.971	2.963	2.956	2.949	2.941	2.934
0.077	2.927	2.920	2.913	2.906	2.899	2.892	2.885	2.878	2.871	2.864
0.078	2.857	2.850	2.843	2.837	2.830	2.823	2.816	2.810	2.803	2.796
0.079	2.790	2.783	2.776	2.770	2.763	2.757	2.750	2.744	2.737	2.731
0.080	2.725	2.718	2.712	2.706	2.699	2.693	2.687	2.681	2.674	2.668
0.081	2.662	2.656	2.650	2.644	2.638	2.632	2.626	2.620	2.614	2.608
0.082	2.602	2.596	2.590	2.584	2.578	2.573	2.567	2.561	2.555	2.550
0.083	2.544	2.538	2.533	2.527	2.521	2.516	2.510	2.504	2.499	2.493
0.084	2.488	2.482	2.477	2.471	2.466	2.461	2.455	2.450	2.445	2.439

Table B.2 - Hole drilling constants 1/K1 for MM strain gauge rosettes.

APPENDIX C

THE OPTICAL UNIT

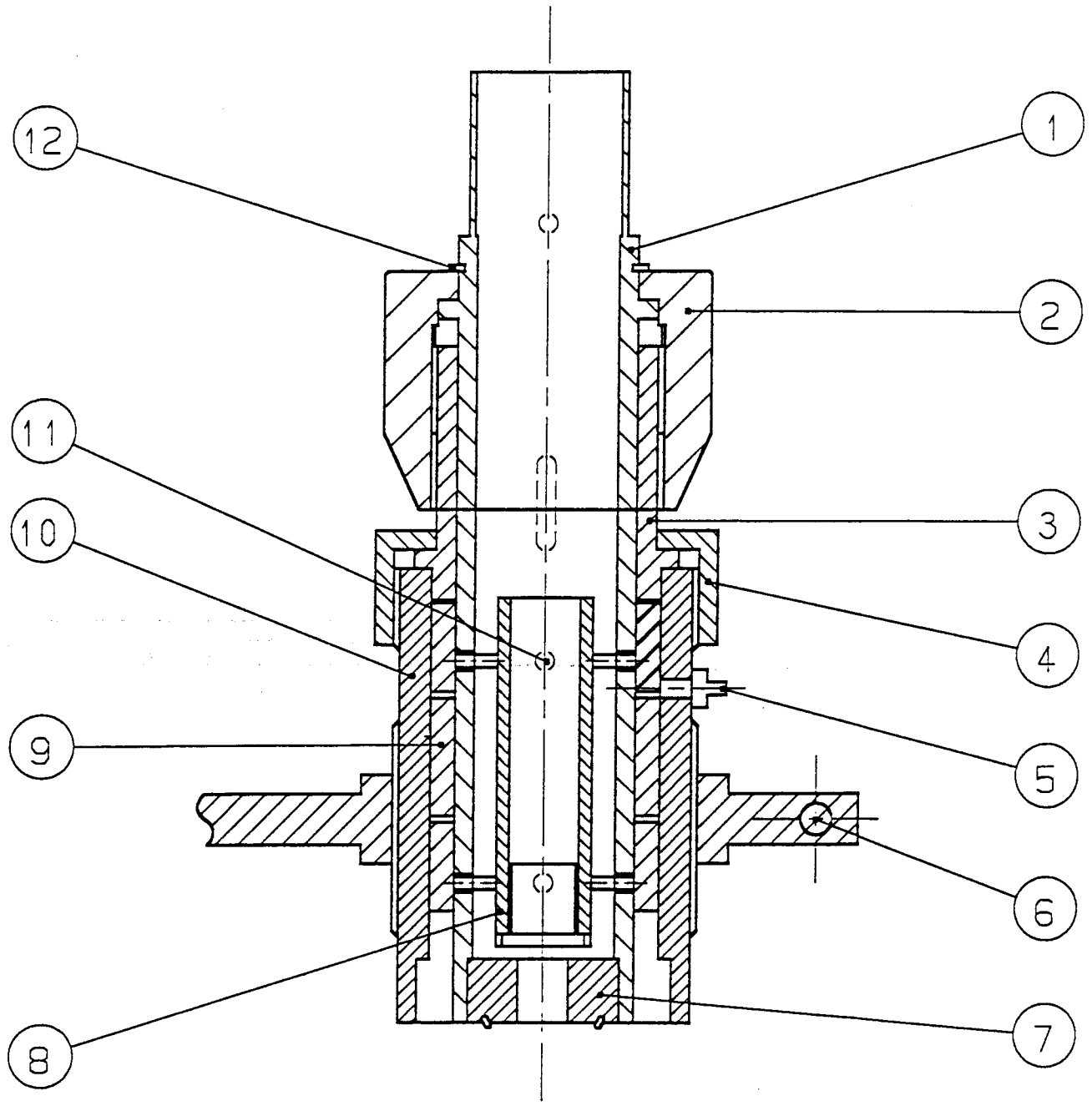

PART NO.	DESCRIPTION	MATERIAL	NO. OFF	REMARKS	SHT. NO.
12	Circlip		1	Std to Fit	
11	Grub Screw		8	M3x0.5 Pitch	
10	Guide Bush	431 Stainless Steel		Modified Original - See Drill Unit	
9	Air-Bearing Bush	431 Stainless Steel		Supplied	
8	Optical Tube	Brass	1	To Fit Objective	3
7	Illumination Ring	Plastic	1	Supplied	
6	Guide Clamp	Mild Steel	1	Supplied	
5	Air Nozzle	Brass	1	Supplied	
4	Securing Ring	431 Stainless Steel	1	Modified Original	
3	Optical Adapter	431 Stainless Steel	1		3
2	Focus Adjuster	431 Stainless Steel	1		2
1	Optical Tube Holder	431 Stainless Steel	1		2

UNIVERSITY OF CAPE TOWN

DEPARTMENT OF MECHANICAL ENGINEERING

OPTICAL UNIT

SCALE: 1:1	SHEET 1 OF 3
DATE: 13/2/94	
DRAWN BY: A.M.SEGAL	

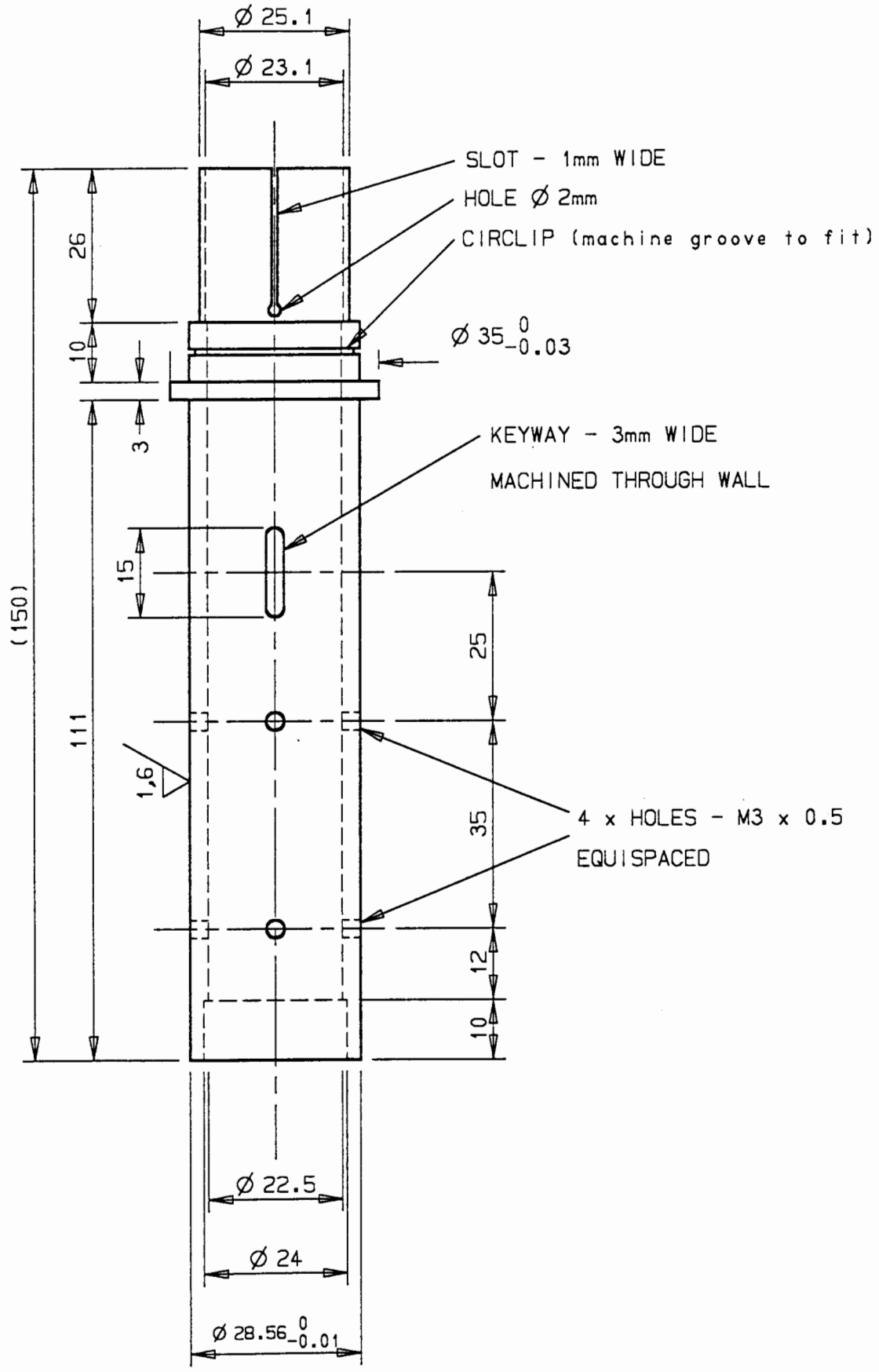

① OPTICAL TUBE HOLDER

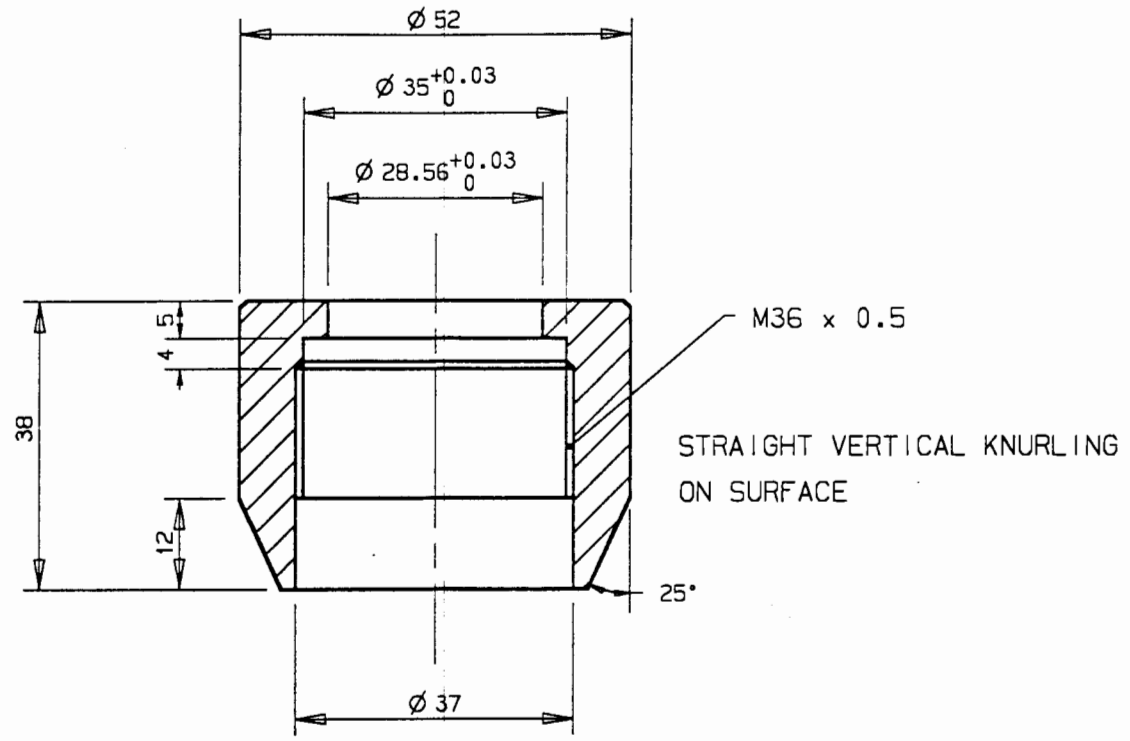

② FOCUS ADJUSTER

UNIVERSITY OF CAPE TOWN DEPARTMENT OF MECHANICAL ENGINEERING	
OPTICAL UNIT PARTS	
SCALE: 1:1	SHEET 2 OF 3
DATE: 13/2/94	
DRAWN BY: A.M.SEGAL	

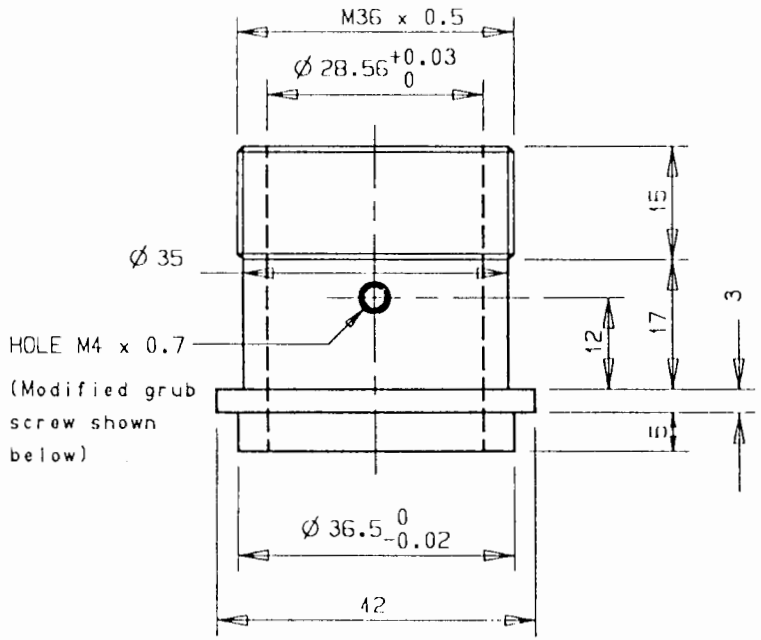

③ OPTICAL ADAPTER

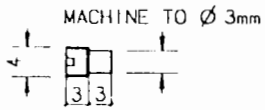

MODIFIED GRUB SCREW REQUIRED FOR OPTICAL ADAPTOR

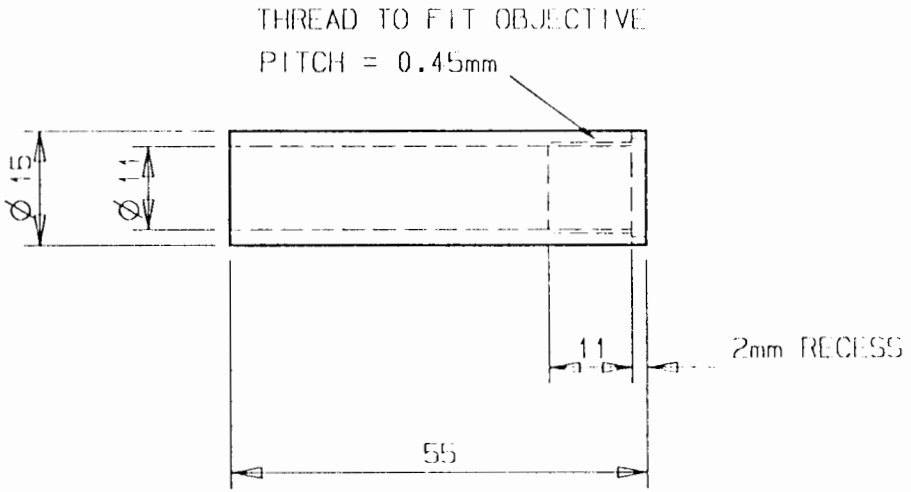

⑧ OPTICAL TUBE

UNIVERSITY OF CAPE TOWN DEPARTMENT OF MECHANICAL ENGINEERING	
OPTICAL UNIT PARTS	
SCALE: 1:1	SHEET 3 OF 3
DATE: 13/2/94	
DRAWN BY: A.M.SEGAL	

APPENDIX D

THE DRILLING UNIT

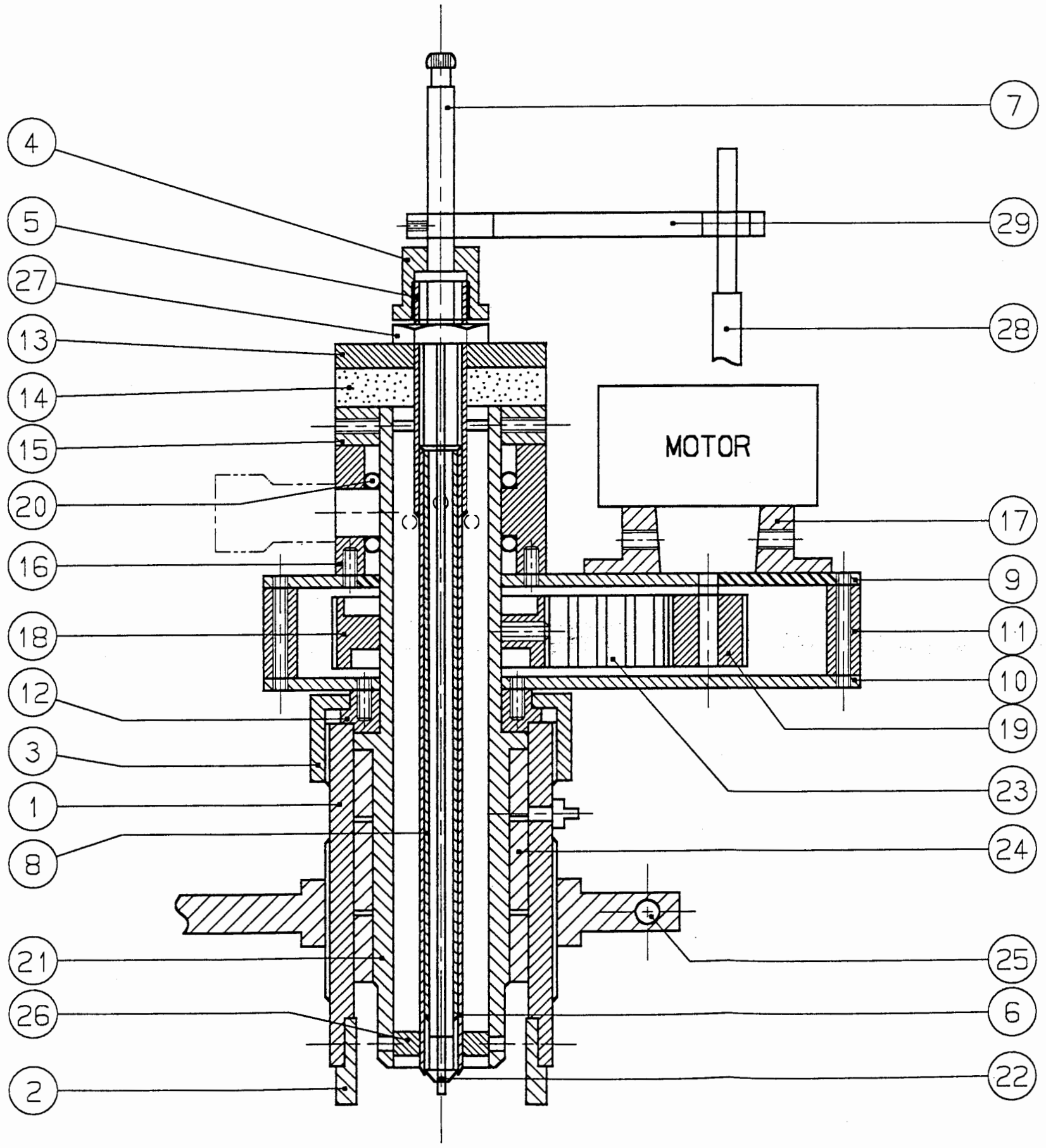

PART NO.	DESCRIPTION	MATERIAL	NO. OFF	REMARKS	SHT. NO.
30	Stabilizer Base	Mild Steel	1	Not Shown	5
29	Stabilizer Arm	Aluminium	1		5
28	Stabilizer Rod	Mild Steel	1		5
27	Fastening Nut	Mild Steel	1	Thread to Fit Adapter	5
26	Offset Gimble	431 Stainless Steel	1		4
25	Guide Clamp	Mild Steel	1	Supplied	1
24	Air Bearing Bush	431 Stainless Steel	1	Supplied	1
23	Timing Belt		1	Uniroyal 90XL	1
22	Sapphire Nozzle		1	Supplied	1
21	Running Tube		1	Supplied	1
20	O-ring		2	ID=25mm W=3mm	1
19	Timing Belt Pulley		1	Uniroyal 11XL Modified	4
18	Timing Belt Pulley		1	Uniroyal 32XL Modified	4
17	Motor Mounting	Mild Steel	1		4
16	Vacuum Housing	431 Stainless Steel	1		4
15	Grub Screw Collar	431 Stainless Steel	1		4
14	Seal	Neoprene	1		4
13	End Washer	Mild Steel	1		4
12	Spigotted Collar	431 Stainless Steel	1		4
11	Belt Casing Wall	Aluminium	2	5mm Plate	3
10	Belt Casing Bottom	Mild Steel	1	3mm Plate	3
9	Belt Casing Lid	Mild Steel	1	3mm Plate	3
8	Air Tube		1	Modified	
7	Inlet Tube	Mild Steel	1	Supplied	
6	Air Tube Housing		1	Supplied	
5	Adapter		1	Supplied	
4	Supply Head	431 Stainless Steel	1		2
3	Securing Ring	431 Stainless Steel	1		2
2	Vacuum Shroud	PVC	1		2
1	Guide Bush	431 Stainless Steel	1	Modified Original	2

UNIVERSITY OF CAPE TOWN
DEPARTMENT OF MECHANICAL ENGINEERING

AIR ABRASIVE ROTARY DRILL

SCALE:	1:1	SHEET 1 OF 5
DATE:	13/2/94	
DRAWN BY:	A.M.SEGAL	

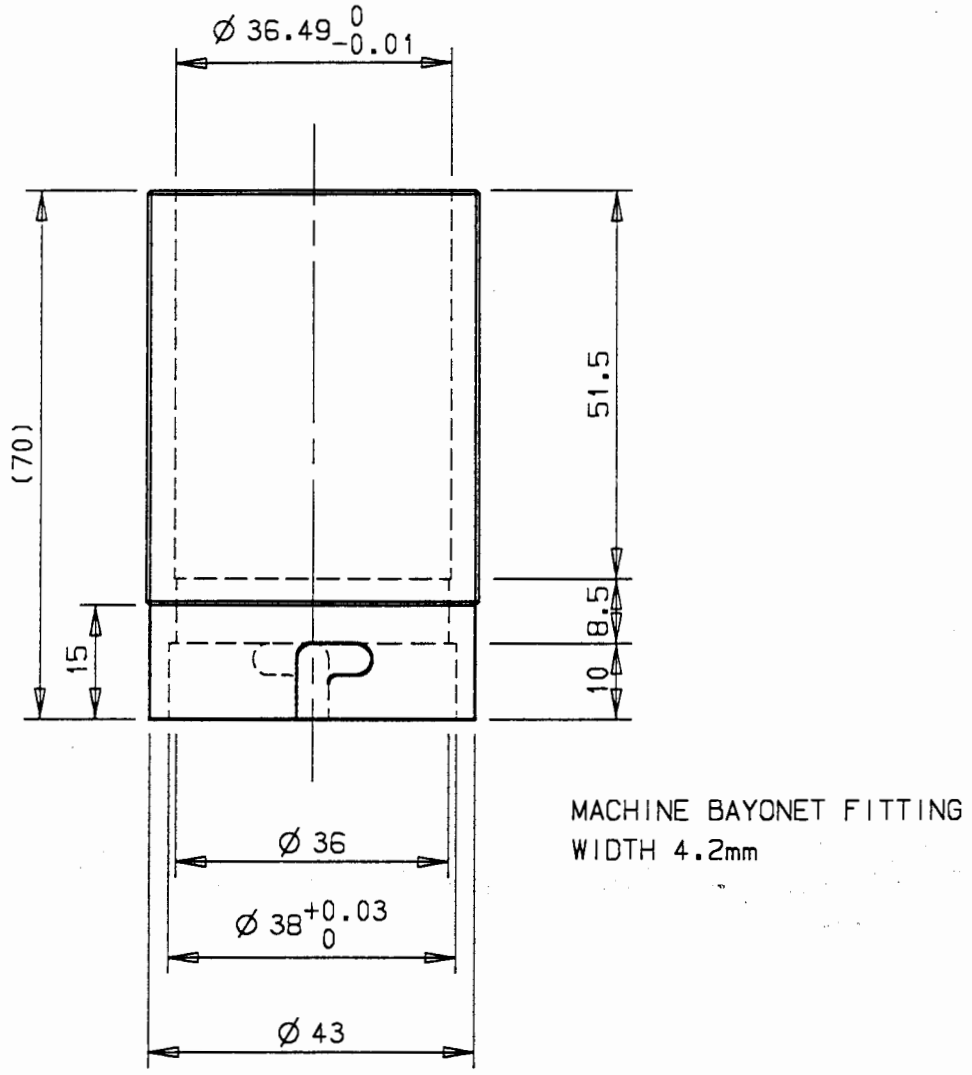

MACHINE BAYONET FITTING
WIDTH 4.2mm

① GUIDE BUSH

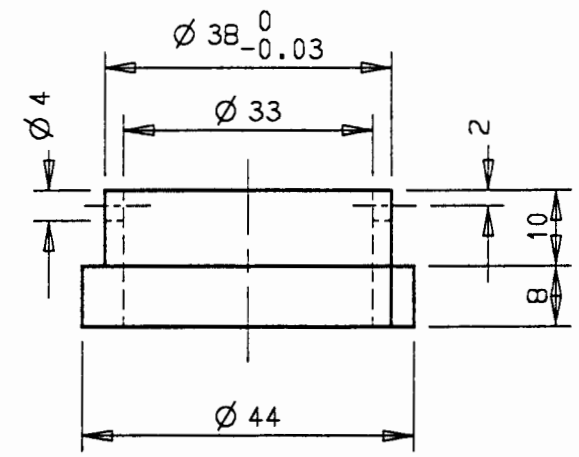

PVC PINS Ø 4mm, 5mm LONG ARE
TO BE INSERTED IN HOLES

② VACUUM SHROUD

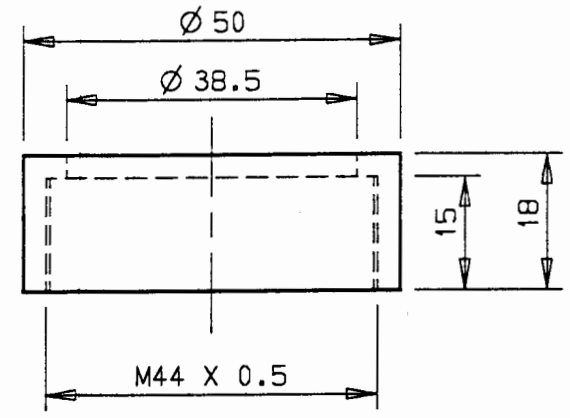

③ SECURING RING

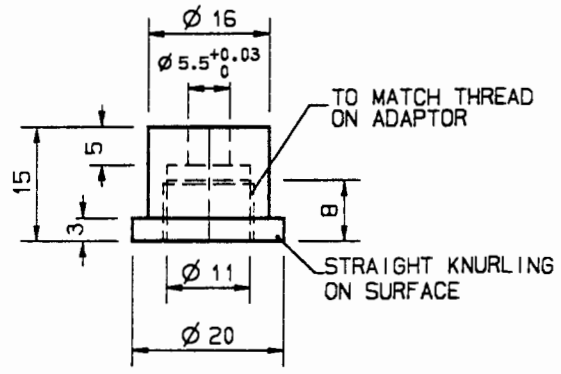

④ SUPPLY HEAD

UNIVERSITY OF CAPE TOWN
DEPARTMENT OF MECHANICAL ENGINEERING

DRILLING UNIT PARTS

SCALE: 1:1	SHEET 2 OF 5
DATE: 13/2/94	
DRAWN BY: A.M.SEGAL	

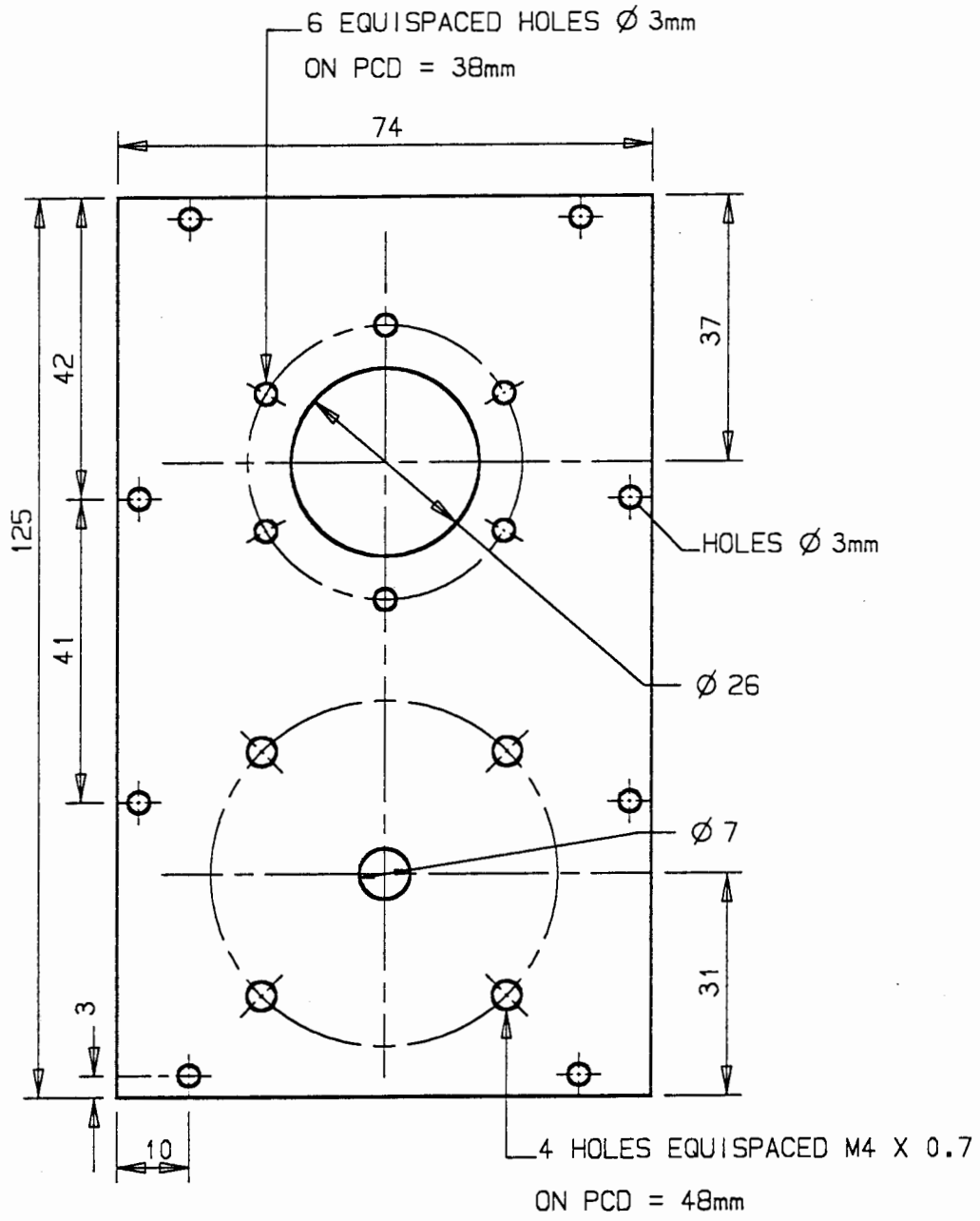

(9) BELT CASING LID

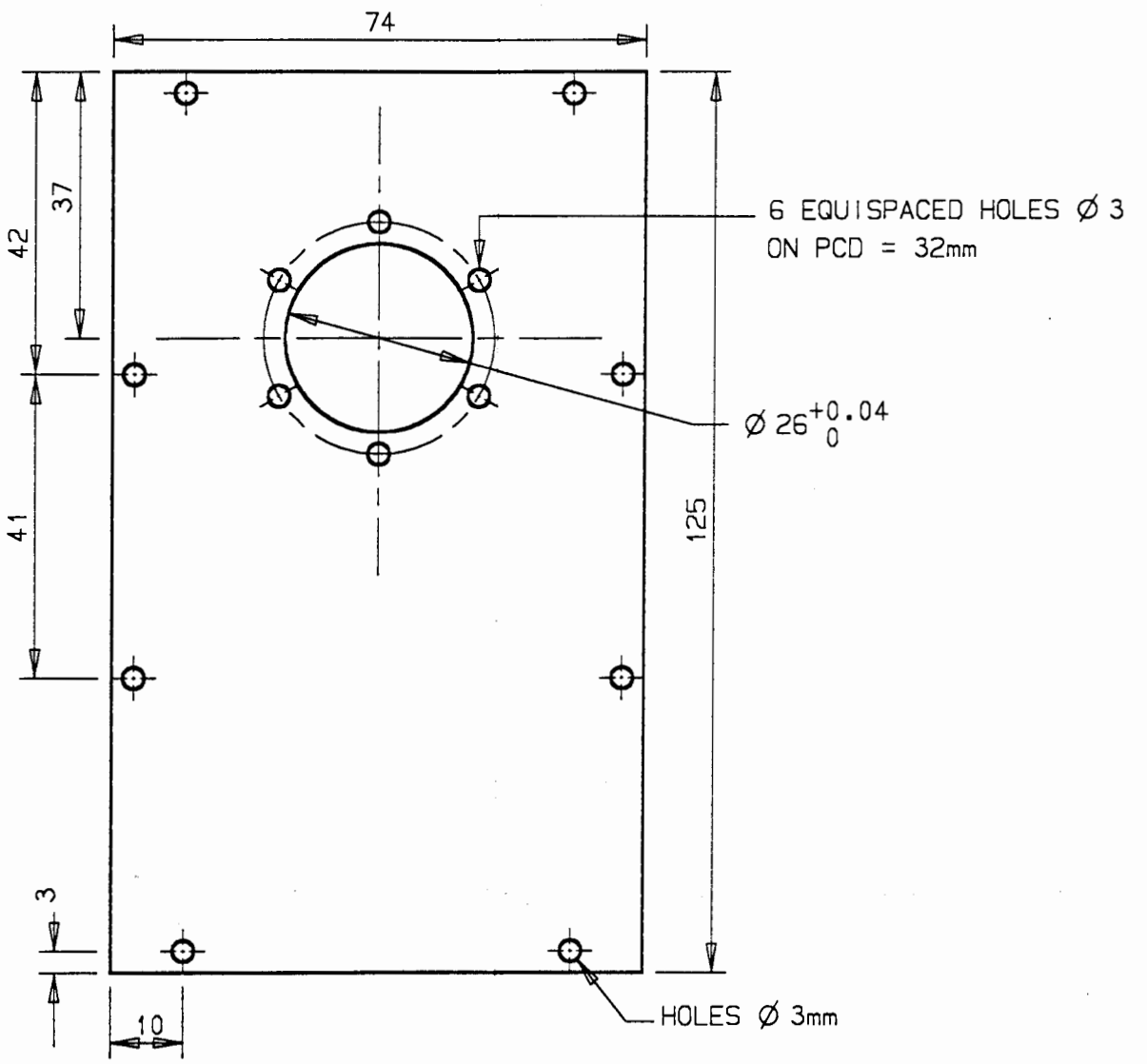

(10) BELT CASING BOTTOM

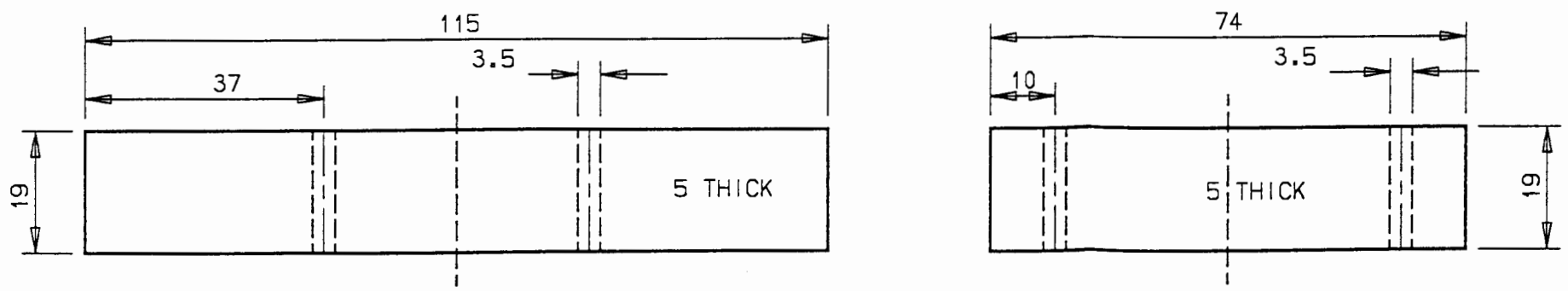

(11) BELT CASING WALL

UNIVERSITY OF CAPE TOWN
DEPARTMENT OF MECHANICAL ENGINEERING

DRILLING UNIT PARTS

SCALE: 1:1	SHEET 3 OF 5
DATE: 13/2/94	
DRAWN BY: A.M.SEGAL	

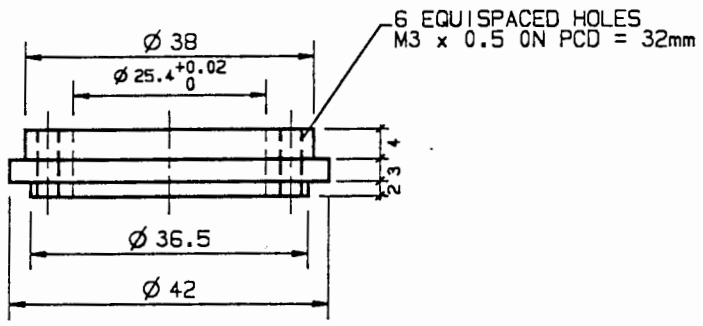

(12) SPIGOTTED COLLAR

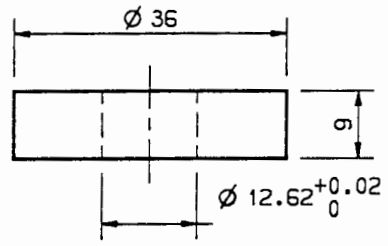

(13) END WASHER

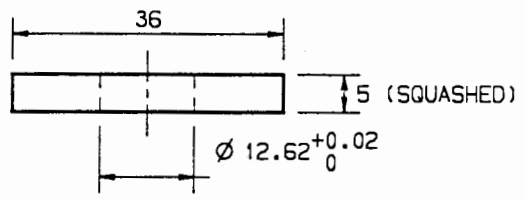

(14) SEAL

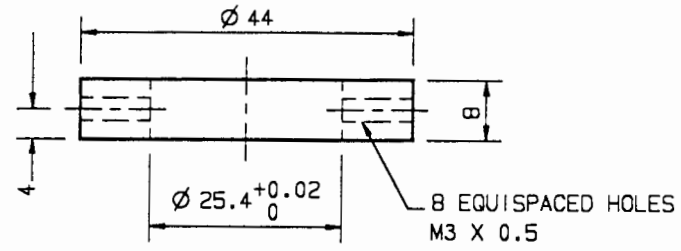

(15) GRUB SCREW COLLAR

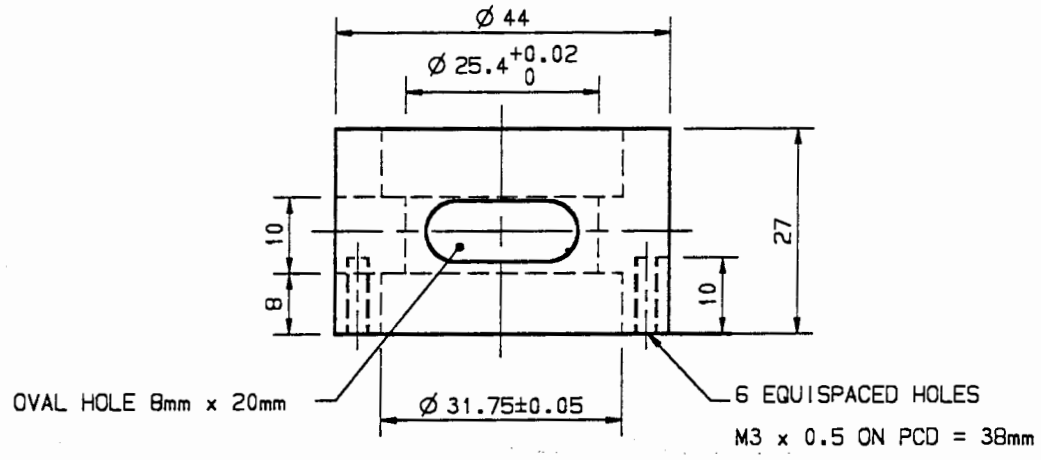

(16) VACUUM HOUSING

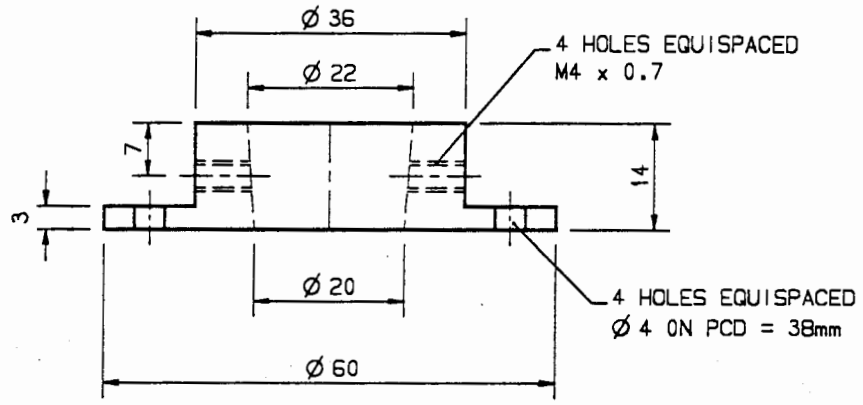

(17) MOTOR MOUNTING

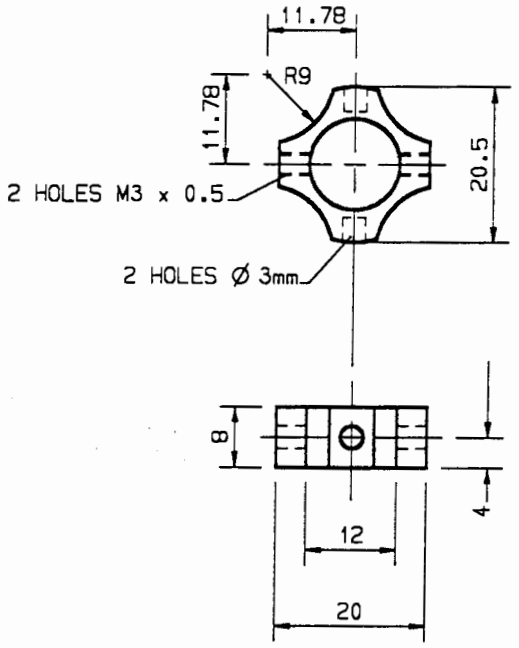

(26) OFFSET GIMBLE

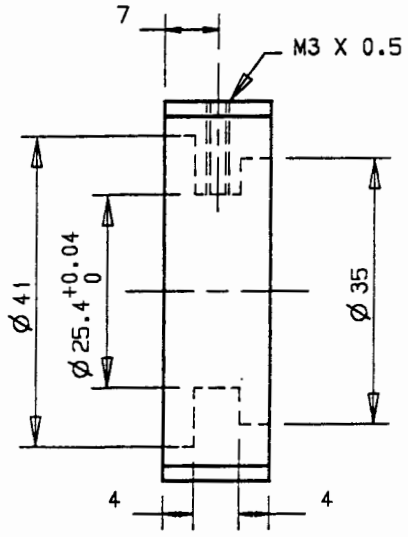

(18) TIMING BELT PULLEY

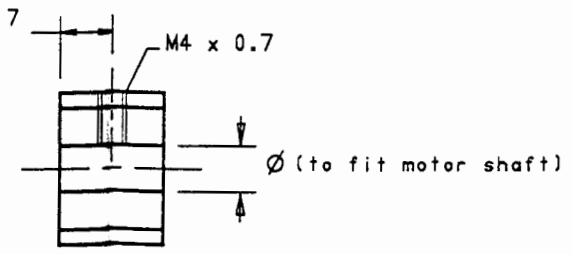

(19) TIMING BELT PULLEY

UNIVERSITY OF CAPE TOWN
DEPARTMENT OF MECHANICAL ENGINEERING

DRILLING UNIT PARTS

SCALE: 1:1	SHEET 4 OF 5
DATE: 13/2/94	
DRAWN BY: A.M.SEGAL	

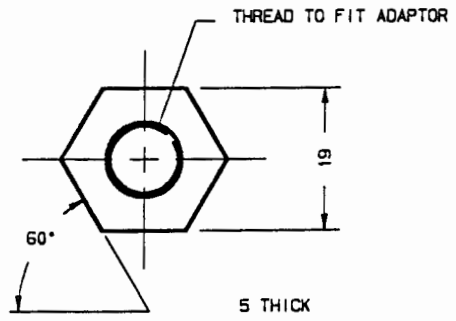

(27) FASTENING NUT

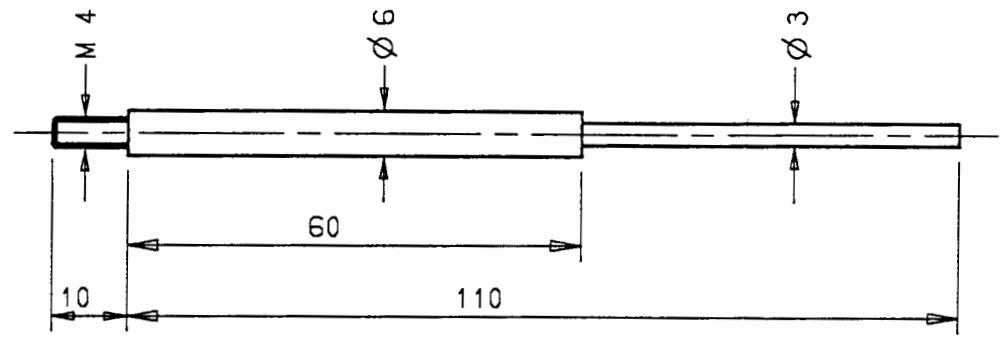

(28) STABILIZER ROD

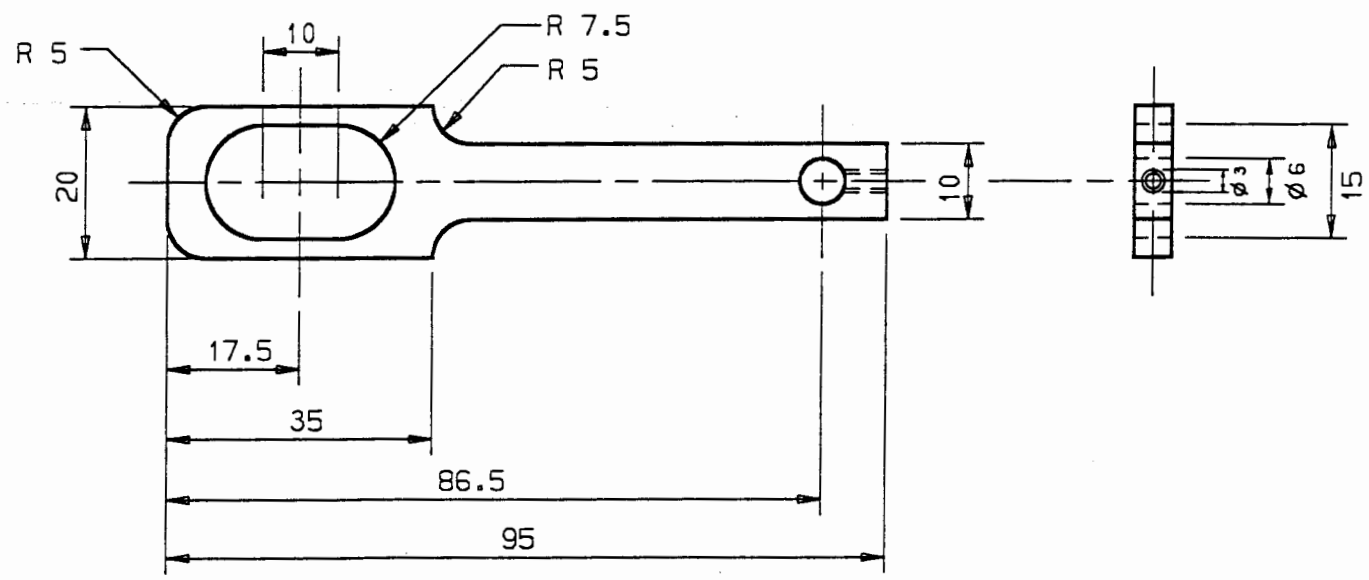

(29) STABILIZER ARM

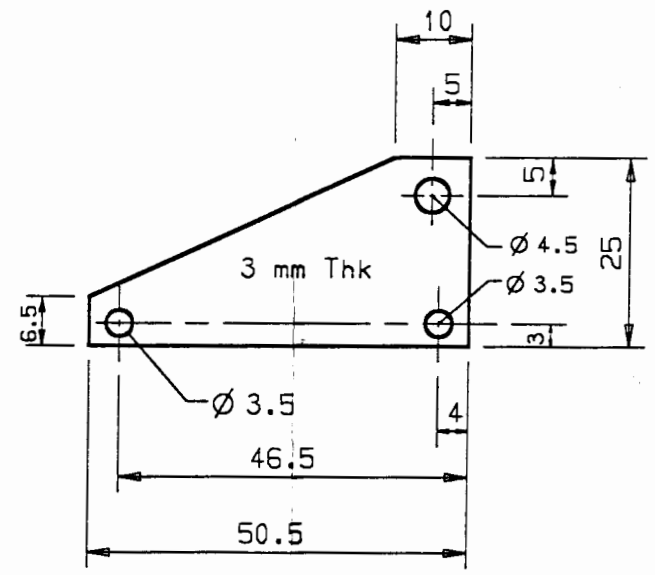

(30) STABILIZER BASE

UNIVERSITY OF CAPE TOWN DEPARTMENT OF MECHANICAL ENGINEERING	
DRILLING UNIT PARTS	
SCALE: 1:1	SHEET 5 OF 5
DATE: 13/2/94	
DRAWN BY: A.M.SEGAL	

APPENDIX E

AUXILIARY COMPONENTS

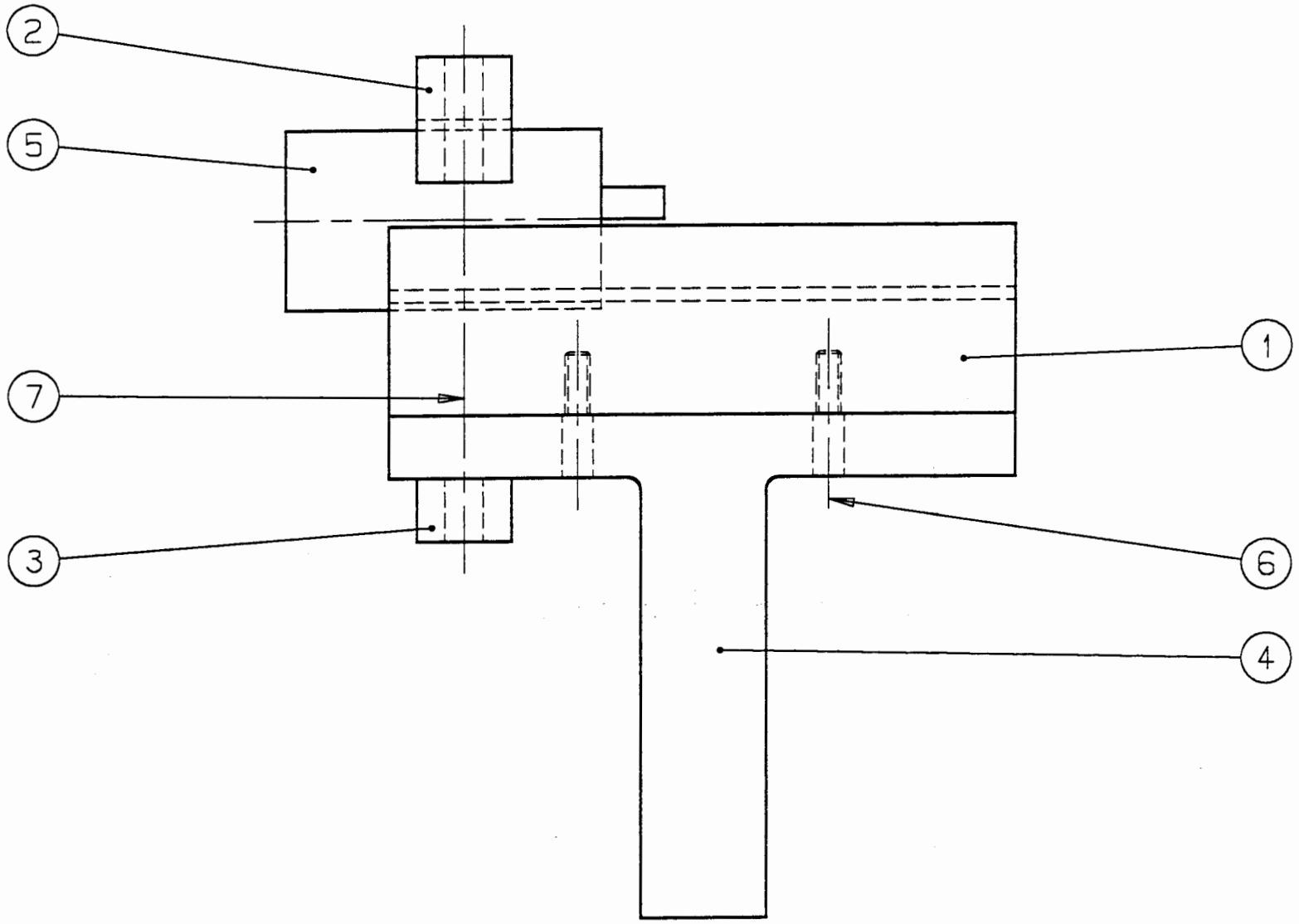

PART NO.	DESCRIPTION	MATERIAL	NO. OFF	REMARKS	SHT. NO.
7	M5 BOLT 80 mm LONG, WING-NUT, 2 WASHERS		4	NOT SHOWN	
6	M4 ALLEN BOLT 15mm LONG		2	NOT SHOWN	
5	ALIGNMENT CYLINDER	431 STAINLESS STEEL	1		3
4	V-BLOCK HOLDER	MILD STEEL	1		2
3	SECURING PLATE	PVC	2		2
2	SECURING BLOCK	PVC	2		2
1	V-BLOCK	MILD STEEL	1		2

UNIVERSITY OF CAPE TOWN
DEPARTMENT OF MECHANICAL ENGINEERING

ALIGNMENT JIG

SCALE: 1:1 | SHEET 1 OF 3

DATE: 13/2/94

DRAWN BY: A.M.SEGAL

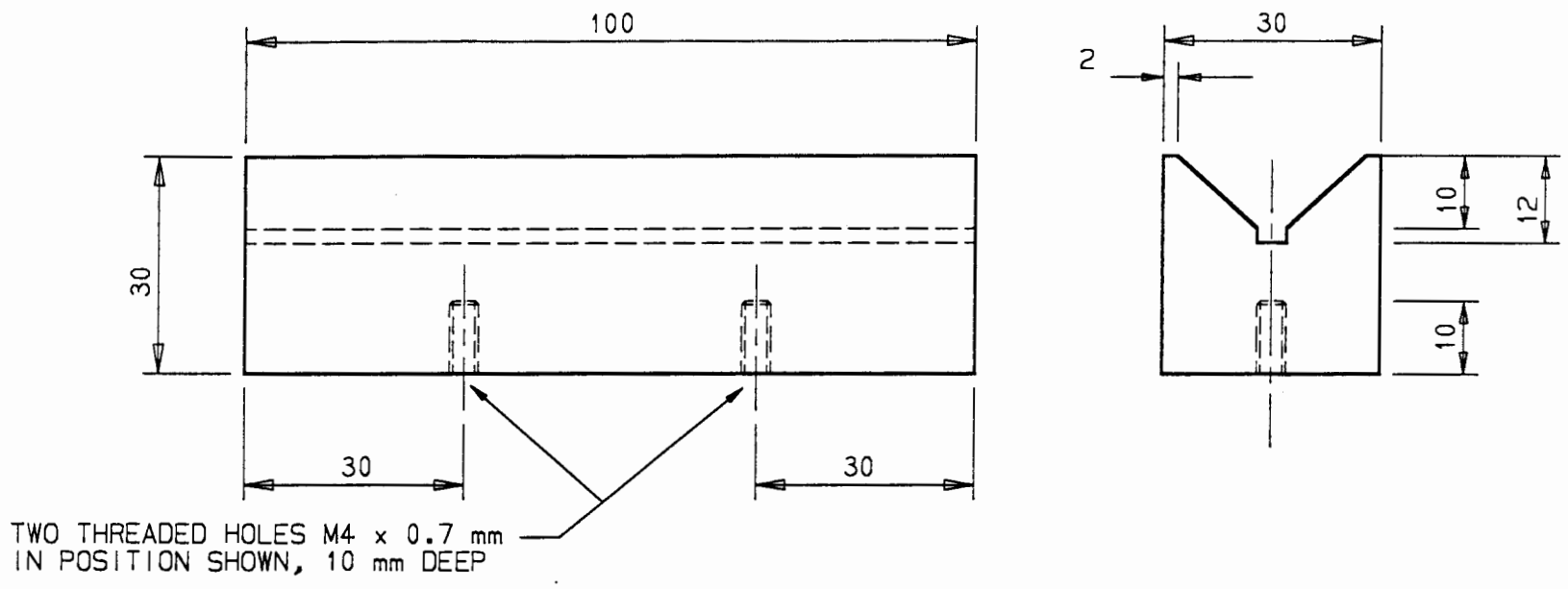

① V-BLOCK

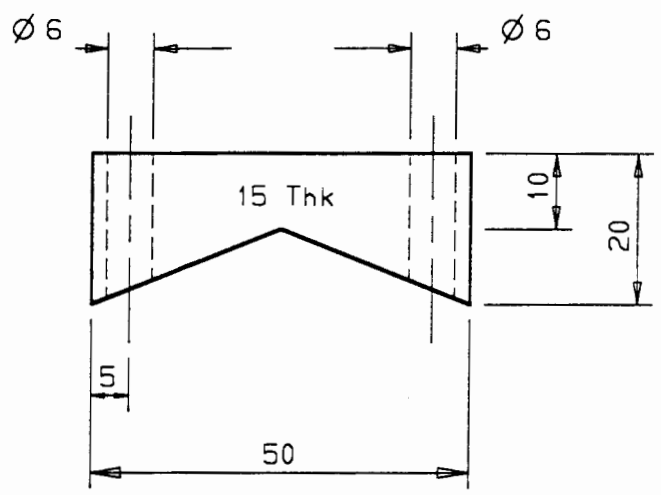

② SECURING BLOCK

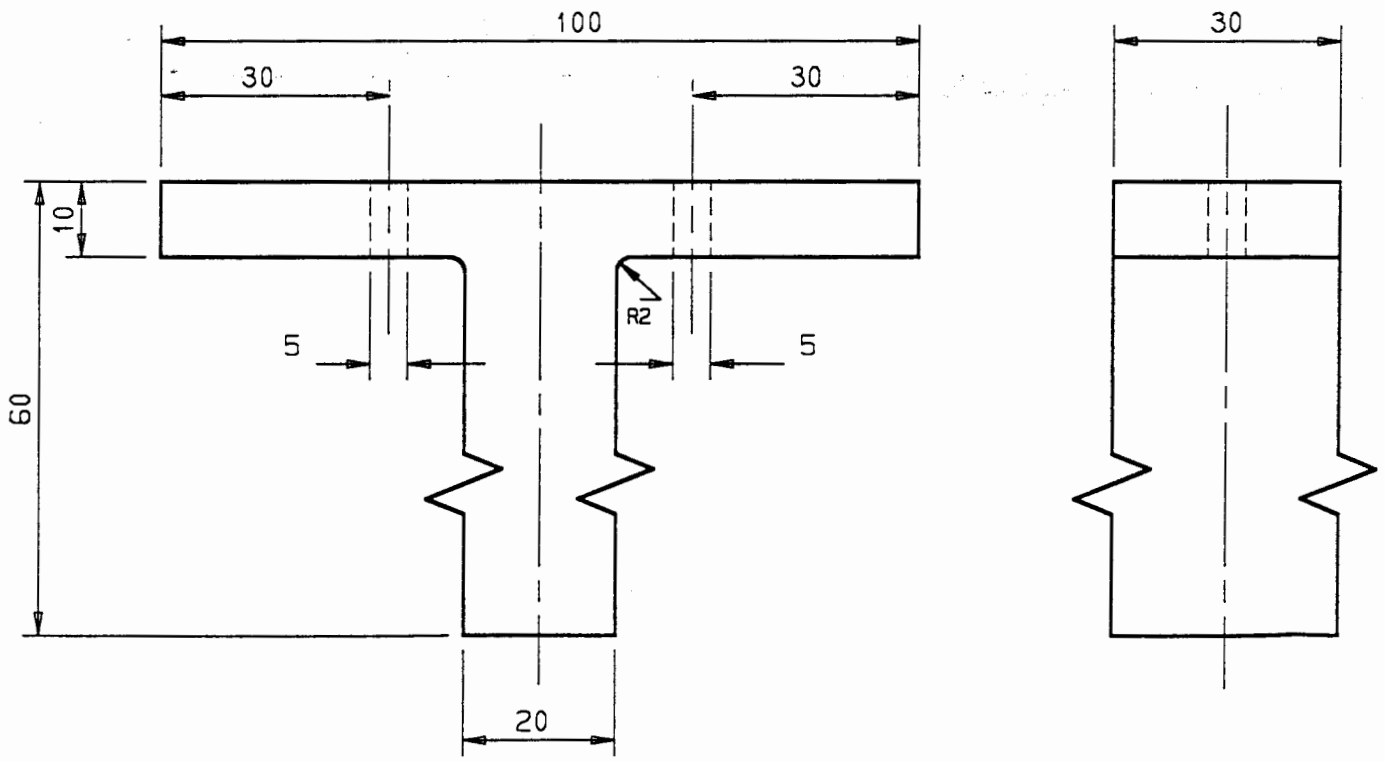

④ V-BLOCK HOLDER

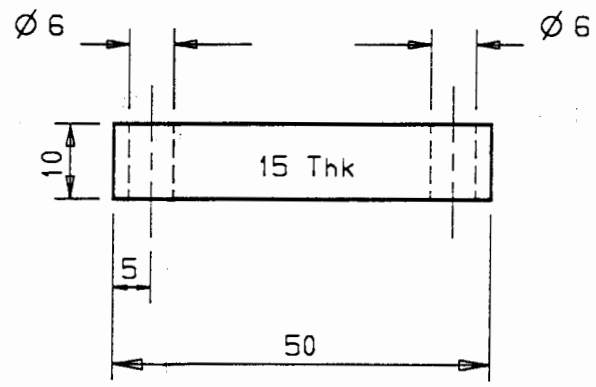

③ SECURING PLATE

NOTE:

ALL CORNERS TO HAVE A
1 mm CHAMFER UNLESS
OTHERWISE SPECIFIED

UNIVERSITY OF CAPE TOWN
DEPARTMENT OF MECHANICAL ENGINEERING

ALIGNMENT JIG

SCALE: 1:1	SHEET 2 OF 3
DATE: 13/2/94	
DRAWN BY: A.M.SEGAL	

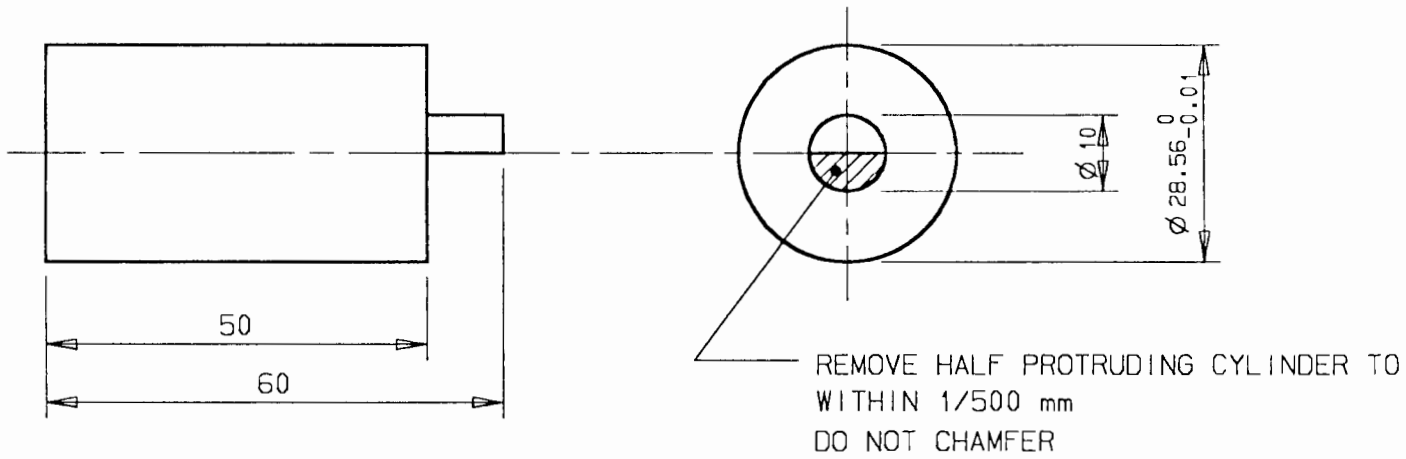

(5) ALIGNMENT CYLINDER

UNIVERSITY OF CAPE TOWN DEPARTMENT OF MECHANICAL ENGINEERING	
ALLIGNMENT JIG	
SCALE: 1:1	SHEET 3 OF 3
DATE: 13/2/94	
DRAWN BY: A.M.SEGAL	

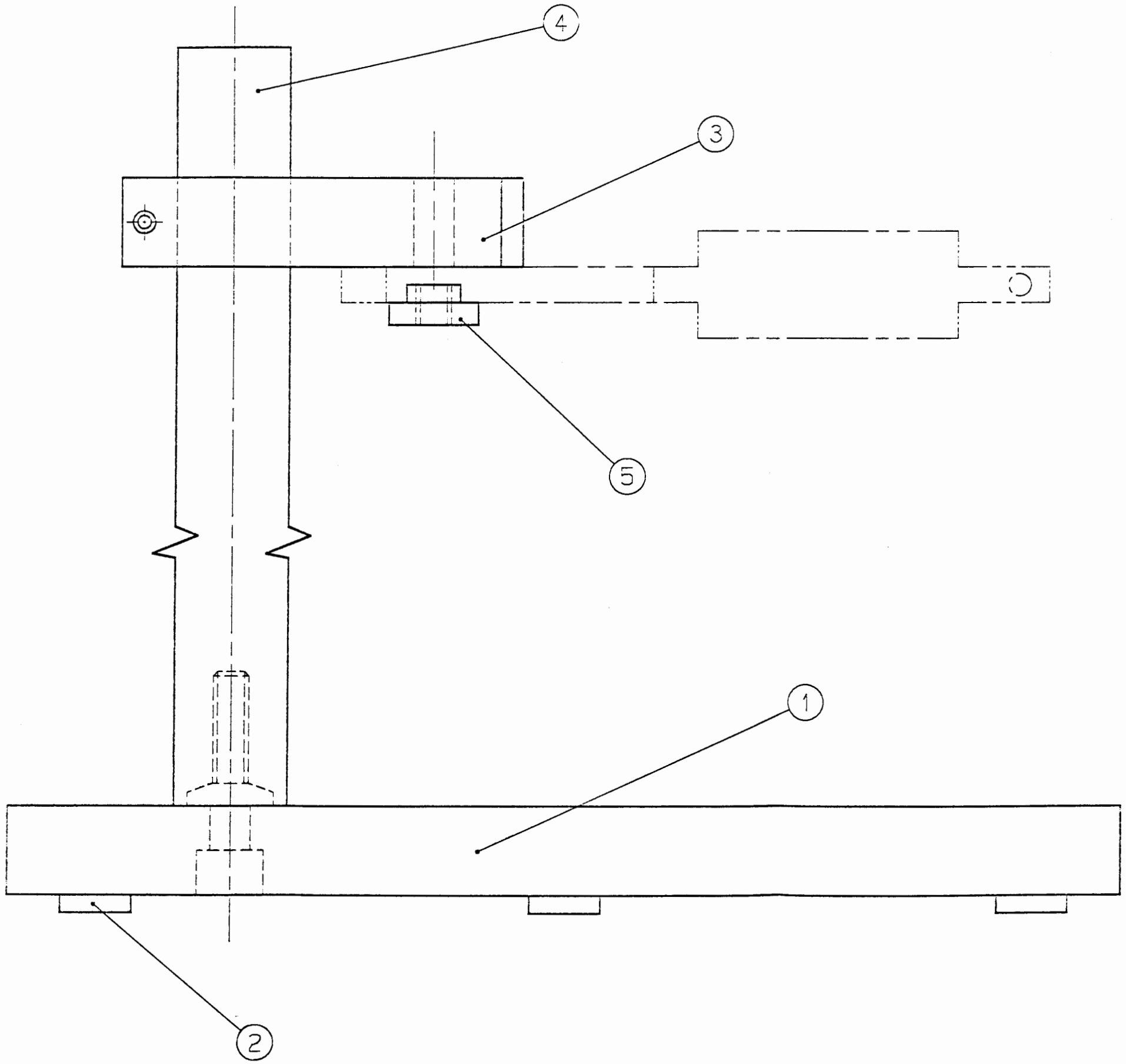

PART NO.	DESCRIPTION	MATERIAL	NO. OFF	REMARKS	SHT. NO.
9	ALLEN BOLT M8		1	NOT SHOWN	
8	SPRING WASHER M8		1	NOT SHOWN	
7	NUT M8		1	NOT SHOWN	
6	THREADED ROD M8		1	NOT SHOWN 55 mm LONG	
5	STEPPED NUT	MILD STEEL	1		3
4	SHAFT	CHROMED MILD STEEL	1	PROVIDED, NEEDS TO BE SHORTENED	3
3	SUPPORT PLATE	MILD STEEL	1		3
2	FEET	RUBBER	5	Ø 20mm, EQUISPACED	
1	BASE PLATE	MILD STEEL	1		2

UNIVERSITY OF CAPE TOWN
DEPARTMENT OF MECHANICAL ENGINEERING

STAND

SCALE: 1:1 | SHEET 1 OF 3

DATE: 13/2/94

DRAWN BY: A.M.SEGAL

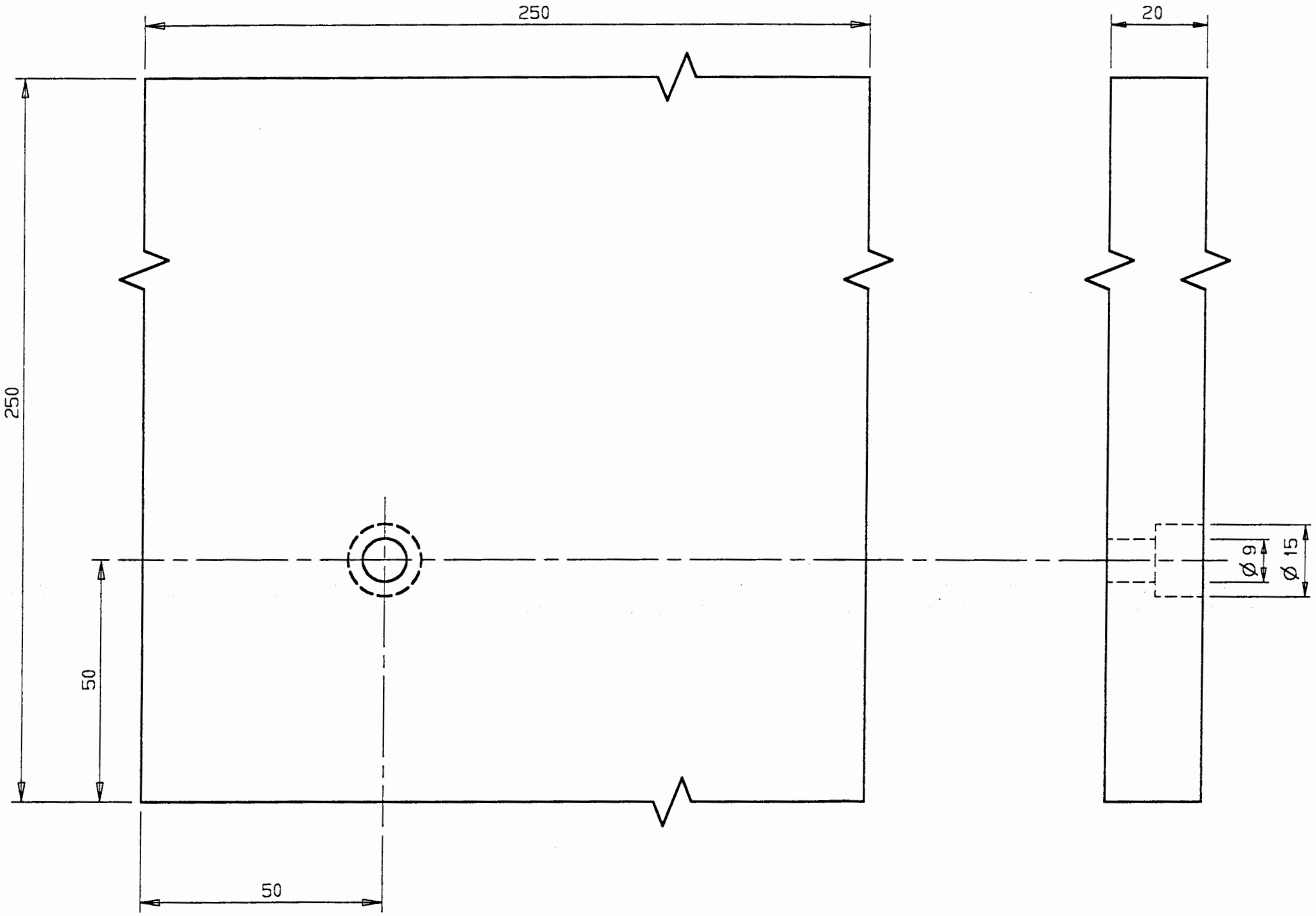

NOTE:

1) RUBBER FEET Ø 20 mm ARE TO BE GLUED TO THE BOTTOM OF THE BASE PLATE 20 mm IN FROM EACH CORNER AND ONE IN THE CENTRE

2) ALL CORNERS ARE TO HAVE A 1mm CHAMFER

① BASE PLATE

UNIVERSITY OF CAPE TOWN
DEPARTMENT OF MECHANICAL ENGINEERING

STAND

SCALE: 1:1	SHEET 2 OF 3
DATE: 13/2/94	
DRAWN BY: A.M.SEGAL	

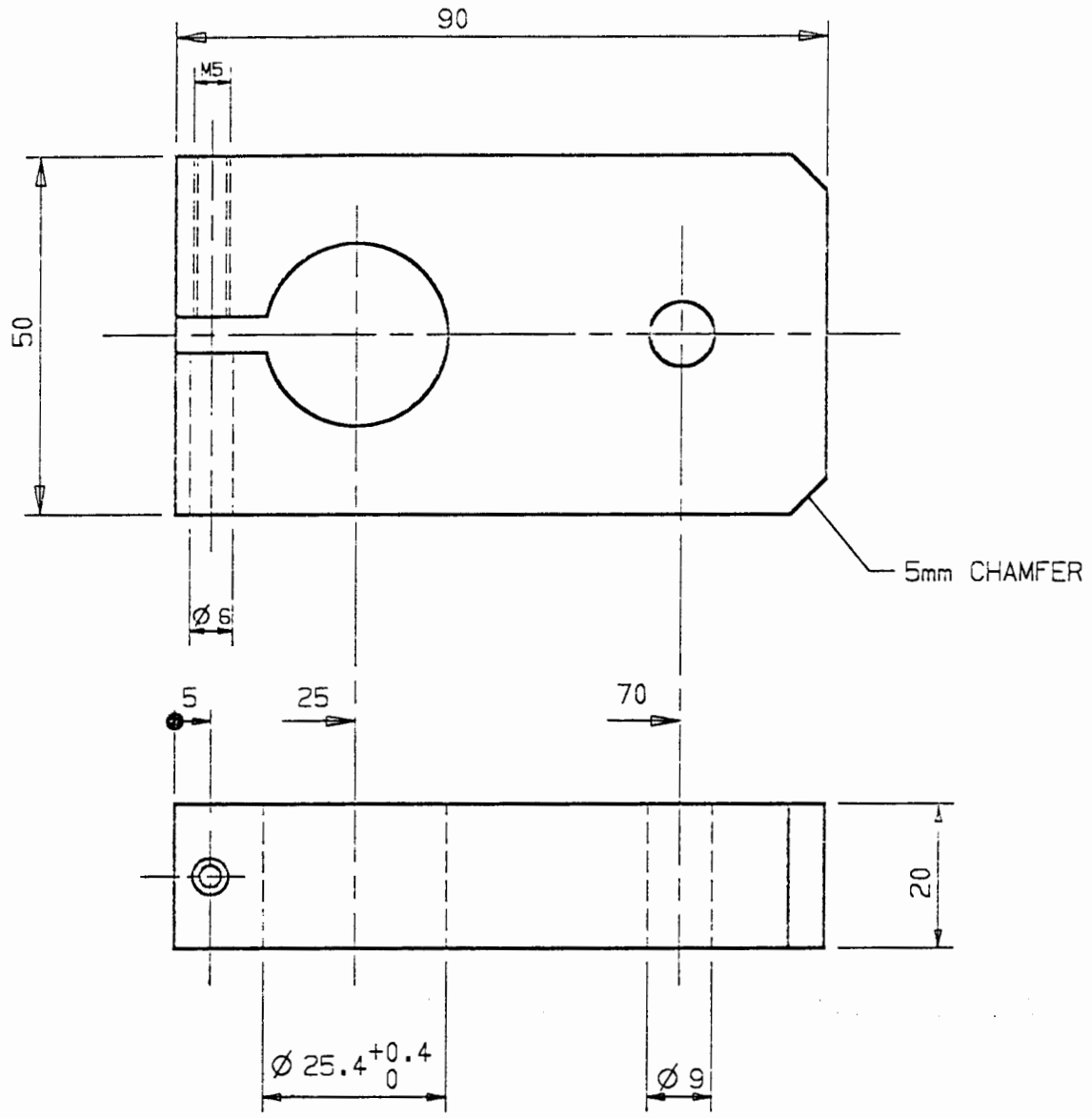

③ SUPPORT PLATE

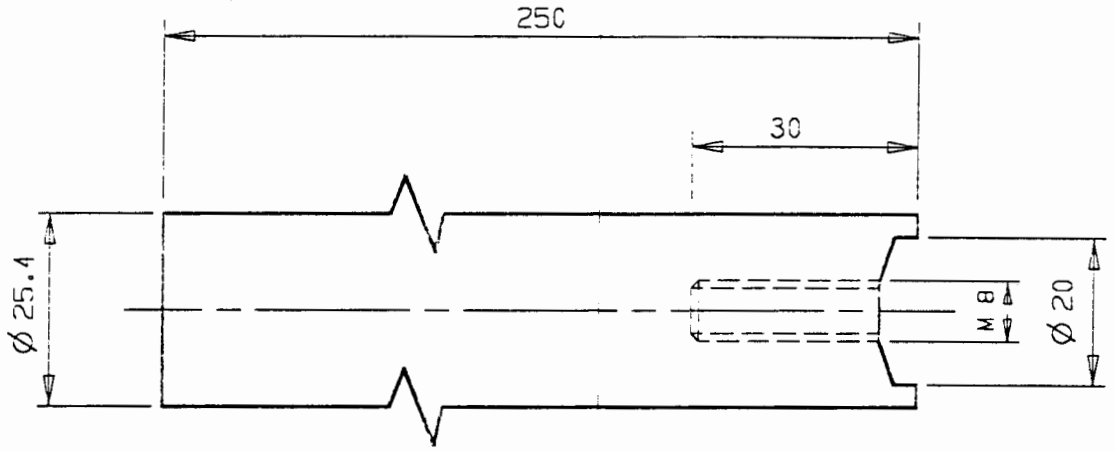

④ SHAFT

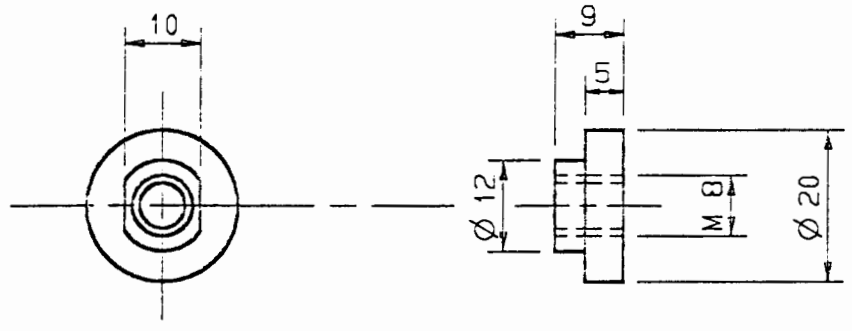

⑤ STEPPED NUT

NOTE:

ALL CORNERS TO HAVE
1 mm CHAMFER UNLESS
OTHERWISE SPECIFIED

UNIVERSITY OF CAPE TOWN
DEPARTMENT OF MECHANICAL ENGINEERING

STAND

SCALE: 1:1	SHEET 3 OF 3
DATE: 13/2/94	
DRAWN BY: A.M.SEGAL	

APPENDIX F

MODIFICATIONS

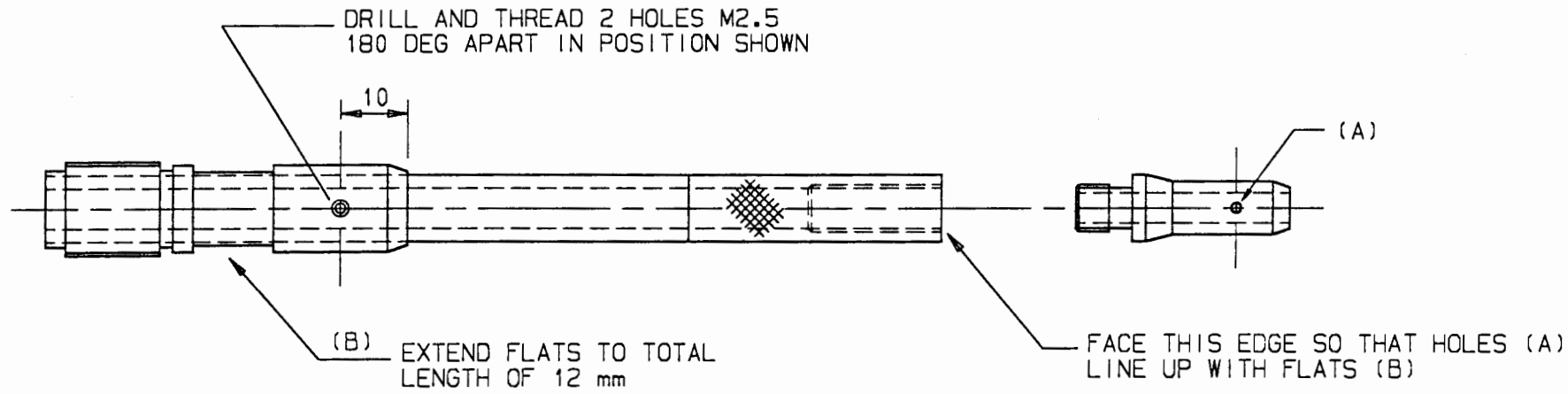

(1) AIR TUBE HOUSING

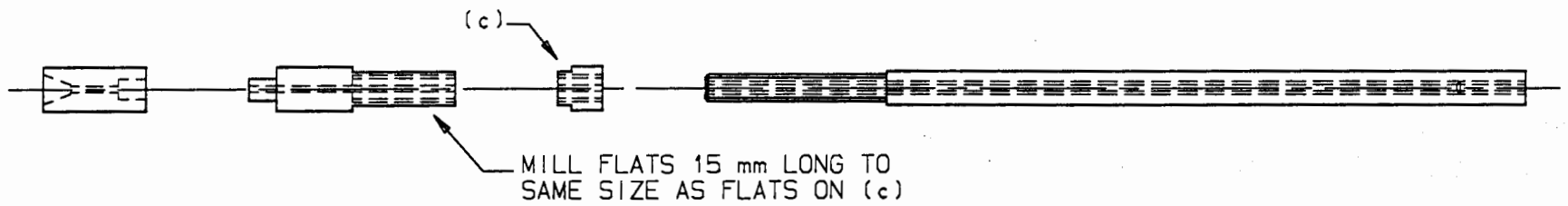

(2) AIR TUBE

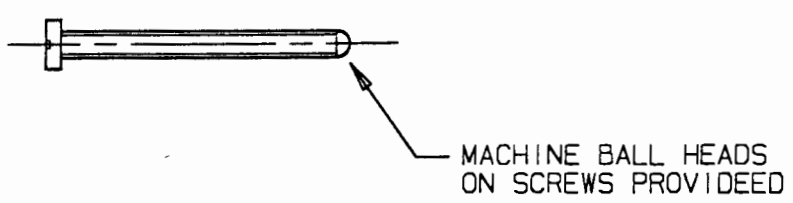

(4) ANGULAR ADJUST SCREWSMENT

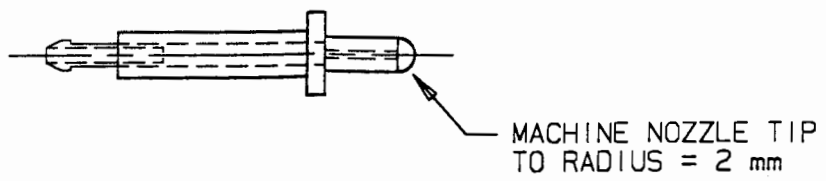

(3) INLET TUBE

UNIVERSITY OF CAPE TOWN
DEPARTMENT OF MECHANICAL ENGINEERING

MODIFICATIONS

SCALE: 1:1	SHEET 1 OF 1
DATE: 13/2/94	
DRAWN BY: A.M.SEGAL	

APPENDIX G

RESULTS OF CALIBRATION

MICRO-STRAINS BEFORE HOLE					
LOAD	SGR 1			SG 7	SG 8
(kN)	AXIAL	45 DEG	90DEG	AXIAL	AXIAL
4.10	143	43	-62	139	87
8.21	286	98	-108	281	201
12.32	427	154	-150	423	325
16.42	570	214	-188	563	451
20.53	712	273	-226	703	584
24.64	840	313	-273	836	710
28.74	978	364	-320	968	836
30.80	1041	382	-346	1033	899

Table G.1 - Strains recorded during the second calibration experiment before hole drilling.

MICRO-STRAINS AFTER HOLE					
LOAD	SGR 1			SG 7	SG 8
(kN)	AXIAL	45 DEG	90DEG	AXIAL	AXIAL
4.10	92	38	-27	164	99
8.21	172	72	-50	312	217
12.32	252	106	-72	454	339
16.42	332	141	-92	595	464
20.53	412	176	-112	740	598
24.64	491	209	-131	879	730
28.74	569	241	-153	1019	866
30.80	613	262	-159	1091	936

Table G.2 - Strains recorded during the second calibration experiment after hole drilling.

CORRECTION FACTORS		
LOAD	BEFORE	AFTER
(kN)	SGR 1	SGR 1
4.10	0.813	0.802
8.21	0.858	0.848
12.32	0.884	0.873
16.42	0.901	0.890
20.53	0.915	0.904
24.64	0.925	0.915
28.74	0.932	0.925
30.80	0.935	0.929

Table G.3 - Correction factors before and after hole drilling for the second calibration experiment.

CORRECTED MICRO-STRAINS						
LOAD	BEFORE			AFTER		
(kN)	AXIAL	45 DEG	90DEG	AXIAL	45 DEG	90DEG
4.10	116.3	35.0	-50.4	73.8	30.5	-21.6
8.21	245.3	84.0	-92.6	145.8	61.0	-42.4
12.32	377.5	136.2	-132.6	220.1	92.6	-62.9
16.42	513.3	192.7	-169.3	295.5	125.5	-81.9
20.53	651.7	249.9	-206.9	372.5	159.1	-101.3
24.64	776.7	289.4	-252.4	449.4	191.3	-119.9
28.74	911.3	339.2	-298.2	526.3	222.9	-141.5
30.80	973.5	357.2	-323.6	569.5	243.4	-147.7

Table G.4 - Corrected strains before and after hole drilling for the second calibration experiment.

RELAXED MICRO-STRAINS			
LOAD	BEFORE HOLE - AFTER HOLE		
(kN)	AXIAL	45 DEG	90DEG
4.10	42.5	4.5	-28.8
8.21	99.5	23.0	-50.2
12.32	157.5	43.6	-69.7
16.42	217.9	67.2	-87.4
20.53	279.3	90.8	-105.6
24.64	327.3	98.1	-132.5
28.74	385.0	116.3	-156.7
30.80	404.0	113.8	-175.9

Table G.5 - Relaxed strains calculated for the second calibration experiment.

RECALCULATED STRESSES (MPa) USING DERIVED CONSTANTS			
APPLIED STRESS	SGR 1		
	SIG(1)	SIG(2)	APLHA
10.0	6.5	-2.6	-1.9
20.0	16.7	-2.5	-0.6
30.0	27.2	-1.9	-0.1
40.0	38.3	-0.7	0.4
50.0	49.7	0.4	0.6
60.0	57.5	-1.3	0.1
70.0	67.6	-1.7	0.2
75.0	70.0	-4.1	-0.0

Table G.6 - Recalculated stresses using experimentally derived constants for the second calibration experiment.

RECALCULATED STRESSES (MPa) USING TABULATED CONSTANTS			
APPLIED STRESS	SGR 1		
	SIG(1)	SIG(2)	APLHA
10.0	6.4	-2.9	-1.9
20.0	16.1	-3.4	-0.6
30.0	26.2	-3.5	-0.1
40.0	36.8	-3.0	0.4
50.0	47.6	-2.6	0.6
60.0	55.2	-4.8	0.1
70.0	64.8	-5.8	0.2
75.0	67.3	-8.3	-0.0

Table G.7 - Recalculated stresses using tabulated constants for the second calibration experiment.

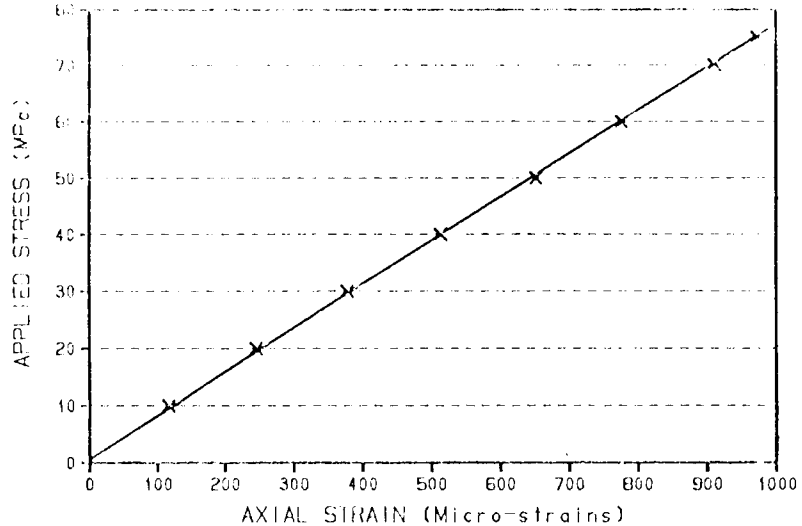

Fig G.1 - Graph of stress-strain data using strain gauge rosette #1 for the second calibration experiment, from which Young's Modulus could be determined.

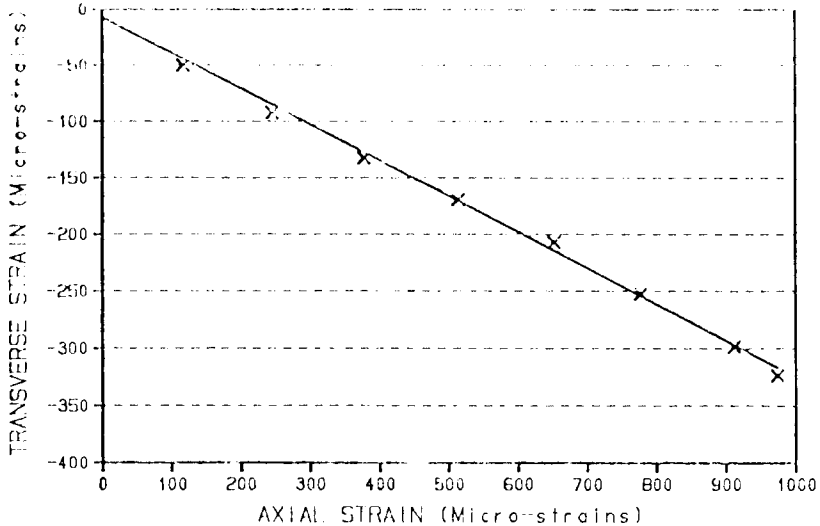

Fig G.2 - Graph of transverse and axial strains using strain gauge rosette #1 for the second calibration experiment, from which Poisson's Ratio could be determined.

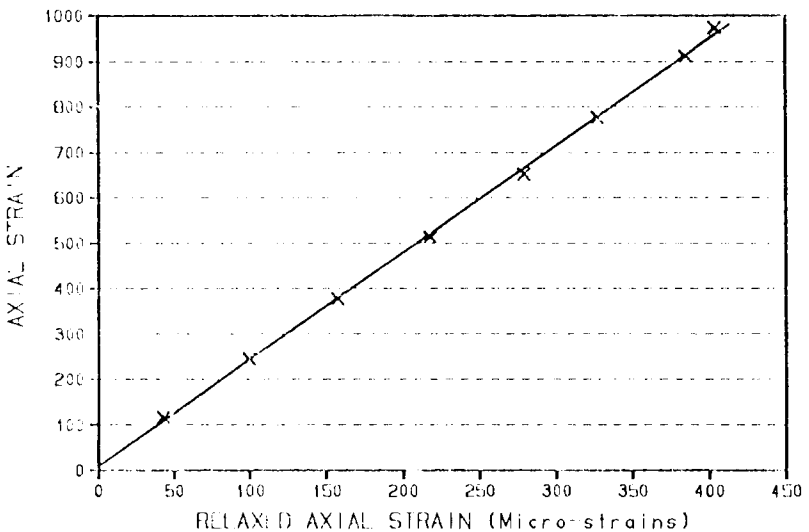

Fig G.3 - Graph of axial and relaxed axial strains using strain gauge rosette #1 for the second calibration experiment, from which 1/K1 could be determined.

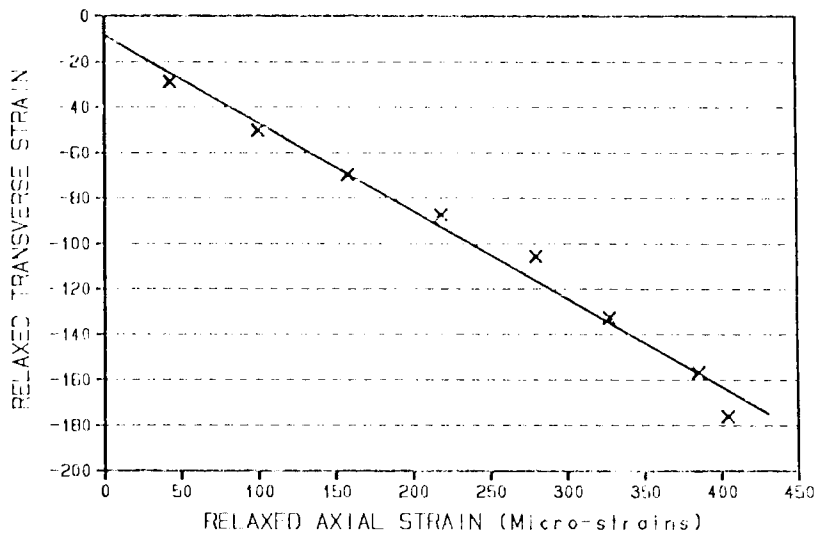

Fig G.4 - Graph of relaxed axial and transverse strains using strain gauge rosette #1 for the second calibration experiment, from which vK2/K1 could be determined.

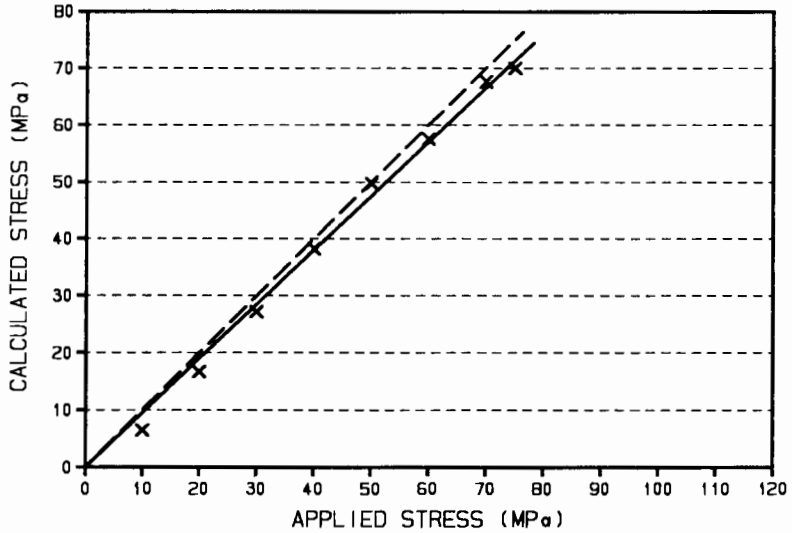

Fig G.5 - Graph of the average calculated relaxed stresses versus the applied stresses using the derived constants for the second calibration experiment. The dashed line represents equal stresses on both axes.

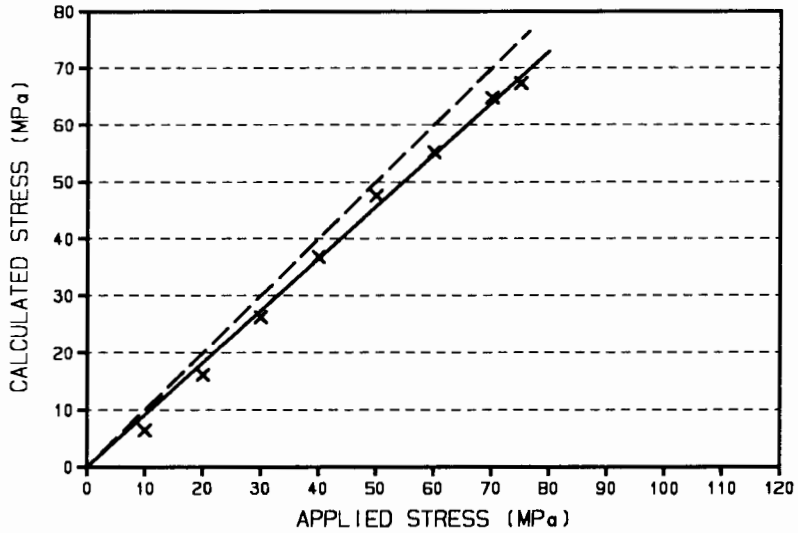

Fig G.6 - Graph of the average calculated relaxed stresses versus the applied stresses using the CEGB[1] constants for the second calibration experiment. The dashed line represents equal stresses on both axes.

APPENDIX H

DETAILED RESULTS OF THE AIR ABRASIVE CENTRE HOLE DRILLING RESIDUAL STRESS MEASUREMENTS

SPECIMEN 8A												
Drill Time (min)	Measured Strain (micro-strain)											
	12 o'clock			3 o'clock			6 o'clock			9 o'clock		
	G1	G2	G3	G1	G2	G3	G1	G2	G3	G1	G2	G3
0	0	0	0	-2	4	-5	-2	-6	-5	1	-1	-2
1	-33	-90	-175	-30	-126	-224	-98	-160	-270	-50	-140	-167
2	-20	-133	-285	-17	-192	-350	-148	-265	-513	-91	-230	-401
3	-2	-152	-406	-14	-249	-442	-207	-340	-620	-105	-290	-463
4	30	-160	-460	10	-272	-500	-224	-366	-700	-120	-286	-510
5	40	-160	-495	28	-266	-520	-224	-373	-730	-111	-281	-512
6	60	-150	-508				-220	-370	-730	-90	-270	-504
6'05"				44	-259	-522						
6'15"										-90	-270	-506
6'30"							-216	-367	-733			

Table H.1 - Recorded strains.

SPECIMEN 8A					
Position (o'clock)		Top 12	3	Bot. 6	9
Final Strain	G1	60	44	-216	-90
	G2	-150	-259	-367	-270
	G3	-508	-522	-733	-506
Max Principal Stress		82.7	87.0	136.9	88.5
Min Principal Stress		16.9	21.9	74.2	42.2
Alpha		-82.7	88.0	-78.7	-86.2
Hoop Stress		81.6	86.9	134.5	88.3
Long Stress		18.0	22.0	76.6	42.4
Shear Stress		8.3	-2.2	12.1	3.1
Hole Diameter		1.584	1.567	1.588	1.598
		1.596	1.572	1.596	1.601
		1.588	1.568	1.585	1.608
Average Diameter		1.589	1.569	1.590	1.602
Hole Depth		1.550	1.605	1.970	1.650
		1.620	1.620	1.840	1.650
Average Depth		1.585	1.613	1.905	1.650
e1+e3-2e2		-148	40	-215	-56
e3-e1		-568	-566	-517	-416
1/K1		2.084	2.134	2.084	2.054

Table H.2 - AACH stresses.

SPECIMEN 18A												
Drill Time	Measured Strain (micro-strain)											
	12 o'clock			3 o'clock			6 o'clock			9 o'clock		
(min)	G1	G2	G3	G1	G2	G3	G1	G2	G3	G1	G2	G3
0	-4	-2	-4	-3	0	0	2	4	0	-1	-4	-1
1	-30	-64	-150	-70	-127	-230	-40	-80	-112			
2	-20	-115	-246	-132	-232	-398	-83	-190	-234			
3	16	-151	-349	-155	-280	-490						
4	44	-169	-385	-147	-288	-513	-100	-275	-362			
5	60	-175	-420	-145	-280	-420	-90	-285	-388			
5'45"				-139	-282	-525						
6	60	-175	-423				-84	-292	-397	-30	-510	-337
6'30"	78	-170	-433									

Table H.3 - Recorded strains.

SPECIMEN 18A					
Position		Top		Bot.	
(o'clock)		12	3	6	9
Final	G1	78	-139	-84	30
Strain	G2	-170	-282	-292	-510
	G3	-433	-525	-397	-337
Max Principal Stress		66.3	106.7	80.3	90.8
Min Principal Stress		9.8	56.8	39.2	-13.2
Alpha		-89.4	-83.0	80.3	58.5
Hoop Stress		66.3	105.9	79.1	62.4
Long Stress		9.8	57.5	40.3	15.2
Shear Stress		0.6	6.0	-6.8	-46.3
Hole Diameter		1.605	1.498	1.494	1.477
		1.588	1.506	1.509	1.471
		1.613	1.501	1.497	1.487
Average Diameter		1.602	1.502	1.500	1.478
Hole Depth		1.650	1.980	1.970	1.650
		1.670	1.950	1.840	1.650
Average Depth		1.660	1.965	1.905	1.650
e1+e3-2e2		-11	-97	109	723
e3-e1		-511	-389	-311	-367
1/K1		2.054	2.317	2.317	2.384

Table H.4 - AACH stresses.

SPECIMEN 27A												
Drill Time (min)	Measured Strain (micro-strain)											
	12 o'clock			3 o'clock			6 o'clock			9 o'clock		
	G1	G2	G3	G1	G2	G3	G1	G2	G3	G1	G2	G3
0	0	0	-1	-2	0	0	0	0	0	1	0	1
1	-23	-30	-95	-38	-73	-125	-68	-117	-165	-21	-61	-124
2	-5	-51	-210	-60	-116	-204	-126	-204	-280	-23	-92	-252
3	12	-59	-283	-77	-140	-283	-168	-297	-428	-24	-132	-248
4	25	-65	-348	-80	-150	-307	-170	-345	-525	-10	-143	-285
5	35	-63	-376	-80	-157	-328	-175	-366	-580	6	-140	-396
6'05"							-169	-369	-588			
6'15"	42	-65	-397	-81	-154	-338				26	-129	-395

Table H.5 - Recorded strains.

SPECIMEN 27A					
Position (o'clock)		Top 12	3	Bot. 6	9
Final Strain	G1	42	-81	-169	26
	G2	-65	-154	-369	-129
	G3	-397	-338	-588	-395
Max Principal Stress		65.1	63.9	105.8	66.0
Min Principal Stress		11.4	31.8	59.5	16.8
Alpha		-76.4	-78.3	87.6	-82.6
Hoop Stress		62.1	62.6	105.8	65.2
Long Stress		14.4	33.1	59.7	17.6
Shear Stress		12.3	6.4	-1.9	6.3
Hole Diameter		1.618	1.564	1.611	1.595
		1.626	1.564	1.605	1.569
		1.613	1.573	1.604	1.581
Average Diameter		1.619	1.567	1.606	1.582
Hole Depth		1.580	1.480	1.470	1.750
		1.580	1.500	1.430	1.850
Average Depth		1.580	1.490	1.450	1.800
e1+e3-2e2		-225	-111	35	-111
e3-e1		-439	-257	-419	-421
1/K1		2.019	2.140	2.048	2.102

Table H.6 - AACH stresses.

SPECIMEN 2A			
Drill Time (min)	Micro-strain 6 o'clock		
	G1	G2	G3
0	-1	-4	2
1	-27	-76	-119
2	-18	-160	-239
3	2	-203	-327
4	27	-230	-398
5	54	-242	-447
6'10"	77	-246	-476
6'40"	96	-233	-477

Table H.7 - Recorded strains.

SPECIMEN 14A			
Drill Time (min)	Micro-strain 3 o'clock		
	G1	G2	G3
0	-5	-2	-3
1	-51	-83	-110
2	-78	-159	-218
3	-91	-212	-321
4	-104	-269	-410
5	-110	-299	-480
6'10"	-108	-322	-518
7'10"	-125	-305	-552

Table H.8 - Recorded strains.

SPECIMEN 2A		
Position (o'clock)		Bot. 6
Final Strain	G1	96
	G2	-233
	G3	-477
Max Principal Stress		71.1
Min Principal Stress		8.1
Alpha		84.5
Hoop Stress		70.6
Long Stress		8.7
Shear Stress		-6.0
Hole Diameter		1.578
		1.583
		1.577
Average Diameter		1.579
Hole Depth		1.500
		1.520
Average Depth		1.510
e1+e3-2e2		106
e3-e1		-546
1/K1		2.109

Table H.9 - AACH stresses.

SPECIMEN 14A		
Position (o'clock)		3
Final Strain	G1	-125
	G2	-305
	G3	-552
Max Principal Stress		99.0
Min Principal Stress		50.3
Alpha		-85.8
Hoop Stress		98.7
Long Stress		50.5
Shear Stress		3.6
Hole Diameter		1.583
		1.594
		1.584
Average Diameter		1.587
Hole Depth		1.630
		1.600
Average Depth		1.615
e1+e3-2e2		-63
e3-e1		-429
1/K1		2.090

Table H.10 - AACH stresses.

SPECIMEN 30A			
Drill Time (min)	Micro-strain 6 o'clock		
	G1	G2	G3
0	-1	-4	1
1	-44	-76	-107
2	-51	-126	-225
3	-50	-159	-303
4	-40	-183	-362
5	-35	-197	-398
6	-22	-196	-422
6'30"	-14	-192	-422

Table H.11 - Recorded strains.

SPECIMEN 15,16,17A			
Drill Time (min)	Micro-strain 3 o'clock (inside)		
	G1	G2	G3
0	-4	-1	0
1	-60	-56	52
2	-90	-92	150
3	-128	-119	243
4	-148	-130	271
5	-154	-145	292
5'30"	-160	-147	297
5"40"	-156	-145	299

Table H.12 - Recorded strains.

SPECIMEN 30A		
Position (o'clock)		Bot. 6
Final Strain	G1	-14
	G2	-192
	G3	-422
Max Principal Stress		73.8
Min Principal Stress		26.0
Alpha		-85.8
Hoop Stress		73.5
Long Stress		26.3
Shear Stress		3.5
Hole Diameter		1.560
		1.572
		1.564
Average Diameter		1.565
Hole Depth		1.530
		1.550
Average Depth		1.540
e1+e3-2e2		-60
e3-e1		-410
1/K1		2.146

Table H.13 - AACH stresses.

15,16,17A-INSIDE		
Position (o'clock)		3
Final Strain	G1	-156
	G2	-145
	G3	299
Max Principal Stress		18.3
Min Principal Stress		-50.2
Alpha		22.0
Hoop Stress		-40.6
Long Stress		8.0
Shear Stress		-25.1
Hole Diameter		1.593
		1.592
		1.589
Average Diameter		1.591
Hole Depth		1.665
		1.650
Average Depth		1.658
e1+e3-2e2		435
e3-e1		451
1/K1		2.078

Table H.14 - AACH stresses.

SPECIMEN 8,9,10E												
Drill Time (min)	Measured Strain (micro-strain)											
	12 o'clock			3 o'clock			6 o'clock			9 o'clock		
	G1	G2	G3	G1	G2	G3	G1	G2	G3	G1	G2	G3
0	2	-1	-1	-2	4	-1	-2	-3	2	2	-2	3
1	-26	-29	-16	44	34	18	25	62	60	20	35	23
2	-26	0	41	73	61	37	22	73	87	55	79	60
3	-16	17	47	84	71	47	19	79	99	71	94	62
4	-9	26	50	86	74	48	20	78	103	81	102	66

Table H.15 - Recorded strains.

SPECIMEN 8,9,10E					
Position (o'clock)		Top 12	3	Bot. 6	9
Final Strain	G1	-9	86	20	81
	G2	26	74	78	102
	G3	50	48	103	66
Max Principal Stress		-1.3	-14.6	-9.4	-14.0
Min Principal Stress		-8.8	-19.9	-20.2	-21.0
Alpha		-5.3	-80.0	-10.8	-52.4
Hoop Stress		-8.7	-14.6	-19.8	-16.6
Long Stress		-1.3	-19.9	-9.8	-19.2
Shear Stress		0.7	0.9	2.0	3.4
Hole Diameter		1.495	1.469	1.510	1.536
		1.481	1.454	1.529	1.524
		1.508	1.478	1.524	1.532
Average Diameter		1.495	1.467	1.521	1.531
Hole Depth		1.600	1.800	2.070	1.420
		1.800	1.800	2.100	1.450
Average Depth		1.700	1.800	2.085	1.435
e1+e3-2e2		-11	-14	-33	-57
e3-e1		59	-38	83	-15
1/K1		2.331	2.414	2.260	2.232

Table H.16 - AACH stresses.

SPECIMEN 17,18,19E						
Drill Time (min)	Measured Strain (micro-strain)					
	12 o'clock			3 o'clock		
	G1	G2	G3	G1	G2	G3
0	-5	-3	-6	0	2	0
1	-7	-4	-9	-5	-6	-12
2	-10	-1	-14	4	9	13
3	-7	11	-11	7	23	32
4	18	39	20	10	28	44
5	19	47	26	13	34	58
6	20	50	32	14	41	65

Table H.17 - Recorded strains.

SPECIMEN 17,18,19E			
Position (o'clock)		Top 12	3
Final Strain	G1	20	14
	G2	50	41
	G3	32	65
Max Principal Stress		-6.0	-12.2
Min Principal Stress		-18.9	-25.1
Alpha		-38.0	-1.7
Hoop Stress		-14.0	-25.1
Long Stress		-10.9	-12.2
Shear Stress		6.2	0.4
Hole Diameter		1.539	1.536
		1.531	1.535
		1.534	1.548
Average Diameter		1.531	1.539
Hole Depth		1.670	1.730
		1.700	1.700
Average Depth		1.685	1.715
e1+e3-2e2		-48	-3
e3-e1		12	51
1/K1		4.710	4.621

Table H.18 - AACH stresses.

SPECIMEN 19E						
Drill Time (min)	Measured Strain (micro-strain)					
	6 o'clock			9 o'clock		
	G1	G2	G3	G1	G2	G3
0	3	4	3	-1	-3	2
1	8	10	11			
2	20	21	27	23	10	-6
3	34	36	39	46	25	2
4	40	44	48	57	33	9
5	42	42	49	64	33	6

Table H.19 - Recorded strains.

SPECIMEN 19E			
Position (o'clock)		Bot. 6	9
Final Strain	G1	42	64
	G2	42	33
	G3	49	6
Max Principal Stress		-9.0	-4.3
Min Principal Stress		-10.0	-10.5
Alpha		22.5	88.0
Hoop Stress		-9.9	-4.3
Long Stress		-9.1	-10.5
Shear Stress		-0.3	-0.2
Hole Diameter		1.659	1.622
		1.657	1.652
		1.630	1.626
Average Diameter		1.649	1.633
Hole Depth		2.050	2.050
		2.000	1.810
Average Depth		2.025	1.930
e1+e3-2e2		7	4
e3-e1		7	-58
1/K1		1.951	1.984

Table H.20 - AACH stresses.

SPECIMEN 27,28,29E												
Drill Time (min)	Measured Strain (micro-strain)											
	12 o'clock			3 o'clock			6 o'clock			9 o'clock		
	G1	G2	G3	G1	G2	G3	G1	G2	G3	G1	G2	G3
0	-1	3	4	2	3	9	3	-2	3	-3	-1	2
1	7	32	49	32	30	34	31	26	70	29	11	20
2	16	72	109	89	87	80	70	66	137	75	62	81
3	13	94	146	100	112	111	85	93	180	80	78	110
4	19	109	161	110	128	133				87	90	123
4'30"	23	116	166									

Table H.21 - Recorded strains.

SPECIMEN 27,28,29E					
Position (o'clock)		Top 12	3	Bot. 6	9
Final Strain	G1	23	110	85	87
	G2	116	128	93	90
	G3	166	133	180	123
Max Principal Stress		-13.4	-27.9	-24.5	-22.0
Min Principal Stress		-30.9	-31.1	-39.6	-27.5
Alpha		-8.4	-14.7	19.9	19.9
Hoop Stress		-30.6	-30.8	-37.9	-26.9
Long Stress		-13.8	-28.1	-26.3	-22.6
Shear Stress		2.6	0.8	-4.8	-1.7
Hole Diameter		1.525	1.525	1.511	1.538
		1.551	1.502	1.511	1.543
		1.559	1.522	1.537	1.545
Average Diameter		1.545	1.516	1.520	1.542
Hole Depth		1.800	1.750	1.500	1.700
		1.750	1.600	1.600	1.600
Average Depth		1.775	1.675	1.550	1.650
e1+e3-2e2		-43	-13	79	30
e3-e1		143	23	95	36
1/K1		2.199	2.274	2.267	2.205

Table H.22 - AACH stresses.

SPECIMEN 17,18 & 19E			
Drill Time (min)	Micro-strain 12 o'clock (inside)		
	G1	G2	G3
0	-2	-2	2
1	-19	-5	-21
2	-27	-14	-34
3	-24	-11	-32
4	-23	-4	-19

Table H.23 - Recorded strains.

SPECIMEN 19E			
Drill Time (min)	Micro-strain 12 o'clock (mid-wall)		
	G1	G2	G3
0	0	0	0
1	18	67	60
2	50	102	110
3	72	127	147
4	87	143	167

Table H.24 - Recorded strains.

17,18,19E - INSIDE		
Position (o'clock)		Top 12
Final Strain	G1	-23
	G2	-4
	G3	-19
Max Principal Stress		6.8
Min Principal Stress		2.9
Alpha		-41.6
Hoop Stress		6.8
Long Stress		2.9
Shear Stress		-0.2
Hole Diameter		1.545
		1.561
		1.553
Average Diameter		1.553
Hole Depth		1.740
		1.790
Average Depth		1.765
e1+e3-2e2		-34
e3-e1		4
1/K1		2.179

Table H.25 - AACH stresses.

SPECIMEN 19E - MID-WALL THK		
Position (o'clock)		Top 12
Final Strain	G1	87
	G2	143
	G3	167
Max Principal Stress		-26.1
Min Principal Stress		-37.0
Alpha		-10.9
Hoop Stress		-29.5
Radial Stress		-33.6
Shear Stress		-5.0
Hole Diameter		1.494
		1.489
		1.505
Average Diameter		1.496
Hole Depth		1.550
		1.600
Average Depth		1.575
e1+e3-2e2		-32
e3-e1		80
1/K1		2.331

Table H.26 - AACH stresses.

SPECIMEN 5,6,7F												
Drill Time	Measured Strain (micro-strain)											
	12 o'clock			3 o'clock			6 o'clock			9 o'clock		
(min)	G1	G2	G3	G1	G2	G3	G1	G2	G3	G1	G2	G3
0	0	5	7	1	-4	1	-3	-3	-2	2	6	0
1	-100	-170	-246	-151	-251	-342	55	-228	-533	-58	-59	-242
2	-130	-249	-386	-207	-401	-577	164	-253	-764	-79	-44	-345
3	-120	-270	-430	-200	-432	-645	206	-257	-810	-64	-10	-362
4	-108	-266	-427	-187	-438	-663	229	-222	-831	-67	-10	-376
4'30"	-110	-267	-436									

Table H.27 - Recorded strains.

SPECIMEN 5,6,7F					
Position		Top		Bot.	
(o'clock)		12	3	6	9
Final	G1	-110	-187	229	-67
Strain	G2	-267	-438	-222	-10
	G3	-436	-663	-831	-376
Max Principal Stress		93.1	153.5	138.5	87.6
Min Principal Stress		49.9	85.9	7.6	22.2
Alpha		-89.0	88.4	-85.8	-63.1
Hoop Stress		93.1	153.4	8.3	74.3
Long Stress		49.9	86.0	137.8	35.5
Shear Stress		0.7	1.8	9.6	26.5
Hole Diameter		1.451	1.401	1.513	1.511
		1.456	1.391	1.517	1.477
		1.458	1.408	1.520	1.506
Average Diameter		1.455	1.400	1.517	1.498
Hole Depth		2.100	1.400	2.000	1.770
		2.000	1.500	1.800	1.800
Average Depth		2.050	1.450	1.900	1.785
e1+e3-2e2		-12	26	-158	-423
e3-e1		-326	-476	-1060	-309
1/K1		2.454	2.640	2.274	2.324

Table H.28 - AACH stresses.

SPECIMEN 12,13,14F						
Drill Time (min)	Measured Strain (micro-strain)					
	12 o'clock			6 o'clock		
	G1	G2	G3	G1	G2	G3
0	-1	1	0	-1	-2	0
1	-50	-88	-144	-42	-81	-117
2	-90	-150	-269	-56	-134	-225
3	-110	-200	-377	-60	-190	-298
4	-115	-218	-427	-54	-238	-368
5	-114	-229	-457	-45	-260	-390
6	-96	-220	-465	-30	-278	-413

Table H.29 - Recorded strains.

SPECIMEN 12,13,14F			
Position (o'clock)		Top 12	Bot 6
Final Strain	G1	-96	-30
	G2	-220	-278
	G3	-465	-413
Max Principal Stress		88.5	151.2
Min Principal Stress		42.7	52.5
Alpha		-80.8	81.8
Hoop Stress		87.3	149.1
Long Stress		43.8	54.4
Shear Stress		7.2	-13.8
Hole Diameter		1.548	1.560
		1.541	1.552
		1.553	1.569
Average Diameter		1.547	1.560
Hole Depth		1.650	1.668
		1.630	1.630
Average Depth		1.640	1.647
e1+e3-2e2		-121	113
e3-e1		-369	-383
1/K1		2.192	4.505

Table H.30 - AACH stresses.

SPECIMEN 19,20,21F												
Drill Time	Measured Strain (micro-strain)											
	12 o'clock			3 o'clock			6 o'clock			9 o'clock		
(min)	G1	G2	G3	G1	G2	G3	G1	G2	G3	G1	G2	G3
0	-3	1	-2	2	-1	2	1	3	1	1	2	-3
1	-63	-111	-204	-117	-150	-306	-218	-381	-562	-69	-95	-240
2	-110	-190	-370	-156	-351	-481	-298	-600	-928	-78	-98	-381
3	-102	-201	-418	-133	-365	-521	-293	-674	-1042	-66	-75	-413
4	-100	-206	-436	-121	-363	-525	-291	-668	-1083	-67	-74	-427

Table H.31 - Recorded strains.

SPECIMEN 19,20,21F					
Position		Top		Bot.	
(o'clock)		12	3	6	9
Final	G1	-100	-121	-291	-67
Strain	G2	-206	-363	-668	-74
	G3	-436	-525	-1083	-427
Max Principal Stress		93.2	104.8	215.2	93.4
Min Principal Stress		46.3	53.8	118.3	30.3
Alpha		-79.9	84.4	-88.6	-68.1
Hoop Stress		91.7	104.3	215.1	84.6
Long Stress		47.7	54.2	118.4	39.1
Shear Stress		8.1	-4.9	2.3	21.9
Hole Diameter		1.460	1.517	1.519	1.504
		1.467	1.503	1.515	1.471
		1.454	1.497	1.517	1.498
Average Diameter		1.460	1.506	1.517	1.491
Hole Depth		1.750	2.000	1.700	1.900
		1.600	1.800	1.800	1.800
Average Depth		1.675	1.900	1.750	1.850
e1+e3-2e2		-124	80	-38	-346
e3-e1		-336	-404	-792	-360
1/K1		2.438	2.302	2.274	2.346

Table H.32 - AACH stresses.

SPECIMEN 5,6,7F			
Drill Time (min)	Micro-strain 6 o'clock (inside)		
	G1	G2	G3
0	-2	1	3
1			
2	101	85	170
3	125	104	223
4	131	106	238

Table H.33 - Recorded strains.

SPECIMEN 19,20,21F			
Drill Time (min)	Micro-strain 6 o'clock (inside)		
	G1	G2	G3
0	2	3	0
1	105	50	98
2	256	120	256
3	330	144	324
4	350	147	350

Table H.34 - Recorded strains.

5,6,7F - INSIDE		
Position (o'clock)		Bot 6
Final Strain	G1	131
	G2	106
	G3	238
Max Principal Stress		-31.6
Min Principal Stress		-53.7
Alpha		27.9
Hoop Stress		-51.8
Long Stress		-33.5
Shear Stress		-6.2
Hole Diameter		1.545
		1.569
		1.557
Average Diameter		1.557
Hole Depth		1.650
		1.550
Average Depth		1.600
e1+e3-2e2		157
e3-e1		107
1/K1		2.166

Table H.35 - AACH stresses.

19,20,21F - INSIDE		
Position (o'clock)		Bot 6
Final Strain	G1	350
	G2	147
	G3	350
Max Principal Stress		-58.8
Min Principal Stress		-107.5
Alpha		45.0
Hoop Stress		-107.5
Long Stress		-58.8
Shear Stress		0.0
Hole Diameter		1.527
		1.527
		1.546
Average Diameter		1.533
Hole Depth		1.700
		1.600
Average Depth		1.650
e1+e3-2e2		406
e3-e1		0
1/K1		2.226

Table H.36 - AACH stresses.

SPECIMEN 7F			
Drill Time (min)	Micro-strain 6 o'clock (mid-wall)		
	G1	G2	G3
0	-2	0	-3
1	-98	37	-27
2	-126	71	-36
3	-145	111	-28
4	-158	132	-16

Table H.37 - Recorded strains.

SPECIMEN 21F			
Drill Time (min)	Micro-strain 6 o'clock (mid-wall)		
	G1	G2	G3
0	-4	0	1
1	-85	41	-21
2	-157	74	-30
3	-189	112	-18
4	-193	136	-10

Table H.38 - Recorded strains.

SPECIMEN 7F - MID-WALL THK		
Position (o'clock)		Bot. 6
Final Strain	G1	-158
	G2	132
	G3	-16
Max Principal Stress		48.9
Min Principal Stress		-6.9
Alpha		-36.0
Hoop Stress		47.6
Radial Stress		-5.6
Shear Stress		-8.7
Hole Diameter		1.523
		1.526
		1.515
Average Diameter		1.521
Hole Depth		1.500
		1.500
Average Depth		1.500
e1+e3-2e2		-438
e3-e1		142
1/K1		2.260

Table H.39 - AACH stresses.

SPECIMEN 21F - MID-WALL THK		
Position (o'clock)		Bot. 6
Final Strain	G1	-193
	G2	136
	G3	-10
Max Principal Stress		56.1
Min Principal Stress		-6.5
Alpha		-34.4
Hoop Stress		53.9
Radial Stress		-4.4
Shear Stress		-11.3
Hole Diameter		1.516
		1.508
		1.511
Average Diameter		1.512
Hole Depth		1.800
		1.600
Average Depth		1.700
e1+e3-2e2		-475
e3-e1		183
1/K1		2.288

Table H.40 - AACH stresses.

APPENDIX I

DETAILED RESULTS OF THE RING SPLITTING RESIDUAL STRESS MEASUREMENTS

SPECIMEN 2A - CUT AT 6 O'CLOCK			
Reading	OD0	ID0	OD1
1	70.086	51.060	70.350
2	70.018	51.049	70.339
3	70.009	51.052	70.338
4	70.048	51.022	70.345
5	70.028	51.055	70.338
6	70.018	50.953	70.337
7	70.023	50.972	70.342
8	70.039	51.002	70.348
9	70.015	50.941	70.339
10	70.065	50.955	70.341
Av Dia.	70.035	51.006	70.342
Av Thk.	9.515		
Calculated Stress =			47.6 MPa
Variance =			3.8 MPa

Table I.1 - Ring split stress.

SPECIMEN 3,4A - CUT AT 6 O'CLOCK			
Reading	OD0	ID0	OD1
1	70.012	50.900	70.417
2	70.017	50.975	70.450
3	70.017	50.920	70.422
4	70.080	50.943	70.388
5	70.012	50.930	70.399
6	70.014	50.900	70.402
7	70.041	50.900	70.378
8	70.082	50.918	70.338
9	70.055	50.931	70.336
10	70.035	50.911	70.317
Av Dia.	70.037	50.923	70.385
Av Thk.	9.557		
Calculated Stress =			54.1 MPa
Variance =			7.4 MPa

Table I.2 - Ring split stress.

SPECIMEN 5,6,7A - CUT AT 6 O'CLOCK			
Reading	OD0	ID0	OD1
1	70.032	50.980	70.472
2	70.035	50.971	70.475
3	70.031	50.995	70.421
4	70.048	50.979	70.413
5	70.041	50.905	70.426
6	70.054	51.038	70.457
7	69.997	51.032	70.458
8	70.040	50.985	70.415
9	70.003	50.979	70.410
10	70.016	50.976	70.370
11	70.058	51.035	70.426
12	70.006	50.961	70.464
13	70.046	50.972	70.453
14	70.003	51.028	70.468
15	70.013	50.963	70.461
Av Dia.	70.028	50.987	70.439
Av Thk.	9.521		
Calculated Stress =			63.7 MPa
Variance =			5.5 MPa

Table I.3 - Ring split stress.

SPECIMEN 8A - CUT AT 6 O'CLOCK			
Reading	OD0	ID0	OD1
1	70.020	50.945	70.645
2	70.025	50.946	70.440
3	70.029	50.960	70.435
4	70.035	50.958	70.439
5	70.018	50.950	70.455
6	70.027	50.948	70.482
7	70.038	50.944	70.464
8	70.012	50.955	70.455
9	70.015	50.971	70.432
10	70.028	50.995	70.478
Av Dia.	70.025	50.957	70.473
Av Thk.	9.534		
Calculated Stress =			69.4 MPa
Variance =			9.4 MPa

Table I.4 - Ring split stress.

SPECIMEN 10A - CUT AT 6 O'CLOCK			
Reading	OD0	ID0	OD1
1	70.022	50.991	70.474
2	70.013	51.013	70.478
3	70.080	50.978	70.422
4	70.025	50.918	70.418
5	70.005	51.003	70.457
6	70.020	50.994	70.475
7	70.010	50.978	70.473
8	70.045	50.980	70.419
9	70.035	50.963	70.532
10	69.998	50.915	70.540
Av Dia.	70.025	50.973	70.469
Av Thk.	9.526		
Calculated Stress =			68.8 MPa
Variance =			7.2 MPa

Table I.5 - Ring split stress.

SPECIMEN 11,12,13A - CUT AT 6 O'CLOC			
Reading	OD0	ID0	OD1
1	70.000	50.963	70.417
2	70.026	50.934	70.388
3	70.058	50.938	70.365
4	70.004	50.960	70.360
5	70.005	50.955	70.366
6	70.038	51.028	70.425
7	70.014	51.011	70.438
8	70.050	50.962	70.448
9	70.018	50.982	70.441
10	70.047	51.031	70.402
11	70.062	50.985	70.393
12	70.059	50.950	70.418
13	70.028	50.980	70.432
14	70.075	51.032	70.419
15	70.025	50.932	70.379
Av Dia.	70.034	50.976	70.406
Av Thk.	9.529		
Calculated Stress =			57.7 MPa
Variance =			5.6 MPa

Table I.6 - Ring split stress.

SPECIMEN 14A - CUT AT 3 O'CLOCK			
Reading	OD0	ID0	OD1
1	70.017	51.022	70.358
2	70.044	51.049	70.349
3	70.031	51.020	70.338
4	70.008	51.009	70.325
5	70.000	50.969	70.327
6	70.034	51.056	70.340
7	70.031	51.029	70.357
8	70.042	51.002	70.355
9	70.026	50.993	70.366
10	70.007	51.005	70.372
Av Dia.	70.024	51.015	70.349
Av Thk.	9.504		
Calculated Stress =			50.3 MPa
Variance =			3.2 MPa

Table I.7 - Ring split stress.

SPECIMEN 15,16,17A - CUT AT 3 O'CLOC			
Reading	OD0	ID0	OD1
1	70.077	51.070	70.466
2	70.066	51.038	70.414
3	70.078	51.039	70.411
4	70.076	51.012	70.464
5	70.078	51.021	70.450
6		51.118	70.401
7		51.104	70.409
8		51.081	70.438
9		51.047	70.472
10		51.032	70.478
11		50.965	70.327
12		50.986	70.369
13		51.030	70.420
14		51.035	70.425
15		50.978	70.418
Av Dia.	70.075	51.037	70.424
Av Thk.	9.519		
Calculated Stress =			54.0 MPa
Variance =			6.1 MPa

Table I.8 - Ring split stress.

SPECIMEN 18A - CUT AT 3 O'CLOCK			
Reading	OD0	ID0	OD1
1	70.020	50.985	70.405
2	70.022	51.018	70.390
3	70.041	51.025	70.375
4	70.062	51.012	70.402
5	70.021	50.986	70.413
6	70.029	50.992	70.385
7	70.031	50.995	70.375
8	70.015	50.990	70.382
9	70.018	50.998	70.388
10	70.018	51.000	70.395
Av Dia.	70.028	50.999	70.391
Av Thk.	9.514		
Calculated Stress =			56.2 MPa
Variance =			2.9 MPa

Table I.9 - Ring split stress.

SPECIMEN 21A - CUT AT 6 O'CLOCK			
Reading	OD0	ID0	OD1
1	70.032	50.995	70.512
2	70.025	50.998	70.531
3	70.046	51.018	70.488
4	70.058	51.011	70.505
5	70.077	51.016	70.532
6	70.034	51.005	70.481
7	70.051	50.982	70.495
8	70.072	50.961	70.541
9	70.024	50.968	70.502
10	70.062	50.970	70.537
Av Dia.	70.048	50.992	70.512
Av Thk.	9.528		
Calculated Stress =			71.8 MPa
Variance =			4.2 MPa

Table I.10 - Ring split stress.

SPECIMEN 24A - CUT AT 6 O'CLOCK			
Reading	OD0	ID0	OD1
1	70.027	50.980	70.411
2	70.003	50.945	70.410
3	70.046	50.885	70.481
4	70.019	50.845	70.410
5	70.002	50.897	70.419
6	70.044	50.930	70.493
7	70.015	50.945	70.418
8	70.008	51.002	70.423
9	70.060	51.002	70.478
10	70.011	50.987	70.420
Av Dia.	70.024	50.942	70.436
Av Thk.	9.541		
Calculated Stress =			63.9 MPa
Variance =			5.8 MPa

Table I.11 - Ring split stress.

SPECIMEN 27A - CUT AT 12 O'CLOCK			
Reading	OD0	ID0	OD1
1	70.048	50.950	70.437
2	70.073	50.919	70.425
3	70.039	50.932	70.452
4	70.037	50.941	70.454
5	70.048	50.940	70.535
6	70.022	50.929	70.425
7	70.103	50.910	70.435
8	70.098	50.905	70.497
9	70.071	50.928	70.468
10	70.062	50.950	70.449
Av Dia.	70.060	50.930	70.458
Av Thk.	9.565		
Calculated Stress =			61.9 MPa
Variance =			6.5 MPa

Table I.12 - Ring split stress.

SPECIMEN 30A - CUT AT 6 O'CLOCK			
Reading	OD0	ID0	OD1
1	70.083	51.038	70.498
2	70.082	51.066	70.480
3	69.986	51.064	70.404
4	69.988	51.065	70.378
5	69.995	51.070	70.350
6	70.028	50.938	70.345
7	69.987	50.935	70.329
8	69.989	50.958	70.328
9	70.085	51.001	70.475
10	70.095	51.002	70.426
Av Dia.	70.032	51.014	70.401
Av Thk.	9.509		
Calculated Stress =			57.1 MPa
Variance =			12.0 MPa

Table I.13 - Ring split stress.

SPECIMEN 33A - CUT AT 6 O'CLOCK			
Reading	OD0	ID0	OD1
1	70.023	50.924	70.481
2	70.094	50.916	70.549
3	70.112	50.932	70.623
4	70.009	50.920	70.516
5	70.064	51.012	70.552
6	70.113	51.005	70.683
7	70.012	51.059	70.485
8	70.063	51.057	70.549
9	70.116	51.067	70.614
10	70.035	50.948	70.540
Av Dia.	70.064	50.984	70.559
Av Thk.	9.540		
Calculated Stress =			76.6 MPa
Variance =			11.3 MPa

Table I.14 - Ring split stress.

SPECIMEN 36A - CUT AT 12 O'CLOCK			
Reading	OD0	ID0	OD1
1	70.016	50.936	70.382
2	70.018	50.928	70.385
3	70.042	50.945	70.392
4	70.058	50.978	70.384
5	70.070	50.976	70.362
6	70.078	50.949	70.350
7	70.069	50.951	70.361
8	70.059	50.956	70.373
9	70.065	50.949	70.383
10	70.054	50.942	70.364
Av Dia.	70.053	50.951	70.374
Av Thk.	9.551		
Calculated Stress =			49.9 MPa
Variance =			3.8 MPa

Table I.15 - Ring split stress.

SPECIMEN 2E - CUT AT 6 O'CLOCK			
Reading	OD0	ID0	OD1
1	69.812	50.860	69.761
2	69.812	50.865	69.762
3	69.816	50.859	69.766
4	69.820	50.861	69.772
5	69.829	50.875	69.772
6	69.821	50.865	69.771
7	69.823	50.831	69.772
8	69.824	50.826	69.786
9	69.828	50.830	69.793
10	69.845	50.810	69.795
Av Dia.	69.823	50.848	69.775
Av Thk.	9.488		
Calculated Stress =			-7.5 MPa
Variance =			2.3 MPa

Table I.16 - Ring split stress.

SPECIMEN 6,7E - CUT AT 6 O'CLOCK			
Reading	OD0	ID0	OD1
1	69.819	50.769	69.732
2	69.818	50.768	69.743
3	69.824	50.767	69.741
4	69.819	50.661	69.751
5	69.825	50.652	69.745
6	69.826	50.713	69.744
7	69.824	50.724	69.741
8	69.823	50.765	69.748
9	69.822	50.795	69.745
10	69.819	50.829	69.743
11	69.818	50.821	69.742
12	69.813	50.832	69.748
13	69.817	50.825	69.749
14	69.822	50.816	69.752
15	69.828	50.797	69.753
16	69.828	50.794	69.752
17	69.832	50.801	69.755
18	69.838	50.851	69.761
19	69.835	50.842	69.760
20	69.840	50.871	69.760
Av Dia.	69.824	50.784	69.748
Av Thk.	9.520		
Calculated Stress =			-11.9 MPa
Variance =			1.6 MPa

Table I.17 - Ring split stress.

SPECIMEN 9E - CUT AT 6 O'CLOCK			
Reading	OD0	ID0	OD1
1	69.857	50.892	69.820
2	69.858	50.855	69.817
3	69.862	50.867	69.818
4	69.860	50.902	69.817
5	69.882	50.913	69.809
6	69.765	50.928	69.810
7	69.875	50.908	69.811
8	69.875	50.896	69.815
9	69.872	50.884	69.816
10	69.873	50.883	69.809
Av Dia.	69.858	50.893	69.814
Av Thk.	9.483		
Calculated Stress =			-6.9 MPa
Variance =			5.0 MPa

Table I.18 - Ring split stress.

SPECIMEN 11E - CUT AT 12 O'CLOCK			
Reading	OD0	ID0	OD1
1	69.841	50.867	69.682
2	69.844	50.837	69.683
3	69.845	50.842	69.682
4	69.841	50.836	69.684
5	69.846	50.826	69.661
6	69.842	50.831	69.679
7	69.840	50.835	69.680
8	69.841	50.851	69.680
9	69.841	50.848	69.690
10	69.848	50.864	69.691
Av Dia.	69.843	50.844	69.683
Av Thk.	9.500		
Calculated Stress =			-25.1 MPa
Variance =			1.4 MPa

Table I.19 - Ring split stress.

SPECIMEN 14,15E - CUT AT 12 O'CLOCK			
Reading	OD0	ID0	OD1
1	69.875	50.905	69.750
2	69.871	50.901	69.760
3	69.857	50.771	69.751
4	69.864	50.823	69.750
5	69.851	50.762	69.750
6	69.854	50.768	69.752
7	69.848	50.818	69.752
8	69.852	50.784	69.757
9	69.848	50.852	69.755
10	69.848	50.869	69.752
11	69.865	50.861	69.752
12	69.865	50.863	69.749
13	69.875	50.901	69.759
14	69.878	50.852	69.750
15	69.869	50.859	69.750
16	69.871	50.860	69.746
17	69.871	50.861	69.751
18	69.869	50.863	69.751
19	69.878	50.864	69.749
20	69.869	50.865	69.748
Av Dia.	69.864	50.845	69.752
Av Thk.	9.510		
Calculated Stress =			-17.5 MPa
Variance =			1.6 MPa

Table I.20 - Ring split stress.

SPECIMEN 17E - CUT AT 12 O'CLOCK			
Reading	OD0	ID0	OD1
1	69.886	50.927	69.796
2	69.889	50.882	69.797
3	69.883	50.891	69.796
4	69.885	50.904	69.797
5	69.876	50.916	69.795
6	69.878	50.923	69.790
7	69.880	50.920	69.790
8	69.880	50.900	69.788
9	69.881	50.887	69.786
10	69.885	50.862	69.787
Av Dia.	69.882	50.900	69.792
Av Thk.	9.491		
Calculated Stress =			-14.1 MPa
Variance =			0.9 MPa

Table I.22 - Ring split stress.

SPECIMEN 16E - CUT AT 3 O'CLOCK			
Reading	OD0	ID0	OD1
1	69.917	50.933	69.875
2	69.928	50.942	69.871
3	69.922	50.945	69.864
4	69.919	50.918	69.875
5	69.917	50.928	69.874
6	69.921	50.947	69.862
7	69.908	50.945	69.873
8	69.916	50.962	69.869
9	69.915	50.942	69.865
10	69.910	50.929	69.868
Av Dia.	69.917	50.939	69.870
Av Thk.	9.489		
Calculated Stress =			-7.3 MPa
Variance =			1.1 MPa

Table I.21 - Ring split stress.

SPECIMEN 20,21E - CUT AT 3 O'CLOCK			
Reading	OD0	ID0	OD1
1	69.862	50.870	69.760
2	69.871	50.869	69.752
3	69.874	50.783	69.742
4	69.880	50.780	69.735
5	69.890	50.771	69.729
6	69.898	50.760	69.730
7	69.895	50.779	69.724
8	69.899	50.841	69.721
9	69.882	50.832	69.718
10	69.876	50.921	69.713
11	69.869	50.879	69.705
12	69.868	50.872	69.711
13	69.861	50.869	69.700
14	69.855	50.831	69.703
15	69.842	50.782	69.704
16	69.840	50.785	69.701
17	69.833	50.826	69.715
18	69.831	50.831	69.718
19	69.832	50.841	69.719
20	69.839	50.881	69.699
Av Dia.	69.865	50.830	69.720
Av Thk.	9.518		
Calculated Stress =			-22.7 MPa
Variance =			4.4 MPa

Table I.23 - Ring split stress.

SPECIMEN 24E - CUT AT 3 O'CLOCK			
Reading	OD0	ID0	OD1
1	69.925	50.842	69.815
2	69.924	50.841	69.819
3	69.929	50.892	69.808
4	69.930	50.818	69.813
5	69.938	50.791	69.804
6	69.946	50.812	69.813
7	69.952	50.820	69.821
8	69.955	50.836	69.829
9	69.958	50.840	69.822
10	69.961	50.841	69.820
Av Dia.	69.942	50.833	69.816
Av Thk.	9.555		
Calculated Stress =			-19.8 MPa
Variance =			2.5 MPa

Table I.24 - Ring split stress.

SPECIMEN 28E - CUT AT 3 O'CLOCK			
Reading	OD0	ID0	OD1
1	69.952	50.501	69.839
2	69.957	50.537	69.837
3	69.972	50.611	69.842
4	69.955	50.579	69.841
5	69.978	50.553	69.843
6	69.967	50.479	69.839
7	69.965	50.568	69.838
8	69.915	50.481	69.842
9	69.954	50.485	69.841
10	69.968	50.497	69.842
Av Dia.	69.958	50.529	69.830
Av Thk.	9.711		
Calculated Stress =			-20.4 MPa
Variance =			2.7 MPa

Table I.25 - Ring split stress.

SPECIMEN 30E - CUT AT 9 O'CLOCK			
Reading	OD0	ID0	OD1
1	69.943	50.961	69.748
2	69.953	50.955	69.751
3	69.954	50.932	69.789
4	69.952	50.921	69.762
5	69.945	50.927	69.761
6	69.945	50.914	69.782
7	69.950	50.915	69.767
8	69.942	50.955	69.728
9	69.936	50.942	69.722
10	69.929	50.961	69.719
Av Dia.	69.945	50.938	69.747
Av Thk.	9.504		
Calculated Stress =			-30.9 MPa
Variance =			3.8 MPa

Table I.26 - Ring split stress.

SPECIMEN 36E - CUT AT 3 O'CLOCK			
Reading	OD0	ID0	OD1
1	69.945	50.961	69.750
2	69.948	50.942	69.761
3	69.948	50.951	69.768
4	69.945	50.932	69.752
5	69.941	50.911	69.751
6	69.955	50.926	69.726
7	69.940	50.938	69.729
8	69.933	50.939	69.721
9	69.930	50.942	69.716
10	69.925	50.951	69.710
Av Dia.	69.941	50.939	69.738
Av Thk.	9.501		
Calculated Stress =			-31.7 MPa
Variance =			3.3 MPa

Table I.27 - Ring split stress.

SPECIMEN 1F - CUT AT 12 O'CLOCK			
Reading	OD0	ID0	OD1
1	69.855	50.764	70.251
2	69.800	50.792	70.248
3	69.860	50.839	70.258
4	69.852	50.798	70.214
5	69.808	50.767	70.188
6	69.875	50.750	70.182
7	69.852	50.810	70.250
8	69.816	50.767	70.245
9	69.845	50.758	70.237
10	69.850	50.728	70.193
Av Dia.	69.841	50.777	70.226
Av Thk.	9.532		
Calculated Stress =			60.0 MPa
Variance =			5.7 MPa

Table I.28 - Ring split stress.

SPECIMEN 2F - CUT AT 6 O'CLOCK			
Reading	OD0	ID0	OD1
1	69.800	50.682	70.387
2	69.879	50.608	70.384
3	69.901	50.700	70.409
4	69.912	50.878	70.438
5	69.803	50.741	70.441
6	69.888	50.760	70.449
7	69.903	50.698	70.450
8	69.827	50.746	70.452
9	69.887	50.783	70.451
10	69.902	50.672	70.445
Av Dia.	69.870	50.727	70.443
Av Thk.	9.572		
Calculated Stress =			89.41 MP
Variance =			7.6 MPa

Table I.29 - Ring split stress.

SPECIMEN 3F - CUT AT 6 O'CLOCK			
Reading	OD0	ID0	70
1	69.878	50.768	70.133
2	69.875	50.892	70.128
3	69.861	50.725	70.135
4	69.860	50.751	70.151
5	69.858	50.887	70.172
6	69.846	50.744	70.193
7	69.831	50.820	70.208
8	69.794	50.752	70.212
9	69.792	50.700	70.256
10	69.795	50.708	70.221
Av Dia.	69.839	50.775	70.181
Av Thk.	9.532		
Calculated Stress =			53.4 MPa
Variance =			8.3 MPa

Table I.30 - Ring split stress.

SPECIMEN 4F - CUT AT 6 O'CLOCK			
Reading	OD0	ID0	OD1
1	69.872	50.798	70.302
2	69.846	50.748	70.301
3	69.824	50.718	70.298
4	69.811	50.701	70.291
5	69.807	50.739	70.291
6	69.828	50.740	70.311
7	69.848	50.724	70.378
8	69.864	50.779	70.410
9	69.883	50.771	70.435
10	69.998	50.785	70.425
Av Dia.	69.858	50.750	70.344
Av Thk.	9.554		
Calculated Stress =			75.8 MPa
Variance =			12.2 MPa

Table I.31 - Ring split stress.

SPECIMEN 5F - CUT AT 6 O'CLOCK			
Reading	OD0	ID0	OD1
1	69.838	50.781	70.461
2	69.832	50.761	70.433
3	69.812	50.755	70.387
4	69.811	50.759	70.351
5	69.815	50.663	70.314
6	69.840	50.708	70.277
7	69.872	50.721	70.223
8	69.663	50.745	70.201
9	69.915	50.751	70.198
10	69.927	50.753	70.188
Av Dia.	69.855	50.740	70.303
Av Thk.	9.558		
Calculated Stress =			70.0 MPa
Variance =			17.7 MPa

Table I.32 - Ring split stress.

SPECIMEN 8,9F - CUT AT 12 O'CLOCK			
Reading	OD0	ID0	OD1
1	69.915	50.699	70.379
2	69.850	50.718	70.386
3	69.831	50.778	70.395
4	69.831	50.746	70.395
5	69.855	50.698	70.396
6	69.869	50.732	70.394
7	69.883	50.651	70.396
8	69.888	50.772	70.396
9	69.892	50.775	70.392
10	69.899	50.704	70.369
11	69.889	50.708	70.324
12	69.898	50.738	70.295
13	69.873	50.770	70.291
14	69.858	50.730	70.302
15	69.817	50.695	70.313
16	69.848	50.745	70.312
17	69.846	50.658	70.306
18	69.821	50.766	70.294
19	69.810	50.761	70.290
20	69.798	50.718	70.286
Av Dia.	69.858	50.728	70.346
Av Thk.	9.556		
Calculated Stress =			76.2 MPa
Variance =			8.7 MPa

Table I.33 - Ring split stress.

SPECIMEN 10F - CUT AT 12 O'CLOCK			
Reading	OD0	ID0	OD1
1	69.838	50.716	70.363
2	69.848	50.691	70.352
3	69.805	50.694	70.352
4	69.744	50.701	70.373
5	69.806	50.702	70.395
6	69.826	50.667	70.421
7	69.855	50.750	70.445
8	69.859	50.779	70.457
9	69.862	50.782	70.457
10	69.875	50.785	70.478
Av Dia.	69.832	50.727	70.409
Av Thk.	9.553		
Calculated Stress =			89.9 MPa
Variance =			9.2 MPa

Table I.34 - Ring split stress.

SPECIMEN 11F - CUT AT 6 O'CLOCK			
Reading	OD0	ID0	OD1
1	69.883	50.935	70.408
2	69.823	50.750	70.382
3	69.876	50.845	70.301
4	69.887	50.730	70.289
5	69.824	50.772	70.300
6	69.877	50.816	70.340
7	69.888	50.771	70.300
8	69.824	50.761	70.300
9	69.858	50.766	70.288
10	69.824	50.762	70.370
Av Dia.	69.856	50.791	70.329
Av Thk.	9.533		
Calculated Stress =			73.6 MPa
Variance =			7.9 MPa

Table I.35 - Ring split stress.

SPECIMEN 13F - CUT AT 12 O'CLOCK			
Reading	OD0	ID0	OD1
1	69.868	50.748	70.412
2	69.868	50.741	70.450
3	69.892	50.749	70.483
4	69.802	50.756	70.493
5	69.894	50.758	70.489
6	69.880	50.761	70.497
7	69.875	50.773	70.495
8	69.878	50.792	70.525
9	69.883	50.800	70.542
10	69.894	50.811	70.560
Av Dia.	69.883	50.769	70.495
Av Thk.	9.557		
Calculated Stress =			95.3 MPa
Variance =			7.6 MPa

Table I.36 - Ring split stress.

SPECIMEN 15,16F - CUT AT 3 O'CLOCK			
Reading	OD0	ID0	OD1
1	69.810	50.722	70.341
2	69.824	50.710	70.332
3	69.852	50.722	70.329
4	69.857	50.755	70.325
5	69.852	50.695	70.318
6	69.850	50.766	70.311
7	69.864	50.681	70.280
8	69.877	50.762	70.261
9	69.878	50.716	70.252
10	69.863	50.728	70.268
11	69.861	50.732	70.298
12	69.857	50.740	70.326
13	69.853	50.730	70.331
14	69.850	50.828	70.334
15	69.851	50.760	70.331
16	69.880	50.782	70.313
17	69.910	50.721	70.294
18	69.922	50.730	70.278
19	69.920	50.737	70.272
20	69.918	50.683	70.282
Av Dia.	69.867	50.735	70.304
Av Thk.	9.566		
Calculated Stress =			68.3 MPa
Variance =			6.5 MPa

Table I.37 - Ring split stress.

SPECIMEN 17,18F - CUT AT 3 O'CLOCK			
Reading	OD0	ID0	OD1
1	69.901	50.790	70.499
2	69.892	50.780	70.456
3	69.882	50.732	70.461
4	69.868	50.739	70.450
5	69.880	50.737	70.432
6	69.885	50.770	70.409
7	69.871	50.545	70.405
8	69.852	50.555	70.401
9	69.842	50.505	70.379
10	69.839	50.789	70.354
11	69.834	50.787	70.145
12	69.850	50.735	70.165
13	69.885	50.611	70.194
14	69.912	50.735	70.219
15	69.913	50.789	70.246
16	69.912	50.704	70.252
17	69.912	50.777	70.267
18	69.924	50.796	70.300
19	69.935	50.740	70.316
20	69.957	50.801	70.312
Av Dia.	69.903	50.748	70.243
Av Thk.	9.578		
Calculated Stress =			53.2 MPa
Variance =			17.0 MPa

Table I.38 - Ring split stress.

SPECIMEN 19F - CUT AT 3 O'CLOCK			
Reading	OD0	ID0	OD1
1	69.860	50.695	70.376
2	69.845	50.711	70.368
3	69.855	50.706	70.381
4	69.862	50.712	70.402
5	69.889	50.725	70.431
6	69.890	50.756	70.440
7	69.836	50.726	70.426
8	69.869	50.724	70.425
9	69.873	50.725	70.421
10	69.888	50.728	70.438
Av Dia.	69.867	50.722	70.411
Av Thk.	9.573		
Calculated Stress =			84.9 MPa
Variance =			5.0 MPa

Table I.39 - Ring split stress.

SPECIMEN 22,23F - CUT AT 9 O'CLOCK			
Reading	OD0	ID0	OD1
1	69.900	50.683	70.380
2	69.875	50.728	70.369
3	69.858	50.742	70.370
4	69.856	50.718	70.374
5	69.862	50.631	70.372
6	69.852	50.740	70.382
7	69.859	50.700	70.363
8	69.877	50.710	70.368
9	69.880	50.691	70.379
10	69.887	50.719	70.400
11	69.905	50.712	70.628
12	69.897	50.866	70.545
13	69.888	50.504	70.581
14	69.882	50.638	70.551
15	69.878	50.877	70.539
16	69.877	50.570	70.522
17	69.883	50.778	70.520
18	69.884	50.610	70.519
19	69.888	50.695	70.508
20	69.908	50.774	70.505
Av Dia.	69.889	50.704	70.542
Av Thk.	9.593		
Calculated Stress =			101.9 MP
Variance =			13.8 MPa

Table I.40 - Ring split stress.

SPECIMEN 24,25F - CUT AT 9 O'CLOCK			
Reading	OD0	ID0	OD1
1	69.864	50.851	70.332
2	69.878	50.660	70.351
3	69.883	50.729	70.370
4	69.878	50.725	70.379
5	69.872	50.608	70.375
6	69.888	50.696	70.374
7	69.887	50.732	70.381
8	69.897	50.668	70.397
9	69.915	50.675	70.428
10	69.928	50.681	70.465
11	69.934	50.800	70.491
12	69.941	50.699	70.500
13	69.941	50.683	70.512
14	69.940	50.716	70.516
15	69.941	50.811	70.528
16	69.942	50.684	70.526
17	69.933	50.706	70.538
18	69.938	50.649	70.541
19	69.945	50.783	70.566
20	69.962	50.682	70.589
Av Dia.	69.915	50.714	70.458
Av Thk.	9.601		
Calculated Stress =			84.9 MPa
Variance =			13.3 MPa

Table I.41 - Ring split stress.